ANALYZING SKID RESISTANCE AND TIRE/ROAD NOISE ON POROUS PAVEMENT USING NUMERICAL MODELING

ZHANG LEI

(M.Eng., Dalian University of Technology)

A THESIS SUBMITTED

FOR THE DEGREE OF DOCTOR OF PHILOSOPHY

DEPARTMENT OF CIVIL AND ENVIRONMENTAL ENGINEERING

NATIONAL UNIVERSITY OF SINGAPORE

2014

DECLARATION

I hereby declare that the thesis is my original work and it has been written by me in its entirety. I have duly acknowledged all the sources of information which have been used in the thesis.

This thesis has also not been submitted for any degree in any university previously.

Zhang Lei
29 Jul, 2014

ACKNOWLEDGEMENTS

I would like to express my utmost appreciation and gratitude to my supervisors, Dr. Ong Ghim Ping Raymond and Prof. Fwa Tien Fang, for their valuable guidance, warm-hearted care, and constant encouragement throughout the research. They not only impart me the critical thinking and research methodology, but also impact me on the principles of behavior and attitude. I sincerely appreciate their contributions.

I would extend my gratitude to Prof. Chew Chye Heng and Dr. Chui Ting Fong May, members of my Ph.D. committee for their insightful and helpful recommendations in improving the research. Thanks are also given to A/Prof. Meng Qiang, Prof. Lee Der-Horng, A/Prof. Chan Weng Tat and A/Prof Chua Kim Huat David for the specialized knowledge they provided.

Special appreciation is given to National University of Singapore for providing the President's Graduate Fellowship to support my research and life. Thanks are also addressed to my colleagues, Dr. Qu Xiaobo, Dr. Pasindu H.R., Dr. Farhan Javed, Dr. Wang Shuaian, Dr. Ju Fenghua, Dr. Yang Jiasheng, Dr. Anupam, Cao Changyong, Lim Emiko, Zhang Wei, Sou Weng Sut, Yin Lu, Fu Rao, Dr. Wang Yueying, Zhang Xiaofeng, Zheng Jiexin, Asif Imran, and Dr. Habibur Rahman, for their kind help and friendship. Thanks are also accorded to Mr. Foo Chee Kiong, Mr. Goh Joon Kiat, Mrs. Yap-Chong Wei Leng, Mr. Farouk and Mrs. Yu-Ng Chin Hoe of the Transportation Engineering Laboratory and Dr. Wang Junhong of NUS Computer Center for their kind assistance and support in the course of research.

Last but not least, I would like to give my heartfelt gratitude to my parents for their tremendous care, support and encouragement. I am especially grateful to my wife, Song Wenwen, for her continuous support and meticulous care.

TABLE OF CONTENTS

SUMMARY

Skid resistance and tire/road noise are two of the major concerns in pavement functional performance in modern road transportation. They are crucial in roadway safety and travel comfort. It is difficult to handle the problems simultaneously using the conventional dense-graded pavement because they have contrary requirements on pavement macrotexture. Wet-pavement skid resistance needs a higher macrotexture level to discharge water underneath tires, while tire/road noise abatement requires a lower texture level to mitigate impact-induced tire vibration. This problem can be well solved by applying porous pavement technologies. Porous pavement enhances skid resistance through inner drainage and reduces tire/road noise through acoustic absorption. Despite its global applications, the mechanisms and influencing factors of skid resistance and tire/road noise on porous pavement have not been completely understood. This is partially due to the lack of mechanistic models to accurately simulate these complex phenomena. Past research efforts on porous surface are largely experimental in nature. This study attempts to explore the development of numerical simulation models in predicting skid resistance and tire/road noise on porous pavements and apply the developed models in influencing factor analysis and porous mixture design.

Porous pavement possesses a superior wet frictional performance because it can rapidly discharge water from tire-pavement contact patch, so that the excessive hydrodynamic pressure can be easily released to avoid undermining the contact force between tire tread and pavement surface. The drainage capacity of a porous surface is modeled by a simplified pore structure of grid network, whose dimension parameters are calibrated through an iterative process, taking effective porosity, clogging effect and measured outflow time into consideration. This porous pavement model is then integrated into the numerical skid resistance model, simulating a lock-wheel smooth tire slides on a flooded porous pavement. This model involves all major mechanisms in skid resistance simulation, such as tire-pavement contact, fluid-structure interaction,

tire deforming behavior, turbulent and multiphase flow. The overall skid resistance model is validated against past experimental results for both porous and nonporous pavements. The effect of porous surface layer on skid resistance enhancement is then analyzed using the developed model from a numerical perspective. The influences of critical factors on porous pavement skid resistance are also investigated quantitatively through a case study. Some suggestions on porous mixture design are provided based on the findings from this parametric study.

Porous pavement surface can reduce tire/road noise emission mainly due to its acoustic absorption capacity resulted from energy dissipation in the pore network. This effect is considered in the development of tire/road noise simulation model. The acoustic characteristics of porous pavement are represented by acoustic impedance (related to acoustic absorption coefficient) which can be either measured in field test or derived from pore structure compositions. Pavement texture serves as excitation input in a form of frequency-domain texture level. The model identifies tire vibration as the major noise source and covers the other sources by model calibration. Tire vibration is reproduced by the finite element method using a mode superposition strategy and sound propagation in free space is modeled by boundary element method. It was found that the developed model needs a careful calibration according to the tire and pavement types before application, and the model validation shows that although this model can predict the overall noise level on porous pavement with a satisfactory accuracy, the generated noise spectrum needs to be corrected with a frequency shift. The developed model is then used to analyze the effect of porous surface on tire/road noise and study the critical influencing factors of tire/road noise on porous pavements. Recommendations on porous mixture designs are drawn from the noise standpoint.

With a better understanding in the mechanisms of wet skid resistance and tire/road noise on porous pavement, as well as the effects of critical influencing factors, this study developed an analysis framework to integrate skid resistance and tire/road noise performances into the porous mixture design process. The fundamental

of this framework is to quantify the safety and comfort benefits brought forth by the application of porous surface using quantitative analysis methods and determine the relevant performance indices through subjective judgments. The developed numerical models are adopted to predict the skid number and noise level generated on porous surfaces. Artificial neural network can be applied to enhance design efficiency. The application of this analysis framework is demonstrated through a hypothetical case study, which illustrates the feasibility and capability of the models and methodologies proposed in this research study.

LIST OF TABLES

LIST OF FIGURES

CHAPTER 1 INTRODUCTION

Pavement structures in modern transportation system not only provide supporting surfaces for vehicles to travel on, but also provide functional purposes to guarantee appropriate traveling quality (Haas et al., 1994; Mallick and El-Korchi, 2013). Among various functional performances, priority is often given to road safety and this requires consideration in pavement design to reduce occurrences of traffic accidents. Comfort is another crucial functional requirement for modern pavements and is evaluated through road users' physical perceptions. With regard to the functional requirements, two critical tasks are to enhance road safety by providing sufficient wet-pavement skid resistance and to improve travel comfort by reducing tire/road noise. Various engineering measures were developed for these purposes, such as surface grooving, surface tining, thin-layer coating, chip seal and porous surface. Among these approaches, porous pavement is found to be an effective and cost-efficient solution which is capable to accomplish skid resistance enhancement and tire/road noise reduction simultaneously. This chapter provides the background of porous pavement technology and its advantages in improving pavement surface performance, followed by the objectives of this research and the organization of thesis.

1.1 Background

Although porous pavement may exhibit various forms (Ferguson, 2005), this research work focuses mainly on the two major types of porous pavements, namely porous asphalt pavements and porous concrete pavements. Different terminologies were used in the development of various porous pavement technologies in different countries, such as porous friction course (PFC), open-graded friction course (OGFC), popcorn mix and pervious concrete in the U.S., drainasphalt in France, flusterasphalt in Germany, as well as drainage mix, permeable pavement or pervious macadam in other countries. The name porous asphalt (PA) was adopted by European Committee

for Normalization to unify the terms for technologies using asphalt binder (Nicholls, 1998). This term is therefore used throughout this thesis. The name porous concrete is used to indicate the porous surface techniques using Portland cement as bonding material.

1.1.1 Introduction of Porous Pavement Technology

Porous pavement is a category of pavement structure whose surface layer contains a large amount of interconnected air voids that allows rainwater to be drained through the surface course. The bonded pavement material is characterized by a high porosity, which can range up to 20% by volume (Anderson et al., 1998) and is much higher than that of a typical conventional mixture (typically around 5%). Such a porous layer is commonly laid on an impermeable dense-graded base course to form an inner-drainage system with a finite vertical thickness. A successful porous pavement system not only improves pavement surface properties, but does not sacrifice its structural capacity.

Porous asphalt was initiated in the Unites States in the mid-twentieth century (Smith, 1992), and was first implemented in Europe on airport runways by British Transport Research Laboratory (TRL) in the late 1950s and then on highways in 1960s (Abbott et al., 2010). Since then, many countries have began using porous asphalt. Today, more than 80% of freeways in the Netherlands are paved with porous asphalt to counterbalance increasing noise level and accident potential resulting from increased speed limit (van der Zwan, 2011). The Japanese strategy is to replace all existing pavements with pervious surface systems to provide benefits on safety and riding comfort (Nakahara et al., 2004). Although porous concrete pavement was developed decades later than the porous asphalt and applied less widely over the world (Offenberg et al., 2010), it is gaining attention from pavement engineers due to its potential superior performance and strength.

Despite the difference in base binder material (i.e. asphalt or cement), the high porosity in porous layer results from the open gradation of its aggregate skeleton. Single-size large particles are commonly used in porous mixture, while small grains are removed from a typical gradation design. The absence of fine aggregates leaves the air voids among coarse aggregates unfilled after stone-on-stone contact is achieved with compaction. High-viscosity modified asphalt or high-strength cement is used to bond the aggregates together, ensuring sufficient integrity and durability. Fibers and/or agents may also be added in the production of porous mixture to improve structural capacity on the premise that no adverse effect is brought to its drainage performance with the addition of fibers/agents.

1.1.2 Advantages and Disadvantages of Porous Pavement

The primary objective of porous pavement applications is to enhance travel safety on high-speed road facilities. This purpose is mostly achieved by improving the skid resistance of wet pavements and preventing the occurrence of hydroplaning. It is widely reported that the skid resistance levels on porous pavement surfaces are generally higher than those of dense-graded asphalt or cement concrete pavements and it is less speed-sensitive (NCHRP, 1978; Isenring et al., 1990; Kandhal and Mallick, 1998; Liu et al., 2010). This is a result of the combined effects of connected air voids and coarser surface macrotexture in the porous pavement structure that allow free water to be quickly discharged from the tire-pavement contact interface. Moreover, the superior drainage capacity of porous surface can also reduce splash and spray, mitigate head light glare and provide better visibility for drivers in raining nights (Smith, 1992). These benefits work together to further improve travel safety on porous pavements.

With the rapid improvement in porous pavement technology, its advantage in tire/road noise reduction has also been found in past research studies (van Heystraeten and Moraux, 1990; Gibbs et al., 2005; Abbott et al., 2010; Liu et al.,

2010). The benefit of porous surface in traffic noise abatement was initially investigated in Europe and has become the main reason why porous pavements are adopted in most European countries. Porous surface is believed to achieve noise reduction primarily through two mechanisms. Firstly, the tire/road noise generation is altered by reducing air pumping at the front and rear edges of tire-pavement contact patch. Secondly, the reflection and scattering of sound wave in the pores result in sound energy absorption and dissipation (Neithalath et al., 2005). Air void content and porous layer thickness affect acoustic performance significantly. The use of porous pavements for the purpose of noise reduction has led to thicker porous layers. Other benefits contributing to traveling comfort include the better rutting resistance of course aggregate skeleton which provides better evenness and less roughness (Huddleston et al., 1991; Younger et al., 1994).

Besides travel safety and comfort, many ancillary advantages are obtained on porous pavement as well. These include improvement in storm runoff management and water quality (Legret et al., 1996; Pagotto et al., 2000; Kuang and Fu, 2013), utilization of rubber from scrap tires (Hori and Furusato, 2001; Shen et al., 2013), and amelioration in urban heat-island effect (Stempihar et al., 2012).

Not all porous surface applications in pavement function enhancement were successful. The major drawbacks are the durability of porous layer due to permeability reduction and clogging (Nicholls, 1998), stripping and raveling after higher exposure to the environment (Kandhal and Mallick, 1998), and deterioration of underlying layers due to improper sealing (Smith, 1992). Various additives are available to address these problems by improving binder properties or increasing binder film thickness over aggregates. Winter maintenance is another widely reported problem for porous pavements. Their rougher textures often result in aggregate removals by snow plows (Huddleston et al., 1993). The higher void content causes the deicing chemicals to flow away faster (Camomilla et al., 1990), while the use of winter sand on porous surfaces has been shown to clog the air voids and reduce

drainage efficiency (Younger et al., 1994). The unit cost of porous pavements is usually higher than that of conventional pavements. This is attributed to the requirement for high-quality or specific materials, extra expenses on treatment of underlying layers, and higher-level quality control in construction and maintenance (Smith, 1992; Nicholls, 1998). The structural contribution of a porous wearing course is usually ignored in pavement design, which results in a need for thicker underlying layers, which in turn drives the total cost of pavement structure even higher. Other disadvantages of porous pavements which were observed in some projects include difficulties in surface patching (Younger et al., 1994), unfavorable wet-friction properties at low speed or in the initial stage when open to traffic (Isenring et al., 1990), and unstable moisture susceptibility (Smith, 1992).

1.1.3 Functional Design of Porous Pavement

Although the porous surface course serves mainly as a functional layer with negligible structural significance, this consideration is not sufficiently looked into in the existing porous mix design specifications. Since the Federal Highway Administration (FHWA) published its first formalized design procedure in 1974 with modifications in 1980 and 1990 (FHWA, 1990), there have been more than 20 different design approaches developed across the United States (Putman and Kline, 2012). All these methods focus on the selection of aggregate gradation and asphalt content to form a skeleton structure with a desired high porosity and stone-on-stone contact. Taking the ASTM standard D7064 (ASTM, 2013a) as an example, the optimum grading is first chosen based on the voids in course aggregate (VCA). The content of modified asphalt is next determined by test results of air voids, draindown, abrasion loss and aging resistance. A minimum air void content of 18% is specified and higher void contents are desirable. Laboratory permeability or porosity testing is optional and no concern is placed on skid resistance or acoustic absorption of the finished porous pavement surface.

Design of porous asphalt in Britain is currently based on a recipe approach. Porous mixtures are specified in BS EN 13108-7 (BSI, 2006). This standard defines the aggregate gradation and binder grade for various application purposes, as well as the selection of additives and modifiers. The target asphalt binder content of 4.5% is considered as a balance between durability and permeability (The Highways Agency, 1999). The British design method involves in-situ hydraulic conductivity tests being conducted after placement but before trafficking. The acceptable relative hydraulic conductivity is in the range of 0.12 s^{-1} to 0.40 s^{-1}. Guideline on pavement edge details for porous asphalt is provided in the design manual (The Highways Agency, 1997) to ensure that the desired function of porous surface (e.g. surface water drainage) is properly delivered. Requirements on porous layer geometry are also specified, such as a nominal thickness of 50 mm and a minimum crossfall of 2.5%. However, all these provisions are targeted at enhancing drainage capacity. There are neither direct guidance on frictional and acoustic properties, nor explicit relationships between drainage capacity and the functional performance.

Besides the United States and Europe, many other countries around the world have also developed their own design specifications. Most countries (such as Spain, Denmark, the Netherland and Australia) specify a minimum air void content as a crucial design requirement. Permeability test is commonly not required in laboratory, but some highway agencies (e.g. Danish Road Institute and Belgium Road Research Center) recommend drainage tests on the finished pavements. A sealed tube is used in Denmark to measure the run-out time of a given volume of water and general guidelines are provided to evaluate the degree of clogging. Belgium also requests in-situ drainage characteristics being evaluated with a drainometer. There are no specific clauses found on the functional performance of porous pavements with regard to skid resistance and noise reduction. It is basically assumed in these design methods that the functional properties are considered adequate if the volumetric and composition requirements are satisfied.

1.2 Objectives

It is concluded from the overview of existing design guidelines that although the main purpose of porous pavement applications is to utilize its advantages in skid resistance improvement and tire/road noise abatement, none of the current porous mixture design specifications explicitly considered wet-pavement friction and sound absorption performances as part of the design targets. This is not unexpected because of the complexities involved in considering both skid resistance and tire/road noise phenomena on porous pavements. The gap between laboratory design indices (such as aggregate gradation, porosity and permeability) and field functional performances (such as skid number and sound pressure level) should be bridged through detailed understandings in the mechanisms. This study attempts to approach the problem from a numerical perspective. The objectives of this research work are:

1. To develop numerical simulation models and analytical frameworks that can analyze skid resistance and tire/road noise performances of porous pavements under different operating conditions.

2. To understand the mechanisms that result in skid resistance enhancement and tire/road noise reduction on porous pavements through the application of the developed models.

3. To analyze the influencing factors of skid resistance and tire/road noise on porous pavement and identify the critical parameters in mixture design.

4. To develop an integrated approach that incorporates skid resistance and tire/road noise performances in the porous mixture design procedures.

1.3 Organization of Thesis

In order to achieve these objectives, research works have been performed as shown in Figure 1.1 which demonstrates the tasks taken to meet the objectives. The figure also provides the logic flowchart of the major components in this thesis. It is seen that two tracks on skid resistance and tire/road noise are developed and then

integrated into the development of mixture design method to numerically investigate the skid resistance and tire/road noise performances of porous pavements. Following this flowchart, the thesis consists of:

Chapter 1 provides the background of porous pavement technique and discusses its ability in improving pavement functional performances. The objectives of the current research work are highlighted as well.

Chapter 2 reviews the existing literature on pavement skid resistance and tire/road noise. The standard measurement methods are introduced. The mechanisms and influencing factors observed in previous experimental studies are discussed as well. Research findings on porous pavements are then described. The existing models for skid resistance and tire/road noise are also extensively reviewed in detail. The needs of current research are highlighted based on the limitations of past studies and the scope of this research work is defined.

Chapter 3 presents in detail the formulation and development of a numerical simulation model that is capable to evaluate the lock-wheel skid number on porous pavements. The critical issues in skid resistance modeling is first discussed and the solutions to these problems are then explained in detail. Emphasis is placed on the representation of porous surface drainage capacity. Model validation is conducted against published experimental results.

Chapter 4 applies the developed numerical simulation model in Chapter 3 to analyze the mechanisms and influencing factors of skid resistance on porous pavements. The effect of porous surface layer on skid resistance is investigated through comparisons between situations on porous and non-porous pavements. The influence of porosity, porous layer thickness, rainfall intensity and vehicle speed is quantitatively analyzed based on hypothetical case studies.

Chapter 5 presents the formulation and development of a numerical model that can estimate the near field noise level resulting from tire/road interaction on porous pavement. Some critical issues in tire/road noise modeling is discussed and

the solutions are provided in the model development. Emphasis is placed on the numerical representation of the acoustic absorption of porous pavements. This model is also validated against reported experimental data.

Chapter 6 applies the developed noise model in Chapter 5 to analyze the mechanisms and influencing factors of tire/road noise on porous pavements. The effect of porous surface layer on noise reduction is investigated through detailed comparisons of noise emissions on porous and non-porous pavements. The influence of porosity, porous layer thickness, pavement surface texture and vehicle speed on tire/road noise emission is analyzed.

Chapter 7 proposes an analysis framework to integrate skid resistance and tire/road noise performances into the design of porous pavement. The considerations in the existing design methods are first introduced. A numerical approach based on extensive simulation results is then established to evaluate and compare the critical functional requirements in mixture design. The feasibility of the proposed method is illustrated through a case study.

Chapter 8 summarizes the main conclusions drawn from the current research and provides recommendations for future work.

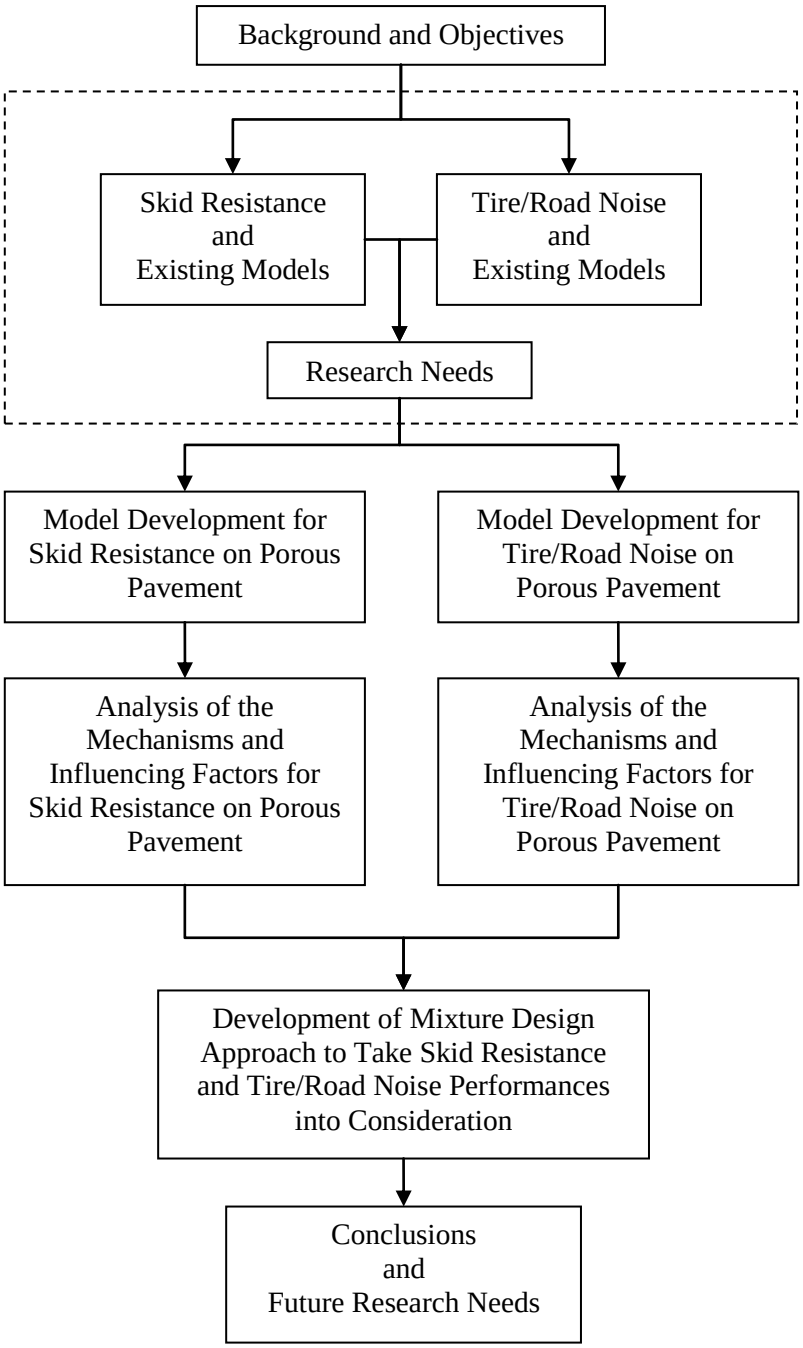

Figure 1.1: Flowchart of thesis organization

CHAPTER 2 LITERATURE REVIEW

This chapter presents a review of the existing literature on the major aspects of this research, i.e. skid resistance and tire/road noise. The mechanisms of skid resistance and tire/road noise are first presented. Various measurement techniques are then described. Major influencing factors on pavement frictional and acoustical performances are next identified, with emphasis placed on their effects of porous pavements. Last but not least, the modeling of skid resistance and tire/road noise is presented. This chapter is then concluded by defining the research needs and the scope of current work.

2.1 Wet-Pavement Skid Resistance

The skid resistance performance of a wet pavement can significantly affect the driving safety in raining weather. Adequate skid resistance plays an important role in reducing the occurrences of wet weather roadway accidents related to hydroplaning, skidding and over-steering, while an insufficient skid resistance level is one of the major causes of traffic crashes. In a recent study, Ivan et al. (2012) indicated that the number of wet-weather vehicle crashes increases when pavement skid number drops, providing all other factors remaining constant. McGovern et al. (2011) noted that 70% of the wet-pavement crashes can be prevented by improving the skid resistance. Similar results were also reported by Mayora and Pina (2009) based on a before-and-after study, where wet-weather crash rates were found to reduce by about 68% through pavement friction improvement campaigns.

Recognizing its importance in safe roadway operation, research efforts have been put forth to understand and improve pavement skid resistance over the past decades. This section presents a comprehensive literature review on the current knowledge of pavement skid resistance. After an overview on skid resistance is described, the classical theories on dry and wet pavement friction are presented. Various skid resistance measurement approaches are then introduced. Some

important factors affecting the wet-pavement skid resistance are discussed, with emphasis placed on past experimental studies on porous pavements. Finally, recent developments in empirical and numerical skid resistance models are presented in detail.

2.1.1 Overview of Wet-Pavement Skid Resistance

Skid resistance is defined as the force developed when a tire prevented from rotating slides on the pavement surface (Highway Research Board, 1972). This term typically refers to the capability of pavements to resist tire sliding in wet condition, because the vast majority of pavement surface types can provide adequate frictional performance in dry condition (Woodside and Woodward, 2002). A resistance force ratio, defined as the force resisting motion divided by the vertical load, can serve as an indicator of pavement skid resistance performance.

Three forms of skidding phenomena have been observed on roads, namely lock-wheel skidding, impending skidding and sideway skidding (Wu and Nagi, 1995). Lock-wheel skidding happens in the travel direction of a vehicle when the brake is suddenly applied. By applying the brake gradually, impending skidding takes place when the wheel is still rolling and skidding is imminent. Sideway skidding occurs to a vehicle travelling along a horizontal curve at a high speed. During sideway skidding, tire attempts to move literally towards outside of the curve. On a wet pavement surface, the lock-wheel condition is usually the most unfavourable skidding situation, because it exhibits the lowest skid resistance among the three forms of skidding at high speeds. Therefore, this research work only focuses on the lock-wheel skid resistance in the safety consideration of porous pavements.

Wet-pavement skid resistance has been considered in design specifications for conventional pavements through several measures. First, sideway coefficient of friction is required in the highway geometric design for determining the minimum curve radius to prevent uncontrollable sideway skidding (AASHTO, 2011a). Second,

cross slope and longitudinal grade should be properly designed to discharge rainwater efficiently to roadside drainage facilities. This measure maintains a sufficiently small water film thickness on the pavement surface and is considered effective in reducing hydroplaning occurrences (AASHTO, 2011a; Wolshon, 2004). Third, an assumed wet friction coefficient is used to derive stopping distance, and wet-weather travel safety should be considered when determining the speed limit (Lamm et al., 1999). Moreover, a minimum polished stone value (PSV) is usually specified in selection of aggregates (The Highways Agency, 2004). Dimensions of artificial texturing on concrete pavements are also recommended to enhance skid resistance (McGovern et al., 2011).

Initially investigated in the late 1920s (Moyer, 1933), research on wet-pavement skid resistance has gained significant progresses. Measurement approaches were developed (Wu and Nagi, 1995) and the mechanisms of skid resistance were proposed through experimental studies (Moore, 1966). It had been found that both pavement characteristics and tire properties are closely related to skid resistance performance (Woodside and Woodward, 2002). Skid resistance is also affected by water film thickness, environmental temperature, vehicle speed, tire inflation pressure, wheel load and many other factors (Hall et al., 2009). The presence of water film on pavement surface, which acts as a lubricant at tire-pavement interface, is critical in wet skid resistance (Delanne and Gothie, 2005). Strategies in design, construction and maintenance (such as asphalt surface treatments, thin asphalt overlays, concrete surface texturing and thin epoxy laminates) were also proposed to enhance the wet weather traveling safety on roadways (McGovern et al., 2011).

2.1.2 Classical Theories on Tire-Pavement Friction

The skid resistance phenomenon on wet pavement surfaces is so complex that to date its mechanisms are still not totally understood. It involves the combined effects of rubber friction, lubrication theory, fluid dynamics and tire mechanics. The

classical tire-pavement friction theory may be a starting point for research in pavement skid resistance performance. Research on friction can be traced back to the 15th century, when Leonardo da Vinci developed the basic laws of friction and introduced the concept of the coefficient of friction (Leonardo and MacCurdy, 1948). Amontons (1699) and Coulomb (1785) later contributed to the five classical laws of friction, most of which are now found to be limitative (Moore, 1975). Equation (2.1) presents a friction theory proposed by Coulomb (1785) considering the works of Amontons (1699) and Desguliers (1734).

$$F = A + \mu N \tag{2.1}$$

where F is the friction force, A represents the component attributed to the adhesive or cohesive effect, and μN refers to the deformation effect. This relationship cannot explain the low friction on lubricated surfaces, and suffers from the variations of parameters with speed and contact pressure. However, it forms the basis of modern contact mechanism modelling.

2.1.2.1 Theories on Rubber Friction

Friction mechanisms turn out to be much more complicated if rubber is involved. The classical laws of friction does not work on elastomers and the coefficient of friction becomes a variable depending on the real contact area, normal load and velocity (Brown, 1996). The study on the relaxation of polymers by Williams et al. (1955) was useful in presenting friction data at different temperatures and speeds. Gough (1958) described the general characteristics of rubber friction and illustrated the variation of frictional force with sliding velocity. The coefficient of friction was found to peak at a certain velocity.

The adhesion and hysteresis effects were the first two components in rubber friction proposed and are based on Coulomb's laws (Moore and Geyer, 1972; 1974). It was assumed that the measured friction force F consists of an adhesion force F_{adh} and a hysteresis force F_{hys} when a rubber block slides on a rough surface under a

uniform loading (Tabor, 1959). As shown in Equation (2.2) and (2.3), adhesion force can be expressed as the product of shear strength and actual contact area, while hysteresis force is related to energy losses within the deformed rubber (Moore, 1966).

$$f_{adh} = \frac{A}{A_n} \cdot \frac{s}{p} \tag{2.2}$$

$$f_{hys} = \frac{QD}{A_n bp} \tag{2.3}$$

where f_{adh} is the adhesion coefficient = $\frac{F_{adh}}{L}$, A is the actual contact area, A_n is the nominal area, s is the interface shear strength, p is the pressure on rubber block, L is the normal load, f_{hys} is the hysteresis coefficient = $\frac{F_{hys}}{L}$, Q is the volume of rubber participating in the deformation, D is the energy dissipated per unit volume of rubber due to damping, and b is the rubber sliding distance.

The formulation of rubber friction was refined by Veith (1986), taking wear component F_{wear} into consideration to express the total friction force as:

$$F = F_{adh} + F_{hys} + F_{wear} \tag{2.4}$$

The adhesion component is usually dominant on smooth surfaces, while the hysteresis term normally governs friction on rough or lubricated surfaces. The wear term depends on the texture and hardness of contacting surfaces. It should be noted that all the three components are affected by the condition of interface, including the actual contact area and the presence of lubricants.

Adhesion Effect

The adhesion effect of skid resistance refers to the shear force developed at the tire-pavement interface when a tire is conformed to the shape of its contact area (Choubane et al., 2003). There exists an adhesion bonding of surface atoms between sliding members, and energy is needed to break this bonding. The dissipation of this energy presents difficulties in the development of adhesion theory for rubber (Veith,

1986). Molecular theory and macroscopic theory are two main categories of adhesion theories (Moore and Geyer, 1972). The former typically takes the van der Waals force as the adhesion between rubber and solid, where a maximum coefficient of friction could be explained by the Eyring rate theory (Bowden and Tabor, 1964). The latter is based on phenomenological theory, assuming rubber is adhered to solid with a number of bonds in each domain, with each bond being able to sustain a finite small force (Savkoor, 1965).

It was indicated in past pavement research that the adhesion component of skid resistance is governed by pavement microtexture (Jayawickrama and Graham, 1995). Microtexture ensures physical penetration of the thin squeeze film at interface and a better tire draping effect at low vehicle speed, so that a good adhesion could develop (Moore, 1969; 1972). Previous studies also showed that the presence of water at the contact interface would reduce the adhesion effect significantly (Persson, 1998). If the surface is completely lubricated, the adhesion component may even disappear (Highway Research Board, 1972). Therefore, appropriate surface drainage provided by pavement macrotexture is also important in maintaining adhesion effect.

Hysteresis Effect

Hysteresis is the resistance due to rubber deformation when energy losses occur in rubber which is subjected to cyclic stress variation. It is a characteristic feature of visco-elastic material when "flowing" over an uneven rigid surface and conforming to the surface contours. Hysteresis theories could be classified into three types: elastic and visco-elastic theories, single and multiple element models and force and energy concepts (Moore and Geyer, 1974). Greenwood and Tabor (1958) applied elastic theory to the concepts of hysteresis and conjectured that a small fraction of input elastic energy from the deformation of elastomers must be dissipated in the form of hysteric friction. Kummer (1966) and Hegmon (1969) proposed a unified theory of friction and a relaxation theory of hysteresis respectively, based on either

semi-empirical analogy or energy concept. It is noted that skid resistance obtained from these works are extremely insensitive to speed, especially at lower sliding speeds. The theory developed by Yandell (1971), using a complex network of spring and dashpot elements, permitted large deformations and any value of Poisson's ratio, rigidity and damping factor. The contribution of hysteric effect due to microtexture and macrotexture can be identified by the superposition principle.

Although Yandell (1971) indicated that both microtexture and macrotexture affects hysteresis friction, it is generally believed that its magnitude is determined by the pavement macrotexture (Jayawickrama and Graham, 1995). The contribution of hysteresis to the total pavement friction is usually small. However, its contribution may become significant when pavement is slippery, due to either lubrication, round microtexture or high speed (Schulze and Beckman, 1965; Highway Research Board, 1972). It was also found that when a tire starts to skid, the adhesion component begins to decrease and the share of hysteresis effect increases relatively (Choubane et al., 2003).

Wear Effect

The wear component of friction results from the work being done to make material loss from one or both surfaces of the sliding pair (Veith, 1986). Three distinct mechanisms have been identified for rubber wear (Moore, 1972): (a) abrasive wear - abrasion and tearing of sliding elastomers caused by sharp texture on base surface; (b) fatigue wear - the failure of elastomers surface under cyclic strain and stress from the repeated deformation on blunt but rough base surface; (c) roll formation - the tearing of rolled fragment when highly elastic materials slide on smooth surfaces. The fatigue wear is relatively less severe than the other two, although all the three forms of wear generally co-exist simultaneously.

The extent of passenger car tire wear was measured on a series of pavements in Transportation and Road Research Laboratory (Lowne, 1970). It was concluded

that microtexture is the governing pavement surface characteristic for tire wear, while macrotexture plays a secondary role. Wear rate increases with an increase in speed or temperature, and is especially high when rubber melting occurs. Wear rate decreases when the amount of water at the interface grows, which was thought by Stachowiak and Batchelor (2005) to be the consequence of hydrodynamic lubricating effect.

2.1.2.2 Lubrication at Contact Interface

Most modern pavement surfaces can provide sufficient skid resistance when they are dry. However, frictional performance decreases dramatically during wet weather, especially when the vehicle is traveling at high travel speeds (Wu and Nagi, 1995). Water film acts as a lubricant between tire and pavement surface and affects skid resistance. This phenomenon can be explained by lubrication theories. The modern lubrication theories were developed from Reynolds' hydrodynamic theory of lubrication for incompressible fluid (Reynolds, 1886). There are two basic methods to derive Reynolds' theory. One is to use the continuity and Navier-Stokes equations, and the other is to apply the principles of mass conservation and the laws of viscous flow (Pinkus and Sterlicht, 1961; Cameron, 1976; Gross et al., 1980; Hamrock, 1994). There are no general closed-form solutions for these equations and typically, numerical methods are required (Bhushan, 2002).

The generalized Reynolds' equation consists of three components, namely the wedge term, the stretch term and the squeeze film term. The wedge term is the most significant of these three due to the film thickness variations and the possibilities of absence of the other two terms (Moore, 1975). Hydrodynamic lubrication, subjected to the surface roughness, contributes to four different forms of load supports, namely directional effect, macro-elasto-hydrodynamic effect, cavitation effect and viscosity effect. If the deformation of surrounding solids has a significant influence on the development process of hydrodynamic lubrication, elasto-hydrodynamic lubrication is said to occur. In this situation, two additional effects should be accounted for in the

classical theory, namely the influence of high pressure on the viscosity of fluid and the substantial local deformation of fluid geometry. Iterative procedure (see Figure 2.1) is often used in the study of elasto-hydrodynamic problems.

In a simple tire traction model developed by Veith (1983), three types of lubricated friction modes were proposed, namely boundary layer lubrication, elasto-hydrodynamic lubrication and mixed lubrication. Boundary layer lubrication mode occurs at low velocity, when tire and pavement are in relatively intimate contact with a molecular thick water film between them. Elasto-hydrodynamic lubrication occurs at high velocity, when an elastic indentation of the tire tread develops due to water accumulating at the leading edge of contact interface and an upward hydrodynamic pressure is generated. Mixed lubrication mode occurs at intermediate velocity. It is a transition between the previous two situations. A part of contact interface (usually the front part) is in the state of elasto-hydrodynamic lubrication while the other part is in boundary lubrication mode. Mixed lubrication mode is the most common situation in practice and it is closely related to the three-zone model discussed below.

2.1.2.3 Three-Zone Model

In order to describe the wet friction phenomenon in tire-pavement interaction, a three-zone model was proposed by Gough (1959) for a lock-wheel skidding on wet pavements. This model was further developed by Moore (1966) for a rolling wheel. The concepts of three-zone model are demonstrated in Figure 2.2.

Zone A: Squeeze-Film Zone

When a vehicle is traveling at a relatively high speed on a pavement surface covered by a thick water film, the front of tire contact area would be deformed by a water wedge. This situation corresponds to the elasto-hydrodynamic lubrication mode. The friction force developed at this zone is mainly determined from the bulk properties of lubricant, such as the viscosity and velocity gradient of water. If the

hydrodynamic uplift force grows to be the same as the vertical load, hydroplaning is said to have occurred (Browne, 1975).

Zone B: Transition Zone

It is also known as draping zone, as it begins when tire elements start to drape over the major asperities of pavement surface and still make contact with some minor asperities. Mixed lubrication mode exists in this zone, and it is a transition between Zone A and Zone C. Partial hydroplaning may still happen, even though the vehicle speed is not as high as that in total hydroplaning (Balmer and Gallaway, 1983).

Zone C: Traction Zone

This region is usually at the tail end of contact interface, where tire elements can attain an equilibrium position on pavement surface after draping. Boundary layer lubrication dominates in this situation, providing a well-developed friction capability by an intimate contact between tire tread and pavement surface. Both properties of contacting solids and characteristics of lubricant are important for the friction force development in this zone.

At a very low speed, only Zone C exists on a wet pavement and it governs the skid resistance performance. With an increase in vehicle speed, the areas of Zone A and Zone B get larger while that of Zone C is reduced. Upon hydroplaning, there is no contact, i.e. Zone C has completely disappeared.

2.1.3 Pavement Skid Resistance Measurement

The classical friction theories are insufficient to completely understand the mechanisms in wet-pavement skid resistance, therefore research efforts were made to better understand skid resistance phenomenon and evaluate the pavement frictional performance. Various measurement devices and methodologies have been developed and used around the world. Each was specially designed in particular aspects. In the United States, standard test methods have been established by the American Society

for Testing and Materials (ASTM, 2004; 2006; 2008a-b; 2009a-d; 2011a-b; 2012b; 2013b-c). Similar specifications have also been issued by organizations in other countries, such as the British Standards Institution (2000a-b; BSI, 2009).

The skid resistance measurement methods can be broadly classified into two groups: direct and indirect approaches. The direct method produces an output in the form of friction coefficient. Lock-wheel method (ASTM, 2011a), slip method (ASTM, 2011b), side-force method (ASTM, 2009b) and British pendulum tester (ASTM, 2013b) are all direct approaches. The indirect method typically measures texture property of a pavement surface and the friction parameters are then deduced through empirical correlations. Sand patch test (BSI, 2000b; ASTM, 2006) and sensor-measured texture depth (ASTM, 2009a; 2009c) are typical indirect measurements of skid resistance. The representative direct skid resistance measurement methods are introduced in the following sub-sections, which are further classified into laboratory measurements and in-situ measurements.

2.1.3.1 Laboratory Measurement of Skid Resistance

British pendulum tester (BPT, see Figure 2.3) is widely used to measure the skid resistance of pavement materials in the laboratory. The procedures of measuring pavement friction using BPT are specified by ASTM E303 standard (ASTM, 2013b). Skid resistance, related to the energy loss during rubber sliding on pavement surface, can be measured in BPT through the difference in pendulum height before and after the interactions between rubber slider and pavement sample (Henry, 2000). BPT can measure the friction level at very low speeds (about 10 km/h) and the resulted British pendulum number (BPN) is usually taken as an indicator of pavement microtexture. A disadvantage of BPT is that it can only evaluate the skid resistance of discrete locations at a single speed, and as such, no continuous measurement is available.

Dynamic friction tester (DFT, see Figure 2.4) was designed to measure the speed dependency of pavement friction (Saito et al., 1996). This test is standardized

in ASTM E1911 (ASTM, 2009d). DFT device consists of a horizontal spinning disk fitted with three spring loaded rubber sliders that contact the pavement surface as the disk rotational speed decreases due to friction. Water is applied to the tested surface. The torque generated by the friction force measured during the spin down is then used to calculate the friction as a function of speed.

Polished stone value (PSV) test (BSI, 2009) is usually employed to evaluate the long term frictional performance of pavements. An accelerated polishing machine (see Figure 2.5) is used to polish the samples before their friction properties are tested by the BPT. The experiment is designed to simulate the polishing effects of traffic on pavement surface materials and to estimate the friction losses due to traffic polishing.

2.1.3.2 Field Measurement of Skid Resistance

The laboratory tests commonly cannot measure high speed skid resistance using the real tires. Therefore, in-field measurements are developed to evaluate the actual friction experienced by vehicles. The field measurements of pavement skid resistance can be generally divided into four classifications: lock-wheel method, slip method, side-force method and stopping distance method. A major advantage of field tests is that the measurement can be conducted at highway operation speeds. The selection of different methods depends on the test purpose and availability of devices.

The lock-wheel skid resistance trailer (see Figure 2.6) is preferred for field measurement of skid resistance by most highway agencies in the U.S. due to its ability to define and control most operational variables (such as water application, tire type, inflation pressure and wheel load). Lock-wheel test represents a critical braking status and the skid resistance measured in this condition is the lowest in the normal tire slip range. Skid number (SN) can be determined from the test procedures specified in ASTM E274 (ASTM, 2011a). The tests can be conducted at various speeds to establish the relationship between skid resistance and sliding speed. A disadvantage of this method lies in its discontinuous piece-wise measurements, which

may overlook some localized low friction spots within a pavement section. Other lock-wheel devices used across the world include Stuttgarter Reibungsmesser, Skiddometer BV8 (Zoeppritz, 1977) and front locked wheel car (Albert and Walker, 1968).

Unlike the lock-wheel approach, slip method is used to measure the braking performance of vehicles with anti-lock systems. Its output is brake slip number (BSN), which depends on travel speed and slip ratio. Both fixed slip and variable slip devices have been developed. The Griptester (see Figure 2.7), available since 1987, is one of the most commonly-used fixed slip devices and its test procedure is specified in the BS 7941-2 standard (BSI, 2000a). ASTM E1859 (ASTM, 2011b) provides a friction evaluation method using the variable slip technique. Slip methods provide continuous measurement without the undue wear on tire. The tests can be used to determine peak braking force coefficient and the relationship between skid resistance and slip ratio.

The sideway-force coefficient (SFC) is defined as the ratio between sideway force (force perpendicular to tire plane, see Figure 2.8) and vertical load. It indicates the ability of pavement surface to keep a vehicle under control when it travels on a horizontal curve. SFC depends not only on vehicle speed, but also on yaw angle, the angle between tire plane and vehicle motion direction (see Figure 2.8). The use of Mu-Meter (see Figure 2.9) in measuring pavement sideway friction is specified by ASTM E670 (ASTM, 2009b). Another famous sideway-force device widely used in Europe is the Sideway-Force Coefficient Routine Investigation Machine (SCRIM, see Figure 2.10). It is specified as the standard device to be used in monitoring the in-service skid resistance of UK trunk roads for maintenance purpose (The Highways Agency, 2004). These devices make it possible to measure wet friction continuously over pavement sections, with a higher probability in detecting the locations with poor skid resistance performance.

Stopping distance method measures the distance required by a given vehicle traveling at a specific speed to stop completely on a wet pavement, usually with all

wheels locked. ASTM E445 (ASTM, 2013c) specifies the standard procedures for this approach. Coefficient of friction is expressed as a function of stopping distance, which is calculated from Equation (2.5) using the energy conservation principle.

$$f = V^2/(30D) \tag{2.5}$$

where f is the average coefficient of friction; V is the initial speed in mph; and D is the stopping distance in feet. Although this method provides an estimation of actual stopping distance on roads, it poses a hazard to both traffic operations and test driver.

All these skid resistance measurement methods have been widely used in pavement friction studies (Wu and Nagi, 1995; Henry, 2000; PIARC, 2005). Correctly selecting the appropriate method for a specific problem is crucial to the proper assessment of pavement frictional performance. The extensive research on skid resistance measurements have led to a comprehensive understanding on the mechanisms of wet-pavement skid resistance.

2.1.4 Factors Affecting Wet-Pavement Skid Resistance

Numerous experimental studies on wet-pavement skid resistance have been conducted globally using various measurement devices and techniques (Wu and Nagi, 1995; Henry, 2000; PIARC, 2005; Woodside and Woodward, 2002). The majority of these research studies focused on analyzing the factors affecting pavement skid resistance performance. For simplification, these factors are broadly classified into four groups: (a) pavement surface characteristics; (b) tire and vehicle properties; (c) presence of lubricant; and (d) environment factors. The following sub-sections shall discuss in detail the influences of the critical factors affecting skid resistance.

2.1.4.1 Pavement Surface Characteristics

Early experiments had emphasized the comparison between frictional performances of different pavement types, for example Moyer (1933) and Stinson and Roberts (1933). Either the towed trailer or the stopping distance method was used

in past experimental studies (Moyer, 1935; Martin, 1939; Michael and Grunau, 1956; Nichols et al., 1956; Clemmer, 1958; Wambold et al., 1986; Roe et al., 1998; Choubane et al., 2003). It was found that pavement surface characteristics have profound effects on its frictional performance. It includes both surface texture and deterioration. Pavement surface textures can be classified into microtexture, macrotexture, megatexture and unevenness based on their wavelengths (ISO, 1997b; PIARC, 1991). Microtexture and macrotexture (see Figure 2.11) are dominant factors in wet pavement skid resistance, while megatexture and unevenness result essentially in poor riding comfort (Wu and Nagi, 1995).

Microtexture

Microtexture refers to the irregularity measured on aggregate surface at micro scale, although the definition of its wavelength range is controversial among different standards (Forster, 1989; PIARC, 2005; ASTM, 2012b). Microtexture is a function of aggregate mineralogy under the conditions of weather, traffic and pavement aging (Kokkalis and Panagouli, 1998). It plays a fundamental role in the skid resistance by enhancing the adhesion effect. A harsh microtexture provides good friction condition, while a polished microtexture commonly gives poor frictional performance even at low speeds (Leland and Taylor, 1965). The mechanisms of microtexture effect are complex because it affects the molecular and electrical interaction between tire and pavement surface (Kummer, 1966). However, it is understood that the microtexture contributes to skid resistance at all speeds and in both dry and wet conditions.

Macrotexture

Macrotexture refers to the irregularity on pavement surface measured in the scale of millimeter, which is usually visible to naked eyes. It is determined by the mixture design, attributed to aggregate size, shape, angularity, spacing and gradation. The main function of macrotexture in skid resistance is to provide necessary surface

drainage to help dispel the water at tire-pavement interface (Martin, 1939; Giles, 1963). It also contributes to skid resistance by inducing deformations on tire tread to produce more hysteresis losses. Rougher macrotexture can make the decline of tire-pavement friction with increasing speed less rapid (see Figure 2.12), so that good skid resistance is maintained at high speed (Sabey, 1966; Highway Research Board, 1972).

Roughness

Pavement roughness, considered to be 50 mm and larger, covers the range of both megatexture (50 to 500 mm) and unevenness (0.5 to 50 m). It affects vehicle dynamics, ride quality, dynamic loading, and drainage (Wu and Nagi, 1995). Studies on traffic safety have noted that multiple-vehicle accidents increase as pavement roughness increases (Al-Masaeid, 1997; Cenek et al., 2004). It was also found that the dynamic changes in normal load with variable pavement roughness may result in skid resistance reductions. A recent experimental study conducted by Fuentes et al. (2010) presented a significantly lower skid resistance on relatively rougher pavement section even though the microtexture and macrotexture were similar. Further analysis showed that dynamic load coefficient (the ratio between standard deviation of dynamic load variation and static normal load) is more appropriate than international roughness index to represent the effect of roughness on skid resistance.

Pavement Deterioration

Most surface distresses not only affect the structural capacity of pavement but also can affect traveling safety. Aggregate polishing directly reduces pavement microtexture and surface wear reduces its macrotexture. Therefore, skid resistance diminishes at all travel speeds as a result of traffic polishing (Gandhi et al., 1991). Bleeding occurs at high temperatures on bituminous pavements due to the excess asphalt. It reduces both macrotexture and microtexture, resulting in a lower skid resistance as well as higher hydroplaning risk. Rutting and pothole collect rainwater

to form thicker water films locally. This excess water may lead to hydroplaning and low skid resistance, as well as splash and spray.

2.1.4.2 Tire Properties and Vehicle Operation Condition

Tire properties and vehicle operation condition were found to significantly affect frictional performance. Patterned tire tread is an effective measure to discharge water from the contact patch, especially on the smooth pavements with poor macrotexture (Giles and Lander, 1956; Marick, 1959; Gengenback, 1968; Lander and Williams, 1968). Sufficient tread depth is required by legal provisions in many countries, such as a minimum tread depth of 1.6 mm specified in UK, and 4 mm in Germany (Woodside and Woodward, 2002). On wet pavements, worn tires cannot provide enough drainage capacity through their treads and may pose serious hazards to drivers and passengers. All the geometric features of tread pattern, such as groove depth, groove width and rib dimension, affect the frictional performance (Marick, 1959; Maycock, 1967; Kelly, 1968). Moreover, Williams and Meades (1975) and Dijks (1976) reported that truck tires normally provide remarkably lower skid resistance than passenger car tires.

Vehicle speed is another important factor known to affect wet-pavement skid resistance. It was reported that most of the wet-skid accidents happens at high speeds (Wambold et al., 1986). As shown in Figure 2.13, skid resistance decreases with an increase in vehicle speed on wet pavements. The early Iowa study (Moyer, 1933), the study at Michigan State University (Mercer, 1958) and the NACA study (Trant, 1959) all provided consistent observations with regard to the speed dependency of skid resistance on wet pavement surfaces.

According to Kummer and Meyer (1967), vehicle tires may be in one of the following three operation modes when running on the roads: skidding, slipping or rolling. The wheel slip condition, including slip ratio and slip angle, was also found to be influential on skid resistance (Moyer, 1933). The slip ratio (S) is defined as:

$$S = 100(\omega - \omega_t)/\omega \tag{2.6}$$

where ω is the angular velocity of a rolling tire corresponding to the travel speed and ω_t is the angular velocity of a slipping tire. As shown in Figure 2.14, the coefficient of friction grows initially with an increase of slip ratio until the peak value at critical slip and decreases afterwards until a lower value at locked wheel condition, namely 100% slip (Wu and Nagi, 1995). The critical slip ratio was reported to be between 7% and 25% slip (Trant, 1959; Holmes, 1970) and can vary with speeds. A similar trend was found with an increase in slip angle, which is defined as the angle between the tire plane and the forward direction of vehicle motion (Gillespie, 1992).

2.1.4.3 Presence of Lubricant

Dry-pavement friction is commonly sufficient and hardly speed-dependent. Moyer (1963) suggested a skid number of 80 ± 10 for the typical dry tire-pavement interfaces. However, significant reductions in skid resistance occur once contaminant such as water or oil is present on pavement surface (Moyer, 1933; Staughton and Williams, 1970; Delanne and Gothie, 2005). It is noticed that even a very thin film of water can cause a remarkable decrease in skid resistance, especially on surfaces with poor microtexture (Leland et al., 1968). As shown in Figure 2.13, at the same travel speed, a thicker water film will cause a greater decrease in skid resistance (Trant, 1959; Benedetto, 2002). Studies (Pelloli, 1976; Balmer and Gallaway, 1983; Veith, 1983) also found that the effect of water depth is more obvious at higher speed. Staughton and Williams (1970) indicated that the influence of water depth on the reduction rate of skid resistance was significant in the first 4 mm water film thickness.

2.1.4.4 Environment Factors

Temperature and precipitation are two major environment factors affecting short-term skid resistance performance. Generally, with all the other variables being equal, a lower skid resistance can be expected at a higher temperature. Changes in

water and asphalt viscosities were suggested by Moyer (1959) as the main reason of decreasing friction with the increasing temperature. Another possible cause may be the lower hysteresis loss in a rubber tire at higher temperature (Giles and Sabey, 1959). Studies on precipitation-related variations of pavement friction indicated that the wet-pavement skid resistance is a bit lower after a dry period and higher after a rainstorm (Barry and Henry, 1981; Saito and Henry, 1983). The accumulation of dust and debris within pavement surface texture is believed to be the reason for such precipitation-related variations.

Pavement skid resistance has been found to vary with season as well. Studies showed that, on the same pavement section, a higher friction level can be expected in winter and spring, while a lower level in summer and autumn (Giles and Sabey, 1959; Burchett and Rizenbergs, 1980; Kulakowski et al., 1990). The varying range can be as large as 25% across seasons (Gargett, 1990; Jayawickrama and Thomas, 1998). Temperature and precipitation are believed to be two important reasons for the seasonal variations in skid resistance (Burchett and Rizenbergs, 1980). It was also observed that pavement microtexture is harsher in winter, providing higher adhesion effect in tire-pavement interaction (The Highways Agency, 2004).

Other influencing factors on wet-pavement skid resistance found in the past experimental studies include tire pressure (Moyer, 1933; Gengenback, 1968), wheel load (Stinson and Roberts, 1933; Giles, 1963) and aggregate property (Nichols et al., 1956; Stutzenberger and Havens, 1958; White, 1958). Quantitative analysis of various influencing factors have provided researchers and engineers the intuitive knowledge on wet-pavement skid resistance and made further understanding of its mechanisms possible. However, most of the previously discussed experiments were performed on conventional pavements. Although similar principles are applicable on porous pavements, there will be more influencing factors affecting porous pavement skid resistance.

2.1.5 Skid Resistance on Porous Pavements

From past research on wet-pavement skid resistance, pavement surface macrotexture has consistently been identified to be critical to the frictional performance at high speed (Highway Research Board, 1972). It governs the drainage capacity of pavement surfaces under a skidding tire. Various engineering measures have been developed to enhance the macrotexture and drainage capacity of pavement surface. This includes tining, grooving, chip seal and porous friction course. Porous pavement, whose high porosity facilitates the drainage of water from tire-pavement interface, is found to be effective in improving pavement skid resistance performance in wet weather (FHWA, 1998).

Porous pavement applications in the U.S. primarily attempt to reduce road accidents in wet weather. Numerous comparison studies have shown the superiority of porous pavements in skid resistance. Moyer (1959) conducted experiments on over 300 pavement sections in California and compared the friction levels of open-graded asphalt surfaces to those of dense-graded asphalt surfaces. It was found that open-graded mixtures had a skid resistance level 10% to 20% higher than that of dense-graded asphalt. In another experimental study sponsored by the Federal Highway Administration, 45 in-service pavement sections with various surface types were tested (Page, 1977). It was found that open-graded asphalt pavements performed better in skid resistance than other pavement types under heavy or medium traffic conditions. Dynamic friction tester was used in a field evaluation in the State of Indiana (McDaniel et al., 2004) to compare the wet frictional performances among porous friction course (PFC), stone matrix asphalt (SMA) and conventional hot mix asphalt (HMA). It was observed that the average DFT value of SMA was lower than that of PFC or HMA, and the higher friction of PFC might have resulted from its higher macrotexture. Furthermore, the long-term frictional performance of Indiana PFC pavements was monitored as well (Kowalski et al., 2009). Both DFT and lock-

wheel trailer were used in the measurements. It was found that the long-term skid resistance performance of PFC was much better than that of conventional HMA. Superior skid resistance on porous pavements was also widely observed in other research studies, such as the FHWA demonstration project "Improved Skid Resistant Pavements" (Pelletier, 1976), the performance evaluation of open-graded asphalt pavements in Oregon (Huddleston et al., 1991), the experiments in Arizona using mu-meters (Hossain et al., 1992), the studies on pavement surface characteristics at Virginia Smart Road (Davis, 2001) , the development of functionally optimized PFC (McGhee et al., 2009) and the application of thin-lift asphalt surface courses in New Jersey (Bennert et al., 2005).

Besides the higher skid resistance at specific speeds, another benefit porous pavements can provide to the road users is the relatively speed-independent frictional performance. Porous pavements were involved in the study of skid number-speed gradients in Colorado (Steere, 1976). The test results provided solid evidences of a significantly less degree of skid resistance deterioration with increasing travel speed on Colorado Type-A open graded plant mix seal coats. Gallaway et al. (1979) found that skid resistance performance of open-graded friction courses was less sensitive to vehicle speed when compared to lightweight aggregate slurry seal and longitudinal grooved concrete pavements. Lock-wheel trailer was used in Florida to measure skid resistance on various types of pavements at different speeds (Page, 1993). The results showed that frictional characteristics remained relatively stable with speed variation on open graded friction courses (OGFC). Friction tests performed by Younger et al. (1994) evaluated the performance of porous pavements used in Oregon and found that the wet friction numbers of porous pavements were retained better at higher speeds than those on conventional dense-graded pavements.

Isenring et al. (1990) also studied the skid resistance variation with vehicle speed on porous pavements in Switzerland, measuring pavement friction properties by Skiddometer BV8. Both lock-wheel and brake-wheel (with a 14% slip ratio) tests

were conducted using a ribbed PIARC skid test tire. Several useful conclusions were drawn from this study: (a) friction values of porous asphalt pavements are hardly speed dependent; (b) skidding properties of porous asphalt is poorer than that of conventional mixtures at lower speeds, where microtexture is more relevant and the function of macrotexture is insignificant; (c) at higher speed, skid resistance of porous pavement is generally higher compared to that of dense-graded surface, due to its higher macrotexture. Although lesser speed dependency was observed in the porous pavement skid resistance when compared to that on conventional pavement, the friction values do decrease with the increase of vehicle speed (McDaniel et al., 2004).

With the consensus that porous pavements are capable to maintain a superior wet skid resistance at high speeds, research efforts were made to relate the frictional performance to various influencing factors. Correlation between British pendulum number and skid trailer measurement on open-graded course was proposed by Mullen (1972) in his research to predict field skid numbers using laboratory test BPN results. It was found that the relationship between SN and BPN of porous pavement was different from that of dense-graded mixture. Seasonal variation of skid resistance on open-graded asphalt pavements was studied using the lock-wheel method in Pennsylvania (Dahir et al., 1979) and a model involving season and weather effects was proposed. Variables considered in this model include rainfall during the previous week, tire and pavement temperature, time in a year and polishing susceptibility and polishing rate of aggregates. McDaniel et al. (2004) indicated that the superior skid resistance of porous friction course may be a result from its higher mean profile depth (MPD), which is an indicator of surface macrotexture level. However, Jackson et al. (2005) showed that there was no clear relationship between MPD and friction number, and macrotexture alone was not a good predictor for overall friction property. It was also found that aggregate gradation has a significant influence on wet skid resistance performance of porous pavements (Xing et al., 2010).

A major adverse effect of porous surface on skid resistance identified from past studies is that a potential skidding hazard may exist on a porous pavement when it is opened to traffic immediately after construction (Younger et al., 1994; Liu et al., 2010; McGhee and Clark, 2010). The lock-wheel test results from the experiments conducted by Isenring et al. (1990) clearly showed that the skid resistance on porous asphalt was relatively lower in the initial stage after construction and increased after the first winter. The generally poorer microtexture and thicker bitumen film on newly laid porous asphalt surfaces were believed to be the causes of such a phenomenon. A Dutch study by Deuss (1994) showed a 25% to 30% lower skid resistance on new porous pavements as compared to new dense-graded pavements . However, friction properties would improve after a certain time range (which can be from weeks to months, depending on the traffic condition) when the binder coating on pavement surface has worn off. These studies also suggested that aggregates with high anti-polish properties and good angular shapes should be used in porous asphalt to provide satisfactory microtexture and macrotexture.

Besides the above mentioned research studies, numerous studies on skid resistance on porous pavements were perfomed in other countries, such as Canada (Ryell et al., 1979), Japan (Yoshiki et al., 2005) and Spain (Miró et al., 2009). Moreover, the application of porous surfaces to enhance skid resistance has been studied on runways (Brownie, 1977) and bridge deck pavements (Brewer, 1971). Although the aspect of porous pavement skid resistance had been studied in past research, applications in the field are still experience-based. There is still a lack of understanding in porous pavement skid resistance mechanisms and how factors can influence skid resistance on porous pavement. This posts difficulties in the efficient design, construction and maintenance of porous pavements and hence limits their applications.

2.1.6 Existing Models for Skid Resistance

Pavement surface characteristics and vehicle operation conditions have been identified as critical factors influencing wet-pavement skid resistance. It is necessary to establish quantitative relationships between skid resistance indices and potential influencing factors so that skid resistance mechanisms can be better understood and pavement frictional performance can be predicted. This is important for both pavement construction and maintenance. Although tire-pavement friction in dry condition has been theoretically studied, fundamental theories describing the physics of tire-water-pavement interaction are still not available to date. The existing skid resistance models can be broadly classified into two categories: empirical approaches and mechanistic methods. The former involves conducting experiments and deriving regression equations to relate skid resistance indices with measurable parameters. The latter relies on finite element method to numerically reproduce the phenomenon. The developments in these two approaches are reviewed in this section, with emphasis being placed on recent progresses.

2.1.6.1 Empirical Models for Skid Resistance

Past researchers had developed empirical relationships to describe the skid resistance performance using some pavement-related factors (Henry, 1986; Meyer 1991; Rezaei et al., 2011). Surface microtexture and macrotexture were identified as two of the most crucial parameters affecting skid resistance. The variations in skid resistance with vehicle sliding speed has been considered in the literature because of the fact that most wet-weather traffic accidents were a result of insufficient skid resistance during high-speed travel. Skid numbers at different speeds can be predicted considering aggregate properties and gradation.

Henry (1986) proposed a regression equation to estimate skid number at 40 mph using the British pendulum number (*BPN*) and mean texture depth (*MTD*) measured on a pavement surface. The linear relationship was presented as:

$$SN_{40} = 0.884 \cdot BPN + 5.16 \cdot MTD - 17.8 \qquad (R^2 = 0.86) \tag{2.7}$$

where *BPN* and *MTD* could be measured following the specifications ASTM E303 (ASTM, 2013b) and ASTM E965 (ASTM, 2006), respectively. Both variables are easy to obtain using portable apparatus. Since *BPN* is normally used as a surrogate microtexture parameter and *MTD* is an alternative measure of the macrotexture, this simple relationship reveals the fact that the skid number at a given speed is closely related to the microtexture and macrotexture of a pavement surface. However, the effect of sliding speed is not included in this model, which cause it fail to predict the skid number at speeds other than 40 mph.

Taking speed variation into consideration, Kulakowski and Meyer (1989) proposed an improved model for skid number at any speed *v* (SN_v):

$$SN_v = SN_0 \cdot e^{-(v/v_0)} \tag{2.8}$$

where SN_0 is the intercept at zero speed, which is an indication of low speed frictional performance. It is seen as a microtexture parameter and is found to be well correlated to the *BPN* measurement by the following equation (Henry and Meyer, 1983):

$$SN_0 = 1.32 \cdot BPN - 34.9 \qquad (R^2 = 0.95) \tag{2.9}$$

v_0 is a speed constant which can be calculated by solving Equation (2.10) if the ribbed tire skidding tests are carried out at two speed v_1 and v_2.

$$v_0 = \frac{v_1 - v_2}{\ln\left(\frac{SN_{v_1}}{SN_{v_2}}\right)} \tag{2.10}$$

This model assumes a simple relationship between the skid number and sliding speed. However, the influence of pavement macrotexture on skid resistance is eliminated by the simple speed constant. Besides, in-field skid resistance tests have to be conducted in order to derive the speed constant before the model can be applied.

To overcome these limitations, Meyer (1991) introduced the concept of *PNG* to improve the empirical model between skid number and vehicle speed:

$$SN_v = SN_0 \cdot e^{-(PNG/100)\cdot v} \tag{2.11}$$

$$PNG = 100 \cdot \left(\frac{d(SN_v)/dv}{SN_v} \right) \tag{2.12}$$

where *PNG* is the percentage normalized gradient of the *SN* versus *v* curve. It actually describes the rate at which the skid number decreases with the sliding speed, and it is found to be closely related to the pavement macrotexture by a non-linear relationship (Henry and Meyer, 1983):

$$PNG = 0.45 \cdot MTD^{-0.47} \qquad (R^2 = 0.96) \tag{2.13}$$

This model is widely used because it involves both the microtexture and macrotexture of pavement surface and is able to predict the skid number at any speed. Many other studies were conducted to develop various models in estimating SN_0 and *PNG*, then use Equation (2.11) to predict SN_v. Despite its successful applications, Meyer's model is feasible only after the construction of pavements, when the in-situ measurements of surface textures are available. This model is more useful in pavement maintenance, but may get less effective in the design phase of pavement mixture.

Recognizing that microtexture of an in-service pavement is decided by the texture of aggregates and its macrotexture depends on the gradation and angularity of aggregates, Rezaei et al. (2011) developed a skid resistance prediction model based on aggregate property and gradation. The aggregate gradation is accounted for by a cumulative two-parameter Weibull distribution. The texture on aggregate surface before and after polishing is obtained by using the aggregate imaging system (Masad et al., 2005). Based on laboratory experiments, the initial aggregate texture ($a_{agg}+b_{agg}$) and the rate of change in aggregate texture (c_{agg}) is derived by:

$$a_{agg} + b_{agg} = 0.9848 \cdot T_{BMD} + 3.1735 \tag{2.14}$$

$$c_{agg} = 0.0217 \cdot ARI^{-0.13/TL} \tag{2.15}$$

$$ARI = \frac{\left(T_{AMD}/T_{BMD}\right)^2}{1-\left(T_{AMD}/T_{BMD}\right)^2} \tag{2.16}$$

$$TL = \frac{T_{BMD} - T_{AMD}}{T_{BMD}} \tag{2.17}$$

where T_{BMD} is the texture before micro-Deval, T_{AMD} is the texture after micro-Deval, *ARI* is the aggregate roughness index, and *TL* is the texture loss. Taking advantage of the concept of international friction index (IFI), the initial IFI value (a_{mix}+b_{mix}), the terminal IFI value (a_{mix}) and the rate of change in the IFI for the mixture (c_{mix}) could be regressed by:

$$a_{mix} + b_{mix} = 0.4984 \cdot \ln[5.656\times10^{-4}\left(a_{agg} + b_{agg}\right) + 5.846\times10^{-2}\lambda - 4.985\times10^{-2}\kappa] + 0.8619 \tag{2.18}$$

$$a_{mix} = \frac{18.422 + \lambda}{118.936 - 0.0013 \cdot AMD^2} \tag{2.19}$$

$$c_{mix} = 0.765 \cdot e^{\left(-7.297\times10^{-2}/c_{agg}\right)} \tag{2.20}$$

where λ and κ are the two variables in Weibull distribution, known as scale and shape parameters. With the initial and terminal IFI values and the rate of change known, the IFI at a given polishing cycles can be calculated by:

$$IFI(N) = a_{mix} + b_{mix} \cdot e^{-c_{mix} \cdot N} \tag{2.21}$$

where *N* is the increments of 1,000 polishing cycles conducted by the National Center of Asphalt Technology (NCAT) polisher on the compacted slab. It could be related to the traffic multiplication factor (TMF) by:

$$TMF = \frac{35,600}{1+15.96 \cdot e^{-4.78\times10^{-2} \cdot N}} \tag{2.22}$$

Closely related to aggregate gradation, the mean profile depth (MPD) of a pavement surface can be estimated from the two variables in Weibull distribution:

$$MPD = 1.8 - \frac{3.041}{\lambda} - \frac{0.382}{\kappa^2} \tag{2.23}$$

Once the *IFI* and *MPD* are determined, the skid number at 50 km/h (SN_{50}) can then be derived from a modified PIARC relationship:

$$SN_{50} = 5.135 + 128.486 \cdot (IFI - 0.045) e^{-20/S_p} \quad (2.24)$$

$$S_p = 14.2 + 89.7 MPD \quad (2.25)$$

This model could be used to decide the desired aggregate properties and gradation in the design process of pavement mixture. It does not consider the influence of binder content and property on pavement textures and skid resistance. The prediction of *IFI* from aggregate tests and the estimation of *SN* from *IFI* and *MPD* in Rezaei et al.'s work are not based on the same set of data, raising concerns in the model feasibility.

A commonality of empirical models is that skid resistance at a specific speed (in terms of SN_v) is related to the microtexture of pavement surface, while the varying rate of skid number with sliding speed is thought to be a function of macrotexture. It is noted that all these equations attempt to interpret experimental observations through regression approaches with limited sample sizes. Although they are able to give some basic trends on pavement skid resistance performance, no mechanistic understandings or scientific explanations are provided. Besides, empirical models are developed under specific conditions (such as materials and environment) which may restrict the application of such models when attempting to apply them in a different situation. Moreover, empirical models are usually less accurate when used on a pavement surface type different from the ones where the models are generated. Therefore, most empirical models developed from non-porous pavements are not applicable for porous pavements.

2.1.6.2 Numerical Models for Skid Resistance

Although empirical models can roughly estimate pavement skid resistance, more advanced numerical models are needed to understand the mechanisms. Numerical models make in-depth skid resistance analysis possible because of their

mechanistic formulations. They are more feasible and flexible to be used on different pavement types, tire characteristics and operation conditions. The finite element method (FEM) is one of the most popular numerical approaches in modeling the dry and wet tire-pavement interactions, especially the frictional effects and skid resistance. In the early days, in-house codes such as NOSAP (Bathe and Wilson, 1973) and AGGIE (Haisler, 1977) were developed to simulate rubber behaviors, but they were powerless in formulating and resolving the whole tire reactions on rough pavements. Recent developments in FEM algorithms allow a more comprehensive and detailed analysis on the frictional contact between tire and pavement surface. More powerful commercial software have been developed and widely used in both tire and pavement researches. ANSYS, ADINA, ABAQUS and NASTRAN are some popular ones that have been used in the literature (Ong and Fwa, 2007a; Jeong and Jeong, 2013).

Behaviors of a rolling or sliding tire on a smooth pavement in dry conditions and its response to friction effects have been modelled in past studies (Tanner, 1996; Johnson et al., 1999; Meng, 2002; Sextro, 2007). The primary purposes of these studies were to allow for the optimum design of pneumatic tire and selection of tire materials. Few efforts were made on exploring skid resistance mechanisms and optimizing pavement surface characteristics. On the other hand, some studies analyzed pavement responses under static or dynamic loads (Al-Qadi et al., 2004; Pelletier et al., 2007; Ayadi et al., 2012), focusing on the stresses and strains developed within pavement materials. A simplified tire or idealized load was usually used in such models. Although complex constitutive pavement material models were adopted, the unrealistic loading condition and contact consideration during modeling render these models infeasible for skid resistance analysis.

Recognizing the fact that pavement surface characteristics have a significant effect on its skid resistance performance, Liu et al. (2003) developed a 3D finite element model simulating the British pendulum test. Load was applied through several beam elements and a spring element. Input with a frictional parameter

measured in the laboratory, the FEM model can provide simulation results with good agreements with experiments. This model was used to analyze the skid resistance of various texture patterns and pavement materials (Liu, 2004). It provided fundamental understandings on the influence of pavement surface texture on the frictional property. However, the model was found inapplicable on complex surface with non-symmetric macrotexture because it suffered excessive distortion in such cases (Lee, 2005). Since lubrication theories are not involved, the model didn't make much improvement in the understanding of wet-pavement skid resistance. Moreover, it does not simulate the realistic scenario of a vehicle tire skidding on a pavement surface at a traveling speed, which may experience different friction mechanisms.

A complete tire-water-pavement interaction was reproduced in the numerical model developed by Ong and Fwa (2007a). This model has been used in prediction of wet skid resistance and hydroplaning potential on smooth pavements, providing more in-depth understandings in the mechanisms. It was developed based on fundamental structural mechanics and fluid dynamics theories, with consideration in tire-pavement contact and fluid-structure interaction. The simulated skid resistance results from this numerical model was validated against published experimental data. The influences of various factors on skid resistance have been studied in their practical ranges. The skid resistance, denoted by *SN*, was found to be most influenced by vehicle speed, followed by water film thickness and wheel load, and least affected by tire inflation pressure. It was noted that the influence of each factor is much more remarkable at higher speeds than at relatively lower speeds. More analyses were conducted on the forces contributing to skid resistance and tire-pavement contact area (Fwa and Ong, 2008). Simulation results indicated that the traction force at tire-pavement interface decreases when sliding speed increases, as a result of which, the total skid resistance gets lower and lower with the increase of vehicle speed. Traction force was found to be the dominant contributor to skid resistance in most of the speed range. The model explicitly presented tire deformations and the variations in tire-pavement contact area

with the increase of speed. The process depicted by the model is quite similar to the conceptual skid resistance theory proposed by Veith (1983), demonstrating the model capability in mechanism interpretations. Despite of its completeness in replicating the practical problem, this initial model was designed only for the standard test tire and a smooth pavement. The variation in pavement textures and tire characteristics is not involved, so their influences on skid resistance are beyond the ability of this model.

To enhance the feasibility, analogous modeling techniques were extended to commercial truck tires (Ong and Fwa, 2010). The model was validated against past experimental data and various factors affecting truck skid resistance were analyzed. Special attentions were paid to the different skidding behaviors between unloaded and fully loaded trucks. The simulation results provided an engineering explanation to the higher skidding accident propensity of unloaded trucks. Moreover, it was found that tire inflation pressure, water film thickness and vehicle speed significantly affect the truck skid resistance as well. More extensions and modifications have been made on the model for ribbed tires (Srirangam, 2009; Cao, 2010), aircraft tires (Pasindu, 2011) and grooved pavements (Anupam, 2011). With broad applications in different tire-pavement combinations, a shortcoming in water depth control was observed for these models. An arbitrary Langrangian-Eulerian (ALE) formulation was adopt to handle the mesh deformation, which forces the geometry of fluid model deform with the tire tread. This makes it difficult to set the water film thickness to a specific value and may create errors during model calibration. Moreover, the simulation may become computationally intensive in the case of extremely thin water film and its numerical accuracy may deteriorate.

In order to provide a more accurate estimation of skid number for the thin water film scenario with a reasonable computational cost, Jeong and Jeong (2013) proposed a hybrid approach to integrate empirical formulations into the numerical analysis. The full numerical simulations of tire-water-pavement interaction were first performed for various thick water cases. An exponential relationship between fluid

uplift force and water film thickness was developed from the simulation results. The uplift force in thin water case was then extrapolated using the exponential function. The same approach was used to derive the traction force and drag force on tire tread under thin water film situations. This approach has been applied in the analysis of standard lock-wheel tests, and was found to reduce analysis time significantly. However, the empirical relationship used to connect the thin water film cases with the thick water film cases has little theoretical basis. Besides, the mechanisms of thin-water skid resistance phenomenon cannot be investigated using this method because water was never simulated in their model.

Numerical models possess a common advantage of mechanically describing interactions between tire and water, as well as between tire and pavement surface. They are able to reproduce the wet skidding phenomenon to some extent and partially explain its mechanisms. However, the existing full tire-water-pavement interaction models only consider dense-smooth pavements or grooved surfaces. Water is not allowed to penetrate into pavement surface layer. Therefore, they are not adequate in simulating the skid resistance on porous pavements, and cannot be used to analyze the influences of porous layer parameters on its skid resistance performance. To date, there is still no numerical model available to appropriately estimate the skid number presented by a porous pavement. This limits the understanding in the mechanisms causing skid resistance enhancement on porous pavements and restricts the functional design of porous surfaces.

2.2 Tire/Road Noise

Road traffic noise is one of the major contributors to the increasing noise pollutions in urban regions today. It is estimated to dominate more than 70% of the environmental noise (Newton et al., 2001). Traffic noise annoys people, disturbs sleep, causes stresses and diseases, and disrupts daily activities. Boer and Schroten (2007) reported that 44% of European population were regularly exposed to a road

traffic noise of over 55 dB - a level may bring negative health effects, with a social cost of €40 billion per year (about 0.4% of total annual gross domestic product). Road traffic noise is the accumulation of noise emissions from all vehicles in traffic stream. The main noise sources on an individual vehicle can be broadly classified into two groups, namely propulsion noise and tire/road noise. As a result of the significant reduction in power train noise brought forth by the rapid development of auto industry, the main noise source on a vehicle traveling at high speed turns to be the one generated from tire-pavement interaction. The contribution of tire/road noise takes over that of power unit noise when vehicle speed is higher than a cross-over speed (see Figure 2.15). It is indicated that tire/road noise dominates traffic noise at speeds above 40 km/h for passenger cars and 60 km/h for trucks (Sandberg and Ejsmont, 2002). Tire noise reduction is crucial in the abatement of traffic noise near high-speed facilities.

The optimization of pavement surface properties plays an essential role in the tire/road noise reduction. Numerous research works have been conducted on tire/road noise in past decades, most of which were experiment-based. This section provides an extensive literature review on tire/road noise. A general overview on the phenomenon of tire/road noise is first presented, followed by a discussion in its generation and amplification mechanisms. Various measurement approaches used in experimental studies are next introduced. Then the critical influencing factors and their effects are discussed, with emphasis placed on the tire/road noise reduction on porous pavements. The existing tire/road noise models are illustrated in the last part of this section.

2.2.1 Overview of Tire/Road Noise

Tire/road noise generally refers to the noise emission resulting from tire-pavement interaction, when a vehicle travels over a road surface. It includes both structural and air-borne noise. Research studies on tire/road noise have been carried out experimentally and analytically since the early 1970s (Dare, 2012). By the early

1980s, it has been recognized that without reduction in tire/road noise, overall traffic noise could not be appreciably controlled (Sandberg, 1982). Gibbs et al. (2005) studied the composition of traffic noise and indicated that tire/road noise represents 75% to 90% of the total noise generated by passenger vehicles. Tire/road noise could also be a significant amount in the noise generated by trucks. The domination of tire/road noise in overall traffic noise is significant at high speeds. The relative contributions of propulsion noise and tire/road noise to the overall traffic noise level were analyzed using the European Harmonoise/IMAGINE traffic noise model (Peeters and van Blokland, 2007). It was found that for passenger cars and car-based vans, tire/road noise contributes about 60% of the acoustic output at 40 km/h, compared to about 80% at 100 km/h.

Many developed countries have introduced regulations on the noise emission control of road vehicles. Tire/road noise has been identified as a transportation noise component which needs most urgent reduction by several major international policies, such as the green paper "Future Noise Policy" from the European Commission (EU, 1996). Following this, the legal limits regarding noise emission from tires have been established by European Union (EU) and United Nations Economic Commission for Europe (UNECE). EU also implemented another environmental noise directive requesting its members to map noise contours along all existing roadways and adopt actions to address problems identified in the noise map (Gibbs et al., 2005). Sandberg (2001) analyzed the effectiveness of vehicle noise regulations in some countries and found that tire/road noise must be substantially reduced to make the regulations effective. It was also highlighted that pavement surface should be subject to noise limitations as well, considering its role in exciting tire/road noise emission.

A large amount of research studies were made to improve acoustic properties of tires, but results turned out to be not very encouraging. Sandberg (1984) compared the noise emissions of several vehicles and tires manufactured in the time period 1920-1982 by coast-by and pass-by tests. The results showed that tire noise

performance was approximately the same over the 60 years studied. Study conducted by Berge (1996) showed that two modern tires were approximately 7 dB(A) noisier at 80 km/h than the noise level predicted by the Nordic traffic noise model, which was developed from hundreds of measurements made in 1974. In the recent decade, tires were claimed quieter by manufacturers, but the effects were not studied extensively and rigorously. This is probably because that the improvement in tire acoustical property is offset by the growths in tire width and vehicle speed on road networks. A consistent conclusion drawn from existing evidences is the fact that tire/road noise reduction cannot solely rely on tire technologies. Innovative pavement technologies should be developed to universally reduce noise emissions from all tires. The concept of "low noise road surface" was proposed and is defined as a road surface that causes at least 3 dB(A) lower vehicle noise than that obtained on conventional and "most common" road surfaces (Sandberg and Ejsmont, 2002). Understanding the generation/amplification mechanisms of tire/road noise is essential to the development of low noise surfaces.

2.2.2 Generation and Amplification Mechanisms of Tire/Road Noise

The mechanisms of tire/road noise have been explored for decades. Various research studies identified an extremely complicated mix of tire/road noise mechanisms (Sandberg and Ejsmont, 2002). The main distinct mechanisms identified from previous studies are listed in Table 2.1. There is generally no disagreement on the existence of such mechanisms, although the relative importance of their contributions is disputable. It is important to note that the term “tire/road noise mechanisms” is rather wide to cover the phenomena related to both the generation and propagation of noise. The noise generation mechanisms mainly include impact-induced vibration, friction/adhesion-induced vibration and air pumping effect, while the noise amplification mechanisms involve horn effect and acoustic resonance. The relative contributions among these mechanisms may vary depending on tire types,

pavement surfaces and operating conditions. This section briefly reviews the major mechanisms and provides some fundamentals on tire/road noise.

2.2.2.1 Impact-Induced Vibration

The structure-borne noise in tire-pavement interaction comes from tire vibrations. The main mechanism responsible for inducing vibrations in tire walls is the sudden displacement of a tread element, in relation to its "rest position" in a rotating tire, when it impacts the road surface (Sandberg and Ejsmont, 2002). At the leading edge, tread element is pushed in and at the trailing edge it is pressed out. These vibrations radiate sound at frequencies generally below 1000 Hz (Descornet and Sandberg, 1980; Nilsson et al., 1980), and radiation is concentrated at the area around contact patch (Kuijpers and van Blokland, 2001; Yum et al., 2006) due to the damping of tire carcass. A rotating tire will be subjected to deflection around its circumference even if the tire and pavement are smooth. The existence of separated tread elements causes a disruption to the smooth displacement at the contact patch edges, leading to a "tread impact" mechanism. On the other hand, pavement surface texture, especially the macrotexture, also applies impacting on the tire tread with an equal importance, which could be named "texture impact". It was highlighted by Sandberg and Ejsmont (2002) that impacts on tire tread by pavement texture or tread elements create substantial vibrations, emitting much higher noise than the case with smooth tire tread and smooth road surface.

The impact-induced vibrations contain both radial and tangential components (Larsson et al., 1999). In the case of "texture impact" (see Figure 2.16), the tire tread is displaced by an asperity at a certain angle relative to the road surface. The impact force is therefore neither perpendicular to the road nor radial to the tire. Similarly, tire tread is displaced both radically and tangentially for the "tread impact" as well. The relative magnitude of each component depends on the texture level, tread pattern and tire radius, while the frequency depending on the distance between tread elements or

texture asperities and the vehicle speed. In the direction perpendicular to tire middle plane, literal vibration also happens when tread and pavement texture are not uniform in the literal direction, but it is much lower than those in other directions (Bergmann, 1980; Dugan and Burroughs, 2003). It was found that differentiating pavement textures in the literal direction may be unnecessary in the tire/road noise modeling (Hamet and Klein, 2000; Wullens et al., 2004).

Besides tire tread, tire sidewalls also vibrate and radiate noise (Nelson, 1986; Ruhala and Burroughs, 2008). Sidewall vibrations were found to be critical in the 500-1000 Hz frequency range (Donavan and Oswald, 1980; Eberhardt, 1984) and most significant near the trailing edge of contact patch (Phillips et al., 1999). Its excitation may come from circumferential tube resonances and tread block vibrations (Ruhala and Burroughs, 1998; Dare, 2012).

2.2.2.2 Friction/Adhesion-Induced Vibration

Besides the impact effect, tire vibrations are also induced by friction and adhesion effects at the tire-pavement interface. There are two major friction/adhesion-related mechanisms, both of which are related to pavement microtexture. The first mechanism is "stick-slip", in which tangential stresses in the rubber-road interface are built up and released. The second one is a "stick-snap" phenomenon due to adhesive bonds between tire tread and road surface, which are broken when rubber is pulled away from road surface. The contribution of these mechanisms to overall emission is low-to-moderate, with the exception of certain abnormal tire/road combinations (e.g. sticky rubber tire and painted smooth pavement) (Sandberg and Ejsmont, 2002).

Stick-Slip Mechanism

The stick-slip mechanism can be visualized when considering a tire in acceleration (Dare, 2012). As a tread block enters the contact patch, it sticks to the pavement initially. As the wheel continues to rotate, tire tread element accumulated a

potential energy when pulled against the vehicle travel direction, until shear forces built up in the tread exceed the static friction forces. At this moment the tread element suddenly "slips" across the pavement to a position it can “stick” again. This process is repeated, resulting in tire vibrations. Another vibration source occurs as a tread element exists the trailing edge of contact patch (Wozniak and Taryma, 2004). It is exposed to accumulated shear stress, which is abruptly released when the friction force suddenly diminishes. The stored potential energy is partly converted to kinetic energy, leading to the free vibrations of tread elements. The friction-induced tread vibrations occur mainly in the tangential direction.

Stick-slip noise source exists at both the leading and trailing edges of contact patch (Richard et al., 1998), and within the patch as well. The frequency of the stick-slip noise is usually around 1-2.5 kHz, depending on normal force and vehicle speed (Kroger et al., 2004; Ryszard, 2001). The stick-slip mechanism is considered to be significant in the situations where great tangential forces are applied to tires, such as acceleration, braking or cornering. During free-rotation or when the driven wheel is rolling at a constant speed, the stick-slip mechanism is considered to be much less important (Sandberg and Ejsmont, 2002). Studies found that increased microtexture decreases the stick-slip vibrations within the contact patch by producing larger friction coefficient which can only be reached at rather high sliding speeds (Kroger et al., 2004). However, in such cases, strains induced by the shearing forces would not be relieved and, as a result, tangential vibrations at the trailing edge of contact patch may increase and become prominent (Ejsmont, 1990).

Stick-Snap Mechanism

Stick-snap is a phenomenon resulted from adhesion at tire-pavement interface. When tire tread surface becomes “sticky” and pavement surface is very smooth, the strength of adhesive bond increases. This bond is stretched and then released at the trailing edge of contact patch. The tread element then gets back to its "rest position",

causing radial and tangential tire tread vibrations. It is difficult to separate stick-snap noise from slip-stick noise. It is also possible that stick-snap mechanism enhances the excitation of "inverse impact" effect when a tread element leaves the contact patch.

Although clearly presented from laboratory experiments, adhesion stick-snap mechanism does not contribute much to field tire/road noise since in-service pavement surfaces are usually covered by dirt that reduces adhesive bonds (Sandberg and Ejsmont, 2002). The stick-snap phenomenon is found mostly occur at the trailing edge of the contact patch (Richard et al., 1998; Kuijpers and van Blokland, 2001), and result in higher noise levels for frequencies above 1000 Hz (Nilsson et al., 1980). The stick-snap noise can be reduced with higher microtexture on pavement surface, where the attraction force between tire tread and pavement surface is decreased (Kroger et al., 2004). It is less significant on wet pavements as well.

2.2.2.3 Air Pumping

Air pumping occurs when a tire rolls as air is compressed and gets pushed out at the front of the contact patch while another portion of air is expanded and sucked in at the rear. It generates vibrations in the surrounding air and constitutes a source of sound. This effect can be more significant if cavities exist on tire tread or pavement surface where air can be enclosed. A common analogy of air pumping mechanism is the sound made by clapping (Nilsson et al., 1980), where hands compress the air between them and force it out and vibrating to create sound.

Air pumping is one of the major sources of tire/road noise (Plotkin et al., 1980; Sandberg and Ejsmont, 2002). It is important at both the leading and trailing edges of contact patch (Richard et al., 1998). Air pumping noise evidently occurs at a 1-3 kHz frequency range (Ejsmont, 1992; Donavan and Lodico, 2009). Both tread pattern and pavement textures can affect air pumping noise. To reduce the noise generated by air pumping, it is necessary to connect all the cavities efficiently to the open air so that pressure gradients are lowered. This could be achieved by increasing

pavement porosity or macrotexture to allow air to escape when it is compressed by a rolling tire (Descornet and Sandberg, 1980; Nilsson, 1982; Fujikawa et al., 2006).

2.2.2.4 Air Turbulence

There is another potential mechanism that may contribute to rolling tire noise, i.e. air turbulence created by a tire rolling in the still air and displacing and dragging the air around the tire. There is a general consensus that this effect is a minor contributor to tire/road noise compared to vibration mechanisms and is relatively insignificant at highway speeds (Donavan and Oswald, 1980; Nilsson et al., 1980; Eberhardt, 1984). From extensive experimental studies, Sandberg and Ejsmont (2002) concluded that air turbulence noise is negligible in most situations and it is unlikely to affect the overall sound level.

2.2.2.5 Horn Effect

It is noticed that most noise generation mechanisms (such as impact-induced vibration, friction-induced vibration and air pumping) exist close to the leading and trailing edges of the tire-pavement contact patch, where a horn-shape geometry is formed by tire tread and pavement surface. This acoustical horn forces a multi-reflection of the sound wave and hence significantly amplifies its magnitude. It provides a better match between the impedance of sound source at the contact patch and sound field around the tire (Schaaf and Ronneberger, 1982). Horn effect is believed to be the most important amplification mechanism for tire/road noise. It enlarges the overall noise level by 10-20 dB in the frequency range up to 2000-3000 Hz (Schaaf and Ronneberger, 1982; Kropp et al., 2000; Graf et al., 2002). The noise amplification is more significant when the excitation is closer to the contact patch. Measurements also found that the horn effect leads greater directivity of sound towards the front and rear of a tire (Ronneberger, 1985).

Iwai et al. (1994) and Kropp et al. (2000) found that horn effect can be reduced when porous surfaces are used. Further studies have indicated that changing the porous layer thickness or adopting a double-layer porous system can optimize the amplification characteristics of horn effect (Lui and Li, 2004). Another horn effect reduction measure is to narrow tire width so that the reflecting area of the "horn" constituted by tire tread and road surface is reduced.

2.2.2.6 Cavity Resonance

The acoustic cavity inside the tire carcass also contributes to tire/road noise amplification (Bschorr, 1985; Scavuzzo et al., 1994). The noise amplified by the cavity resonance is less important for exterior-vehicle noise emission than for interior-vehicle noise. The cavity resonance commonly does not affect tire vibration characteristics (Bolton et al., 1998), unless in some special cases where a structural resonance may couple with the cavity resonance resulting in further amplification. The frequency of the cavity resonance is determined by tire and rim geometry. Typical resonance frequencies for passenger car tires are 220-280 Hz while that for heavy truck tires is around 150 Hz (Sandberg and Ejsmont, 2002).

2.2.2.7 Helmholtz Resonance

Helmholtz resonance occurs as an action in a simple mass-spring vibration system. Applied to tire/road noise, the volume of tread cavity leaving contact with the road surface acts as a spring, and the air present between tread and pavement acts as a mass. This mechanism is observed when a trapped volume of air is connected to the outside through a narrow channel (Kinsler et al., 2000). As a cavity moves out of the contact patch, a mass-spring system is suddenly created at the moment when the cavity opens to the surrounding air. Along with the cavity moving further away from the contact patch, the volume and mass of the air immediately outside the cavity will increase. The resonance frequency is determined by the mass, spring and damping

constants, thus there is a “tone burst” associated with each cavity leaving the contact patch, starting at a high amplitude at a medium frequency and fading-off at a higher frequency. Nilsson et al. (1979) found that the Helmholtz resonance has most of its energy concentrated in the frequency range of 1000-2500 Hz.

Helmholtz resonance could be suppressed by good “ventilation” of the cavity formed by tire tread and road surface. The ventilation may be provided by a porous pavement or a ventilated tread pattern. The resonance frequencies may be shifted by changing the tread cavity volume or altering the tire diameter and thus contact patch length (Sandberg and Ejsmont, 2002). It is indicated that the Helmholtz resonance is closely related to the air pumping mechanism and these two mechanisms should be studied simultaneously (Kim et al., 2006).

2.2.2.8 Pipe Resonance

Another resonance mechanism existing in tire/road noise emission is the pipe resonance occurring within the tread grooves. In a pipe of length *L* and open at both ends, an air displacement may create a standing wave with a fundamental wavelength of *2L*. If a pipe is closed at one end and open at the other, the fundamental resonance will be at a quarter of a wavelength. All tread grooves (with different shapes and dimensions) serve as pipe resonators to some extent when they are in contact with a smooth road surface. Pipe resonance is considered a major noise amplification for grooved tires on smooth pavement (Koiki et al., 1999). Saemaan and Schmidt (2002) found that a tire with longitudinal grooves is about 3.5 dB(A) noisier when compared to the same slick tire. The frequency of pipe resonance generally depends on the groove geometry (Oswald and Arambages, 1983), and is believed to concentrate in high frequency range.

Pipe resonance reduction may be realized in two ways. One is to avoid the tread pattern having a resonance frequency close the impact frequency. Another is to efficiently ventilate the grooves, which can be achieved by porous pavement surface

(Koiki et al., 1999). Similar as the Helmholtz resonance effect, pipe resonance cannot be completely separated from air pumping mechanism either (Kim et al., 2006). These phenomena have to be considered simultaneously in the investigations of tire/road noise generation and amplification.

This section discussed the critical mechanisms in tire/road noise generation and amplification. It is important to note that all the mechanisms coexist in tire/road noise emission and interact with each other. It is impossible to extract each individual mechanism explicitly in practice. The relative importance of a specific mechanism varies with tire-pavement combination and operation condition. Nevertheless, some general consensuses can still be obtained from this literature review. Tire vibrations and air pumping are the most important noise generation mechanisms, while air turbulence noise is negligible to the overall noise level at highway speeds. Horn effect has a significant influence on tire/road noise amplification, while acoustic resonances are less important, especially for smooth tires. Some of the mechanisms can be reduced by applying porous pavement surfaces, such as the air pumping, horn effect, Helmholtz resonance and pipe resonance.

2.2.3 Tire/Road Noise Measurement

To compare acoustical performances between different tires and pavements, various experimental techniques have been developed to measure tire/road noise. These techniques can be broadly divided into two major categories, namely in-field measurements and laboratory measurements. The former involve full-scale test pavement sections, while the later are commonly conducted on test drums covered by pavement samples. Some techniques specify the vehicles and tires being used and others adopt statistical approaches to deal with the vehicle and tire variations. The widely accepted in-field measuring methods include the statistical pass-by method (SPB), controlled pass-by method (CPB), coast-by method (CB), close-proximity method (CPX) and on-board sound intensity method (OBSI). Most of these in-field

techniques have been standardized. The laboratory measurements vary from one to another without international specifications being established. They may use either a stationary wheel or a stationary pavement test set-up. These measurement methods are briefly introduced in this section, and their advantages and disadvantages are discussed.

2.2.3.1 Statistical Pass-By Method

Statistical pass-by method is a far field noise measurement approach utilizing a random sample of typical vehicles selected from the traffic stream, under constant or nearly constant speed conditions. This test is standardized by ISO 11819-1 (ISO, 1997a) in detail. The test site configuration is illustrated in Figure 2.17, in which a stationary microphone is located 7.5 m from the central line of the travel lane. The vehicles measured are those cruising-by the test site without disturbances from other vehicles. At the passage, the maximum A-weighted sound level is measured together with the vehicle speed. The vehicle is also classified into one of the preset categories. After measuring at least 100 cars and 80 heavy vehicles, the measured sound levels are plotted against the measured speeds by vehicle category. Statistical methods are then used to assess the noise levels and derive the statistical pass-by Index (SPBI).

Statistical pass-by method is easy to conduct at a normal operation condition without traffic control. It provides a quick and direct evaluation on noise level near the roadway, and takes into account the vehicle and tire variation in the realistic traffic flow. SPB is particularly useful to compare the acoustic performance of several pavement sections constructed on the same road (Abbott and Phillips, 1996) and to conduct a "before-and-after" study when a new pavement treatment is performed on an existing road (Sandberg, 1997). The main disadvantage of SPB method lies in its loose definition of “normal” traffic condition. It assumes that the randomly selected vehicle sample is representative, however traffic composition depends on location and time and is not a constant. This makes it difficult to compare two pavements with

significantly different traffic compositions. SPB method measures the noise generated by the entire vehicle, including power unit noise and aerodynamic noise as well, other than tire/road noise. Another disadvantage of SPB method is the long measurement time it takes due to the large sample size collected. Moreover, as shared by all roadside noise measurement methods, the results are susceptible to environmental factors such as wind and temperature.

2.2.3.2 Controlled Pass-By Method

The test configuration of controlled pass-by method is similar to that of SPB method. Instead of a statistical traffic sampling, the vehicles and tires being tested in CPB method are prescribed. For each test location, a specific vehicle cruises by at a given speed with its engine running at normal condition and a maximum A-weighted noise level is measured at the roadside. Multiple test locations are necessary for each test section to derive the average noise level representing the full test section. The CPB method is specified by a national French standard (NF S 31-119-2), which makes use of two cars and four tire sets. It is used to survey the French road network, establishing a database on the acoustical properties of all the major French roadways (Sandberg and Ejsmont, 2002).

One of the primary advantages of the CPB method is that it can control most test variables, such as the vehicle, tire and test speed, making it easier to compare the acoustic properties of different pavement surfaces. CPB measurement can be performed much faster compared to SPB method because fewer runs are needed for generating reliable results. It also allows for passes at different speeds to derive the speed dependency of noise level. A drawback of CPB method is that it does not account for the variation in traffic composition and thus cannot estimate the perceived noise level at roadsides. CPB method requires test vehicles to be isolated from other traffic, and background noise has to be kept as low as possible. Therefore, potential problems may occur when conducting the measurements on highly trafficked roads.

This may lead to traffic control or closure of the road, causing inconvenience to road users. Similar to SPB measurement, the CPB method also measures the overall noise generated by the entire vehicle, rather than the separated tire/road noise.

2.2.3.3 Coast-By Method

Coast-by approach was developed to eliminate engine noise from the noise levels measured at roadsides. The test configuration is the same as CPB method, except that the test vehicle is coasting through the test area with the engine switched off and the transmission put in neutral. The vehicle is driven only by the inertia force and is assumed to emit only tire/road noise. During coasting, the vehicle will slightly slow down. This is usually neglected and the speed at the maximum noise level or the average speed is used in the data processing. The Coast-by method is standardized by ISO 13325 (ISO, 2003).

The principal advantage of CB method is that it eliminates the interference of power unit noise. The noise levels measured with this method can be directly used to estimate the tire/road noise emitted from individual vehicle at particular speeds. The CB method has disadvantages similar to the CPB approach and the CB measurement result is affected by the performance of test vehicle. Besides, narrow-band frequency analysis (narrower than 1/12 octave band) is inapplicable to all roadside measurement methods unless advanced Doppler compensation methods are employed. The Doppler effect has a negligible effect on one-third octave band frequency analysis.

2.2.3.4 Close Proximity Method

The close proximity method, previously named the trailer method, is a near field measurement technique specially designed to focus on the tire/road noise. This method is standardized by ISO 11819-2 (ISO, 2013). In the CPX measurements, a test tire is mounted on a trailer lined with the sound-absorbing material (see Figure 2.18). Two microphones are fixed near the leading and trailing edges of the contact

patch at 200 mm from tire side wall and 100 mm above road surface (see Figure 2.19). The trailer is hooded by an enclosure to reduce the influence of wind noise and pulling vehicle noise. To control the uncertainties from test tire, standard reference tires are used in CPX measurements, as specified in ISO/TS 11819-3 (in preparation). Some of the most widely used reference tires are illustrated in Figure 2.20. In the CPX tests, the average A-weighted sound pressure levels emitted from the tire-road interaction are measured over a specified distance, together with the vehicle speeds. The close-proximity sound index (CPXI) is then derived at a reference speed and the spectrum analysis could be performed based on the time series data.

The CPX technique makes possible direct near-source measurements of tire/road noise. The primary advantage of this method is that measurements are fast and efficient. Once the test vehicle and devices are available, a large distance of pavement sections can be measured continuously within a single test run. Comparing to roadside methods, the CPX method is less susceptible to suffer from the variations of environmental conditions. Because of the enclosure installed around the test tire, no strict requirements on background noise are specified in the CPX method, and it can be conducted on roads with considerable traffic. Besides, narrow-band spectrum analysis is feasible with this method. However, there are still several disadvantages coming with the CPX method. It only measures a limited number of vehicles and tires, therefore it cannot represent the actual traffic composition, nor can it measure perceived noise in the far field. In CPX tests, the variation of measuring results due to different test vehicles and trailers is large. Higher investment is needed for the equipments and vehicles used in the tests, making it more expensive compared to the roadside methods.

2.2.3.5 On-Board Sound Intensity Method

The on-board sound intensity method was developed in the NCHRP Project 1-44 (Donavan and Lodico, 2009) to measure the tire/road noise at near field. It has

been standardized by AASHTO Specification TP 76-11 (AASHTO, 2011b) and ASTM WK26025 (ASTM, 2009e). The test configuration of OBSI technique is illustrated in Figure 2.21. The probes are mounted on one of the tires of a test vehicle instead of a trailer. A significant difference between the OBSI and CPX methods is that the OBSI method measures sound intensity instead of sound pressure (as in CPX method). Sound intensity measurement makes use of two phase-matched microphones arranged in a particular direction in one probe to measure sound intensity perpendicular to the travel direction. With this feature, sounds from other sources in other directions (i.e. wind noise, engine noise etc.) are attenuated, increasing the reliability in measuring tire/road noise. The standard reference test tire P225/60R16-97S (ASTM, 2008c) is adopted in the OBSI method and sound intensity probes are fixed at specific positions near the leading and trailing edges of contact patch. The OBSI method has advantages and disadvantages similar to the CPX method. OBSI method is found to better correlate mathmatically with roadside noise measurements (Donavan and Lodico, 2009).

2.2.3.6 Laboratory Measurement

Besides the above mentioned in-situ approaches, tire/road noise can also be measured in the laboratory. The laboratory measurement usually requires access to some "drum facility". In the stationary wheel method, a test tire is fixed on a stationary axle and rolls on a rotating drum. The test tire is installed in a way that it can roll against either the inside or the outside of drum (see Figure 2.22). In the stationary pavement method, test tire is usually mounted on a rotating arm and rolls around a stationary drum. The moulded replicas of road surfaces are fitted onto the drum in segments to simulate the interactions between tires and real pavements. Near-field measurements can be conducted with microphones installed in a configuration similar to the CPX or OBSI method.

Laboratory measurements do not need test vehicles or real pavement sections. They can be used to predict the acoustical properties of new pavement technologies even before the test sections are constructed (Scofield, 2009). It is suitable when high precision is required, because most test parameters can be strictly controlled in the tests, such as wheel loading, rolling speed and test temperature. The measurement of tire vibrations using laser-Doppler vibrometers can be conducted in the stationary wheel method, since the test set-up makes it possible to focus the laser. Implemented properly, laboratory measurements can be used to predict the coast-by measurements (Sandberg and Ejsmont, 1984). Nevertheless, laboratory measurements also have several disadvantages. It is very difficult to reproduce the pavement surface on a drum, even with the same construction procedures. This may reduce measurement accuracy when the method is used to predict acoustical performance of to-be-constructed pavement. Background noise (such as the noise generated from drum power unit and the sound reflected by surrounding objects) is another concern in this approach. Moreover, the drum curvature caused by restricted device dimension may result in a significant difference from the flat road surface in practice.

2.2.4 Factors Affecting Tire/Road Noise

Using the tire/road noise measurement techniques introduced in Section 2.2.3, the noise emitted from tire-pavement interactions were extensively studied at various conditions (Ejsmont, 1982; Storeheier and Sandberg, 1990; Köllman, 1993; Sandberg and Ejsmont, 2002). Many factors have been identified affect tire/road noise generation, amplification and propagation. These factors can be classified into four groups, namely vehicle operations, tire characteristics, pavement properties and environmental conditions. Factors related to vehicle operations include vehicle speed and vehicle maneuver (braking, accelerating and cornering). Tire composition, dimension, tread pattern design, inflation pressure and wheel load are the main tire characteristics affecting acoustical performance. Pavement surface texture, acoustic

impedance and mechanical impedance are believed to be the most important pavement properties influencing tire/road noise. Temperature and water presence at tire-pavement interface are the most influential environmental conditions. All these factors interact with each other and affect tire/road noise simultaneously. Most effects of these factors can be explained based on one or more mechanisms discussed previously. The noise variation amplitudes due to some major influencing factors are estimated by Sandberg and Ejsmont (2002) and are illustrated in Table 2.2. This section presents a discussion on the current understanding of these influencing factors.

2.2.4.1 Vehicle Speed

From Table 2.2, it was found that vehicle speed is the most important operational parameter affecting tire/road noise. An illustration of the tire/road noise variation with vehicle speed is shown in Figure 2.23. Generally, noise level increases rapidly with an increase in vehicle speed, but the rate of increase varies among vehicle categories and pavement types. A higher vehicle speed may induce more severe tire vibrations and increase the air pumping effect. It can also develop larger tangential stresses on the tire contact patch when vehicle negotiates a curve or applies brake. Moreover, it is suspected that the stick-slip and stick-snap noise are enlarged as well. All these mechanisms work together to generate more noise at higher speed.

Experimental studies (Ejsmont, 1982) have suggested a logarithmic linear relationship between tire/road noise and vehicle speed. This relationship, as shown in Equation 2.26, has been found to be a general feature of tire/road noise (Sandberg and Ejsmont, 2002).

$$L = A + B \cdot \log(V) \tag{2.26}$$

where L is the sound pressure level, V is the vehicle speed, and A and B are the speed coefficients. This relationship is widely used to describe the speed dependencies of noise emissions at different conditions. Some speed coefficient results are illustrated in Table 2.3. Further analysis found that there is a strong linear correlation between

coefficient *A* and *B*, and their values can be used in the selection of tires and/or road surfaces (Sandberg and Ejsmont, 2002).

2.2.4.2 Vehicle Maneuver

When a vehicle accelerates, brakes or turns, the excess tangential forces will develop on the tire contact patch and the noise emitted could be higher than that at a constant speed. Extremely high slip may cause tonal-type tire squeal and significantly increase the overall noise level. Longitudinal slip is usually resulted from the driving or braking torque acting on a tire. It was thought to increase tire/road noise by as high as 12 dB (Steven, 1989). The influence of slip is larger at lower speeds than at higher speeds (Wozniak, 2002). A comprehensive experimental study conducted by Steven (1991) found that the average noise increase for a torque of 800 Nm was about 10 dB at the speed 20 km/h, 8 dB at 30 km/h, 4.5 dB at 50 km/h and only 3.5 dB at 70 km/h. The largest sound level increase happens at a slip of 10% to 15%. It stabilizes at higher slips because the further increase of slip does not increase the frictional force any more. Lateral slip will develop with a side force when a vehicle changes its travel direction. Noise level increases during cornering by 0-2 dB at lower speeds, 0-5 dB at medium speeds and 1-7 dB at higher speeds. With regard to spectrum analysis, the influence of cornering on noise is found to be constant and low at frequencies below 1 kHz, but is much more significant at higher frequencies. Most of the effects occur in the range of 2-10 kHz (Ejsmont and Sandberg, 1988).

The noise increase due to tangential forces is thought to be closely related to the stick-slip mechanism at the contact patch and may also connect with the friction between tire tread and pavement surface. This mechanism can result in both the stick-slip vibrations within the contact patch and the free tangential vibrations immediately after a tread element has passed the contact patch and released the high strains. It may also cause an excitation for the air resonant mechanism at high frequencies.

2.2.4.3 Wheel Load and Tire Inflation Pressure

Inconsistent results were obtained across various tires in past research studies investigating the influences of wheel load and tire inflation pressure on the tire/road noise emission (Sandberg and Ejsmont, 2002). However, the common trend from those studies is that the tire/road noise increases with an increasing wheel load or a decreasing tire inflation pressure. Ejsmont and Taryma (1982) tested the typical radial tires of passenger cars and found that noise increased by 1-2 dB(A) per doubling of load, with inflation pressure adjusted to the load. With constant pressure, the increase was found to be 0.7-1.5 dB(A). From the acoustic measurements on more than 100 car tires, Köllman (1993) found a 2.4 dB(A) noise level increase when doubling the tire load from 170 to 340 kg. The noise variations for truck cross-ply tires was observed by Kilmer (1976) as follows. With a constant inflation pressure, changing the load from 50% to 100% of the maximum tire load produced around 2-3 dB(A) noise increase for crossbar tires, but was negligible for rib tires. If the inflation pressure was adjusted according to the load, more complex behaviors were observed. Increasing the load from 50% to 75% increased noise by 2 dB(A) but further increases of load decreased noise. According to Underwood (1981), the noise increase for a loaded truck (13.23 tons) in comparison to an empty one (5.58 tons) was as high as 6.5 dB(A) for traction tires but only 0.5 dB(A) for rib tires.

The effects of wheel load and tire inflation are very complicated, involving various mechanisms. Increased inflation pressure could stiffen the tire carcass and change the vibration characteristics, especially for tire sidewalls. Contact area is affected by wheel load and tire inflation, so does contact pressure distribution within the contact patch, which may cause different parts of the tire tread to be excited. The horn shape geometry next to the contact patch will also be changed, affecting the amplification effect. Besides, the air channels in tire tread pattern may become longer or shorter, wider or narrower, influencing the air pumping and pipe resonance effects.

2.2.4.4 Tire Properties

The width of pneumatic tire has increased over the past decades due to wider tire benefitting from better dry traction and steering response. However, tire/road noise is adversely affected by the increase of tire width. Research studies have observed significant noise level increases on wider tires (Ullrich and de Veer, 1978; Sandberg and Ejsmont, 1992; Phillips and Abbott, 2001). The increase of noise level was found to be around 0.4 dB per 10 mm increase in tire width when the tire width is below 200 mm. For tires wider than 200 mm, the influence of tire width becomes lower. Tire/road noise grows with increasing tire width because a wider tire results in more tread blocks impacting on pavement and more air being displaced from the contact patch. As a result, both tire vibration and air pumping mechanisms are intensified. Moreover, horn effect is also amplified by wider tire tread.

Tire/road noise is weakly correlated to tire diameter (Storeheier and Sandberg, 1990). An increase in tire diameter may result in lower noise level (Nilsson, 1979; Ejsmont and Taryma, 1982) because a larger tire diameter reduces the "attack angle" on road surface and produces a gentle impact between tire tread and pavement surface. A smaller tire-pavement angle, on the other hand, may amplify the horn effect and hence increase tire/road noise. The overall effect of tire diameter on noise level depends on which mechanism dominates the noise emission.

Tire composition affects noise emission as well. It is observed, statistically, radial tires are less noisy than bias tires (Anonymous, 1980). Ejsmont (1982) indicated that increased tread bending stiffness can reduce noise generation. Muthukrishnan (1990) found that tread modulus has larger influences on tire/road noise than sidewall modulus and a significant interaction exists between the tread and sidewall properties. Watanabe et al. (1987) showed that rubber hardness has a substantial effect on truck tire noise. Sandberg and Ejsmont (2002) concluded that by selecting an appropriate rubber hardness, noise level can be reduced by at least 2

dB(A). Their further work found that the overall noise levels increase 1-2.5 dB per 10 unit increase in Shore A hardness (Sandberg and Ejsmont, 2007).

Tread pattern is usually specially designed to control tire/road noise. It affects all the generating mechanisms to some extent. Tires with a constant pitch generate a tonal noise due to the periodical impact of the pattern. A simple solution to this problem is to introduce a varied tread segment pitch. Air pumping and pipe resonance effects will decline if all the grooves on tire tread are well connected to the open air. Therefore, in order to reduce noise level, any closed pockets, cavities with narrow outlets and long grooves without ventilated side branches should be avoided in the tread pattern design.

2.2.4.5 Pavement Textures

Variation of tire/road noise level on different pavements was found up to 13 dB at highway speed (Donavan, 2008), which is attributed to the pavement properties. Sandberg and Ejsmont (2002) summarized influence of road surface characteristics on tire/road noise emission and the results are listed in Table 2.4. It is seen from the table that pavement texture is a major factor affecting tire/road noise. Dare (2012) also indicated that pavement texture determines tire/road noise levels more than any other tire or pavement properties.

The influence of macrotexture and megatexture on tire/road noise are interrelated and they should be considered together. Experimental studies have shown that noise levels increase with increasing mean texture depth (MTD) as measured from the sand-patch method (Franklin et al., 1979) or with increasing mean profile depth (MPD) as measured from a laser profilometer (Steven et al., 2000). This weak correlation is valid only for slick tire or the tire with a shallow tread pattern. There is no correlation observed for an aggressive tread pattern. The influence of pavement texture on tire/road noise emission may not be adequately explained by a sole parameter describing the overall texture level (such as MTD and MPD). This is

because the different generation mechanisms have contradicting dependencies on pavement surface texture. The effect of macro- and mega-texture on the tire/road noise, therefore, has to be investigated using spectral bands. Sandberg and Descornet (1980) found that the noise levels at low frequencies (generally below 1 kHz) increase with texture amplitude within the wavelength range of 10-500 mm, while noise levels at high frequencies decrease with texture amplitude within the wavelength range 0.5-10 mm. A positive correlations was also found between OBSI noise levels in the 630-1000 Hz range and texture levels in the 5-100 mm wavelength range (Rasmussen et al., 2006; Cesbron et al., 2009). Similar conclusions were obtained from other research studies (Clapp and Eberhardt, 1984; Nelson and Phillips, 1997; Anfosso-Lédéé and Do, 2002), although it was found to be difficult to isolate the texture effects in narrow wavelength band. The influence of pavement texture on tire/road noise at low frequencies is thought to be a result of tread impact mechanism. The texture effect at high frequencies is related to air pumping and resonance mechanisms. Pavement macrotexture also affects stick-slip mechanism by varying the contact area between tire tread and road surface, while megatexture may affect tire dynamic loading and thereby influence tire/road noise as well.

Microtexture also influences tire/road noise, but inconsistent observations are found among past research works (Franklin et al., 1979; Nilsson, 1980; Beckenbauer, 2001; Dare and Bernhard, 2009). Microtexture was commonly measured indirectly using friction test. Most studies observed a positive correlation between friction and tire/road noise, especially for tires with smooth tread (Franklin et al., 1979; Nilsson, 1980; Sandberg and Ejsmont, 2002). It was found significant at high frequencies and negligible at low frequencies. Beckenbauer (2001) and Dare and Bernhard (2009) found that the presence of microtexture decreases noise level at high frequencies. Sandberg (1987) and Oshino et al. (2001) reported that no clear relationship was detected between noise and friction. Such apparent inconsistency is not unexpected as pavement microtexture affects tire/road noise generation mechanisms in different

ways. An increased microtexture generally increases pavement friction, enhances the stick-slip phenomenon to generate higher noise at high frequencies. However, it may also decrease the adhesion strength between tire tread and pavement surface which in turn will reduce the stick-snap effects.

The orientation of pavement texture also affects its acoustic property. In this sense, texture is usually distinguished as positive or negative. The difference is illustrated in Figure 2.24. Positive texture is formed by particles or ridges protruding above the plane of pavement surface, while negative texture is normally formed by voids between particles whose upper surfaces form a generally flat plane. Pavements with an identical texture spectrum but different texture directions can induce different tire/road noise responses (Paje et al., 2007; Abbott et al., 2010). With regard to noise reduction, negative texture is normally preferred. A positive texture can increase impact-induced vibrations, while a negative texture, with appropriate ventilation, can reduce air pumping, resonance and impact.

2.2.4.6 Pavement Acoustic Absorption

Besides surface texture, acoustic absorption is another important pavement property affecting tire/road noise generation and propagation. Porous surface is an effective and efficient pavement technology for noise reduction (Praticò and Anfosso-Lédée, 2012). Its acoustic absorption can be related to porosity, thickness, air flow resistance and tortuosity of porous surface layer. Porous pavement is able to reduce noise generation and dissipate more sound energy compared to conventional non-porous surfaces, resulting in a 3 to 5 dB reduction in tire-related noise (Bérengier et al., 1997). This is achieved through the following mechanisms. Firstly, interconnected pores effectively reduce the compression and expansion of air entrapped in the contact interface, and air pumping and air resonant effects are reduced. Secondly, porosity reduces noise amplification of the acoustical horn existing between tire tread and road surface near the contact patch. Thirdly, acoustic absorption influences

reflection and propagation of sound waves. Finally, negative surface macrotexture exhibited by porous surfaces reduces texture impact mechanism in noise generation.

2.2.4.7 Environment Factors

It has not been realized until the 1980s that temperature can affect tire/road noise emission. This effect requires temperature corrections in noise measurements. Some linear relationships were found between temperature and measured tire/road noise (Ejsmont and Mioduszewski, 1994; Kuijpers, 2001; Landsberger et al., 2001). The current consensus is that noise from automobile tires is reduced by about 1 dB per 10°C temperature increase. Testing in a cold climate may get up to 3 dB higher noise than in a hot climate. However, for truck tires, it is more difficult to observe any consistent temperature influence. The temperature effect is frequency-dependent. It affects more in the 1-4 kHz frequency range. The frequencies corresponding to the spectral peaks are generally unaffected by temperature, because they are mostly connected with the tread impact frequency. The mechanisms through which tire/road noise is influenced by temperature are not yet properly understood. The variations in rubber hardness, pavement impedance and interface adhesion with temperature may be some potential reasons (Dare, 2012).

It has been indicated that the rainwater accumulated on road surface heavily affects the tire/road noise level. The noise levels on an SMA pavement in dry and wet conditions were compared under a rainfall intensity of 1 mm/h (Phillips and Abbott, 2001). It was found that the noise level increases rapidly at the start of the rainfall. A maximum increase of 6 dB(A) was observed after the occurrence of the maximum rainfall intensity and the higher noise level may last for several hours after the rainfall has ceased. Studies also found that wet pavement surfaces are louder at frequencies above 1000 Hz (Boullosa and Lopez, 1987; Descornet, 2000), which may be attributed to the acceleration of water droplets and their fragmentation.

This section discussed the effects of critical influencing factors on tire/road noise performance. Vehicle operating conditions, tire properties and pavement characteristics were identified as significantly influential on tire/road noise. With regard to pavement surface properties, macrotexture and acoustic absorption were found to be important in the determination of pavement acoustical performance. This leads to the utilization of porous pavements to reduce tire/road noise.

2.2.5 Tire/Road Noise on Porous Pavement

Porous pavements were originally developed to improve road safety by enhancing pavement skid resistance and reducing splash and spray in rainy days. However, their superior performance in tire/road noise reduction was soon recognized (Gibbs et al., 2005; Abbott et al., 2010). Various experimental studies on the acoustical performance of porous pavements have been performed, leading to recommendations on porous pavement design (von Meier et al., 1990; Neithalath et al., 2005; Kowalski et al., 2009).

2.2.5.1 Experimental Studies on the Noise Reduction on Porous Pavements

Younger et al. (1994) conducted a study on the acoustical performance of porous pavements in Oregon. Three sections along the I-5 interstate highway were evaluated before overlay (conventional asphalt surface) and after overlay (porous asphalt surface). Roadside A-weighted noise levels were measured in the study, using a Brüle and Kjær 2221 sound level meter and a Rion Sa-27 1/3 octave band analyser. It was found that porous pavements could reduce the noise level at higher frequencies. The overall roadside noise reduction was observed to be 0.9-2.0 dB(A), and 1-4.5 dB(A) for 1/3 octave band in the frequency range of 600 to 4000 Hz. The superior acoustic property of porous pavements, compared to dense asphalt surfaces, was also detected in the field measurements performed by the Danish Road Institute (Bendtsen, 1998). However, the lower-noise benefit of porous surfaces lasted only for six years

after construction (see Figure 2.25). The acoustical performance of porous pavements became similar to that of dense-graded pavements since the seventh year.

Kowalski et al. (2009) investigated the long-term acoustical performance of porous pavements under Indiana traffic and climatic conditions. The porous friction course (PFC) located on I-74 east of Indianapolis, with a design air void content of 23%, were compared with stone matrix asphalt (SMA) and dense graded asphalt (DGA). Both close proximity and controlled pass-by tests were conducted shortly after construction, before the road was opened to traffic, and statistical pass-by tests were conducted periodically in the 4-year study period. It was found that the PFC surface had the best noise performance and was about 4 to 5 dB(A) quieter than the SMA section. Seasonal variation in noise was not significant on PFC, but an increasing trend in sound pressure level with traffic loading could be noticed.

An experimental study on the tire/road noise from trucks was conducted in the Netherlands (der Graaff et al., 2005). 15 types of commercial truck tires were selected to be tested on twelve test tracks with various pavement surface types. Measurements were performed at speeds between 40 and 90 km/h. The sound levels were measured using the controlled pass-by and close proximity methods. The effect of pavement surface type on tire/road noise level measured in the pass-by tests is shown in Figure 2.26. The measurement results showed that the double-layer porous asphalt pavement (field A02) was the quietest surface type, with a noise level about 9 dB(A) lower than that of SMA surface with epoxy resin (field A11), which was the loudest. The single-layer porous asphalt pavement (field A01) was slightly louder than the double-layer one by about 2 dB(A). All the other surface types produced similar noise levels, about 4 to 5 dB(A) louder than the double-layer porous asphalt surface. Similar results were observed in the near-field measurements as well. It was concluded that, in general, the porous asphalt pavement is quieter than other surface types.

Similar conclusions were drawn from other research studies. The acoustical performance of porous pavement on Yan-Tong expressway in China was reported by Xu et al. (2010). It was found that porous pavement produced the lowest noise level among the different pavement types being tested, although the observed noise level do increase with pavement age and vehicle speed. In another application of porous pavement on Nanning express ring road in China, it was found that by providing a 40 mm porous overlay on existing cement concrete pavement, a noise reduction of 3 to 6 dB(A) can be achieved, compared against an asphalt overlay alternative (Yang et al., 2009). Table 2.5 summarizes the observed benefits of porous pavements in terms of noise reduction from various countries. Direct comparisons between these results are extremely difficult because of the variations in reference surfaces, test vehicles, traffic conditions and measuring approaches adopted by different countries.

More than 8 dB(A) noise reduction was reported by Ishida et al. (1996) and Fujiwara (2005) on specially designed porous pavements. In such a case, it was likely that the surface had some other means of noise reduction besides sound absorption, for example a lower stiffness or a negative texture.

2.2.5.2 Design Recommendations on Acoustic Absorption

The acoustic absorption of porous pavements is a complicated function of several variables, such as porosity, tortuosity, porous layer thickness and air flow resistance. Theoretically, these variables can be adjusted to optimize the acoustic absorption of a particular porous surface. The design objective is normally to obtain the maximum absorption coefficient at a frequency around 1000 Hz for high speed facilities and 600 Hz for low speed ones (von Meier, 1992). In addition, the frequency width of high absorption coefficient should be as broad as possible.

It appears that the porosity value governs both magnitude and bandwidth of the peak absorption, whereas the air flow resistance governs mainly the bandwidth. The tortuosity and layer thickness determine the peak absorption frequency and also

affect, to some extent, the bandwidth and magnitude of maximum acoustic absorption. Considering the effect of air void content, higher porosity increases the bandwidth of absorption peak. The optimum air flow resistance was reported to be in the range of 20-50 kNs/m^4 for high speed roads and 12-30 kNs/m^4 for low speed roads (von Meier et al., 1990). The tortuosity is a measure of the path length of the pores throughout the porous layer. Higher tortuosity apparently leads to a lower frequency of the maximum absorption.

An illustration of porous pavement acoustic absorption spectra at different porous layer thicknesses is shown in Figure 2.27. The general effect of increasing porous layer thickness is to make the absorption peak shift to a lower frequency. It also introduces the secondary peaks into the critical frequency range of tire/road noise (i.e. 0.3 to 2 kHz) at high frequencies (Neithalath et al., 2005; Losa and Leandri, 2012). Meanwhile, absorption spectrum becomes peaky when porous layer thickness increases. The noise reduction on porous pavement can be enhanced by adjusting porous layer thickness to make sound absorption spectrum fit tire/road noise spectrum. For acoustical performance optimization, von Meier et al. (1990) suggested a 32-50 mm porous layer thickness to have the absorption peak at 1000 Hz. It would be unwise to make porous surface too thick, considering noise reduction efficiency and material cost.

2.2.6 Existing Model for Tire/Road Noise

Besides experimental studies, research were also performed to develop tire/road noise models (Descornet and Sandberg, 1980; Kropp, 1992; Sandberg and Ejsmont, 2002; Nachenhorst, 2004; Kuijpers et al., 2007; Yang, 2013). Existing tire/road noise models are broadly classified into three categories, namely empirical models, theoretical models and numerical models. Due to the complexity of tire/road noise phenomena, none of the existing models is able to appropriately cover all the mechanisms in noise generation and amplification, nor are they capable enough to

consider all the influencing factors. Each model in the literature involves only several major mechanisms to make it work well in specific scenarios. This section presents a brief review on the major developments in tire/road noise modeling and the emphasis should be placed on the noise prediction using pavement surface properties.

2.2.6.1 Empirical Models

A relatively simple method to derive the tire/road noise prediction models is to correlate the emitted noise levels with measured tire and pavement properties using statistical regression approaches. The most significant factors are identified and included into the models, although there is no theoretical representations of the various mechanisms. Such methods were initially used to estimate the noise level from tire properties and tread pattern (Varterasian, 1969; Fong, 1998; Ejsmont, 2000), and then models considering pavement effects were developed as well.

To predict noise level from pavement properties, an early effort was made by Descornet and Sandberg (1980) in the analysis of the relations between noise levels and texture spectra. This work led to a simple prediction equation:

$$ERNL = a \cdot L_{80} - b \cdot L_5 + c \tag{2.27}$$

where, ERNL is the estimated road noisiness level [dB(A)], L_{80} is the texture level in the octave band centred at 80 mm wavelength in relation to the reference level of 10^{-6} m, L_5 is the texture level in the octave band with centre wavelength of 5 mm, and a, b and c are constants derived from regression. The constants depend on the vehicle and tire types, speed range and measurement method. This simple relationship provides a rough estimation of the acoustical performance of pavements and is feasible for a general comparison between surface textures. However, it is only valid for car tires and non-porous pavements. One major drawback of this model is the arbitrariness of the absolute noise level, c, which causes the model unable to provide the typical noise emission levels. This model assumes that L_{80} and L_5 are representative of the course and fine textures, respectively, which may not always be true, especially for a surface

with periodical grooves or blocks. Some other studies also attempted to reveal the relationship between texture spectra and noise spectra (Rasmussen et al., 2006; Klein and Hamet, 2007; Dare and Bernhard, 2009). It was concluded that pavement textures in the wavelength range of 30-100 mm correlates positively with noise levels in the frequency range of 500-1000 Hz, and those with wavelengths shorter than 2 mm affects noise levels higher than 2000 Hz negatively.

In order to address some of the limitations in the original model described by Equation (2.27), Sandberg and Ejsmont (2002) introduced the effects of pavement age, porous surface and heavy vehicle into the model to make it more comprehensive. The overall model for passenger cars is then presented as:

$$ERNL = 0.5 \cdot L_{80} - 0.25 \cdot L_5 - u \cdot (2 - T) - q \cdot \ln(\Omega d) + 67 \tag{2.28}$$

and the relationship for trucks is shown as:

$$\begin{aligned} ERNL = {} & 0.35 \cdot L_{80} - 0.175 \cdot L_5 - 0.7 \cdot u \cdot (2 - T) - 0.7 \cdot q \cdot \ln(\Omega d) \\ & -0.2 \cdot \left[70 - 20 \cdot \log\left(MPD / 10^{-6} \right) \right] + 81 \end{aligned} \tag{2.29}$$

where T is the surface age in years, u is a constant depending on T, Ω is the porosity (%), d is the porous layer thickness (mm), q is a constant depending on Ωd, and MPD is the mean profile depth (m). The model constant increases from 67 for cars to 81 for trucks, in order to approximately reflect the difference in noise emissions between cars and trucks at a somewhat average travel condition. These models can only be used to compare acoustical performances of different pavements. The absolute noise levels calculated from the equations may not agree with measurements due to the lack of considerations in tire types and vehicle speeds. Therefore, the applications of such models require careful calibrations.

The statistical physical explanation of rolling noise (SPERoN) model is another well developed empirical model, initially developed for the German Road Authority by M+P and Müller-BBM in the Sperenberg project (Kuijpers et al., 2007). The first version aimed to explain the texture-induced noise for passenger car tires.

Further parallel developments included more and more mechanisms into the model. The latest version of SPERoN model has become a hybrid model combining both the physical and statistical approaches. The core of this model is a multivariate regression relationship describing the various mechanisms of tire/road noise generation. This interaction model defines a sound energy at the measurement position and assumes that the sound energy emission results from five components, namely tire vibration, airflow related sources, tire cavity, vehicle body aerodynamic and friction/adhesion. It further assumes that contributions are uncorrelated with each other and the total sound power is a linear superposition of the individual sources. The model is described as:

$$p_{total}^2 = p_{vibration}^2 + p_{airflow}^2 + p_{cavity}^2 + p_{vehicle}^2 + p_{friction}^2 \tag{2.30}$$

where p_{total}^2 is the total sound power, $p_{vibration}^2$ is the component resulting from tire vibration, $p_{airflow}^2$ is the component related to air flow within the contact patch, p_{cavity}^2 is the source of tire carcass cavity resonances, $p_{vehicle}^2$ is the aerodynamic noise around car body, and $p_{friction}^2$ is the contribution due to friction and adhesion. The values of these components can be obtained from the following expressions:

$$p_{vibration}^2 = a \cdot F_c^2 \Gamma^{\alpha_1} B^{\alpha_2} S^{\alpha_3} \tag{2.31}$$

$$p_{airflow}^2 = b \cdot \left(F_c^2 \Gamma^{-1.5} S^{-2} \right)^{\beta_1} B^{\beta_2} V^4 \tag{2.32}$$

$$p_{vibration}^2 = c \cdot G_{pattern}^{\gamma} \tag{2.33}$$

$$p_{vibration}^2 = d \cdot V^{\delta} \tag{2.34}$$

$$p_{vibration}^2 = e \cdot \left(G_{pattern} \Gamma X^{-1} \right)^{\varepsilon} V^4 \tag{2.35}$$

where *a, b, c, d, e* are the regression coefficients, α_1, α_2, α_3, β_1, β_2, γ, δ, and ε are the regression exponents, F_c is the tire-pavement contact force derived from analytical approaches, Γ is the air flow resistance of pavement, B is the tire width, S is the tire tread stiffness, V is the traveling speed, $G_{pattern}$ is the spectral power of tread pattern

variation, and X is the micro-roughness. It is noted that the regression coefficients (*a* through *e*), the contact force (F_c) and the tread pattern effect ($G_{pattern}$) are frequency-dependent, and $G_{pattern}$ also depends on the traveling speed (V). The noise absorption of porous pavement could be integrated into the model through a representation of noise level reduction:

$$\Delta L_p = A \cdot H_{horn}(f) \cdot \alpha\left(\frac{f}{f_{sh}}\right) \tag{2.36}$$

where ΔL_p is the difference between the noise emissions on dense and porous surfaces, A is an amplification factor, $H_{horn}(f)$ is a weighting curve expressing the horn effect strength as a function of frequency, α is the absorption coefficient at frequency f, and f_{sh} is the frequency shifting factor (normally with a value of 1.25-1.30). The primary advantage of SPERoN model is that it covers most of the important noise generation mechanisms and provides the possibility to address various tire-road combinations. However, because of the large number of regression coefficients and exponents, it is very difficult to calibrate this model, especially considering the frequency dependency of the coefficients and variables. Comprehensive measurements on tire and pavement properties are needed in model validation and application, which may not always be available. Therefore, while the SPERoN model is popular in the literature, its application in industrial practice is still limited to date.

The SPERoN model takes the CPB noise spectrum as the dependent variable which contains sound other than tire/road noise and most of its independent variables represent tire properties rather than pavement properties. Another statistical model is recently developed to estimate the influence of concrete pavement surface textures on OBSI noise measurement (Izevbekhai, 2012). Tire/road noise is isolated from the other sources in this model, which was derived from an unforced stepwise regression process and is expressed as:

$$OBSI = 99.023 + 20.164\left(\frac{293 - T}{T}\right) + \left(\frac{ASPT}{ASP}\right)(1.513DIR + 0.098)$$

$$+5.849\left(\frac{IRI}{IRIT}\right)+1.684SP \tag{2.37}$$

where T is the air temperature in °K, ASP is the asperity interval in pavement texture (the average interval of repeating patterns of asperity), $ASPT$ is the asperity interval of tire, DIR is the texture striation direction (transverse = 1 and longitudinal = 0), IRI is the international roughness index describing the pavement smoothness, $IRIT$ is a reference value of 15 m/km, and SP is the texture spikiness variable (i.e. the texture direction, positive = 1 and negative = 0). This model has been shown to be capable to reproduce more than 90% of the field measurements within a 1.5 dB(A) error criteria. This prediction model considers both small scale and large scale texture variables as well as an environmental variable, but the texture profile depth was not identified as a significant influencing factor. This model is feasible for noise estimation of a standard reference test tire (SRTT) running on cement concrete pavements at a constant speed of 60 mph. It may not be valid for other tire types or asphalt pavements. The noise variation with speed is not involved in the model. Moreover, this model is infeasible to predict the noise levels on porous pavements.

Other empirical models were also developed with different considerations (Fujikawa et al., 2005; Losa et al., 2010; Mak et al., 2011; Dubois et al., 2013; Yu and Lu, 2013). They are capable, to some extent, to estimate the noise levels for particular tire and pavement types under given traveling conditions, but none of them can be extensively applied to various situations. Although theses models adopt most of the critical variables and attempt to cover the major influencing factors in their formulations, it is not possible to obtain any theoretical explanations on the tire/road noise mechanisms from such statistical models.

2.2.6.2 Theoretical Models

In order to better explain tire/road noise emission mechanisms, various theoretical models have been developed since the late 1980s. Most of these models

focused mainly on tire vibration noise. An early model was initially developed by Kropp (1989a-b) based on a linear tire assumption, where the tire is modelled by a continuum circular ring with excitations at discrete points. The analysis showed that below 250 Hz tire tread behaves like a string under tension, while between 250 and 400 Hz it works like a beam with high material losses. At approximately 400 to 2000 Hz tread band has an input admittance similar to that of a flat plate and behaves like a two-dimensional bending waveguide. The model was then refined (Kropp, 1992) to simulate a smooth tire rolling over a rough pavement surface at a constant speed. The model was formulated in the time domain to capture the nonlinear interactions between tire tread and pavement surface. Tire responses were calculated with a convolution technique between the Green's functions and the contact forces. The functions were solved as an orthotropic plate under tension on an elastic "Winkler bedding" foundation. Larsson (2000) developed an approach to define the stiffness of individual springs in the bedding, in which the effect of local stiffness was included in the Green's functions directly. This model was found to agree well with field noise measurements up to 2500 Hz. A major limitation of this model is that it considers only the tire vibration and neglects the air displacement mechanisms. Moreover, tire rotating conditions are not properly reproduced and there is a lack of the complete description on sound radiation in this model.

Molisani et al. (2003) developed a closed form analytical model for the tire structure/acoustic cavity evaluation. The acoustic-structure coupled problem is solved simultaneously to incorporate the dynamics of tire cavity on the mechanical response of tire. The tire was modelled as an annular cylindrical shell where only the tire tread was assumed elastic and flexible. Tire sidewalls and wheel were considered rigid. The tire was assumed to be stationary without rotation and the external excitation was a point force acting normally to the tire tread. The equations of motion for this thin circular cylindrical shell follow the Donnell-Mushtari theory. The structural responses were expanded in terms of eigen-functions based on the analytical solutions

of the eigen-problem. The acoustic mode shapes and natural frequencies for a rigid annular cavity were derived in order to integrate the effects of tire acoustic cavity responses into the structural responses. The acoustic-structure interaction problem was solved based on the structure eigen-properties and the interior acoustic eigen-properties. The approach to solve this coupled problem was to include the force resulting from interior pressure into the tire's equations of motion, while the fluid force in turn depended on the tire structure responses. This model is more efficient in analysing the coupling between acoustic cavity and tire structure, comparing to the numerical simulations. Although case studies (Molisani et al., 2003) demonstrated the capability of this model in capturing the main mechanisms of the tire cavity acoustic effect on the tire dynamics, it has never been validated against measurements. The stationary tire framework and the point load excitation make the modeling different from reality. Furthermore, the assumptions of rigid tire sidewalls and single-layer thin shell tire significantly reduce the reliability in reproducing the real tire vibrations.

A more complex theoretical model for the structure-borne tire/road noise was developed by O'Boy and Dowling (2009). This model is able to predict the noise emission of a multilayer patterned tire rolling on a rough road surface. A viscoelastic multilayer tire belt model was first developed to derive tire vibration characteristics [see Figure 2.28 (a)]. Tire was modelled as an infinitely long cylinder with multilayer belt material. Each layer was assumed to be homogeneous isotropic viscoelastic. The boundary conditions on the inner belt surface included a mathematical representation of an inflated air cavity and the outer surface was exposed to the atmosphere with an localised force excitation. Mechanical responses on tire tread (displacement and velocity) could be determined with the material properties from tire design process. The authors then developed an approach to derive parameters for a simple bending plate model to yield equivalent responses as the multilayer tire belt. This equivalent bending plate model was further modified to make it capable to include the effect of tire sidewalls into the prediction of tire mechanical response. Transfer functions were

derived to relate the radial acceleration of tire surface to a normal force excitation on tire tread using the finite width tire plate [see Figure 2.28 (b)]. The accelerations on tire surface as the tire rolls over a rough pavement surface at a constant speed were next determined from the transfer functions and the contact force. The accelerations were used to predict the sound pressure distribution around the tire, taking the noise amplification due to horn effect into consideration. This model is capable to estimate the tire vibration characteristics and the structure-borne noise. It has been validated against experimental results with satisfactory agreements. This model employs a relatively complicated representation of tire tread and considers, to some extent, the effect of tire sidewalls and inflation pressure. However, the model focuses mainly on tire characteristics, thus does not appropriately consider pavement surface properties. It involves only the noise generated by tire vibration and amplified by the horn effect. Other mechanisms are neglected in the model formulation.

Some other theoretical models are also available in the literature. Kim (2003) studied the sound radiation from tire tread vibration using a circular ring model. This work led to further analysis on the flexural wave propagation in the tire shell using the plate and shell models (Kim et al., 2007). A spring-mass system, an elastically supported beam and a cylindrical shell model were adopted to investigate the tire vibrations at different frequency ranges respectively. The tire structure modes were then coupled with the inner cavity modes and the sound radiation from a tire shell could be derived. Berckmans et al. (2010) evaluated the tire noise emission using a sound synthesis technique with behaviouristic source models. The running tire is substituted by a monopole distribution covering the static tire. The quantification of the monopoles was based on both the tire vibration and airborne sources. Loudness and sharpness were taken as the output indexes in the evaluation to represent the perceived sound quality. Besides, researchers have developed some analytical models to describe the tire vibration characteristics, which may be further developed to provide noise prediction (Kim and Bolton, 2004; Kozhevnikov, 2012). A common

limitation of the analytical models is that they are mostly research-orientated and are difficult to be implemented in practice. The comprehensive theories lying behind the phenomena force the formulations to be complicated and make the solving process difficult. Due to the imperfection in tire mechanics and air acoustics theories, analytical models can actually only partially explain and replicate the mechanisms. Such models normally focus on one or two noise emission mechanisms (such as tire wall vibrations and horn effect) and neglect all the others (such as air pumping and acoustic resonance).

2.2.6.3 Numerical Models

Numerical methods (such as FEM, BEM and CFD) have been developed to simplify the mathematical formulation of physical problems and solve governing equations more efficiently. Clapp et al. (1987; 1988) proposed a three-step model to describe the noise generation based on the tire vibrations excited by contact pressure. The first step was named "excitation", where the contact pressure, footprint length and tread penetration in the tire/pavement contact patch were approximated from the surface texture effects. The problem was simplified as a rigid indenter contacting an elastic half plane. The pavement surface profile and tire inflation pressure were requested as the only input data in this step. In the second step a dynamic tire structural response model was developed. Orthotropic properties of tire ply materials were adopted and shell elements were used to define the tire carcass. The tire model was excited by a time varying pressure distribution resulting from the first step. The dynamic solutions of displacement and acceleration were Fourier transformed to derive the frequency response of tire/road interaction. In the third step, the noise radiation from a vibrating tire surface was computed by a finite element model. The acoustic domain was treated as a stationary compressible fluid and the sound waves were generated from a boundary with prescribed accelerations. The acoustic problem was then transformed to a structural dynamic problem by taking the fluid as a solid

with a zero shear strength. Although the dynamic tire model has been validated against experiments, the noise radiation results have not been validated. The fluid-structure analogy used in the model formulation may reduce the accuracy and reliability of the noise prediction. The three-step framework of this model established a general procedure for tire vibration noise analysis. Many later model developments followed this excitation-response-radiation workflow and made further improvements in the three modules.

A progress was achieved by the TINO model developed from the EU project "Measuring, understanding and reducing tire noise emission under realistic vehicle operation conditions including the contribution of the road surface" (Gelosa and Cervi, 1999; Guisset and Augusztinovicz, 1999). The tire vibrations were reproduced by a transient finite element approach and the noise radiation was modelled by the infinite element method. A numerical acoustic holography technique was developed using the inverse boundary element method (I-BEM) and validated against experimental results. Introducing the boundary element method and infinite element method into the noise radiation analysis simplified the representation of the acoustic field around a vibrating tire. The acoustic Helmholtz equation could be appropriately solved numerically, therefore, the efficiency of the "radiation" step was significantly improved in this model. However, the transient tire vibration model in the "response" step may be quite time and resource consuming, since very small time steps were necessary to replicate the high frequency noise and a sufficient total time was also needed to capture the low frequency characteristics. To overcome this shortcoming of the transient response model, tire vibration could be analyzed in the frequency domain rather than the time domain.

Nachenhorst (2004) made a significant improvement to the contact-induced rolling tire vibration analysis in frequency domain. Two challenges were identified for the model development, one is the physically correct description of rolling tire in a stationary framework and the other is the large mode density of tire structure at the

high frequencies (Brinkmeier and Nackenhorst, 2008). The first problem was solved using an arbitrary Lagrangian Eulerian (ALE) formulation and the second one was addressed by an approach for large-scale gyroscopic eigenvalue analysis. The weak form of the equation of motion was developed from the kinematic description of the ALE-formulation of rolling structure and an additional flux contribution describing the material motion was derived. The basic kinematic relations were presented within the large deformation framework. The contact status was formulated on the case of a deformable wheel rolling on a rigid surface. A complex eigenvalue analysis was then performed for this stationary rotating system. An efficient algorithm was developed based on a Lanczos-type subspace iteration with a proper numerical treatment of the eigenvalue problem. A large number of eigenvalues and eigenvectors can be solved efficiently by splitting frequency band and using shifting techniques. This stationary rolling tire vibration model was further developed to simulate the tire rolling noise (Brinkmeier et al., 2008). The normal velocities of tire surface were computed by a modal superposition approach with a frequency domain excitation derived from the pavement surface texture. Noise generated from the tire vibration was then calculated using the BEM approach, taking tire surface velocities as a boundary condition. The ALE formulation is successfully adopted to describe the rolling tire with a stationary framework in this model and the eigenvalues at high frequencies can be efficiently solved. These advantages make possible the analysis of tire/road noise in frequency domain. The main limitation of this model is that only the mechanical excitation due to pavement texture is considered and the acoustic characteristics of pavement surfaces remains neglected.

Another significant improvement was achieved by Kropp et al. (2012) in the modeling of sound radiation from rolling tires. The wave guide finite element method (WFEM) was adopted to develop an advanced tire response model, which was then integrated with a boundary element model (BEM) to predict the sound pressure level. The smooth tire was considered as a homogeneous wave guide in the circumference

direction. A 2D FE model of tire cross section was applied in the WFEM formulation and the tire vibration was described by a group of waves along the circumference. This formulation would lead to a set of coupled partial differential functions and their solutions could interpret the waves physically. The contact model was formulated in the time domain, where the tire structural responses to the time-varying forces were computed as a convolution between forces and impulse response functions. The latter was derived by inverse Fourier transformation from the WFEM results and transferred receptances in the frequency domain. A stationary tire relative motion framework was adopted, i.e. the contact patch was rotating around the tire. With the contact geometry and forces obtained from the contact model, cross section modes and circumferential waves were derived from kinetic equations and the vibration field on tire was composed of lateral modes combined with the waves propagating around the tire. Some examples of low-order modes are illustrated in Figure 2.29. This tire vibration served as an input in the BEM radiation model where the horn effect was also involved. The model included an impedance plane to describe the pavement reflection and absorption by means of an appropriate Green's function (Brick, 2009). The overall model was validated against some noise measurements on an ISO replica surface with, somehow, a grooved tire. The numerical results showed very good agreements to experimental measurements. This is one of the most advanced tire/road noise models up to date. It can efficiently calculate the tire response and sound radiation. It is also capable to take the pavement texture and acoustic absorption into consideration. Although the model should be able to include the pavement acoustic property, the model validation on porous pavements has not been presented. Due to the homogeneous wave guide assumption, the model is only valid for smooth tires and may need further developments to cover patterned tires. Besides, similar to other tire vibration noise models, the air-related generation mechanisms are not considered.

Yang (2013) recently developed a computational fluid dynamic (CFD) model to predict the noise emission from a rolling tire, attempting to combine the air-related

mechanisms with the FEM tire vibration simulation. This model worked in the time domain, physically modeling the tire and pavement using shall elements in an FEM structure sub-model and modeling the surrounding air using tetrahedral elements in a CFD fluid sub-model. The fluid-structure interaction (FSI) algorithm was adopted to connect the two sub-models and transfer data between them. A smooth tire rolling on a smooth pavement at a constant speed was simulated in the structure sub-model with a stationary rolling frame of reference, where a standing tire was rotating around its axle without translational displacement and the pavement surface moved horizontally towards the stationary tire at the traveling speed. The tire surface displacements were calculated and transferred to the fluid sub-model, where the stationary air was excited by the boundary movement and the air pressure variation was captured as the sound radiation. The turbulence effect was considered using the large eddy simulation and the adaptive mesh approach was adopted to automatically adjust the element sizes and shapes according to the calculation results. This model was validated against the experimental measurements. The primary advantage of this model is that it simulates more mechanisms than the tire vibration, such as the aerodynamic effect and horn effect. However, the pavement texture is not considered in the tire vibration modeling, which may make the model inadequate for the rough pavement surfaces. The air is set stationary without a relative motion towards the tire axle, which restricts the model's capability to simulate the air pumping effect. The effect of pavement porosity on tire/road noise is not included in this model, although it has the potential to be simulated on porous surfaces.

There are many other numerical models available in the literature that simulate different tire/road noise mechanisms. The representatives include the FEM model on the horn effect introduced by Graf et al. (2002), the modal tire model developed by Gauterin and Ropers (2005), the prediction of air-pumping noise described by Kim et al. (2006) and the representation of porous pavements in BEM models proposed by Anfosso-Lédée et al. (2007). The existing works illustrate the

potential of numerical modeling in the tire/road noise simulation and prediction. More and more mechanisms have been investigated using numerical models. The formulation of numerical models is much simpler comparing to that of theoretical models, provided various commercial software available, and its efficiency is improved significantly with the development in computational capacity. However, there is still a lack of validated numerical model to evaluate the tire/road noise on porous pavements. This restricts the understanding of tire/road noise mechanisms on porous pavement and limits the applications of porous pavements in the traffic noise reduction.

This section extensively reviewed past research on tire/road noise with emphasis on experimental studies and model developments. Tire vibration and air pumping effects are identified as the kay noise generation mechanisms, and horn effect is believed to have a significant influence on tire/road noise amplification. Pavement surface textures and its acoustic absorption are found to be the most essential influencing factors to tire/road noise, with regard to pavement properties, and the increase of noise level with increasing vehicle speed is very significant. Porous pavement is found to be effective in the abatement of tire/road noise, and the noise reduction effect can be optimized through appropriate porous mixture design. Tire/road noise modeling has achieved significant progress in recent years. However, numerical simulation of tire/road noise on porous pavement is still unavailable to date.

2.3 Summary

This chapter has reviewed past research works on skid resistance and tire/road noise, covering generation mechanisms, measurement approaches, influencing factors, porous pavement effects and prediction models.

Skid resistance mechanisms can be interpreted by the classical rubber friction theories. The elasto-hydrodynamic lubrication theory explains the reduction of frictional force on wet pavements, which can be described by the three-zone model.

Among the various skid resistance measurement approaches, lock-wheel trailer test is a well-developed and widely-used standard method. It evaluates the most adverse skidding situation for a braking vehicle. From extensive experimental measurements, pavement surface characteristics, tire properties, vehicle speed and environmental factors are found influential on skid resistance. Pavement texture and water film thickness are identified as key influencing factors. Porous pavement exhibits superior skid resistance performance from its higher macrotexture and inner drainage capacity. These features help to reduce water film thickness and discharge water from tire-pavement interface, so that high friction can be better maintained at high speeds. Numerical tire-water-pavement interaction models have been developed for dense-graded pavements to simulate lock-wheel test and predict skid number. These models are complements to experimental studies and help to understand skid resistance phenomenon. However, no numerical skid resistance model for porous pavements is currently available.

Tire vibration and air pumping are identified as the dominant noise generation mechanisms. Horn effect significantly amplifies the noise generated near the contact patch. The near-field measurement techniques (such as CPX and OBSI methods) are superbly suitable for tire/road noise investigation and serve as the most appropriate tire/road noise measuring method to date. Vehicle operations, tire characteristics, pavement properties and environmental conditions can affect tire/road noise. For a pavement surface, macrotexture and acoustic absorption are the most important properties determining its acoustical performance. Porous pavement provides negative macrotexture and higher acoustic absorption, which can aid in tire/road noise reduction. The noise reduction effect can be optimized in the porous mixture design by adjusting porosity, tortuosity, airflow resistance and porous layer thickness. Past studies have demonstrated the potential of numerical methods in tire/road noise modeling. However, due to the complexity of tire/road noise phenomenon, none of existing models can include many mechanisms or influencing

factors, and the valid numerical simulation model for tire/road noise prediction on porous pavement is still unavailable to date.

2.4 Research Needs and Scope of Work

From the extensive literature review conducted in this chapter, it is concluded that existing experimental studies are insufficient to allow a thorough understanding on the mechanisms of skid resistance and tire/road noise on porous pavements. The lack of appropriate numerical models discourages the optimization of porous pavement functional performance. Porous pavement design, therefore, fails to directly consider the frictional and acoustical performances simultaneously. To address this problem, the following research needs are identified.

- To develop numerical simulation models of skid resistance and tire/road noise for porous pavements, with proper representations of the porous layer properties.
- To analyze the phenomena of skid resistance improvement and tire/road noise reduction on porous pavements and to quantify the effects of major factors affecting porous pavement frictional and acoustical performances.
- To optimize the functional performances of porous pavements according to the numerical results and to improve the porous mixture design process to include the consideration of functional performances.

The primary objective of this study is to develop and apply numerical models to analyze the skid resistance and tire/road noise on porous pavements. The numerical simulations are cost- and time-saving and are easy to be implemented. They can serve as a complementary research approach to experimental studies. This study should enhance the understanding in the mechanisms of skid resistance and tire/road noise on porous pavements and provide a clear picture on the influencing factors. When integrated with existing design practices, the findings in this study should be able to predict the functional performance of finished porous pavements and could be used to optimize the mixture design. Furthermore, the models and analyses could also be

used in the maintenance management of porous pavements to help in deciding the maintenance strategies.

The present study will focus on the simulations of lock-wheel trailer skidding test and close-proximity noise measurement. These two tests are the most popularly used methods to date and the test conditions are clearly defined in the specifications. Only the simple situation of straight traveling of vehicles at a constant speed is considered, since it is the standard test scenario and also the most common traveling condition on roads. Moreover, to simplify the problem and focus on pavement properties, only smooth tires with no tread patterns are adopted in the current simulation models. This is also because smooth tire experiences the most adverse skid resistance on wet pavements and generates a noise level with no much difference from that of a treaded tire on porous pavements. Based on the scope of this work, the following tasks are identified to be carried out in the remaining chapters.

- To develop a numerical methodology to replicate the drainage capacity of porous pavements using the finite element method, and apply this approach in the skid resistance modeling of porous pavements. The resulted overall FE model should be able to simulate the ASTM E274 lock-wheel trailer test on porous pavements and should be validated against experimental data.
- To develop an analytical framework to compare the frictional performance of porous and non-porous pavements under the same condition. This framework is then used to explain the mechanisms of skid resistance improvement on porous pavements and analyze the effects of major factors (such as porosity, porous layer thickness, rainfall intensity and vehicle speed) that can affect skid resistance on a porous pavement.
- To develop a numerical model simulating the close-proximity tire/road noise measurement according to ISO 11819-2 specification. The model should cover the major noise generation, amplification and reduction mechanisms, such as the

tire vibration, horn effect and pavement acoustic absorption. It may involve both the finite element method and the boundary element method. The model needs to be calibrated and validated against the experimental measurements as well.

- To apply the tire/road noise model to compare the noise levels on porous and non-porous pavements, and explain the mechanisms. The developed model is then used to analyzed the effects of major factors affecting porous pavement acoustical performance. These factors include porosity, porous layer thickness, surface texture and vehicle speed.
- To integrate skid resistance and tire/road noise performances into porous pavement design. The developed models serve as a tool to predict the frictional and acoustical performances of the finished porous pavement in the design phase and the extensive analysis results are used to optimize the mixture design. The identification of key variables and design criteria is an essential challenge in this task, as well as the valuation of safety and comfort benefits.

Table 2.1: Major mechanisms in tire/road noise generation and amplification

<table>
<tr><td rowspan="6">Generation mechanisms</td><td rowspan="4">Structure-borne mechanisms</td><td rowspan="3">Impact-induced vibration</td><td>Tread impact</td></tr>
<tr><td>Texture impact</td></tr>
<tr><td>Running deflection</td></tr>
<tr><td rowspan="2">Friction/adhesion-induced vibration</td><td>Stick-slip</td></tr>
<tr><td>Stick-snap</td></tr>
<tr><td colspan="2" rowspan="2">Air-borne mechanisms</td><td>Air pumping</td></tr>
<tr><td>Air turbulence</td></tr>
<tr><td rowspan="4">Amplification mechanisms</td><td colspan="2">Tire-pavement configuration</td><td>Horn effect</td></tr>
<tr><td colspan="2">Tire carcass</td><td>Cavity resonance</td></tr>
<tr><td colspan="2" rowspan="2">Tread patterns</td><td>Helmholtz resonance</td></tr>
<tr><td>Pipe resonance</td></tr>
</table>

Table 2.2: Effects of major influencing factors on tire/road noise variation (Sandberg and Ejsmont, 2002)

Influencing factor	Noise level variation (dB)
Vehicle speed (30-130 km/h)	25
Road surface (conventional)	9
Road surface (including extremes)	17
Truck tire type (same width)	10
Car tire type (same width)	8
Car tire type (including width influence)	10
Studs in tire	8
Wheel load and tire inflation (±25%)	5
Road condition (wet/dry)	5
Temperature (0-40°C)	4
Torque on wheel (0-3 m/s^2 acceleration)	3

Table 2.3: Coefficients in the linear equation describing the speed-dependency of tire/road noise

Source	A	B	Method	Remarks
Anonymous (1971)	24.1	30.5	CB	Truck, rib
	9.3	41.6		Truck, Lug
Steven and Pauls (1990)	26.2	32.9	CPX	Porous 0/5
	27.3	33.5		Porous 0/8
	23.4	37.3		ISO surface
	24.4	36.9		SMA 0/5
	24.6	37.2		Surface dressing
	21.9	39.9		PCC pavement
	27.9	35.5		AC 0/11
	27.1	36.7		Asphalt 0/11
Ivannikov et al. (1998)	7.1	37.6	CB	ISO surface
	11.8	36.3		SMA
	10.7	36.8		porous
Steven et al. (2000)	30.6	34.9	CPX	AC 0/16 with chippings on surface
	33.5	33.0		SMA 0/4
	34.2	32.6		SMA 0/6
	30.4	34.9		SMA 0/8
	27.8	37.0		Surface dressing 5/8
	39.5	29.2		Porous 6/16
	37.1	29.0		Porous 4/8+11/16
	34.4	29.2		Porous 2/4+11/16
	38.9	30.9		Gussasphalt 0/11+2/5+5/8
	20.3	42.0		PCC transversely brushed
	32.7	34.2		PCC with epoxy-durop 3/4
	24.3	37.8		PCC burlap drag
	27.6	36.9		PCC exposed aggregate

Table 2.4: Potential influences of pavement properties on tire/road noise (Sandberg and Ejsmont, 2002)

Parameter	Degree of influence
Macrotexture	Very high
Megatexture	High
Microtexture	Low to moderate
Unevenness	Minor
Porosity	Very high
Porous layer thickness	High
Adhesion	Low to moderate
Friction	Low to moderate
Stiffness	Uncertain

Table 2.5: Noise reduction on porous pavements in selected countries

Country	Noise reduction [dB(A)]
Denmark	3 to 5
The Netherland	more than 3 to 5
United Kingdom	5 to 6
France	more than 5
United States	3 to 6
Sweden	7 to 12
Switzerland	7 to 9
China	3 to 6
Japan	4 to 6

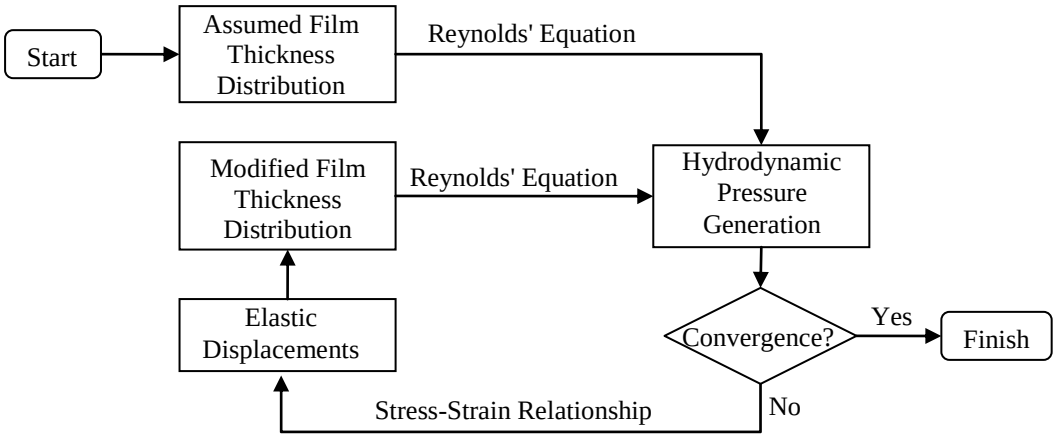

Figure 2.1: General iterative procedure for elasto-hydrodynamic lubrication

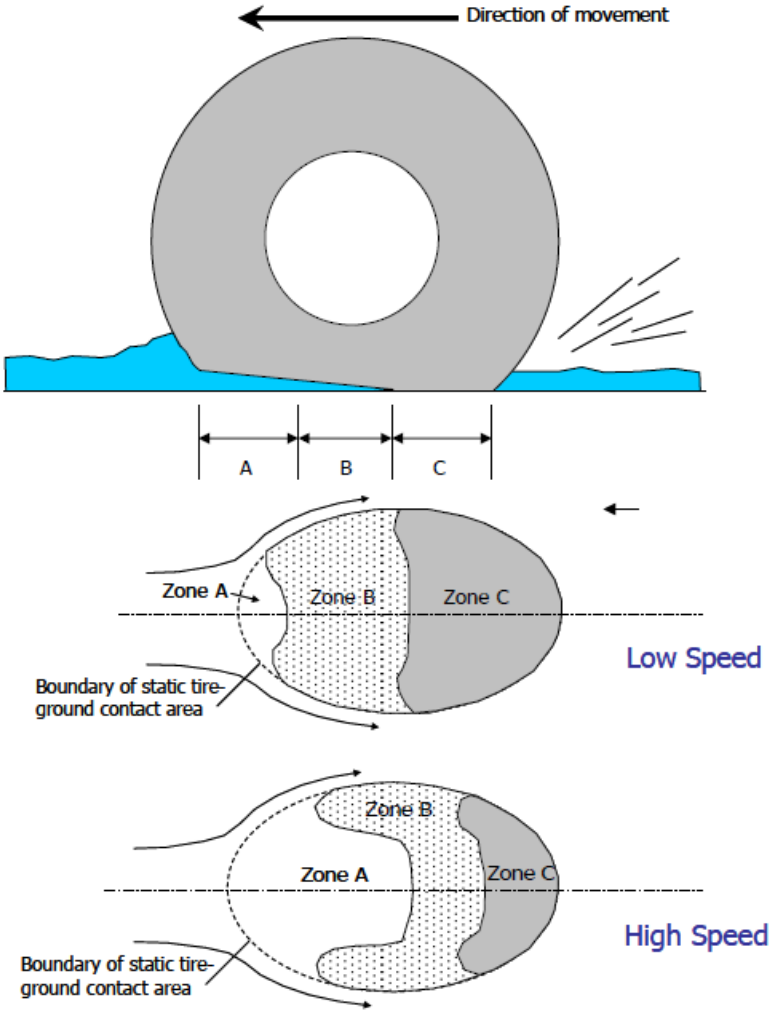

Figure 2.2: Three-zone model for sliding tire on wet pavement (Moore, 1966)

Figure 2.3: British pendulum tester

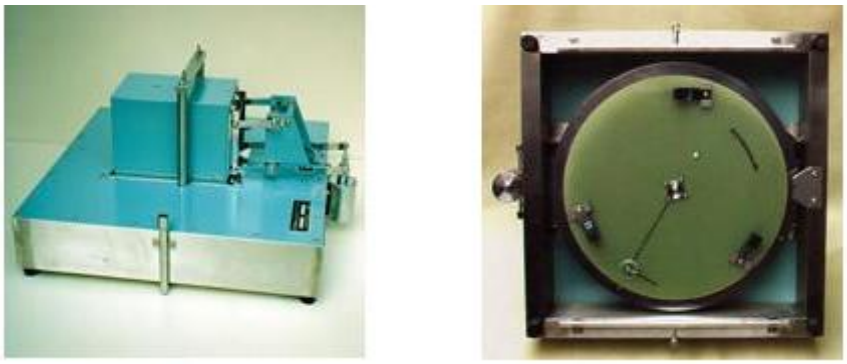

Figure 2.4: Dynamic friction tester

Figure 2.5: Accelerated polishing machine

Figure 2.6: Lock-wheel skid resistance trailer

Figure 2.7: Griptester

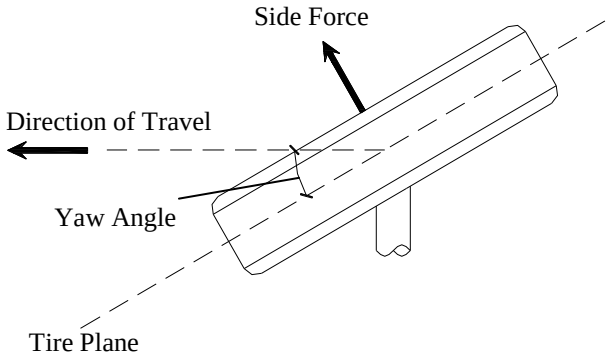

Figure 2.8: Side force and yaw angle

Figure 2.9: Mu-meter

Figure 2.10: Sideway-force coefficient routine investigation machine (SCRIM)

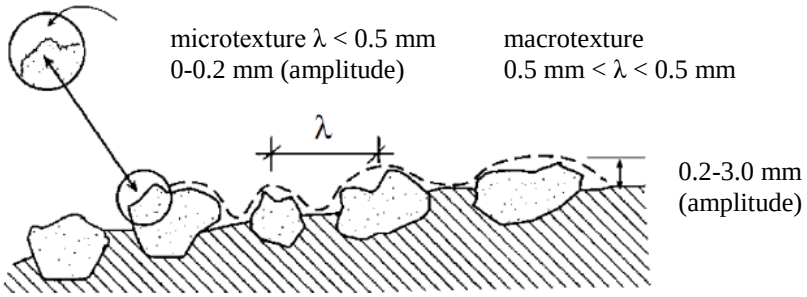

Figure 2.11: Pavement microtexture and macrotexture (Flintsch et al., 2003)

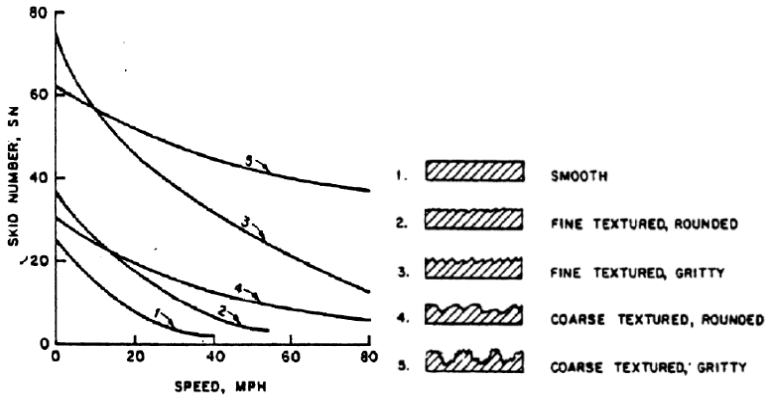

Figure 2.12: Skid numbers of different texture characteristics (Sabey, 1966)

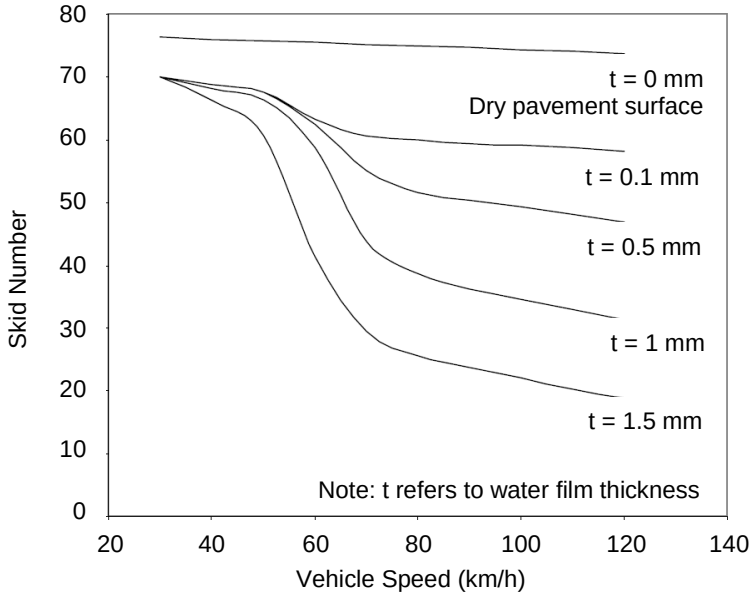

Figure 2.13: Effects of vehicle speed and water film thickness on skid number (Benedetto, 2002)

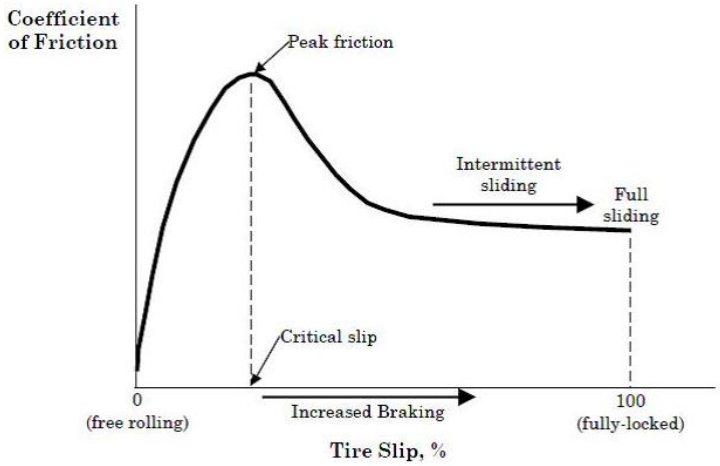

Figure 2.14: Friction coefficient at different slip ratios (Hall et al., 2009)

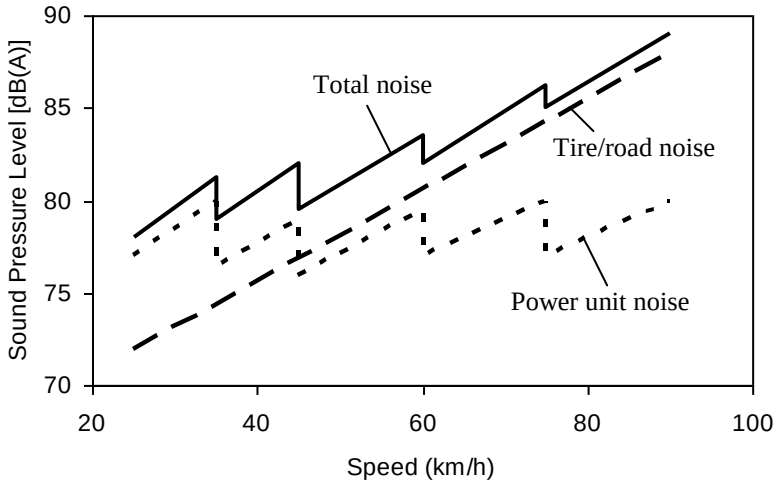

Figure 2.15: Illustrative relationship of tire/road noise and power unit noise with vehicle speed (Rasmussen et al. 2007)

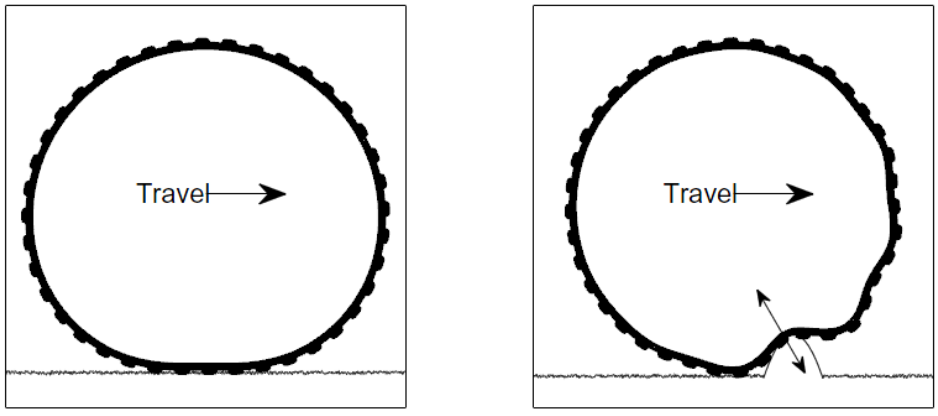

Figure 2.16: Texture impact and resulted tire vibration (not to scale) (Dare, 2012)

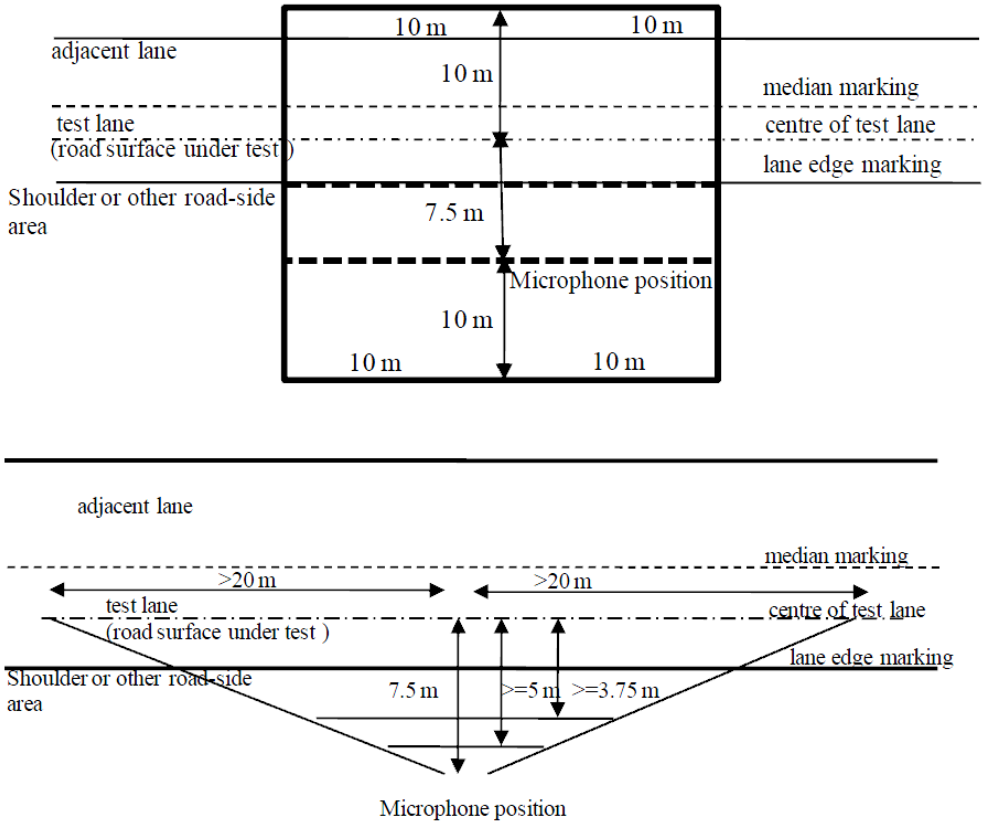

Figure 2.17: Test site configuration in SPB measurement (ISO, 1997a)

Figure 2.18: CPX trailer (Bakker et al., 2012)

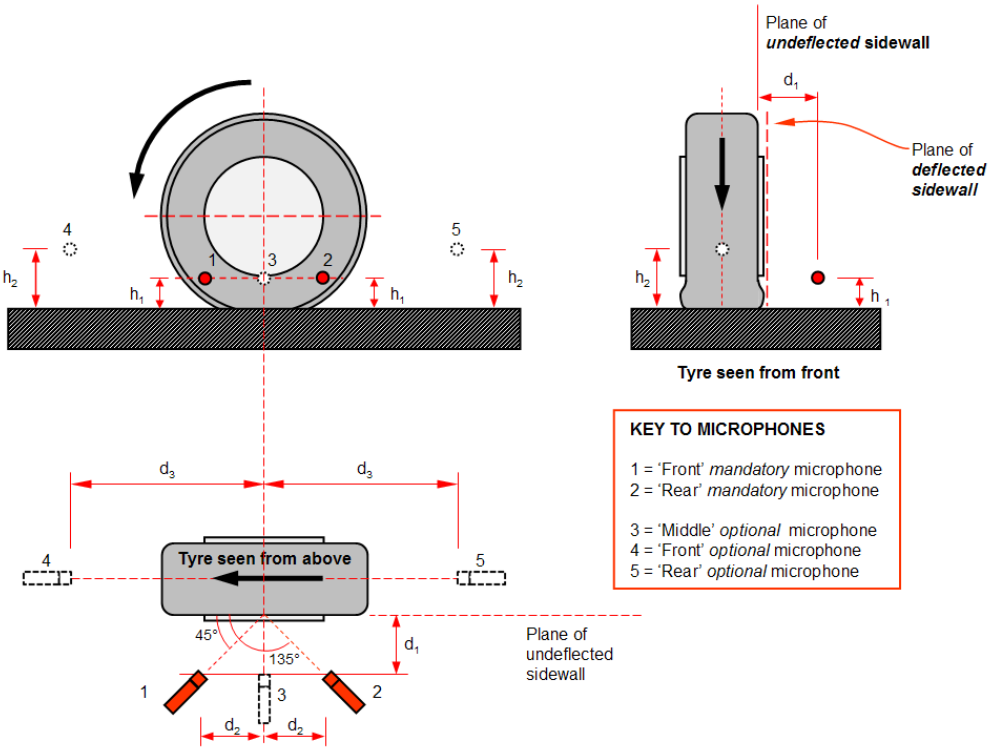

Figure 2.19: Microphone positions in CPX measurement (ISO, 2013)

(a) CPX reference tire P1

(b) CPX Reference tire H1

Figure 2.20: CPX reference tires and tread patterns (Bakker et al., 2012)

(a) Single probe (b) Dual probe

Figure 2.21: Configuration of OBSI measurement (Rasmussen et al., 2011)

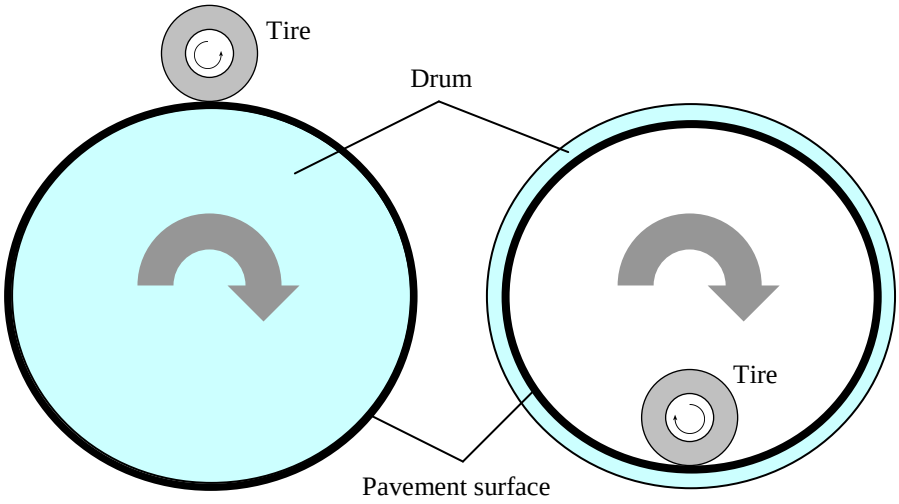

(a) Outer drum (b) Inner drum

Figure 2.22: Illustration of the two types of drum facilities used in laboratory

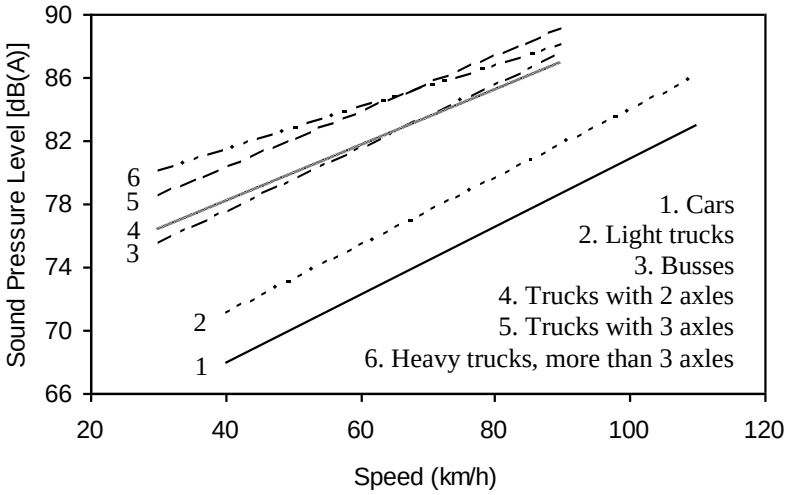

Figure 2.23: Illustrations of the speed dependency of tire/road noise

(a) Positive texture (b) Negative texture

Figure 2.24: Pavement texture direction

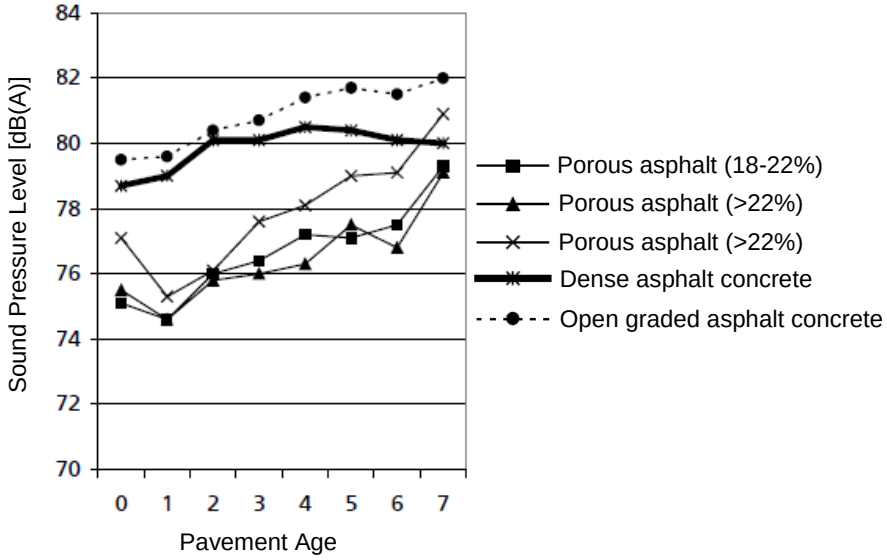

Figure 2.25: Noise level variations of different surface types with pavement age (Bendtsen, 1998)

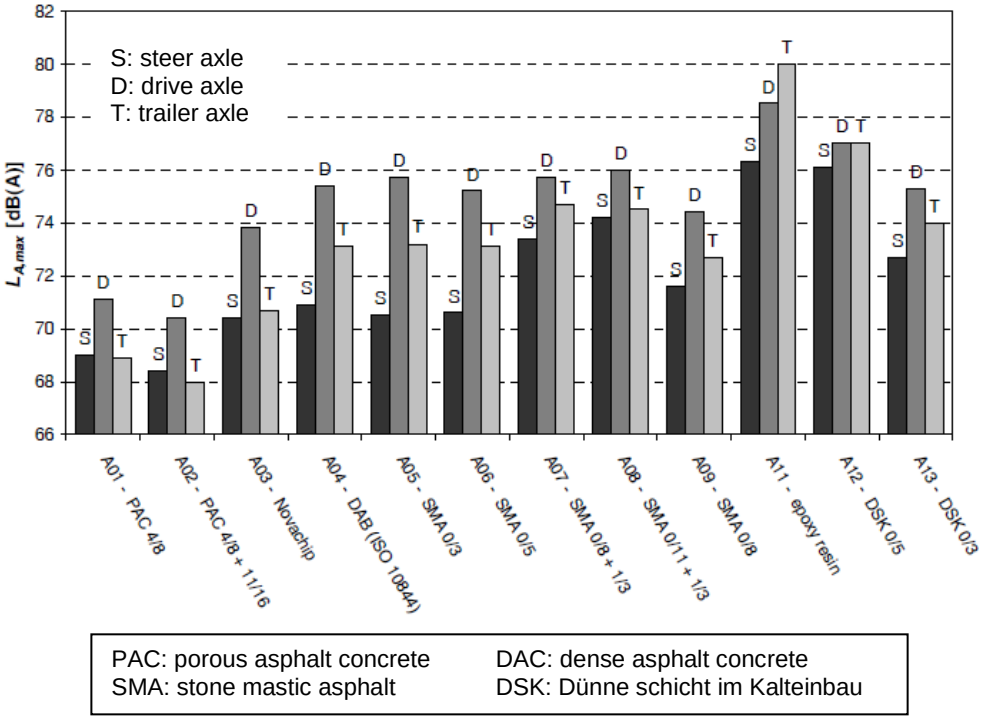

Figure 2.26: Measured sound levels on different types of pavement surfaces (der Graaff et al., 2005)

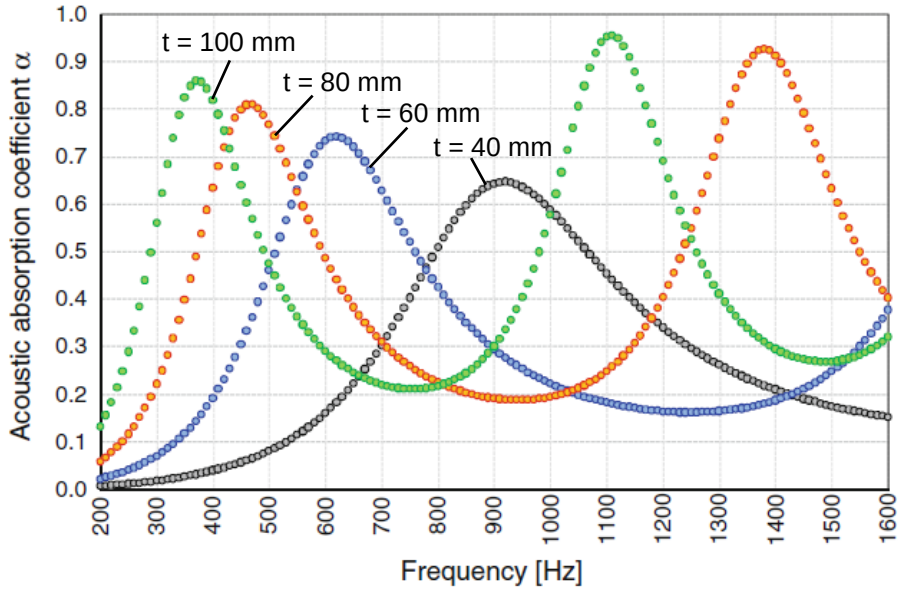

Figure 2.27: Acoustic absorption spectra of porous layers with different thicknesses (Losa and Leandri, 2012)

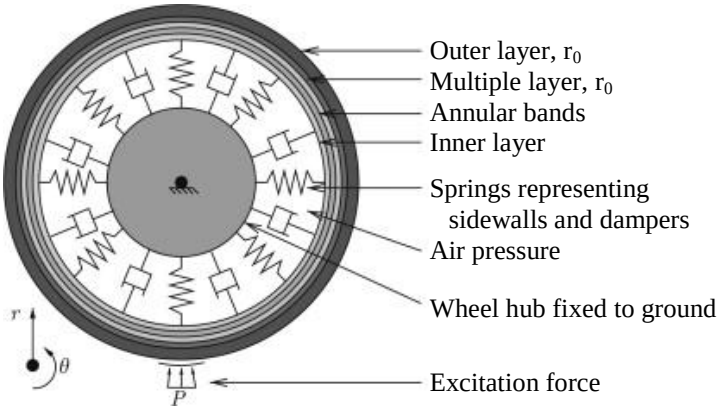

(a) Complete viscoelastic cylindrical model or the tyre belt

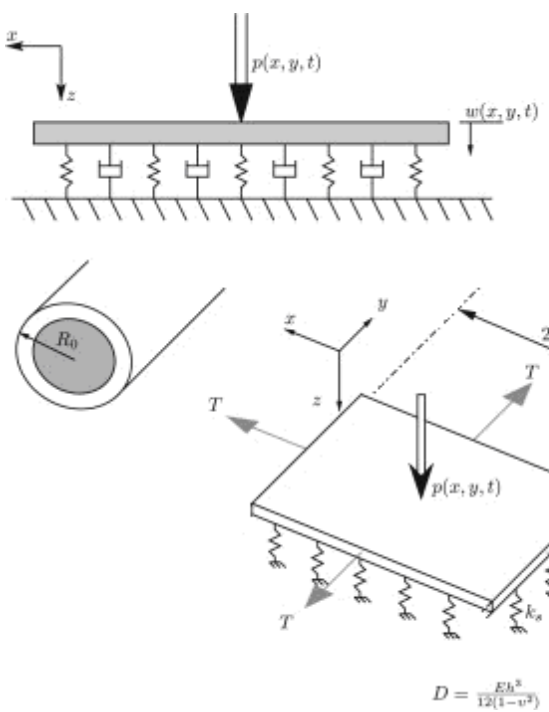

p: applied load per unit area
w: normal displacement
x, *y*: plane coordinate
t: time
h: thickness
R_0: radius of tire
E: Young's modulus
v: Poisson's ratio
D: bending stiffness
T: in-plane tension

(b) A thin bending plate with finite width and in-plane tension

Figure 2.28: O'Boy and Dowling's model (2009)

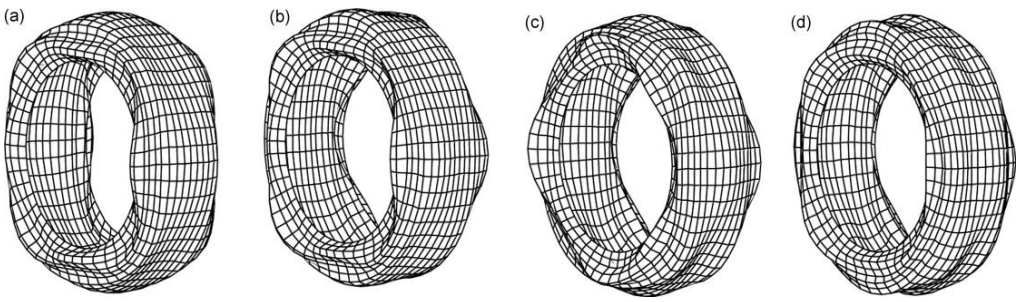

Figure 2.29: Examples of low-order modes in the WFEM model developed by Kropp et al. (2012)

CHAPTER 3 DEVELOPMENT OF NUMERICAL MODEL FOR SKID RESISTANCE ON POROUS PAVEMENT

With the rapid development in computational power, numerical simulation has been widely used in pavement research in recent decades. Although it cannot fully replace the need for experiments, it provides a less expensive and more efficient alternative. This chapter presents the development of a numerical simulation model for skid resistance on porous pavements. The critical issues in developing such a model are first addressed, followed by a description on the numerical modeling using finite element method. The core of this simulation model is to appropriately reproduce the drainage capacity of porous pavements. An iterative process based on a structural grid pore network is proposed to model the porous pavement layer with consideration on porosity, permeability and clogging. This porous pavement model is then integrated with a tire model and a fluid model to simulate tire-pavement-fluid interaction occurring near the tire-pavement contact patch. The overall porous pavement skid resistance model is then validated against experimental measurements.

3.1 Issues Considered in Modeling Skid Resistance on Porous Pavement

The wet skid resistance on porous pavement is a complex phenomenon involving various mechanisms. Its modeling requires both finite element method (FEM) and computational fluid dynamics (CFD) formulation. In the simulation of porous pavement skid resistance, following issues should be considered numerically in order to get more accurate results.

3.1.1 Tire-Pavement Contact

The interactions between tire and pavement are critical in skid resistance modeling. A numerical study conducted by Ong and Fwa (2007a) has indicated the importance of realistic contact modeling in the prediction of skid resistance on conventional smooth pavements. The adopted non-linear contact algorithm must

include friction computation so that tire footprints at different wheel loads, as well as contact and friction forces, could be reproduced closely.

3.1.2 Fluid-Structure Interaction

The interaction between water on road surface and the pneumatic tire is an important element in wet-pavement skid resistance and has to be properly addressed. It includes the hydrodynamic pressure applied on tire tread by water and the effect of tire deformation on water flow. It should be a two-way coupling process, where fluid force is transferred to the solid model and solid deformation is transferred back to the fluid model. The iteration continues until errors in both pressure and displacement satisfy certain convergence requirements.

3.1.3 Tire Deformation Behavior

Tire deformations under loading have to be correctly described in the simulation model. The deformed tire geometry is essential to model water flow patterns and hydrodynamic pressure underneath and around the tire. The entire tire structure should be modeled with different material properties for different tire components (i.e. rim, sidewall and tread). The modeling of tire behavior can be calibrated through a comparison between the simulated tire footprints and experimental measurements under different wheel loads.

3.1.4 Turbulence in Fluid Flow

Previous studies (Chuai, 1998; Ranieri et al., 2012) have already shown that the water flow within porous layers is turbulent rather than laminar Moreover, water flow under tires is also found to be turbulent due to the high relative velocity and small flow channel dimensions (Schlichting, 1960). Various numerical formulations are available to date to simulate the turbulent flow and special care should be placed when selecting appropriate turbulence model and calibrating model parameters.

3.1.5 Multiphase Flow

In the moving wheel frame of reference proposed by Ong and Fwa (2007a), both water and air are moving towards the stationary tire. Although the uplift and drag forces applied on the tire tread by air are relatively small comparing to those by water, it is still necessary to properly capture the free surface at water-air interface because it provides a simple way to control the inlet water quantity during the simulation process. The modeling of water-air interaction could be attained using a multiphase flow algorithm such as the volume of fluid (VOF) method (Hirt and Nichols, 1981).

3.1.6 Drainage Capacity of Porous Media

Experimental studies have implied that the superior skid resistance on porous pavement may be a result of its inner drainage channels and surface macrotexture. These features significantly influence the under-tire drainage capacity at high speeds, which is essential for deterring skid resistance loss with increasing sliding speed. Therefore, it is important for porous pavement skid resistance models to accurately simulate the drainage capacity of porous surfaces. As drainage capacity depends on randomly distributed pores and channels within a porous layer, it is extremely challenging to reproduce such a pore structure in the porous pavement. As such, some reasonable simplifications are necessary to solve this complex problem numerically.

Four of the problems discussed above, i.e. the tire-pavement contact, flow-structure interaction, tire deforming behavior and turbulence flow, have already been addressed by Ong and Fwa (2007a) in their previous studies on skid resistance modeling of conventional smooth pavements. Although a different software package is used in their work, similar modeling methods and algorithms could be applied. The multiphase flow has been considered in another model proposed by Ong and Fwa (2006) in a numerical study on hydroplaning. That application, despite the lack of flow-structure interaction, provided useful insights on the modeling of multiphase

flow in skid resistance simulations. However, the drainage capacity of porous pavements has never been included in their skid resistance simulations. This research focuses on the modeling of porous surface layers using a geometrically simple pore structure network which is capable to provide the same drainage capacity as in-situ porous pavements. Parameters such as porosity, permeability, clogging percentage and outflow time may be used as indicators of drainage capacity in this study.

3.2 Numerical Representation of the Drainage Capacity of Porous Pavement

Most of the benefits provided by a porous pavement come from the higher percentage of air voids within the porous mixture and the associated inner drainage capacity as a result of the interconnected pores. To date, studies on porous pavement permeability are mainly experimental in nature. There are a few research studies exploring the numerical simulations of water flow within the porous surface layer (Abustan et al., 2012; Umiliaco and Benedetto, 2012; Benedetto and Umiliaco, 2014). Such models are essential for numerical modeling of skid resistance on porous pavements. This section therefore introduces a model that can reproduce the drainage capacity of in-situ porous pavements. Noting that it is almost impossible to rebuild the actual pore structure of a porous surface layer in a full-scale skid resistance model, a grid pore network is proposed to geometrically simplify the drainage channels in the porous layer. Through a simulation of outflow tests, dimensions of the pore network are determined by an iterative process. This porous pavement model is then validated against past experimental results. It can be applied in the numerical simulations of porous pavement skid resistance.

3.2.1 Concepts of Permeability and Hydraulic Conductivity

Permeability, commonly symbolized as κ, is a measure of the ability of a porous media to allow fluids to pass through it. Hydraulic conductivity, symbolically represented as k, is a property of porous material that describes the ease with which

fluids can move through its pore spaces. The hydraulic conductivity depends on the intrinsic permeability of a porous media and its degree of saturation. The relationship between permeability and hydraulic conductivity is

$$\kappa = k\frac{\mu}{\rho g} \tag{3.1}$$

where μ is the fluid dynamic viscosity, ρ is the fluid density, and g is the acceleration due to gravity. Hydraulic conductivity is also known as the permeability coefficient. In practice, it is more convenient to measure the hydraulic conductivity through a constant-head or falling-head outflow test before converting the result to permeability.

Darcy's law indicates that the instantaneous discharge rate through a porous medium is proportional to the viscosity of the fluid and the pressure drop over a given distance. Three-dimensional hydraulic conductivity for Darcy flow could be derived from the steady-state continuity equation (Charbeneau et al., 2011). For an isotropic porous specimen located in cylindrical coordinates (see Figure 3.1), the continuity equation is

$$\frac{1}{r}\frac{\partial}{\partial r}\left(r\frac{\partial h}{\partial r}\right)+\frac{\partial^2 h}{\partial z^2}=0 \tag{3.2}$$

and the boundary conditions are expressed as:

$$h(r,z)=h_s(t) \qquad \left[0\le r\le R_s; z=0\right] \tag{3.3}$$

$$h(r,z)=0 \qquad \left[r=R_c; 0\le z\le b_c\right] \tag{3.4}$$

$$\frac{\partial h(r,z)}{\partial z}=0 \qquad \left[R_s<r\le R_c; z=0\right] \tag{3.5}$$

$$\frac{\partial h(r,z)}{\partial z}=0 \qquad \left[0\le r\le R_c; z=b_c\right] \tag{3.6}$$

where R_s is the radius of standpipe, h is the hydraulic head, R_c is the radius of porous specimen and b_c is the specimen thickness. r and z are the coordinates in radial and vertical directions respectively.

Assuming that R_c and b_c are infinite, the solution of the above equations is

given by Carslaw & Jaeger (1959) as:

$$h(r,z) = \frac{2}{\pi} h_s \sin^{-1}\left(\frac{2R_s}{\sqrt{(r-R_s)^2 + z^2} + \sqrt{(r+R_s)^2 + z^2}} \right) \tag{3.7}$$

It is related to the discharge (Q) through

$$Q = -2\pi k \int_0^{R_s} r \frac{\partial h(r,0)}{\partial z} dr = 4kh_s R_s \tag{3.8}$$

where k is the isotropic hydraulic conductivity of the porous material. The effect of finite specimen dimensions is addressed approximately by a shape factor F, which is a function of specimen size and standpipe radius, and is independent of the standpipe head h_s, as follows:

$$F = F\left(\frac{R_s}{R_c}, \frac{b_c}{R_c} \right) \tag{3.9}$$

The isotropic hydraulic conductivity k can then be computed as:

$$k = \frac{Q}{4h_s R_s F} \tag{3.10}$$

The inertial effects caused by head gradients usually result in non-Darcy flow in permeability tests. To take account of the nonlinear effect, a heuristic correlation can be made and the following relationship is proposed (Chuai, 1998):

$$i = pv^n \tag{3.11}$$

Where i is hydraulic gradient, v is head falling velocity, n is an index determined from the experiments and can vary from 1 to 2. An n value of 1 indicates fully laminar flow, while a value of 2 represents fully turbulent flow. p is an empirical parameter. After rearranging Equation (3.11), a modified equation is obtained as:

$$v = ki^m \tag{3.12}$$

where k is the pseudo hydraulic conductivity and m is the flow condition index (m = 1 indicates a fully laminar flow and m = 0.5 represents a fully turbulent flow). Applying the natural logarithmic to Equation (3.12), we get

$$\ln(v) = \ln(k) + m\ln(i) \tag{3.13}$$

For a falling-head outflow test, the variation of standpipe head with time (t) can be approximated with a cubic function:

$$h = a_0 + a_1 t + a_2 t^2 + a_3 t^3 \tag{3.14}$$

The average velocity of falling hydraulic head is computed by differentiating Equation (3.14) with respect to time:

$$v = \frac{dh}{dt} = a_1 + a_2 t + a_3 t^2 \tag{3.15}$$

Noting that $i = h/l$ (where h is the hydraulic head measured from the bottom of the porous sample and l is the thickness of the sample), the values of v and i can be derived from test data at different times t. Permeability k can then be obtained through linear regression, using Equation (3.13). For a constant-head test, the flow rate Q is measured at different hydraulic gradients i, and the corresponding head-falling velocities v can be easily derived from the flow rate and outflow meter dimension.

3.2.2 Modeling the Drainage Capacity of Porous Pavement

Although the permeability of a porous surface layer is closely related to its porosity, using porosity alone to predict porous pavement permeability is inadequate and perhaps misleading (Chuai, 1998; Liu and Cao, 2009; Kuang et al., 2011) due to the following reasons: (a) the nominal air void content includes closed pores which contribute little to drainage capacity; (b) pore clogging affects the drainage capacity significantly, and is difficult to be quantified by existing porosity measuring methods; (c) the size of each single pore and the tortuosity of capillaries also have an influence on drainage capacity. Therefore, besides porosity, other drainage-related parameters, such as outflow time, clogging percentage and pore dimension, have to be considered.

This work attempts to develop a pore network model that is computationally efficient for drainage capacity and skid resistance modeling applications. The model

geometry (see Figure 3.2) has straight channels in all the longitudinal, transverse and vertical directions with a cubic pore element spatially repeated in the three directions. Two variables are required to specify this structure, namely the edge length of each drainage channel as denoted by *x*, and the distance between centers of two successive parallel channels (i.e. the edge length of a cubic pore element) as denoted by *y*. The ratio between *x* and *y* is constant (i.e. $x/y = c$) for a specific porosity ϕ.

$$\phi = \frac{V_{pore}}{V_{total}} = \frac{3x^2 y - 2x^3}{y^3} = c^2\left(3 - 2c\right) \tag{3.16}$$

A family of infinite pairs of x and y is available to provide the same ratio, and it cannot guarantee the desired drainage capacity. Therefore, an iterative process has been developed to determine the parameters of this grid pore network structure (i.e. *x* and *y*). The computational framework is shown in Figure 3.3. A minimum feasible *x* value is predetermined based on the computational capacity of the computers so that the pores are not too small as it may result in the problem size being overly large. A maximum clogging percentage is preset based on engineering experience. This is the clogging level at which a porous surface basically loses its inner drainage capacity. The convergence criterion is a sufficiently small residual between the numerical and experimental results, typically set at 5%. As an initialization step, a nominal porosity ϕ_0 can be obtained from design mixtures or pavement cores and the initial clogging percentage is set as 0%. With the ratio *c* (= *x/y*) calculated from the nominal porosity, the initial *x* and *y* values can be determined using the findings from previous studies [e.g. Acharya et al. (2004) or Xu & Yu (2008)].

A numerical simulation of constant-head or falling-head outflow tests can be performed on the proposed porous pavement model. Figure 3.4 illustrates an example of such model which simulates a cylinder filled with water flowing through a porous specimen. Simulation conditions, including temperature, initial hydraulic head and

pavement condition are specified based on the actual test conditions. A quarter model is adequate since the model is essentially symmetric in both *x* and *y* directions.

Closed pores and clogging of capillaries can significantly reduce the effective porosity of a porous pavement layer. Fwa et al. (1999) and Mallick et al. (2000) have indicated that clogging in porous pavement can reduce its permeability. Therefore, the proposed model should also consider the presence of closed pores and the effect of clogging. For this purpose, the iteration algorithm in Figure 3.3 chooses a clogging percentage (i.e. λ) of the drainage channels to be blocked. This percentage should be adjusted after each run to ensure convergence. The presented iterative process can provide the dimension of pore size (*x* and *y*), the effective porosity (ϕ_{eff}) and the clogging percentage (λ) as the key outputs.

3.2.3 Validation of the Drainage Capacity Model

The proposed pore network structure model is next validated against past experimental measurements made available in literature. These experiments include the constant-head outflow tests conducted by Charbeneau et al. (2011) and Chuai (1998), measuring the hydraulic conductivity of porous asphalt specimens. Table 3.1 compares the experiment data obtained by Charbeneau et al. (2011) and the simulation results from the developed pore network structure model. All the errors of flow rate are less than 2 ml/s and all the percentage errors are within 12%. Figure 3.5 further compares the goodness of fit for the data presented in Table 3.1 and good agreement between simulation and experiment results can be observed. Similar observations can be made for the other model validation case presented in Table 3.2 and Figure 3.6. The good agreement between simulation and experimental results illustrates the capability of the proposed model in simulating the drainage capacity of porous pavements. This model is next integrated into the numerical skid resistance simulation model to predict the frictional performance of porous pavements.

3.3 Development of Skid Resistance Simulation Model for Porous Pavement

Porous pavement skid resistance model is developed based on the numerical representation of porous layer drainage capacity. The proposed model attempts to simulate the phenomenon of a lock-wheel smooth tire skidding on a flooded porous pavement under a set of pre-specified conditions (such as sliding speed, water film thickness, pavement drainage capacity, wheel load and tire inflation pressure). Fluid-structure interaction and multiphase flow method are adopted to provide a more realistic depiction of the field condition.

3.3.1 Model Framework and Basic Elements

The moving wheel frame of reference (Ong and Fwa, 2007a) is adopted in this model, in which pavement and fluid move relatively towards stationary tire, (see Figure 3.7). The overall simulation model consists of two computational processes, namely the structure model (tire and pavement) and the fluid model (water and air). These two processes are coupled with each other and the overall workflow is shown in Figure 3.8. The model illustrated in this thesis is built and calibrated in ANSYS Workbench (ANSYS, 2009a), with ANSYS Static Structure (ANSYS, 2009b) for the structure model and ANSYS CFX (ANSYS, 2009c) for the fluid model.

The principle of the whole model is to solve the fluid model and the structure model iteratively, using a fluid-structure interaction (FSI) interface connecting them. Through this interface, the stresses developed on fluid boundaries can be transferred to the structure model, and the deformation of structure surface can be transferred to the fluid model. The fluid model provides a solution of fluid stresses acting on the FSI interface after one computation. This stress solution, although may have large errors, is transferred to the structure model by the FSI algorithm and then treated as a pressure load applied on tire tread surface. The tire deformation is then computed by the structure model with all the preset input properties as well as the fluid pressure acting on its FSI surface. This deformation is transferred back to the fluid FSI surface

by the FSI algorithm and causes deformation on the boundaries of fluid model. With the new geometry, the fluid model calculates a new set of stress solution which will be transferred to the structure model again. The iterative process carries on until the convergence criteria of sufficiently small stress and deformation residuals are reached.

The overall skid resistance simulation model consists of three basic elements: pneumatic tire sub-model, porous pavement sub-model and fluid sub-model. The sub-models interact with each other either through a fluid-structure-interaction or a tire-pavement contact. Given detailed information on tire, pavement and fluid properties, key information on contact and traction forces acting on the tire as well as fluid uplift and drag forces can be computed from the model simulations. Table 3.3 shows the major input and output variables of the proposed model.

3.3.2 Tire Sub-Model

As shown in Figure 3.7, the tire sub-model is built according to ASTM E524 standard smooth tire (ASTM, 2008b). Three structural components, namely tire rim, tire sidewalls and tire tread are being individually modelled within the tire sub-model. The tire is in contact with pavement surface under a downwards wheel load acting on tire rim and a uniformly distributed inflation pressure on the inside tire walls. All the degrees of freedom of tire rim are fixed except for vertical translational displacement, which is set to be free moving. The three structural components are modelled using the four-node finite strain shell elements, with homogeneous isotropic elastic material properties. The application of shell elements in tire friction modeling has been proved to be successful (Ong and Fwa, 2007b; Tanner, 1996), since such element is well suited for large strain nonlinear simulation (ANSYS, 2009d).

The simplified material properties for each tire component are assumed to be homogeneous isotropic elastic, which can be represented by three parameters: elastic modulus, Poisson's ratio and density. It was indicated by Ong and Fwa (2007a) that the elastic modulus of tire tread needs a careful calibration to make the tire sub-

model adequate for skid resistance simulation. This calibration is conducted using the measured tire footprint dimensions published by PIARC (1995). The other material properties are set constant in the model calibration, according to the normal ranges of rubber tire properties (see Table 3.4). It is observed that mesh dimension affects the calibration of material properties. Therefore, material calibration should be performed in conjunction with the mesh convergence study. This means first calibrating material properties with a fixed mesh design to get a value of tire tread elastic modulus and then conducting a mesh convergence study with this elastic modulus to achieve a new convergent mesh design, which is then used in the next iteration of material property calibration. The results of the last round of material calibration and mesh convergence study are shown in Figure 3.9. It turns out that a model with 27900 elements and a tread elastic modulus of 90 MPa is sufficient with an error of 1.02% in footprint area.

3.3.3 Pavement Sub-Model

The pavement sub-model serves two major functions. Firstly, it provides a rigid surface for tire-pavement contact. In this case, the pavement surface can be assumed to be perfectly rigid and smooth for interaction between the tire and pavement sub-models. Secondly, the pavement sub-model should allow the fluid flow modeling on and within porous pavement layer. In this sense, it is necessary to model the effect of pore structure on drainage capacity of the porous layer in this sub-model.

An impermeable surface is adequate for the contact modeling applications. Comparing with the tire deformation, the pavement surface deflection is so small that pavement can be taken to be relatively rigid. Therefore, the pavement material is assumed to have an elastic modulus of 30 GPa, a Poisson's ratio of 0.15, and a density of 2200 kg/m^3. The top surface of pavement model is set as a contact interface and the bottom surface is fixed in both translation and rotation. Eight-node structural solid element is used to model pavement in the structure model.

The drainage capacity of porous pavement is considered and simulated in the fluid model. The simplified pore network structure discussed in Section 3.2 is used for this purpose. The pore structure diameters are calibrated against in-field outflow measurement conducted on the same porous pavement section, as the skid resistance is tested, following the iterative process presented in Figure 3.3. The resulted pore network geometry provides the boundaries of water flow channels in the fluid sub-model.

3.3.4 Fluid Sub-Model

Fluid behaviour is modelled through the Navier-Stokes equations in the fluid sub-model. It adopts the multiphase flow formulation where both water and air are considered. Since the fluid flow around a sliding tire and within the porous pavement layer is known to be turbulent, a proper turbulence model is needed to simulate the fluid turbulence. These techniques provide a closer depiction of the actual tire-fluid-pavement interactions.

3.3.4.1 Multiphase Flow Model

The primary purpose of modeling multiphase flow in this work is to capture the free surface of water. Free surface flow is one of the most common applications of the homogeneous multiphase flow, which is a limiting case of Eulerian-Eulerian multiphase flow where all fluids share the same flow field as well as other relevant fields, such as temperature and turbulence (ANSYS, 2009e). For a given transport process, the same transported quantities (with exception of volume fraction) for all phases are assumed in a homogeneous model, i.e.,

$$\phi_\alpha = \phi \qquad 1 \le \alpha \le N_p \tag{3.17}$$

where ϕ is a general variable, N_p is the number of phases. The bulk transport equation is sufficient to solve for the shared fields:

$$\frac{\partial}{\partial t}(\rho\phi)+\nabla\cdot(\rho U\phi-\Gamma\nabla\phi)=S \tag{3.18}$$

where

$$\rho=\sum_{\alpha=1}^{N_p}\gamma_\alpha\rho_\alpha\,,\quad U=\frac{1}{\rho}\sum_{\alpha=1}^{N_p}\gamma_\alpha\rho_\alpha U_\alpha\,,\quad \Gamma=\sum_{\alpha=1}^{N_p}\gamma_\alpha\Gamma_\alpha \tag{3.19}$$

The hydrodynamic equations for homogeneous multiphase flow are derived based on the basic equations of computational fluid dynamics (CFD), taking the same velocity field and pressure field into consideration, i.e.

$$U_\alpha=U\,,\qquad p_\alpha=p\qquad 1\le\alpha\le N_p \tag{3.20}$$

Continuity equations:

$$\frac{\partial}{\partial t}(r_\alpha\rho_\alpha)+\nabla\cdot(r_\alpha\rho_\alpha U)=S_{MS\alpha}+\sum_{\beta=1}^{N_p}\Gamma_{\alpha\beta} \tag{3.21}$$

where r_α is the volume fraction of phase α, $S_{MS\alpha}$ is the user specified mass sources of phase α, and $\Gamma_{\alpha\beta}$ is the mass flow rate per unit volume from phase β to phase α.

Momentum equation:

$$\frac{\partial}{\partial t}(\rho U)+\nabla\cdot\left(\rho U\otimes U-\mu\left(\nabla U+(\nabla U)^T\right)\right)=S_M-\nabla p \tag{3.22}$$

where S_M is the momentum source, and

$$\rho=\sum_{\alpha=1}^{N_p}r_\alpha\rho_\alpha\,,\qquad \mu=\sum_{\alpha=1}^{N_p}r_\alpha\mu_\alpha \tag{3.23}$$

Volume conservation equation:

$$\sum_{\alpha=1}^{N_p}r_\alpha=1 \tag{3.24}$$

Continuum Surface Force model (Brackbill et al., 1992) is adopted to model the surface tension. A volume force concentrated at the interface is given by:

$$F_{\alpha\beta}=f_{\alpha\beta}\delta_{\alpha\beta} \tag{3.25}$$

where α indicates a primary fluid (the liquid phase) , β indicates a secondary fluid (usually a gas phase), and

$$f_{\alpha\beta} = -\delta_{\alpha\beta}\kappa_{\alpha\beta}n_{\alpha\beta} + \nabla_s\sigma \tag{3.26}$$

$$\delta_{\alpha\beta} = \left|\nabla r_{\alpha\beta}\right| \tag{3.27}$$

$$\kappa_{\alpha\beta} = \nabla \cdot n_{\alpha\beta} \tag{3.28}$$

where σ is the surface tension coefficient, $n_{\alpha\beta}$ is the interface normal vector pointing from the primary fluid to the secondary fluid, ∇_s is the gradient operator on the interface, and $\kappa_{\alpha\beta}$ is the surface curvature.

3.3.4.2 Turbulence Model

The length scale of eddies in turbulent flow may be much smaller than the smallest finite volume mesh dimension. Direct numerical simulation of turbulent flow by the Navier-Stokes equations is impracticable at present due to limitations in computational power. Therefore, an appropriate turbulence model is essential for turbulent flow simulation. It was indicated that the *k*-ε model (a two-equation eddy viscosity turbulence model) can be used to model the flow under a loaded skidding tire (Ong and Fwa, 2006). The variables and constants of the *k*-ε model for multiphase flow should be phase-dependent and eddy viscosity hypothesis is assumed to hold for each fluid phase. However, the bulk turbulence equations solved in the homogeneous multiphase flow have the same expressions as those in the single phase case, with the exception of mixture density and mixture viscosity. The continuity and momentum equations are defined as:

$$\frac{\partial \rho}{\partial t} + \nabla \cdot \left(\rho U\right) = 0 \tag{3.29}$$

$$\frac{\partial \rho U}{\partial t} + \nabla \cdot \left(\rho U \otimes U\right) = -\nabla p' + \nabla \cdot \left(\mu_{eff}\left(\nabla U + \left(\nabla U\right)^T\right)\right) + S_M \tag{3.30}$$

where S_M is the sum of body forces, p' is the modified pressure which is equal to $p + \frac{2}{3}\rho k + \frac{2}{3}\mu_{eff}\nabla U$, and μ_{eff} is the effective viscosity ($\mu_{eff} = \mu + \mu_t$).

The turbulence viscosity μ_t is calculated by:

$$\mu_t = C_\mu \rho \frac{k^2}{\varepsilon} \tag{3.31}$$

where k is the turbulence kinetic energy, ε is the turbulence eddy dissipation and C_μ is a model constant. The values of k and ε come from the differential transport equations:

$$\frac{\partial(\rho k)}{\partial t} + \nabla \cdot (\rho U k) = \nabla \cdot \left[\left(\mu + \frac{\mu_t}{\sigma_k} \right) \nabla k \right] + P_k - \rho \varepsilon \tag{3.32}$$

$$\frac{\partial(\rho \varepsilon)}{\partial t} + \nabla \cdot (\rho U \varepsilon) = \nabla \cdot \left[\left(\mu + \frac{\mu_t}{\sigma_\varepsilon} \right) \nabla \varepsilon \right] + \frac{\varepsilon}{k} (C_{\varepsilon 1} P_k - C_{\varepsilon 2} \rho \varepsilon) \tag{3.33}$$

where $C_{\varepsilon 1}$, $C_{\varepsilon 2}$, σ_k and σ_ε are model constants, which are set to be 1.44, 1.92, 1.0 and 1.3, respectively, in the skid resistance model, P_k is the turbulence production due to viscous and buoyancy forces, which is formulated by:

$$P_k = \mu_t \nabla U \cdot \left(\nabla U + \nabla U^T \right) - \frac{2}{3} \nabla \cdot U (3\mu_t \nabla \cdot U + \rho k) + P_{kb} \tag{3.34}$$

where P_{kb} is the buoyancy production term, which is included in the equation only if buoyancy turbulence is considered.

3.3.4.3 Material Properties and Boundary Conditions

Water and air are simulated as continuous fluids in the fluid model. Their material properties at 25°C and 1 atm are used in the simulations. The density and dynamic viscosity of water are set 997 kg/m^3 and 8.899×10^{-4} kg/ms, respectively, while those of air are 1.185 kg/m^3 and 1.831×10^{-5} kg/ms. The four-node tetrahedral elements, which is widely used in the modeling of flow with high Reynolds' number, are adopted in this study. Because water plays a dominant role in skid resistance compared to air and air flow characteristics are beyond the interest of this part of the study, the mesh design for water is made much denser than that for air. A mesh convergence study was performed and satisfactory results have been found to be provided by a fluid sub-model with around 3,200,000 elements (see Figure 3.10).

The boundary conditions of fluid sub-model are presented in Figure 3.11. A specified percentage of uniformly distributed channel outlet ends are set to be wall

boundaries to model the clogging effect in porous layer, as discussed in Section 3.2.2. The inlet water depth and volume fractions are specified as input parameters using the CFX Expression Language (ANSYS, 2009f).

3.3.5 Tire-Pavement Contact Algorithm

As a part of tire-pavement-fluid interaction, contact analysis between tire tread and pavement surface is critical to the entire model. A contact pair is defined, with tire tread as contact surface, modelled by 3-D 8-node surface-to-surface contact elements, and pavement top surface as target surface, modeled by 3-D target elements. These elements are commonly applied in general 3-D contact analyses between solid bodies or shells. The contact detection points are the integration points located either at the nodal points or the Gauss points, and a pinball region is used to search for contact (ANSYS, 2009d). The reaction force on target surface is calculated from the summation of all nodal forces of associated contact elements.

The friction at contact interface is considered by the Coulomb's Law. The state of sticking/sliding is identified by the relative magnitude of equivalent shear stress between two contacting surfaces to a limit frictional stress.

$$\begin{cases} \|\tau\| \le \tau_{\lim} & \textit{sticking} \\ \|\tau\| \ge \tau_{\lim} & \textit{sliding} \end{cases} \tag{3.35}$$

where $\tau_{\lim}$ is the limit frictional stress, and $\|\tau\|$ is the equivalent shear stress.

$$\tau_{\lim} = \mu_f P + b \tag{3.36}$$

$$\|\tau\| = \sqrt{\tau_1^2 + \tau_2^2} \tag{3.37}$$

where μ_f is the coefficient of isotropic friction, P is the contact normal pressure and b is the contact cohesion. A maximum equivalent frictional stress $\tau_{\max}$ can be defined for the contact element to perform the function of limit frictional stress $\tau_{\lim}$.

The augmented Lagrangian algorithm is used in nonlinear contact analysis. It searches for the Lagrange multiplier for each element by iteratively updating penalty. The contact pressure is defined by:

$$P = \begin{cases} 0 & if \quad u_n > 0 \\ K_n u_n + \lambda_{i+1} & if \quad u_n \leq 0 \end{cases} \tag{3.38}$$

$$\lambda_{i+1} = \begin{cases} \lambda_i + K_n u_n & if \quad |u_n| > \varepsilon \\ \lambda_i & if \quad |u_n| < \varepsilon \end{cases} \tag{3.39}$$

where ε is the compatibility tolerance and λ_i is the Lagrange multiplier component at iteration i.

3.3.6 Fluid-Structure Interaction Algorithm

The interaction between tire tread and water flow significantly affect the tire wall deformations with changes in skidding speed or water film thickness, which in turn determines the variations in tire-pavement contact and fluid uplift force. This important feature has to be taken into consideration in the skid resistance modeling through a special numerical treatment known as "two-way fluid-structure coupling", which requires mathematical coupling of the fundamental equations from each field.

There are two categories of coupling algorithms, namely strong coupling and loose coupling, respectively. In the strong coupling approach, the CFD equations describing fluid behavior and the mechanics equations describing structure behavior are treated as a coupled system of equations that are solved simultaneously. In the loose coupling approach, the CFD and mechanics equations are solved independently of each other in an iterative process. The proposed model employs the loose coupling approach, because it requires relatively less computational resources and is able to achieve comparable accuracy to the strong coupling approach.

The kinematic condition (i.e. displacement compatibility) and the dynamic condition (i.e. traction equilibrium) are the fundamental requirements applied onto the fluid-structure interface in the coupling analysis.

$$d_f = d_s \tag{3.40}$$

$$\vec{n} \cdot \tau_f = \vec{n} \cdot \tau_s \tag{3.41}$$

where d_f and d_s are the displacements at the fluid-structure interface for fluid sub-model and structure sub-model, respectively, and τ_f and τ_s are the stresses at that interface for the two sub-models, respectively. The residuals in stresses (from fluid sub-model) and displacements (from structure sub-model) computed from the two subsequent iterations are used as convergence criteria, which are defined as:

$$r_\tau = \frac{\left\| \tau_f^k - \tau_f^{k-1} \right\|}{\max\left\{ \left\| \tau_f^k \right\|, \varepsilon_0 \right\}} \leq \varepsilon_\tau \tag{3.42}$$

$$r_d = \frac{\left\| d_s^k - d_s^{k-1} \right\|}{\max\left\{ \left\| d_s^k \right\|, \varepsilon_0 \right\}} \leq \varepsilon_d \tag{3.43}$$

where ε_τ and ε_d are the tolerances for stress and displacement convergence, and ε_0 is a preset constant for the purpose of overriding the stress and displacement in case they are too small to monitor convergence. The stress and displacement tolerances are both set to be 0.1% and ε_0 takes the value of 10^{-8} in this study.

3.4 Validation of Skid Resistance Simulation Model

The proposed skid resistance simulation model is next validated against published experimental results for both conventional dense-graded pavements and porous pavements. Although previous models developed for dense-graded pavements have been validated in past research studies (Ong and Fwa, 2006; Ong and Fwa, 2008), neither of them involves coupled VOF-FSI simulation. Therefore, it is necessary to validate the proposed model for dense-graded pavements first to ensure its capability in simulating skid resistance on conventional surfaces. The model is then validated for porous pavements using past experiments.

3.4.1 Derivation of Skid Number from Numerical Simulation Model

The skid number at speed v (denoted as SN_v), based on the lock-wheel skid resistance test (ASTM, 2011a), can be determined from the simulation. Skid number is defined as the ratio between horizontal resistance force and vertical loading force acting on the same test tire, normalized by a scale of 100. A higher skid number indicates a better skid resistance performance. Skid number can be calculated as:

$$SN_v = (F_x / F_z) \times 100 \tag{3.44}$$

where F_x is the horizontal backwards resistance force acting on tire model, and F_z is the vertical downwards load applied on the tire. Both these two variables could be obtained from the numerical simulation model. Horizontal resistance force F_x and vertical load F_z are further explained by:

$$F_x = F_{traction} + F_{drag} \tag{3.45}$$

$$F_z = F_{contact} + F_{uplift} \tag{3.46}$$

where $F_{traction}$ is the traction force developing at tire-pavement interface, F_{drag} is the fluid drag force developing at tire-fluid interface, $F_{contact}$ is the contact force between tire and pavement surface, and F_{uplift} is the fluid uplift force acting on tire surface. In these variables, F_{drag} and F_{uplift} are direct outputs from the fluid model, F_z is an input parameter, and $F_{traction}$ is derived from $F_{contact}$:

$$F_{traction} = \mu \cdot F_{contact} = \mu \cdot \left(F_z - F_{uplift}\right) \tag{3.47}$$

where μ is the coefficient of friction between tire tread and pavement surface at wet condition. It is usually determined through experiments in laboratory or field, and varies with the surface properties of contact materials. Combining Equations (3.44) to (3.47), the skid number SN_v could be expressed as:

$$SN_v = \frac{\mu \cdot \left(F_z - F_{uplift}\right) + F_{drag}}{F_z} \times 100 \tag{3.48}$$

The friction coefficient μ is commonly represented by the skid number at an extremely low speed SN_0, and it is assumed that the wet friction coefficient maintains

constant with the increase of speed. In the case that experimental SN_0 values are unavailable, an iterative back calculation approach developed by Fwa and Ong (2006) can be used to derive the friction coefficients from field skid resistance tests, using the simulation model. The detailed procedures are shown in Figure 3.12 and described below.

Step 1: For each set of experimental results with the same pavement and tire, a measurement of skid resistance at a speed v is randomly selected. The measured skid number is SN_v;

Step 2: Assume a reasonable initial SN_0 value (normally 50) as the friction coefficient used in the proposed model and run the model at sliding speed v to derive a numerical skid number SN_v* from the model outputs;

Step 3: Adjust the value of SN_0 based on the difference between numerical SN_v* and measured SN_v, according to the equation (new trial SN_0) = (last trial SN_0) + 0.5(SN_v* - SN_v);

Step 4: Perform the simulation again using the new trial SN_0 as the friction coefficient to get a new numerical skid number SN_v*;

Step 5: Repeat steps 3 and 4 until the error between numerical and measured results (i.e. $\varepsilon = SN_v$* - SN_v) is sufficiently small; and

Step 6: The resulted SN_0 value is taken as the wet friction coefficient at tire-pavement interface and all the skid numbers at other sliding speeds are predicted by the proposed model with the back-calculated SN_0.

3.4.2 Validation of the Model for Conventional Pavement

Numerous experimental studies were performaed on wet-pavement skid resistance using in-field measurements under different operation conditions defined by various parameters, such as sliding speed, water film thickness and wheel load. Many of such studies were conducted according to the ASTM E274 standard (ASTM, 2011a) with standard smooth tires as specified in the ASTM E524 standard (ASTM,

2008b). The experiments conducted by Horne (1969) and Agrawal and Henry (1977) were used to validate the proposed model on conventional dense-graded pavements. The experimental data are shown in Table 3.5.

The numerically simulated results of skid resistance experiments conducted by Horne (1969) and Agrawal and Henry (1977) are presented in Table 3.6. Further comparisons on simulated curves against measured values are shown in Figure 3.13. As indicated by the ASTM E274 standard, the acceptable standard deviation of this test is ±2 SN units. Therefore, the 95% confidence interval of this test has a range of ±3.92 SN units. As seen in Table 3.6, only one simulation got a result out of this range (with an error of +4.8 SN units from the measured value), and all the percentage errors are below 12% except this case. It is seen that most high percentage errors correspond to lower skid numbers.

3.4.3 Validation of the Model for Porous Pavement

Although the amount of skid resistance tests on porous pavements is not as extensive as that on conventional pavements, there are still some measured experimental results that can be used to validate the proposed model on porous pavements. In an experimental study conducted by the Oregon Department of Transportation and Oregon State University in the early 1990s, skid resistance performances of several porous asphalt pavement sections were evaluated using the lock-wheel trailer test (Younger et al., 1994). Different road sections were selected to provide a mix of traffic conditions and pavement ages. All the tested sections were constructed with the same porous asphalt mixture named ODOT F-mix, but the porosities of different sections differed a lot due to the different service and traffic histories. Variations in porous layer thickness were also available among these projects. The same water application mechanism was adopted in all the tests, providing a water film thickness of 0.55 mm (ASTM, 2011a).

The porosities of selected porous pavement sections were measured using core samples (inner and outer wheel paths) in the laboratory, while the permeability was measured in the field using a specially designed falling-head outflow device. The skid numbers of each section at different skidding speeds were measured according to the ASTM E274 standard (ASTM, 2011a). The pavement properties and skid resistance performance of each tested section are listed in Table 3.7.

The proposed model is next validated against this experimental study by Younger et al. (1994). The average measured porosity and permeability values are input to the model to predict the skid numbers. There is no permeability measurement available for the Jumpoff Joe section in the experiment report. However, its porosity is very similar to that of the Grants Pass section and the locations of these two sections are quite near to each other. Therefore it is reasonable to assume the same permeability range as Grants Pass for Jumpoff Joe. Numerical results derived from the proposed model are shown in Table 3.8 and Figure 3.14.

It can be seen from Table 3.8 that most numerical prediction errors are less than 2 SN units and all the percentage errors are less than 8%. This indicates that the proposed model can simulate skid resistance on porous and non-porous pavements. However, the simulation results of Jumpoff Joe seems to be less satisfactory, with two errors near 3 SN units. This may be a result of the incomplete information for Jumpoff Joe in the experimental measurements, demonstrating the importance of proper permeability evaluation for an accurate skid resistance prediction.

Besides the estimation of the average performance trends, the range bounds for skid numbers of Murphy Road-Lava Butte and Hayesville-Battle Creek are predicted based on the extreme porosity and permeability values. The skid numbers at a zero speed, SN_0, used in the prediction of skid resistance range are back calculated from the average curves shown in Figure 3.14. The range of SN_0 thus reflects the prediction error of SN_0 due to the measurement errors in lock-wheel skidding tests, while the difference in curve shapes reflects the different decreasing trends of skid

number with increasing skidding speed due to the errors or variances in porosity and permeability measurements. Therefore, this approach considers both experimental errors and pavement property inconsistency. Figure 3.15 shows the simulation results. This approach is not applied to Grants Pass and Jumpoff Joe because of their narrow porosity range (i.e. 1.1% porosity variation).

From Figure 3.15, all the measured data points fall into the predicted SN ranges, demonstrating the capacity of the model to predict a range of skid resistance performance that vehicles may experience on the road. The prediction range depends on the quality of input data, as well as the sliding speed as seen in Figure 3.15 where prediction ranges are larger at higher speeds. The decrease in skid number with sliding speed is steeper on a surface with lower porosity compared to that on a surface with higher porosity. Therefore, the decreasing rate of the upper bound, which is derived from the maximum porosity, is less than that of the lower bound, which is derived from the minimum porosity. The practical meaning of this phenomenon is that the actual skid resistance a vehicle experiences on a porous pavement may not be identical spatially, especially at high speed, because of the porosity/permeability variation.

3.5 Summary

A numerical simulation model of skid resistance on porous pavements was developed and validated in this chapter. The proposed model considers all the critical issues associated with porous pavement skid resistance modeling, including frictional contact between tire tread and pavement surface, fluid-structure interaction at tire-water interface, tire mechanical properties and its deforming behaviour, turbulent and multiphase free-surface flow, and most importantly, the drainage property of porous pavements.

After discussing the critical issues that should be addressed in the simulation model, the appropriate modeling of porous pavement drainage capacity was identified

as a major task in the development of porous pavement skid resistance model. A phenomenology approach to numerically reproduce the drainage capacity of a porous pavement was first proposed in this chapter. The pore structure geometry of porous surface was modeled by a simplified grid network that provides the same drainage capacity as porous pavements observed in the field. The dimensional parameters of this geometry (i.e. pore size and pore spacing) should be calibrated using the measured results from falling-head or constant-head outflow tests. An iterative procedure based on numerical simulation of outflow test was developed for this purpose, taking porous layer porosity, permeability and clogging potential into consideration. This drainage capacity representation approach can significantly simplify the model and make the problem numerically feasible.

The proposed porous pavement drainage model was next integrated with the skid resistance simulation model which simulates the lock-wheel trailer skidding test specified by the ASTM E274 standard (ASTM, 2011a). The standard smooth tire (ASTM, 2008b) was modelled by shell elements and elastic material properties and the model was calibrated against tire footprints measured from experiments. The k-ε model and VOF method were adopted to simulate turbulence and multiphase flow, respectively. Standard properties of water and air at test conditions are used in the fluid model. The porous pavement was modelled as a rigid surface in the analysis of tire-pavement interaction and its drainage capacity was simulated in the fluid model using the simplified pore network geometry. The two-way structure-fluid interaction algorithm connected the two major components of this skid resistance model, namely structural model and fluid model. The stresses and deformations at the FSI interface were transferred iteratively between these two components until the convergence was reached and the fluid forces were obtained.

The entire skid resistance model was next validated against published in-field measurements for both dense-graded surfaces and porous pavements. The simulated results on conventional smooth pavements were compared to the tests conducted by

Horne (1969) and Agrawal and Henry (1977), while the numerical results on porous pavements were compared to the measurement performed by Younger et al. (1994). The numerical simulations were found to agree well with experimental measurements. The percentage errors of simulations on porous pavements were found less than 8%. To further demonstrate the validity of porous pavement skid resistance model, the bounds of skid number were deduced from the simulation and compared against two sets of experimental data. All the measured data points fall into the predicted ranges. The validation work illustrated the ability of the proposed model in predicting the skid resistance performance of porous pavements. The model can be used to analyze the mechanisms and influencing factors in the skid resistance enhancement on porous pavements. It should be able to provide valuable and useful information that is difficult to obtain in experiments.

Table 3.1: Validation of drainage model against Charbeneau et al. (2011)

Hydraulic head (cm)	Flow rate (mL/s)		Error	Percentage error
	Measured value from experiment	Numerical result from simulation model		
0.05	1.5	1.503	0.003	0.22%
0.60	5.5	6.156	0.656	11.93%
1.10	8.0	8.474	0.474	5.93%
1.50	9.0	9.974	0.974	10.83%
2.30	12.0	12.441	0.441	3.68%
4.10	16.0	17.570	1.570	9.81%
5.00	18.0	19.454	1.454	8.08%
5.80	20.0	20.978	0.978	4.89%
7.30	23.0	23.579	0.579	2.52%
8.20	24.5	25.008	0.508	2.07%
9.10	26.0	26.364	0.364	1.40%
10.00	28.0	27.653	-0.347	-1.24%
11.00	29.5	29.152	-0.348	-1.18%
12.30	31.5	30.704	-0.796	-2.53%
13.30	33.0	31.944	-1.056	-3.20%
14.80	35.0	33.719	-1.281	-3.66%
15.80	36.0	34.854	-1.146	-3.18%

Table 3.2: Validation of drainage model against Chuai (1998)

Hydraulic gradient (mm/mm)	Specific velocity (mm/s)		Error	Percentage error
	Measured value from experiment	Numerical result from simulation model		
6.04	47.57	41.91	-5.66	-11.90%
5.40	43.12	39.11	-4.01	-9.30%
5.31	38.71	38.70	-0.01	-0.02%
4.67	35.12	35.67	0.55	1.56%
3.35	30.62	28.43	-2.19	-7.14%
2.97	27.00	25.99	-1.01	-3.73%
2.39	23.90	21.76	-2.14	-8.95%

Table 3.3: Input and output parameters of skid resistance simulation model

Input parameters	Direct outputs	Derived outputs
• Tire geometry and dimensions • Tire wall material properties (elastic modulus, Poisson's ratio and density for each tire components) • Tire inflation pressure • Wheel load • Sliding speed • Pavement material properties (elastic modulus, Poisson's ratio and density) • Water properties (density and dynamic viscosity) • Air properties (density and dynamic viscosity) • Friction coefficient at wetted tire-pavement interface	• Fluid uplift force • Fluid drag force • Tire deformation • Tire-pavement contact area • Fluid stress distribution • Flow pattern	• Tire-pavement contact force • Traction force • Skid number at given speed • Force contribution in skid resistance • Hydroplaning speed

Table 3.4: Material properties of tire model

	Elastic modulus (MPa)	Poisson's ratio	Density (kg/m^3)
Tire rim	100,000	0.30	2700
Tire sidewall	20	0.45	1200
Tire tread	90*	0.45	1200

note: * means the value comes from model calibration

Table 3.5: Experimental results of selected skid resistance tests in the literature

Experimental studies	Pavement type	Tire inflation pressure (kPa)	Wheel load (N)	Water film thickness (mm)	Sliding speed (km/h)	SN_v
Horne (1969)	Concrete	165.5	4800	5.08-10.12 (7.62 in the model)	8	60
					16	55
					32	45
					48	35
					64	20
					80	15
	Asphalt	165.5	4800	5.08-10.12 (7.62 in the model)	48	45
					64	30
					80	10
Agrawal and Henry (1977)	Concrete	165.5	2891	1.27	48	30
					64	20
					72	15
					80	12

Table 3.6: Validation of skid resistance model on conventional pavements

Experimental studies	Sliding speed (km/h)	Measured SN_v from experiment	Numerical SN_v from simulation model	Error	Percentage error (%)
Horne (1969)	8	60	59.2	-0.8	-1.33
	16	55	56.1	1.1	2.00
	32	45	46.7	1.7	3.78
	48	35	34.2	-0.8	-2.29
	64	20	20.8	0.8	4.00
	80	15	10.2	-4.8	-32.00
	48	45	42.8	-2.2	-4.89
	64	30	26.5	-3.5	-11.67
	80	10	9.8	-0.2	-2.00
Agrawal and Henry (1977)	48	30	29.2	-0.8	-2.67
	64	20	20.9	0.9	4.50
	72	15	16.7	1.7	11.33
	80	12	13.2	1.2	10.00

Table 3.7: Properties and skid resistance of tested porous pavements (Younger et al., 1994)

Project	Porosity (%)	Permeability test (s)	Depth of porous layer (mm)	Test speed (km/h)	Skid number
Murphy	16.0 - 23.9	1.01 - 1.41	50	64	47.2
Road-Lava				80	44.7
Butte				88	43.6
Hayesville-	14.5 - 22.6	0.76 - 1.00	50	50	45.8
Battle Creek				66	43.1
				80	40.6
				88	39.3
				48	45.8
				64	43.1
				80	40.9
				88	39.8
Grants Pass	14.4 - 15.5	0.66 - 1.26	100	50	52.6
				66	48.9
				80	45.6
				88	43.6
				100	41.9
Jumpoff Joe	15.0 - 16.1	N.A.	50	50	45.1
				64	44.0
				80	42.5
				97	41.2

note: N.A. means not available

Table 3.8: Validation of skid resistance model on porous pavements

Project	Sliding speed (km/h)	Measured SN_v from experiment	Numerical SN_v from simulation model	Error	Percentage error (%)
Murphy	64	47.2	47.7	0.5	1.06
Road-Lava	80	44.7	44.5	-0.2	-0.45
Butte	88	43.6	42.8	-0.8	-1.83
Hayesville-	50	45.8	45.4	-0.4	-0.87
Battle Creek	66	43.1	43.7	0.6	1.39
	80	40.6	41.5	0.9	2.22
	88	39.3	40.4	1.1	2.80
	48	45.8	45.4	-0.4	-0.87
	64	43.1	43.7	0.6	1.39
	80	40.9	41.5	0.6	1.47
	88	39.8	40.4	0.6	1.51
Grants Pass	50	52.6	52.1	-0.5	-0.95
	66	48.9	49.5	0.6	1.23
	80	45.6	46.5	0.9	1.97
	88	43.6	45.0	1.4	3.21
	100	41.9	43.4	1.5	3.58
Jumpoff Joe	50	45.1	48.0	2.9	6.43
	64	44.0	44.8	0.8	1.82
	80	42.5	42.2	-0.3	-0.71
	97	41.2	38.3	-2.9	-7.04

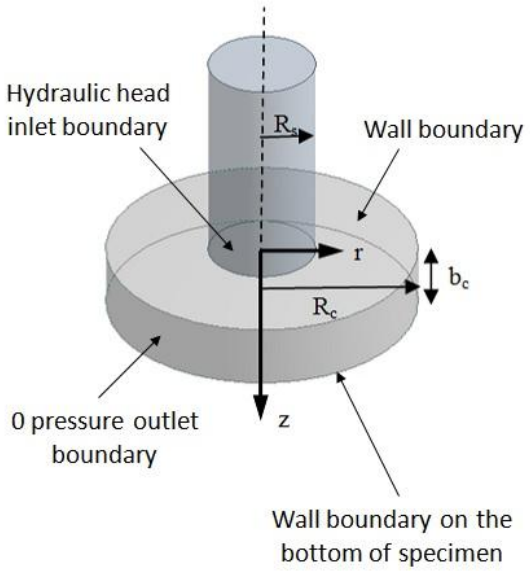

Figure 3.1: Sketch of outflow test in cylindrical coordinates

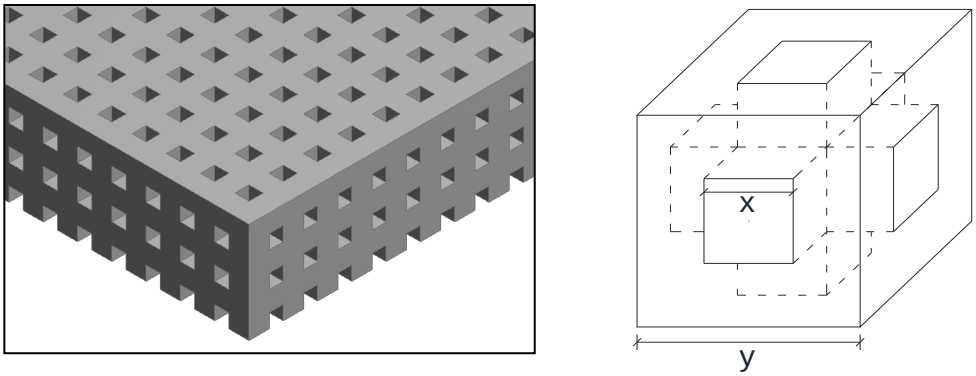

(a) Geometry of pore network structure of porous pavement layer

(b) Cubic pore element of porous pavement model

Figure 3.2: Pore network structure of porous pavement model

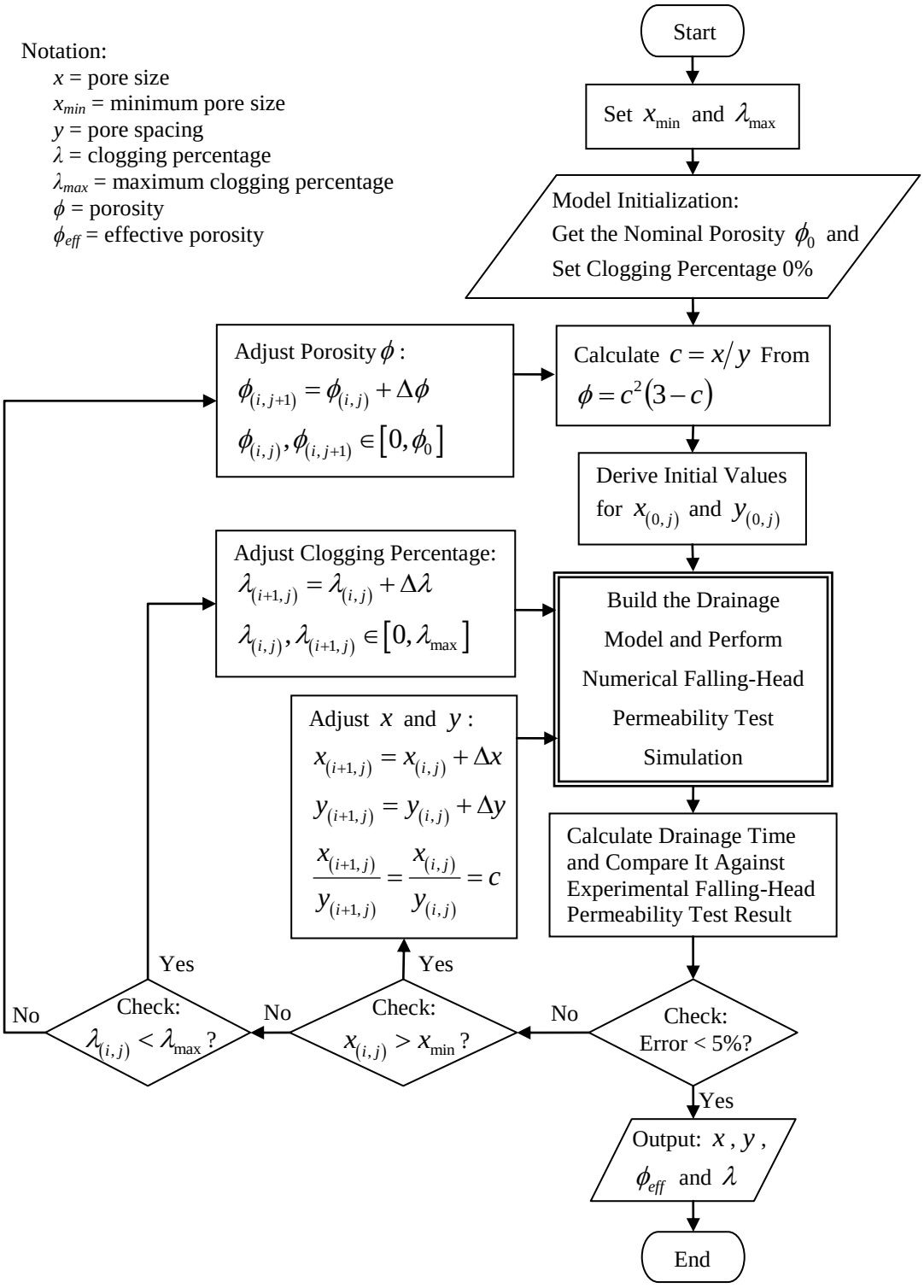

Figure 3.3: Computation framework to determine pore structure dimensions in the porous pavement model

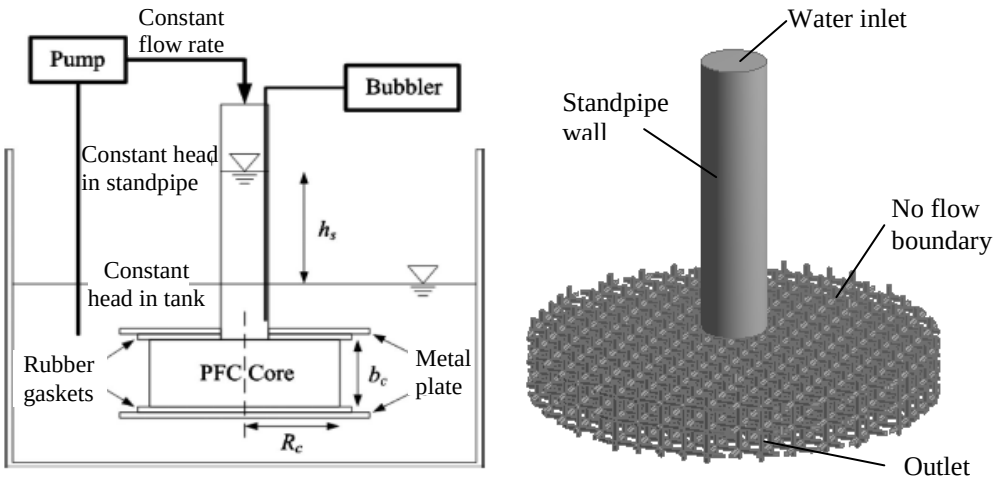

(a) Constant-head outflow test (Charbeneau et al., 2011)

(b) Finite volume model

Figure 3.4: Illustrative device and model of constant-head outflow test

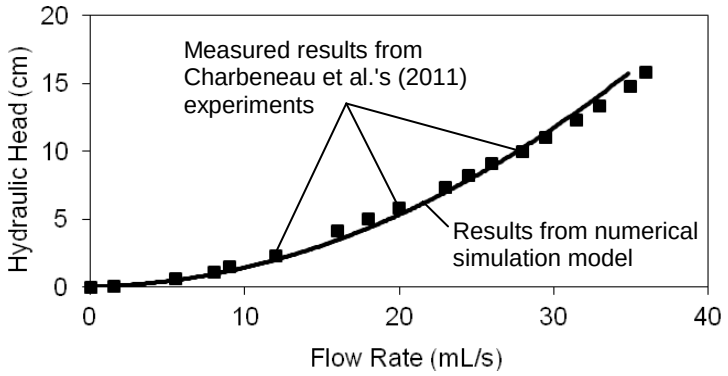

Figure 3.5: Comparison between numerical and experimental results for Charbeneau et al. (2011)

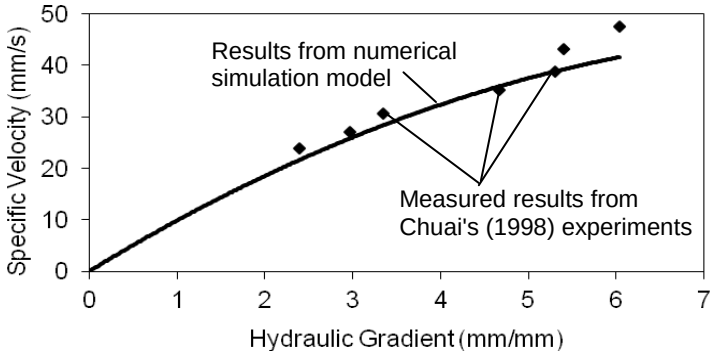

Figure 3.6: Comparison between numerical and experimental results for Chuai (1998)

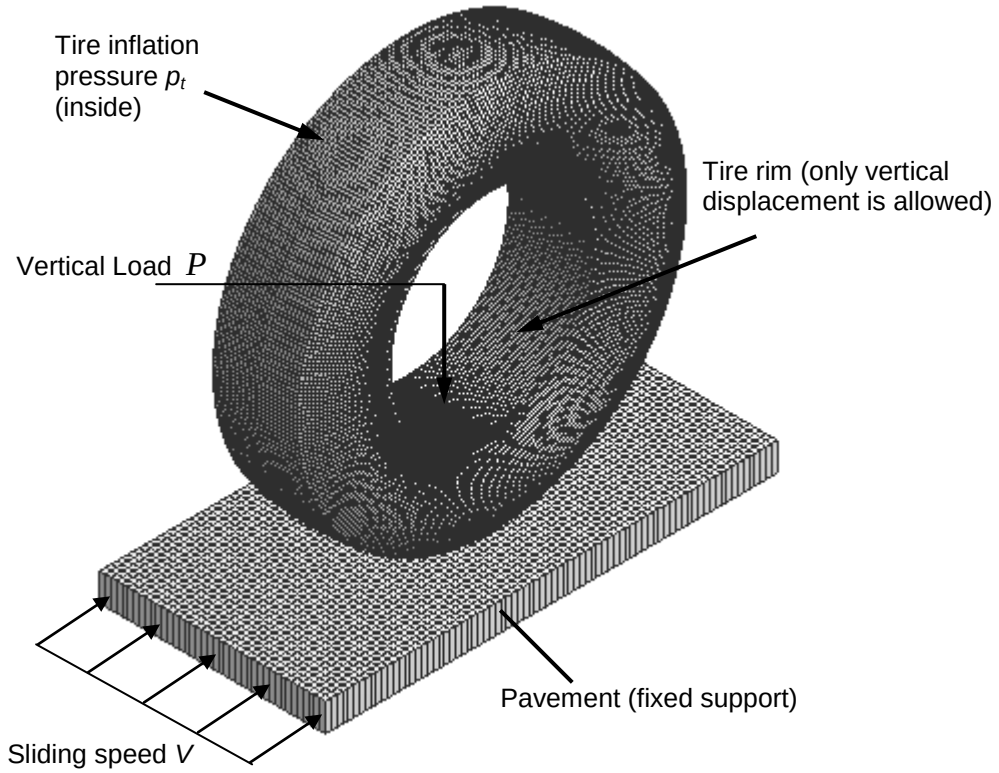

Figure 3.7: Moving wheel frame of reference

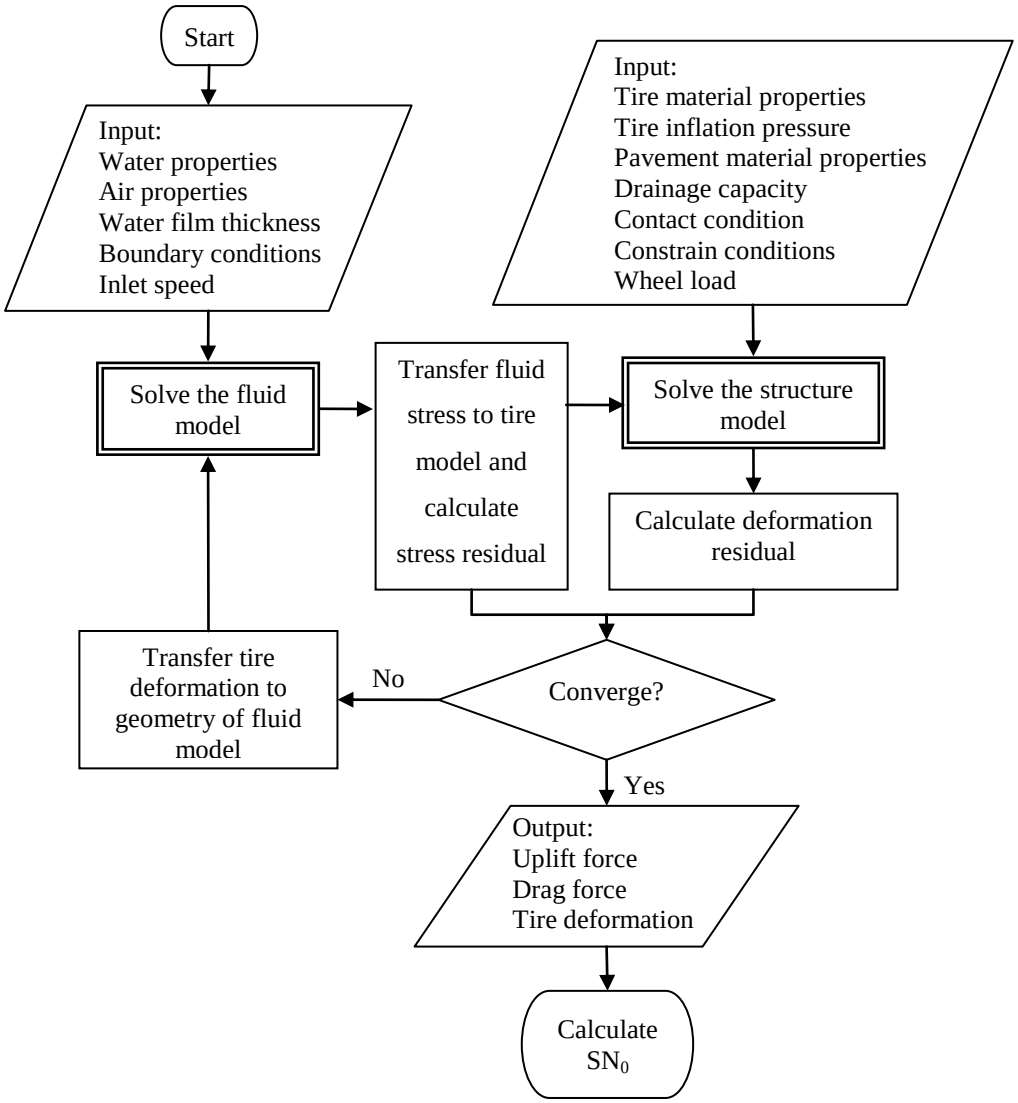

Figure 3.8: Iteration between fluid and structure models

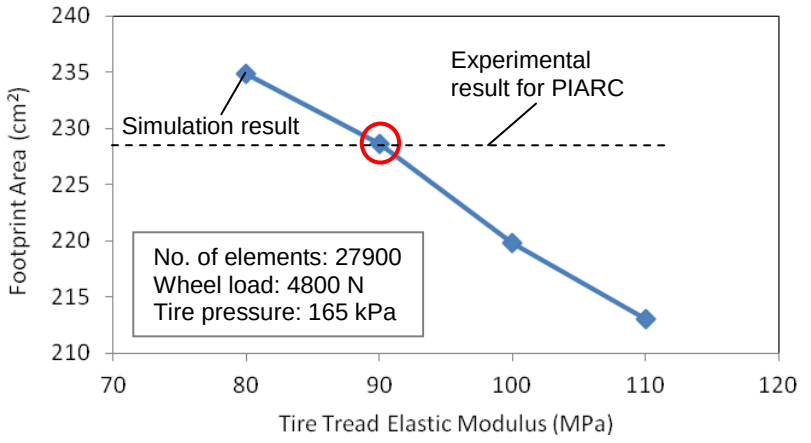

(a)

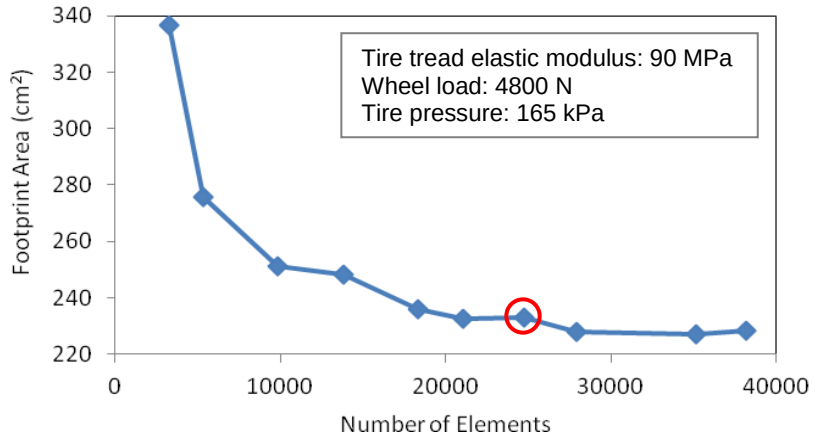

(b)

Figure 3.9: Final stage of (a) model calibration and (b) mesh convergence study for tire sub-model

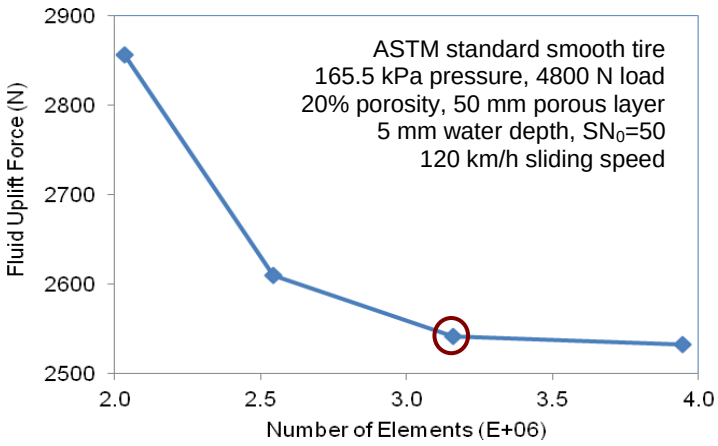

(a) Fluid Uplift Force

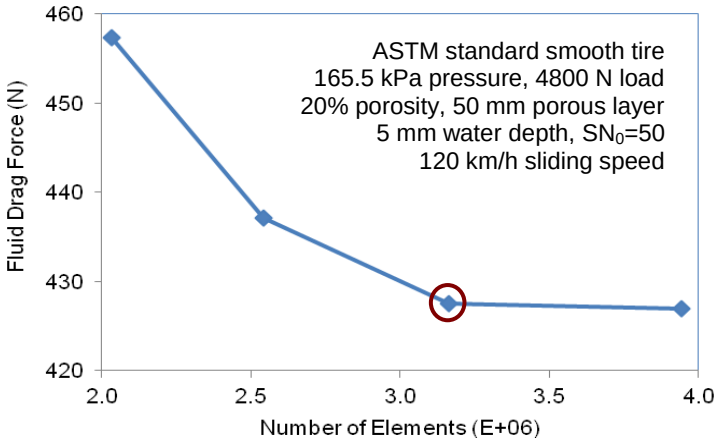

(b) Fluid Drag Force

Figure 3.10: Mesh convergence study for fluid sub-model

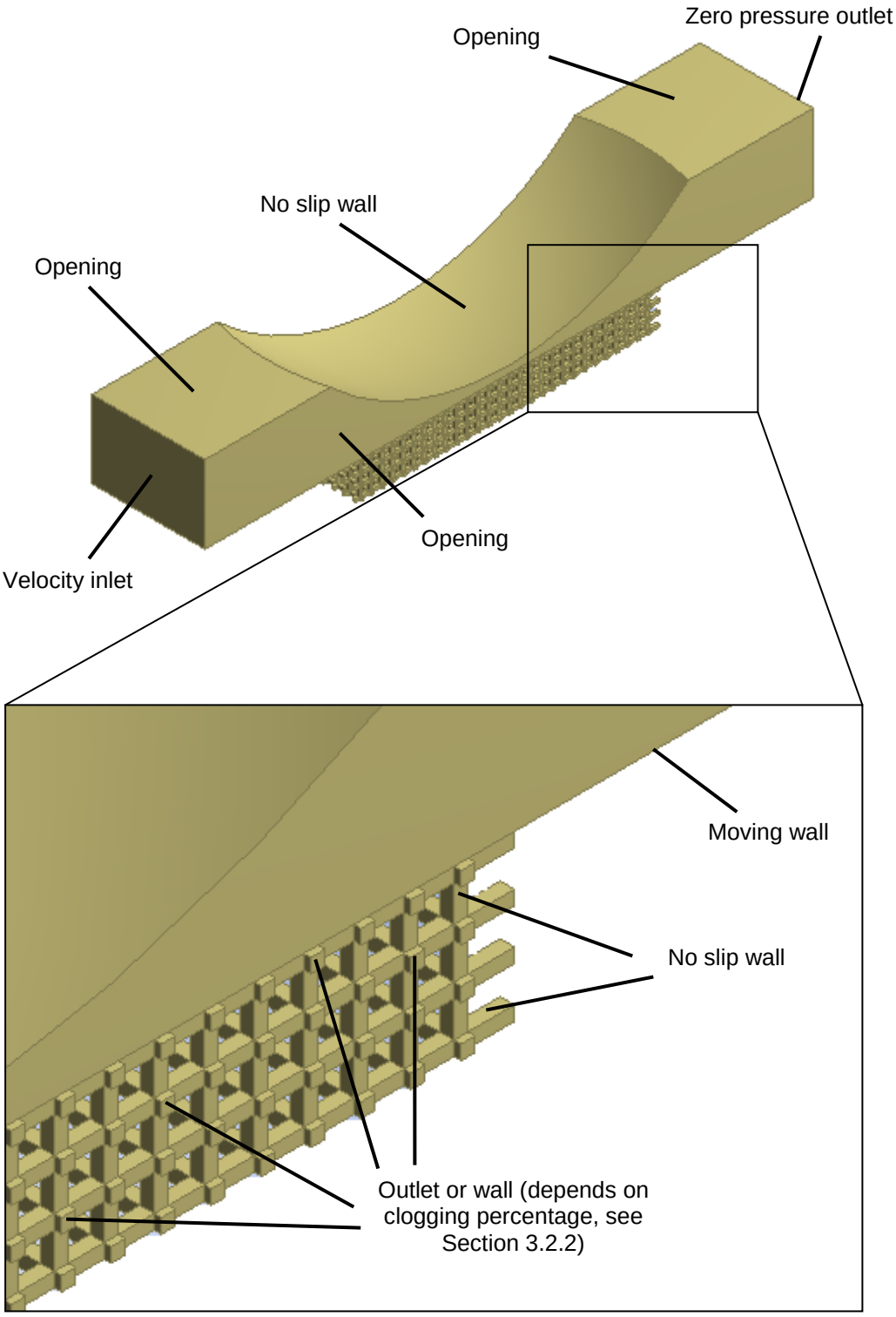

Figure 3.11: Boundary conditions of fluid sub-model

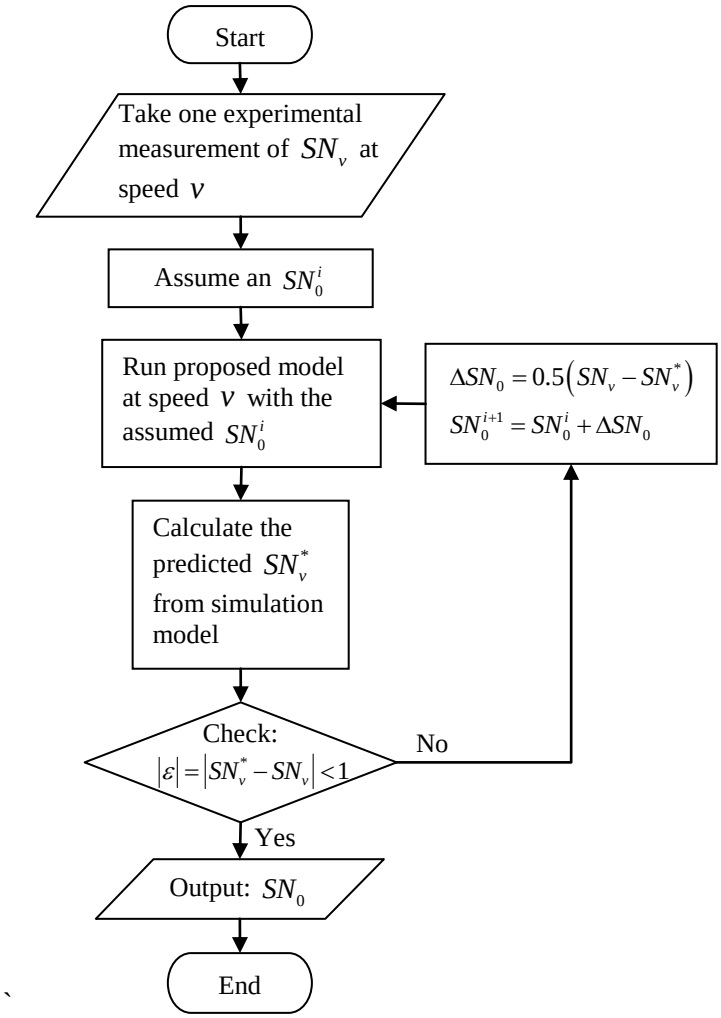

Figure 3.12: Iterative procedures of numerical derivation of SN_0

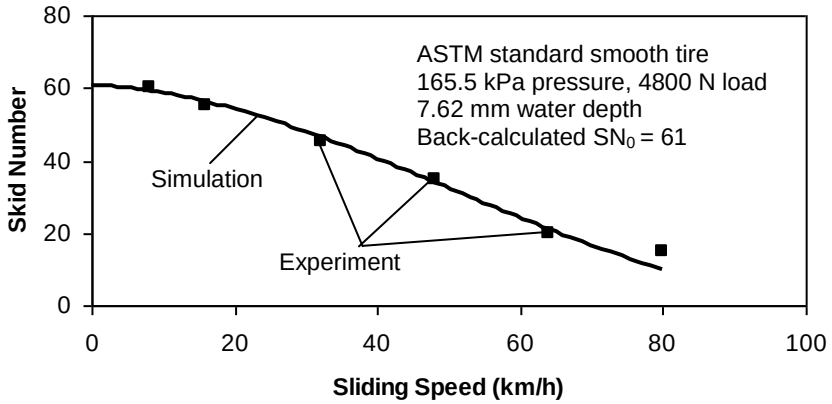

(a) Concrete Pavement (Horne, 1969)

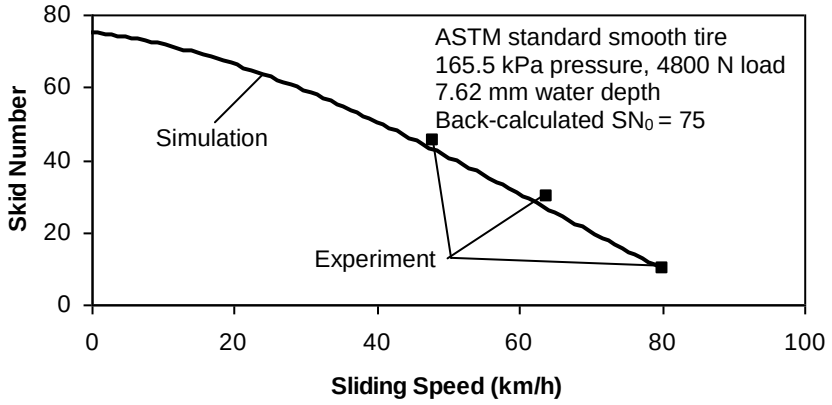

(b) Asphalt Pavement (Horne, 1969)

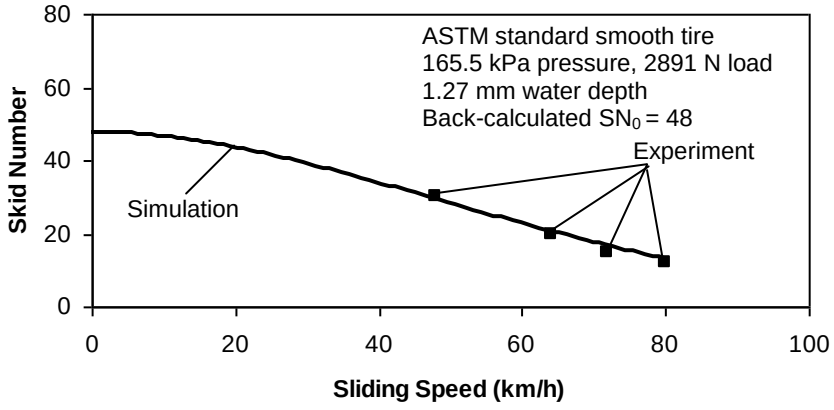

(c) Concrete Pavement (Agrawal and Henry, 1977)

Figure 3.13: Comparison of numerical SN_v and experimental results (conventional pavements)

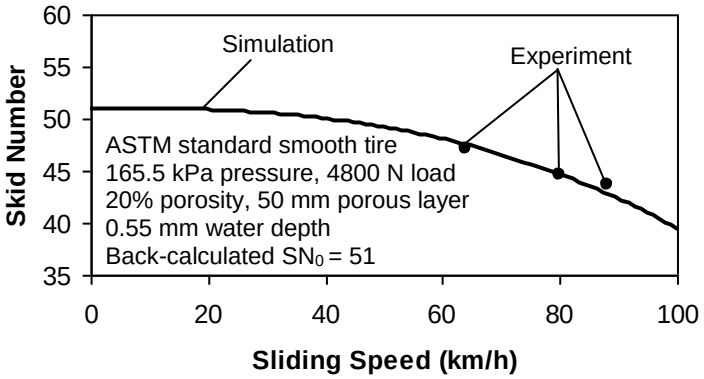

(a) Murphy Road-Lava Butte

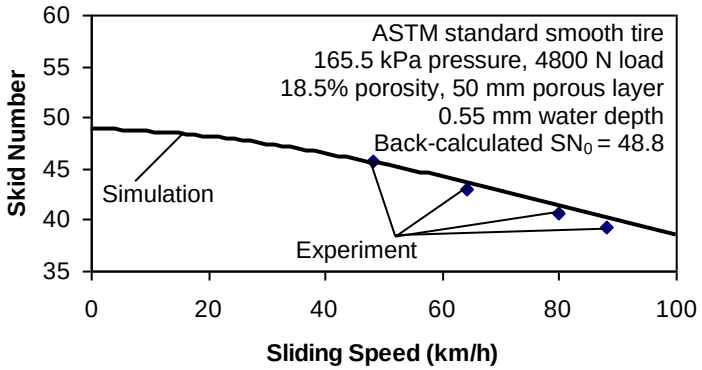

(b) Hayesville-BattleCreek

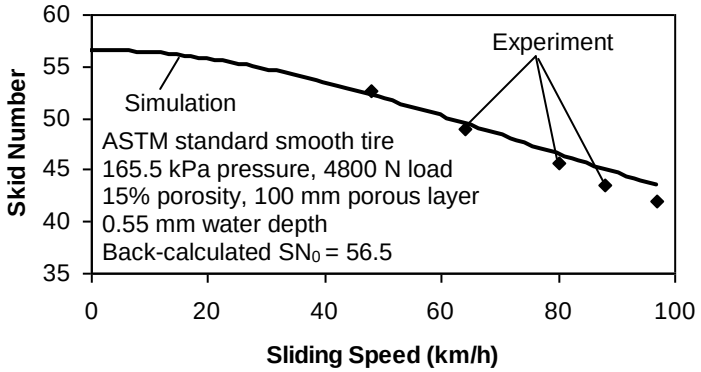

(c) Grants Pass

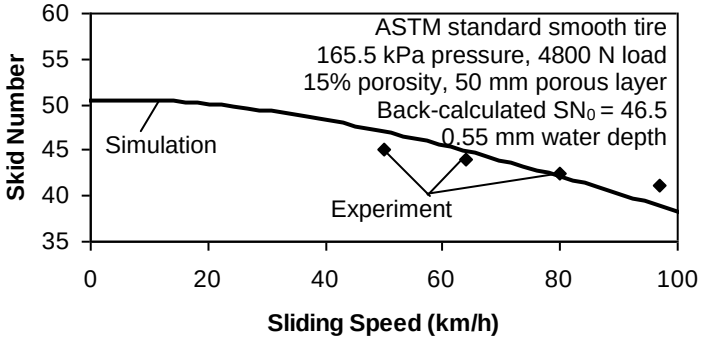

(d) Jumpoff Joe

Figure 3.14: Comparison of numerical SN_v and experimental results (porous pavements)

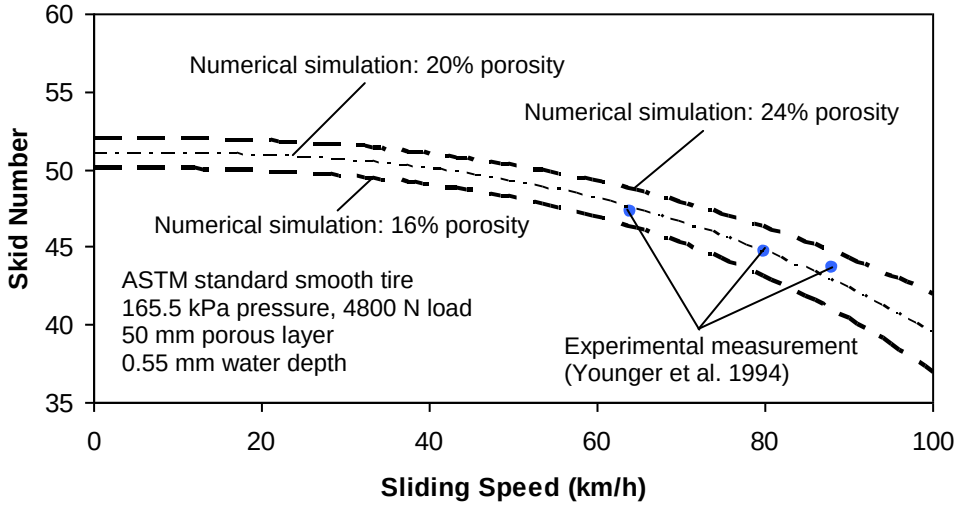

(a) Murphy Road-Lava Butte

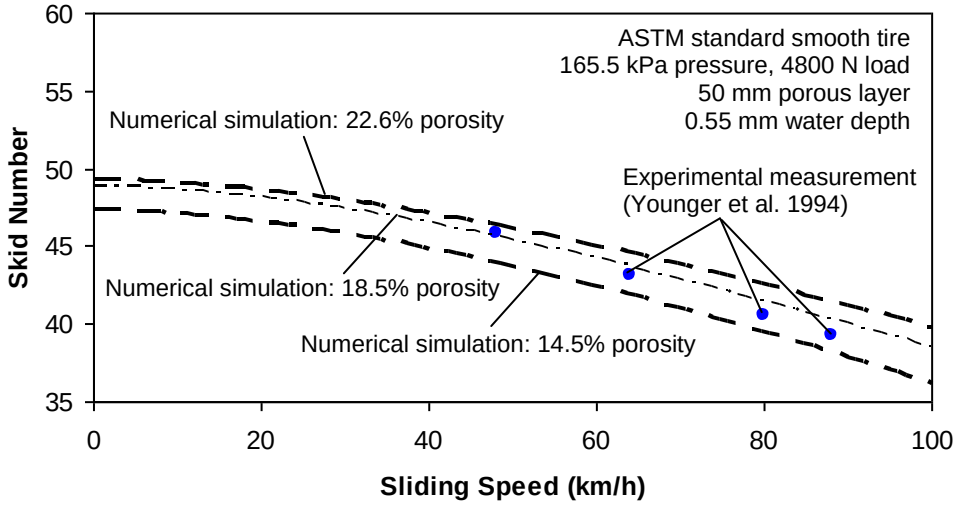

(b) Hayesville-BattleCreek

Figure 3.15: Numerical prediction of SN_v ranges on porous pavements

CHAPTER 4 ANALYSIS OF THE INFLUENCING FACTORS ON SKID RESISTANCE OF POROUS PAVEMENT

As discussed in Section 2.1.4, many operational and environmental factors can significantly affect the skid resistance performance of pavements. There are even more parameters affecting skid resistance on porous pavements. The porosity and thickness of porous surface layer are identified as crucial parameters in the porous pavement design. Rainfall intensity is a critical environmental factor and sliding speed is an important parameter in vehicle operation. The influence of these factors on skid resistance performance of porous pavements are analyzed quantitatively in this chapter using the developed numerical simulation model presented in Chapter 3. An analytical approach integrating water film thickness estimation into the skid resistance evaluation framework is first introduced to allow an accurate prediction of porous pavement frictional performance under a given rainfall intensity. The overall effects of a porous surface layer on wet skid resistance are then analyzed for both porous and non-porous pavements. The effect of each factor influencing skid resistance is next studied to understand the mechanisms of skid resistance enhancement on porous pavements.

4.1 Consideration of Water Film Thickness in the Analysis Framework

Because rainfall results in a layer of water on pavement surfaces and skid resistance is heavily dependent on the water film thickness on pavement surfaces (Rose and Gallaway, 1977), it is essential for the analysis framework to first compute the thickness of water film accumulated on porous and non-porous surfaces before the determination of wet-pavement skid number. Taking this concern into consideration, an analysis framework to determine the skid resistance on a flooded pavement is developed and shown in Figure 4.1. The proposed framework consists of two modules: (a) water film thickness computation module; and (b) numerical skid resistance simulation model. The intermediate solution derived from the first module

is the water film thickness accumulated on the pavement surface. It serves as one of the input parameters required by the skid resistance simulation model where the skid number under a given set of operational and environmental conditions is determined.

4.1.1 Water Film Thickness Computation Module

Various methods have been proposed in the literature to analyze the drainage characteristics of porous pavements and to compute the water film thicknesses on porous and non-porous pavements (Anderson et al., 1998; Charbeneau and Barrett, 2008; Ranieri et al., 2010; Ranieri et al., 2012). Whilst any of these porous surface drainage analysis methods can be used in the analysis framework, this study adopts the water film thickness calculation model for porous and non-porous pavements developed by Anderson et al. (1998). This model computes the depth of water accumulated on pavement surfaces using:

$$t_w = \left[\frac{nL(i-f)}{\alpha S^{0.5}} \right]^{0.6} - MTD \tag{4.1}$$

where t_w is the water film thickness (mm), n is the Manning's roughness coefficient, L represents the length of drainage path (m), i is the rainfall intensity (mm/h), f denotes the infiltration rate into pavement surface (mm/h), S represents the slope of drainage path (m/m), α is a model constant and MTD is the mean texture depth of pavement surface (mm). The Manning's roughness coefficient accounts for the hydraulic effect of pavement surface type on the water depth, and it is surface-specific. Anderson et al. (1998) derived various expressions of Manning's roughness coefficients for different pavement surfaces.

The infiltration rate for dense-graded pavement surface can be taken as zero (i.e. impermeable). For porous pavement, the infiltration rate is related to the drainage capacity of porous surface layer (Charbeneau and Barrett, 2008) and can be roughly estimated by:

$$f = \frac{khS}{L} \tag{4.2}$$

where k is the hydraulic conductivity of the porous surface layer (mm/h) and h is the thickness of the porous surface layer (m).

Equations (4.1) and (4.2) have been incorporated into the PAVDRN software (Anderson et al., 1998). Given information on rainfall intensity, roadway geometry and porous pavement properties, the water film thicknesses accumulated on porous and non-porous pavement surfaces can be computed and used as inputs to the skid resistance simulation model.

4.1.2 Numerical Skid Resistance Simulation Module

A mechanistic evaluation of wet-pavement skid resistance on non-porous pavement surfaces would ideally consider the following: tire structural mechanics, fluid dynamics, tire-pavement contact and tire-fluid interaction; while in the modeling of skid resistance on porous pavements, the additional consideration of drainage capacity of the porous surface layer has to be made. The three-dimensional skid resistance simulation model developed in Chapter 3 would be used to serve this purpose, taking into consideration of both the tire-fluid-pavement interactions and water flow within the porous layer. When the model is adopted on non-porous pavements, the pavement sub-model is assumed to be smooth and rigid in both the structure and fluid models; while applied on porous pavements, the pavement sub-model is still a smooth and rigid plate in the structure model, but is modelled by the proposed grid pore network structure in the fluid model.

As described in Chapter 3, this numerical model consists of three sub-models: pneumatic tire sub-model, pavement sub-model and fluid sub-model, which interact with each other through either fluid-structure interaction or tire-pavement contact (see Figure 4.2). Given detailed information on tire, pavement and fluid properties, vehicle operating conditions, as well as the water film thickness, key information on contact

and traction forces acting on the tire as well as fluid uplift and drag forces can be computed from the simulation model. The skid numbers at specific conditions are then derived from fluid forces and wheel load using Equation (3.48).

4.2 Effect of Porous Surface Layer on Skid Resistance Performance

Porous pavements have been extensively used worldwide to improve the skid resistance and reduce the accident occurrences in wet weather. These benefits mainly result from their capability to drain water off the pavement surface and hence achieve better frictional performance during wet weather. Most of the past research studies on the effectiveness of porous pavements in improving skid resistance and restraining hydroplaning are experimental or empirical in nature (Deuss, 1994; Huddleston et al., 1991; Isenring et al., 1990). It is essential to mechanistically compare and analyze the skid resistance performances of porous and non-porous pavements under identical wet weather condition. This section presents a study to analyze the overall effect of a porous surface layer on skid resistance and interpret how porous pavements provide friction control during wet weather. An illustrative case study is investigated to quantify and compare the skid resistance performances between porous and non-porous pavements, with considerations of the influence of pavement surface type on rain water accumulation.

4.2.1 Description of Hypothetical Problem

Numerous experimental studies in literature (Isenring et al., 1990; Kowalski et al., 2009; McGhee and Clark, 2010; Dell'Acqua et al., 2012; Ivan et al., 2012) have indicated that porous pavements tend to have better skid resistance performance compared to conventional dense-graded pavements. However, two critical questions remain unanswered from past experimental studies: (a) how does porous pavement improve skid resistance? and (b) what is the expected skid number increase when a porous layer is used? The first question is aimed at understanding the mechanisms of

skid resistance on porous pavements and how the improvement in skid number comes about, while the second question aims to determine quantitatively the improvement in skid resistance performance brought forth when using porous pavements instead of non-porous pavement surfaces.

In order to answer the above questions, the developed analysis framework in Section 4.1 could be applied to quantify and compare the skid resistance performance between porous and non-porous pavements. The following hypothetical case study is analyzed to illustrate the differences in skid resistance behavior on porous and non-porous pavements:

- Case I: A dense-graded smooth asphalt pavement on a two-way four-lane tangent section with a 2% cross slope and 15 m road width. The pavement surface course is assumed to be impermeable, with a macrotexture of 0.5 mm mean texture depth (MTD = 0.5 mm). The wet friction coefficient of the tire-pavement interface is assumed to be 0.5 (SN_0 = 50, μ = 0.5).

- Case II: A porous friction course overlaid on a dense-graded asphalt pavement on a two-way four-lane tangent section with a 2% cross slope and 15 m road width. The porous layer thickness is 50 mm with a porosity of 20%. In this study, a hydraulic conductivity of 5.6 mm/s at 20% porosity is assumed based on the past experimental studies (Chuai, 1998; Tan et al., 1999). The wet friction coefficient of tire-pavement interface for this case is also assumed to be 0.50 for comparison basis.

The lock-wheel skid resistance test in accordance to the ASTM E274 method (ASTM, 2011a) is simulated using the proposed numerical model. The ASTM E524 smooth tire (ASTM, 2008b) is considered to be used with a tire inflation pressure of 165.5 kPa and a wheel load of 4800 N. Skid tests are assumed to be performed under different speeds (40 km/h, 60 km/h and 80 km/h) and rainfall intensities (60 mm/h, 150 mm/h and 300 mm/h).

4.2.2 Results and Discussions

The numerical analysis results of water film accumulation and skid number prediction on porous and non-porous pavements are presented and compared in this section. The skid number improvement is quantified and discussed as well. The mechanisms of skid resistance enhancement on a porous pavement is analyzed based on comparisons in fluid force development, tire deformation and tire-pavement contact status.

4.2.2.1 Reduction of Water Film Thickness on Porous Pavements

A direct consequence of the porous pavement applications is the reduction in water accumulation on pavement surfaces during wet weather. Figure 4.3 compares the water film thicknesses on Case I and Case II pavements for different rainfall intensities, which were obtained from the PAVDRN software (Anderson et al., 1998). It can be seen from the figure that water film thickness increases as the rainfall intensity increases on both porous and non-porous pavements. More importantly, water film thickness is higher for impermeable surface than for porous pavement under the same rainfall intensity and the difference is larger at higher rainfall intensity. For Case II, rain water does not start to accumulate on porous pavement surface until the rainfall intensity is higher than a threshold level of about 30 mm/h. The reduction in water-film thickness on porous pavement is highly associated to its drainage capability and may have a significant impact on its frictional performance in wet weather. These computed water-film thicknesses serve as input parameters to the skid resistance simulation model.

4.2.2.2 Quantifying Skid Resistance Performance

Using the water film thicknesses presented in Figure 4.3 at a specific rainfall intensity, the skid numbers at different sliding speeds can be computed using the skid resistance simulation model developed in Chapter 3. Figure 4.4 compares the skid

numbers on Case I and Case II pavements at different speeds and rainfall intensities. The following observations can be made from this figure:

- For Case I, there is a significant decrease in skid number with an increase in sliding speed or an increase in rainfall intensity. At a rainfall intensity of 150 mm/h, the loss in skid number is as high as 57% when the sliding speed increases from 40 to 80 km/h. At a speed of 60 km/h, the loss in skid number is as high as 19% when rainfall intensity increases from 60 to 300 mm/h. These findings indicate that non-porous pavements are highly susceptible to low skid resistance at high sliding speeds and high rainfall intensities.

- For Case II, the decrease in skid number with an increase in sliding speed or an increase in rainfall intensity is relatively small (less than 5 SN units). At a rainfall intensity of 150 mm/h, the loss in skid number is only 6% when the speed increases from 40 to 80 km/h. At a 60 km/h sliding speed, the loss in skid number is a mere 3% when the rainfall intensity increases from 60 to 300 mm/h. Such a small variation in skid number may have given researchers such as Isenring et al. (1990) and McDaniel et al. (2004) the impression that the skid number of porous pavements is "hardly speed-dependent".

- Case II has a consistently higher skid number than Case I for an identical rainfall intensity and sliding speed. The percentage increase in skid number achieved by applying the porous pavement technology ranges between 15% and 215% for the different speeds and rainfall intensities tested in this study and the difference is more pronounced at higher sliding speeds and higher rainfall intensities. This demonstrates that porous pavements can provide superior skid resistance performance in wet weather.

Based on the above findings, it can be seen that Case II is better than Case I in providing high-speed skid resistance and hence ensuring better braking and directional control in wet-weather traffic operations. The benefit can reach up to more

than 200% skid number at 80 km/h sliding speed and 300 mm/h rainfall intensity, according to the presented numerical computations.

4.2.2.3 Contribution of Forces Acting on Tire to Skid Resistance

In order to achieve a fundamental understanding on why porous pavement exhibits a higher skid number than non-porous pavement under the same wet-weather condition, there is a need to examine the major force components acting on the tire in the presence (or absence) of a porous surface course. Figure 4.5 compares the normal contact forces, the fluid uplift forces and the wheel loads acting on the tire for Cases I and II at different traveling conditions. It is clearly observed that the porous surface results in a lower fluid uplift force compared to the dense-graded pavement under the same condition. This may be due to the presence of additional drainage paths within the porous layer, reducing the hydrodynamic pressure build-up underneath the sliding tire. As a consequence, a higher contact reaction force is observed for Case II as opposed to Case I.

Another interesting noteworthy point in Figure 4.5 is that for Case I, the fluid uplift force is equal to the wheel load at about 84 km/h under a rainfall intensity of 300 mm/h. At this point, hydroplaning is said to occur and the tire is separated from the pavement surface by a thin film of water. This hydroplaning speed of 84 km/h corresponds well to that computed by the well-known NASA hydroplaning equation (Horne and Dreher, 1963). For Case II, however, the tire will remain in contact with the pavement surface for the whole practicable range of highway operation speeds. This indicates that adopting of porous surfaces can effectively prevent the occurrence of hydroplaning even at an extreme rainfall intensity of 300 mm/h.

As a result of tire-water-pavement interaction, the skid resistance develops from the traction force at the tire-pavement interface and the drag force at the tire-fluid interface. The former is proportional to tire-pavement contact force, and the latter is the fluid drag force computed from the numerical simulation model. Figure

4.6 illustrates the percentage contributions of traction force and fluid drag force to skid resistance. It is obvious that, for Case I, fluid drag force becomes the dominant component of skid resistance beyond 73 km/h sliding speed at a 300 mm/h rainfall intensity, and at the hydroplaning speed of 84 km/h, a vehicle will only be experiencing the fluid drag (since the wheels are "lifted" off the pavement surface). For Case II, it was noted that even at high sliding speeds, traction force is still the main component of skid resistance. This stark contrast indicates that a major reason why porous pavements can maintain the excellent skid numbers at high speed is to keep fluid uplift and drag forces low while maintaining the contact between tire tread and pavement surface and relying on the traction forces resulting from the tire-pavement contact. This is further demonstrated in Figure 4.7 where it can be seen that at high speed, there is a significant tire deformation causing loss in tire-pavement contact for Case I as compared to Case II at the same rainfall intensity.

From the above case study, it can be concluded that porous pavement is an effective engineering measure to improve wet pavement skid resistance. The superior skid resistance performance of porous pavements is mainly due to its higher porosity and inner drainage capacity. Such characteristics result in a significant reduction in fluid uplift force, providing better contact between tire tread and pavement surface even at extremely high speeds. This develops higher traction force, which dominates the skid resistance on porous pavements. Resulting from the same mechanisms, porous pavements can also prevent the occurrence of hydroplaning at highway operational speed.

4.3 Effect of Influencing factors on Porous Pavement Skid Resistance

The effects of some critical factors on the skid resistance of porous pavements are quantitatively analyzed using an illustrative hypothetical case study. The parameters being examined include the porosity, porous layer thickness, rainfall intensity and sliding speed. The analysis considers the interaction between different

influencing factors. The hypothetical problem is first defined based on a porous asphalt overlay project. The skid resistance performance on porous pavements with various design parameters are then evaluated using the developed simulation model and the numerical results are compared and analyzed for each factor. Some recommendations on porous pavement design are made based on the conclusions drawn from the parametric study.

4.3.1 Description of Hypothetical Problem

A hypothetical problem is defined for illustration purpose in this study. It is assumed that a two-way four-lane crowned tangent highway section with a total width of 15 m is considered to be rehabilitated using a porous asphalt overlay. The existing impermeable dense-graded pavement surface has a longitudinal grade of 0% and a cross slope of 2%. The overlaid surface will preserve the same geometric features as the old pavement. An identical wet tire-road friction coefficient of 0.5 (SN_0 = 50) is assumed for all the porous surface candidates for comparison basis since the asphalt binder and aggregates are assumed to be from the same sources for all porous mixtures. Alternative porous overlay designs with different porosities and thicknesses are considered in design period with focus on their frictional performance. The skid numbers on these porous surfaces under different rainfall intensity levels at different vehicle sliding speeds are predicted and analyzed using the developed numerical simulation model.

The levels of porous layer porosity used in this study cover the common porosity range of porous pavements found in practice. The typical porosity of a newly paved porous layer usually ranges from 18% to 22% (Alvarez et al., 2011). Higher porosity values of as much as 25% have also been used to enhance the safety benefits and reduce the tire-pavement noise (Alvarez et al., 2011). The porosity of porous pavement tends to reduce with time due to the clogging effect. To cater for the deterioration of porosity with time, some road agencies adopt a design terminal value

of 15% for porosity (Liu and Cao, 2009). These considerations form the basis for selecting five porosity levels in this study, i.e. 15%, 17.5%, 20%, 22.5% and 25%.

The levels of porous layer thickness considered in this analysis cover the regular thickness range of porous surface course found in practice as well. It is noticed from the extensive review of porous pavement projects that most of porous layers used as overlays or wearing courses vary from 50 mm to 100 mm thick (Smith, 1992; Moore et al., 2001). There are also instances where thin lift of porous layers with a thickness of 25 mm are used (Smith, 1992). Moreover, porous surface layers in the United States are usually paved in an integer multiple of 1 inch (25.4 mm). Therefore, four porous layer thicknesses are considered in this study, namely 25 mm, 50 mm, 75 mm and 100 mm.

The levels of rainfall intensity considered in this analysis have to be sufficiently large so that a significant thickness of free standing water film can form on the porous pavement surfaces. The upper bound of examined rainfall intensity is determined according to the meteorology of project location.. From past research studies on extreme rainfall intensities (Hershfield, 1984; De Toffol et al., 2009; Langousis and Veneziano, 2009) and computations of water film thickness on porous pavements (Anderson et al., 1998), five rainfall intensity levels are involved in this study, i.e. 60 mm/h, 100 mm/h, 150 mm/h, 225 mm/h and 300 mm/h.

The range of vehicle sliding speeds considered in this analysis cover the common operating conditions encountered by passenger cars on the roadways in a raining weather. A 20 km/h speed step is selected in order to properly develop the speed-dependency of skid number on porous pavements. Five speed levels are included in this study, namely 20 km/h, 40 km/h, 60 km/h, 80 km/h and 100 km/h.

The skid resistance performance of the various porous overlays is evaluated and compared under the above defined conditions using the proposed analysis framework. The range of values examined for each variable are believed to be adequate for most porous pavement applications and common wet-weather operating

conditions. The simulation results are analyzed for each individual influencing factor, taking the interactions between different factors into consideration.

4.3.2 Influence of Porosity

As recognized from past experimental studies (Page, 1993; Younger et al., 1994), the superior skid resistance performance of porous pavements mainly results from their excellent drainage capacity. Rainwater on pavement surfaces can be easily discharged through the inter-connected pores and the surface macrotexture. It not only reduces the water film thickness on pavement surface, but also releases hydrodynamic pressure developing between tire tread and pavement surface. In most applications, the porous surface layer serves only as a functional surface course without structural contribution. Therefore, porous pavement design typically focuses on its drainage capacity if the primary purpose is to enhance skid resistance. From this perspective, the porosity of a porous surface layer is the most crucial factor closely related to its drainage capacity. The influence of porosity on the frictional performance of porous pavements is quantitatively analyzed in this section.

Based on the skid numbers computed by the developed numerical simulation model, Figure 4.8 is plotted to illustrate the influence of porous layer porosity on the skid resistance for different levels of porous layer thickness, rainfall intensity and vehicle speed, respectively. In general, higher skid numbers are seen on pavements with higher porosity levels, when all the other three parameters are held constant. This is expected because more interconnected air voids are available when the porosity of a porous pavement increases, thereby resulting in more effective water discharge underneath the vehicle tires and enhancing the skid resistance performance of the porous pavement. It is noted from Figure 4.8 that skid number increases with porosity increase in an approximately linear manner. This indicates that skid resistance is constantly improved as porosity increases. Taking a closer look at the three plots, the following additional observations can be made from Figure 4.8:

- Figure 4.8(a) illustrates the variations of skid number with porosity for the four porous layer thickness levels under the same operation condition with a 150 mm/h rainfall intensity and an 80 km/h vehicle sliding speed. This plot could be used to examine the effect of porous layer thickness on the efficiency of porosity-induced skid resistance improvement. When the porosity increases from 15% to 25%, the skid number increases by 1.6, 1.9, 2.0 and 2.1 SN units respectively for 25, 50, 75 and 100 mm porous layer thickness. These results suggest that increasing porosity in a thicker porous surface layer produces better results in improving skid resistance.

- Figure 4.8(b) examines the effect of increasing porosity under different rainfall intensities, for the case of 50 mm porous layer thickness and 80 km/h vehicle sliding speed. Skid resistance improvement resulted from the increasing porosity is found to be more effective at higher rainfall intensities. When porosity value increases from 15% to 25%, the skid number increases by 1.4 SN units at 60 mm/h rainfall intensity, and increases by 2.1 SN units at 300 mm/h rainfall intensity.

- Figure 4.8(c) compares the skid number variation with porosity increase for different vehicle speeds under the travel condition of 150 mm/h rainfall intensity and 50 mm porous layer thickness. When the porosity value increases from 15% to 25%, the skid resistance improvement is 2.6 SN units at a vehicle speed of 100 km/h. The corresponding increase at vehicle speed of 20 km/h is only 0.2 SN units. These results show that the skid resistance improvement due to increasing porosity is more efficient and more significant at higher sliding speed than at lower speed.

To summarize, the above observations indicate that wet skid number on porous overlay increases with increasing porous layer porosity and the enhancing effect of porosity becomes more significant in the case of thicker porous layer, higher rainfall intensity and higher vehicle speed. Therefore, porous mixture with a larger porosity value should be used for skid resistance enhancement, as long as the large air void content does not adversely affect other performance such as durability, revelling

resistance and rutting resistance. In addition to skid resistance improvement, larger porosity may also give benefits in splash/spray reduction and clogging resistance.

4.3.3 Influence of Porous Layer Thickness

In addition to porosity value, the thickness of porous surface layer is also a critical factor in porous pavement design. It affects the drainage capacity of porous pavement system. A thicker porous layer is capable to store more rainwater within its pores in raining weather before a significant water film appears on pavement surface. A thicker porous layer may also provide a larger outlet area at roadsides to make the lateral drainage of water more efficient. The influence of porous layer thickness on porous pavement skid resistance performance is analyzed in this section based on numerical simulation results.

Figure 4.9 illustrates the skid numbers computed from numerical simulation models for pavements with different porous layer thicknesses. Skid number variations with porous layer thickness are plotted with respect to pavement porosity, rainfall intensity and vehicle speed in each sub-figure, respectively. The following trends are observed from these plots:

- Generally, all the plots show increasing trends of skid number as porous layer thickness increases, although the rates of increase in skid number tend to diminish when porous surface becomes thicker. These increasing trends indicate that, all other parameters being equal, a pavement with thicker porous surface layer produces a superior skid resistance performance.

- Figure 4.9(a) illustrates the relationships between skid number and layer thickness for porous overlay courses with different porosities at an identical operating condition of 150 mm rainfall intensity and 80 km/h vehicle speed. This plot actually interprets the same set of data as shown in Figure 4.8(a) from a different perspective. It is observed that the increase of skid number with porous layer thickness is slightly higher on a surface with a larger porosity. At 25% porosity, the skid number increases

by 2.4 SN units when the porous layer thickness increases from 25 to 100 mm, while at 15% porosity, the corresponding increase is 1.9 SN units.

- In Figure 4.9(b), the variation of skid number with porous layer thickness at different rainfall intensities is presented. Vehicle speed and pavement porosity are fixed at 80 km/h and 20%, respectively. The trends of curves show that, provided all other conditions being equal, higher skid resistance improvement can be obtained at higher rainfall intensity when porous layer thickness increases. In the examined thickness range (i.e. 25 to 100 mm), skid number increases by 2.8 SN units at 300 mm/h rainfall intensity, and 1.6 SN units at 60 mm/h rainfall intensity.

- Figure 4.9(c) shows the effect of vehicle sliding speed on the relationship between porous pavement layer thickness and skid resistance. In this plot, surface porosity and rainfall intensity are held constant at 20% and 150 mm/h respectively. The skid resistance improvement through thickening porous surface layer is found to be more effective at higher skidding speed. When porous layer thickness increases from 25 mm to 100 mm, the skid number increases by 3.6 SN units at a vehicle speed of 100 km/h, but only increases by 0.2 SN units at 20 km/h.

To summarize, skid resistance on porous pavement increases with increasing porous layer thickness. The influence of porous layer thickness on skid resistance is found to be more significant in the case of larger porosity, higher rainfall intensity or higher vehicle speed. A thicker porous surface layer should be used to enhance skid resistance performance if the added materials do not reduce the cost effectiveness of the whole pavement structure. In addition to skid resistance improvement, larger porous layer thickness may also provide benefits in terms of reduction of splash/spray and improvement of urban runoff quality.

4.3.4 Influence of Rainfall Intensity

The present of rainwater on pavement surface is the essential cause of friction reduction in wet weather. Since water viscosity is much lower than the frictional bond

between tire rubber and aggregate, the water film serves as lubricant at the tire-pavement interface. The hydrodynamic pressure developed within the water film underneath a traveling tire is closely related to the water film thickness accumulated on pavement surface, which is directly determined by the rainfall intensity. Therefore, it is necessary to examine the skid resistance performance of porous pavements under different rainfall intensities in order to further understand the frictional properties of porous pavements. The influence of rainfall intensity on the skid resistance of porous pavements is analyzed in this section.

The results of numerical simulation analysis are summarized in Figure 4.10 to illustrate the influence of rainfall intensity on porous pavement skid resistance. Each of these three plots shows the variation of skid number with rainfall intensity for different values of pavement porosity, porous layer thickness or vehicle speed. The following characteristics of the rainfall effect are observed:

- All three plots in Figure 4.10 show the general decreasing trend of skid number with rainfall intensity. This is expected because for a specific porous surface, its drainage capacity is identical at various rainfall intensities. Heavier rainfall can cause a thicker water film on pavement surface, where more water may be trapped underneath the tires when a vehicle slides over, resulting in a reduced skid resistance performance. Furthermore, it is also observed that the skid number decreases with the increase of rainfall intensity in a concave manner. It declines more rapidly in the beginning as rainfall intensity rises from 60 mm/h, and tends to level off at higher rainfall intensities.

- In Figure 4.10(a), the vehicle speed and porous layer thickness are kept constant (i.e. 80 km/h and 50 mm, respectively), while varying the pavement porosity. Skid resistance appears to be affected marginally more by rainfall intensity at a lower porosity level. At a 15% porosity, skid resistance drops by 3.5 SN units when rainfall intensity increases from 60 to 300 mm/h; while at a 25% porosity level, the reduction is 2.8 SN units.

- In Figure 4.10(b), vehicle speed and pavement porosity are kept constant (i.e. 80 km/h and 20%, respectively), while varying the thickness of porous surface layer. It is seen that the largest fall of skid number with rainfall intensity occurs when the porous surface layer is the thinnest at 25 mm. The reduction of skid resistance is 3.7 SN units for 25 mm thick porous layer when rainfall intensity increases from 60 to 300 mm/h, while it is 2.5 SN units on the 100 mm thick layer. Similar decreasing rates of skid number with increasing rainfall intensity are observed on porous surfaces thicker than 50 mm.

- In Figure 4.10(c), the pavement porosity and surface layer thickness are maintained constant (i.e. 20% and 50 mm, respectively), while varying the vehicle sliding speed. It is apparent from the plot that skid resistance reduction due to increasing rainfall intensity is more significant at high sliding speeds. The skid resistance performance is reduced by 4.9 SN units at a 100 km/h vehicle speed when the rainfall intensity increases from 60 to 300 mm/h, while it is only 0.1 SN units at 20 km/h under the same rainfall intensity increment.

In summary, the simulation results demonstrate that tire-pavement skid resistance is adversely affected by increasing rainfall intensity. The influence of rainfall intensity on porous pavement frictional performance is more severe when pavement surface porosity is lower, porous layer thickness is thinner, or when vehicle speed is higher.

4.3.5 Influence of Vehicle Speed

Vehicle sliding speed is another critical factor influencing porous pavement skid resistance. It may be the most important parameter in vehicle operation that has a significant impact on the wet-pavement skid resistance performance. In the standard lock-wheel measurement (ASTM, 2011a), test speed is specified as 40 ± 1 mph (65 ± 1.5 km/h). However, the operational traveling speeds on roads vary dramatically between different locations and vehicle types. The benefits in skid resistance

improvement obtained from applying porous pavements may differ significantly at different sliding speeds. The influence of vehicle sliding speed on porous pavement skid resistance is numerically investigated in this section.

The illustrative numerical simulation results are presented in Figure 4.11 to analyze the effects of vehicle sliding speed on tire-pavement skid resistance. These plots provide insights on how vehicle speed influence skid resistance when surface porosity, porous layer thickness, and rainfall intensity are varied. The following observations on skid number variations with vehicle sliding speed can be achieved:

- In general, the three plots show that wet-pavement skid resistance on porous pavements reduces as vehicle speed increases. This observation is similar to that on dense-graded pavements (Fwa and Ong, 2008). It is understood that when a vehicle skids on road at a higher speed, there is more water to be discharged from tire-pavement contact patch in a certain time instant. More water may be trapped underneath the tire, resulting in a reduced skid resistance at higher speed. All the curves are convex in shape, indicating that skid resistance reduces faster with unit speed incremental at higher sliding speeds.

- Figure 4.11(a) shows how surface layer porosity affects the decreasing trend of skid resistance with vehicle speed. The results are plotted for the case of 150 mm/h rainfall intensity and 50 mm porous layer thickness. It is found that the fall of skid number with speed is more severe on porous pavement with lower porosity. When vehicle speed is raised from 0 to 100 km/h, the fall in skid resistance is 8.4 SN units at 15% porosity, and 5.8 SN units at 25% porosity.

- Figure 4.11(b) shows how different porous layer thicknesses affect the decreasing trend of skid resistance with vehicle speed. The illustrated data are for the case of 20% porous layer porosity and 150 mm/h rainfall intensity. The plot indicates that larger skid resistance reduction is observed on the surface with a thinner porous course for a certain vehicle speed increase. With a 25 mm thick porous surface, the

skid number reduces by 9.4 SN units when vehicle speed increases from 0 to 100 km/h; while with a 100 mm thick porous surface, the reduction is 5.8 SN units.

- Figure 4.11(c) illustrates the effect of rainfall intensity on the relationship between skid resistance and vehicle speed. The plotted data are for the case of 20% porous layer porosity and 50 mm porous layer thickness. The influence of vehicle speed on skid resistance is found more significant at higher rainfall intensity. The skid number is reduced by 8.4 SN units at a 300 mm/h rainfall intensity when vehicle speed increases from 0 to 100 km/h. For the same speed incremental, the skid number only drops by 3.5 SN units at the rainfall intensity of 60 mm/h.

Overall, the above findings show that skid number on porous pavements deteriorates as vehicle sliding speed increases. The effects of vehicle speed on tire-pavement skid resistance is more significant at lower pavement porosities, thinner porous layer thicknesses and higher rainfall intensities. Therefore, increasing the porosity and thickness of porous surface layers can help to reduce the speed-dependency of wet skid number and provide a more consistent frictional condition in wet-weather traveling.

4.4 Summary

This chapter applied the developed numerical simulation model to analyze the mechanisms and influencing factors of wet skid resistance enhancement on porous pavements. An analysis framework was first developed to integrate the wet pavement surface condition into the skid number prediction. Water film thickness computation module and skid resistance simulation model are the two major components of this framework. The former determines the water film thickness accumulated on a porous or non-porous pavement, which is a important input parameter in the skid resistance simulation. The latter is capable to predict the skid number at a given environmental and operational condition.

The proposed analysis framework was next used to analyze the overall effect of a porous surface layer on wet-pavement skid resistance. This application aimed to quantify skid resistance improvement achieved on porous surfaces as compared to conventional dense-graded surfaces. It was found in the illustrative case study that porous pavement can be an effective engineering measure to improve wet-pavement skid resistance at different rainfall intensities and vehicle speeds. The use of porous pavement results in a lower fluid uplift force, better tire-pavement contact status, higher traction force and less tire deformation - all of which are essential to achieving a higher skid number. Furthermore, tire-pavement contact can be well maintained on porous surfaces even at high sliding speeds.

The analysis framework was next used to investigate the influence of various pavement parameters and vehicle operating conditions on the tire-pavement skid resistance. The availability of the analytical model enables one to study in detail the effects of individual factors (e.g. pavement surface porosity, porous layer thickness, rainfall intensity and vehicle speed) through a hypothetical case study. The following findings have been made from the simulation analyses conducted in this study:

- Skid resistance of porous pavements in wet weather increases when either the porosity or the thickness of porous surface layer increases, but decreases when either the rainfall intensity or vehicle speed increases.
- Skid resistance increases with surface layer porosity approximately linearly in the porosity range of 15% to 25%. The beneficial effect of porosity in skid resistance improvement is more prominent in the situations with thicker porous surface layer, higher rainfall intensity and higher vehicle speed.
- Skid resistance increases nonlinearly with an increase in porous layer thickness. The increasing trend of skid number is more pronounced for thin porous layers, and tends to flatten as the porous layer becomes thicker than 75 mm. The skid resistance benefit of increasing porous layer thickness is more substantial for porous

pavements with higher porosity, and operating conditions under higher rainfall intensity and higher vehicle speed.

- Skid resistance decreases with the increase of rainfall intensity in a concave manner. The reduction rate is higher at lower rainfall intensity levels. The adverse effect of increasing rainfall intensity on skid resistance reduction is more significant for pavements with lower porosities and thinner porous surface layer, and at higher traffic speeds.
- Skid resistance decreases with the increase of vehicle sliding speed in a convex manner. Skid resistance reductions become more significant as vehicle speed increases. The effects of vehicle speed on skid resistance reduction are more critical in the cases of lower porosity, thinner porous layer and higher rainfall intensity.

Based on the findings above, some recommendations can be made for porous pavement design from the perspective of wet-weather driving safety. A high porosity in the surface layer is preferred to better utilize its advantage in wet skid resistance improvement, as long as it does not adversely affect other structural and functional performance of porous pavements. It does not only increase the skid resistance, but also reduces the negative influence of rainfall intensity and vehicle speed, so that a more consistent driving behaviour can be maintained in rainy days. The findings also suggest that, from the safety point of view, a minimum of 50 mm thickness of porous surface layer should be used. A thickness of 75 mm is recommended at a reasonable material cost. Thickness higher than 75 mm may not be cost effective as it does not provide much additional skid resistance benefits.

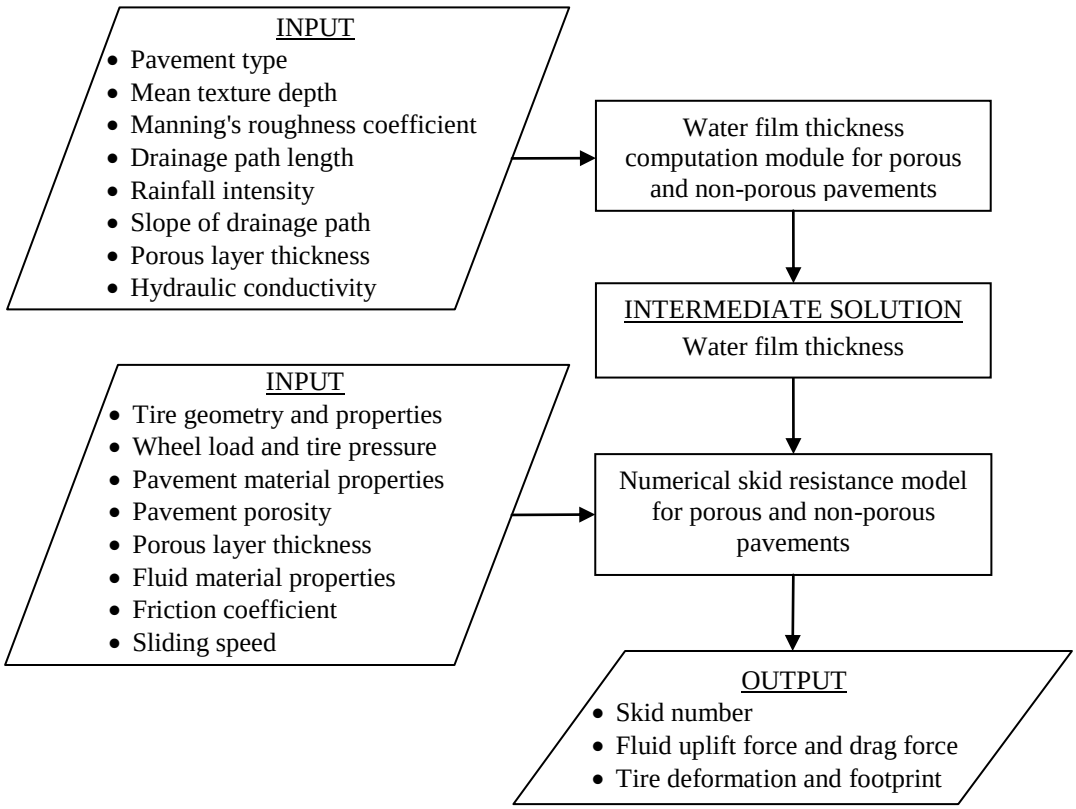

Figure 4.1: Analysis framework of skid resistance on wet pavements

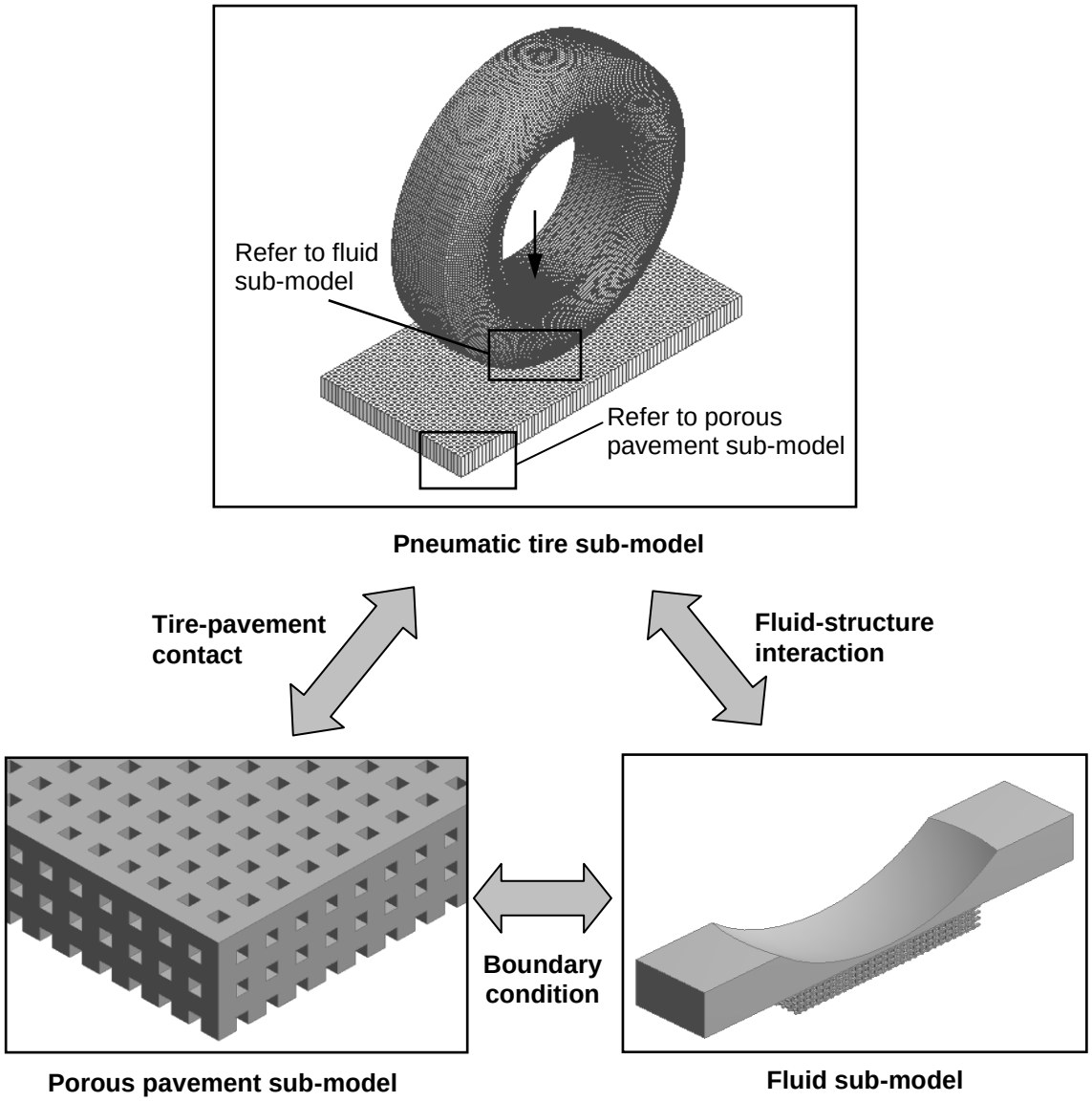

Figure 4.2: Skid resistance model for porous pavements

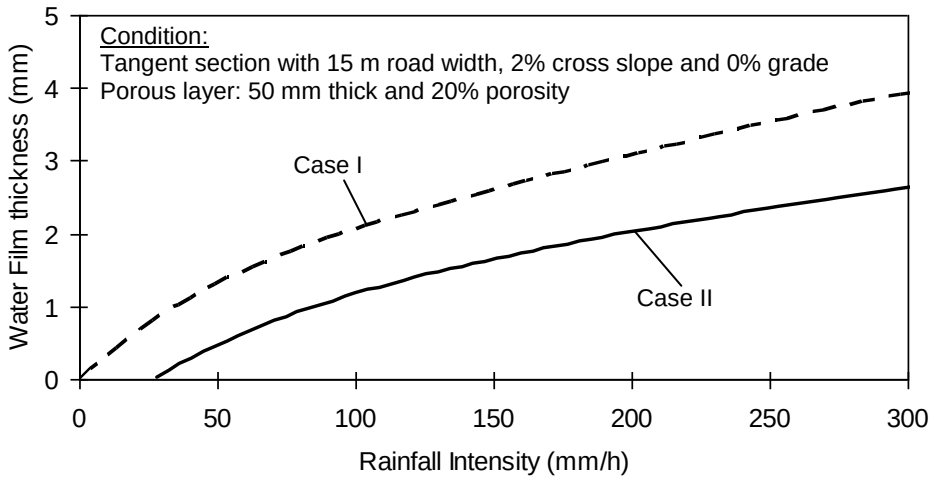

Figure 4.3: Water film thickness on pavement surfaces at different rainfall intensities

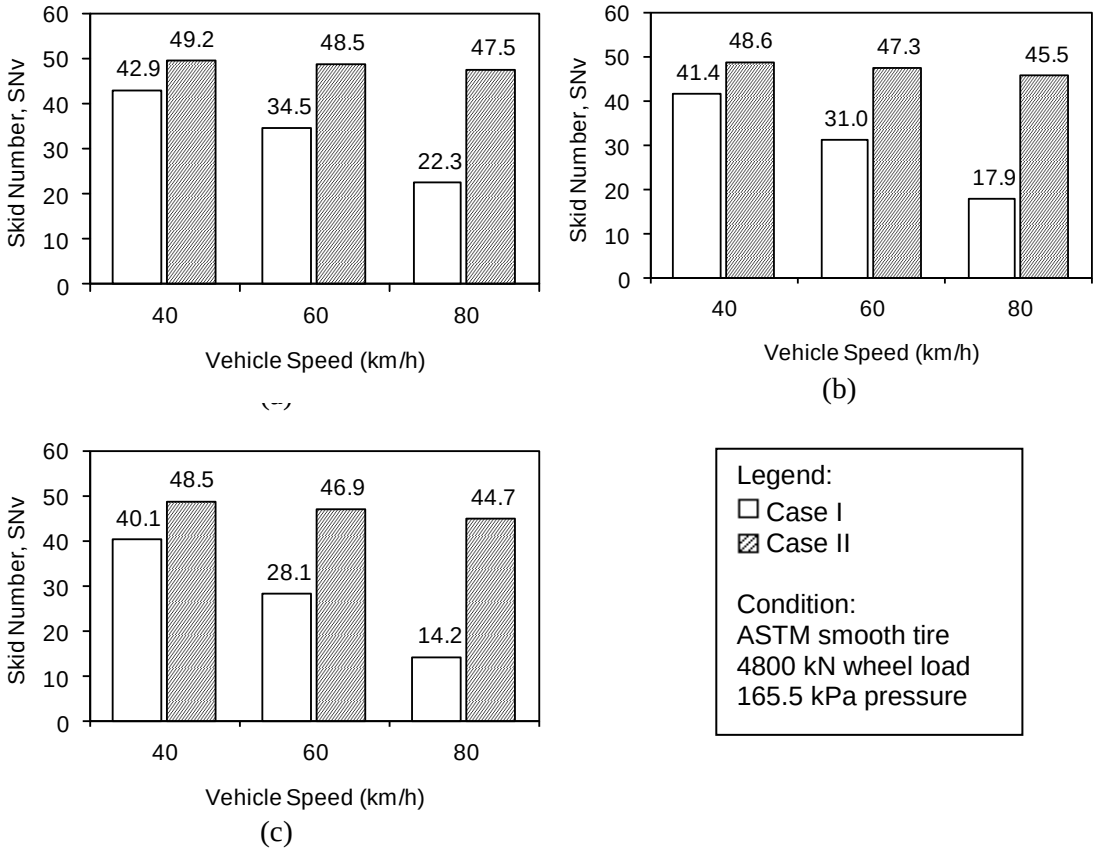

Figure 4.4: Comparing skid resistance on Case I and Case II pavements: (a) 60 mm/h rainfall intensity, (b) 150 mm/h rainfall intensity, (c) 300 mm/h rainfall intensity

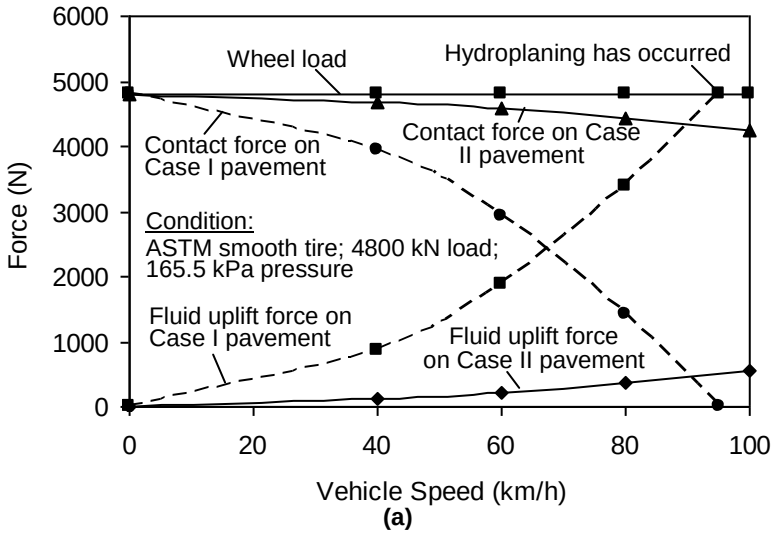

(a)

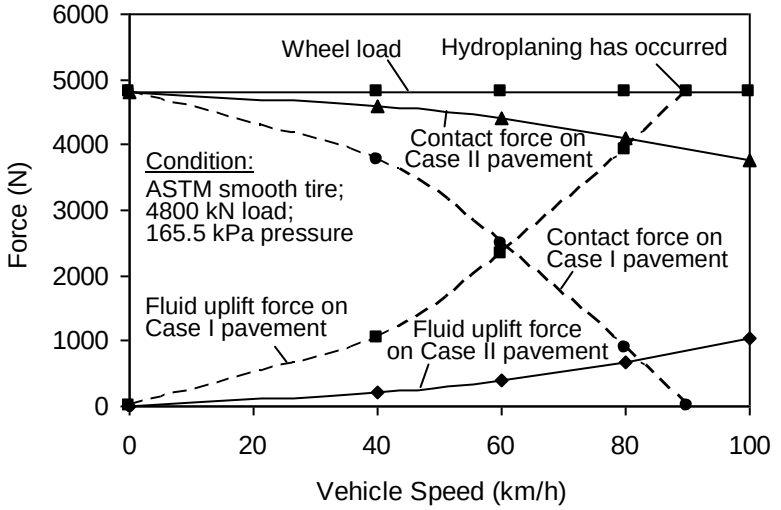

(b)

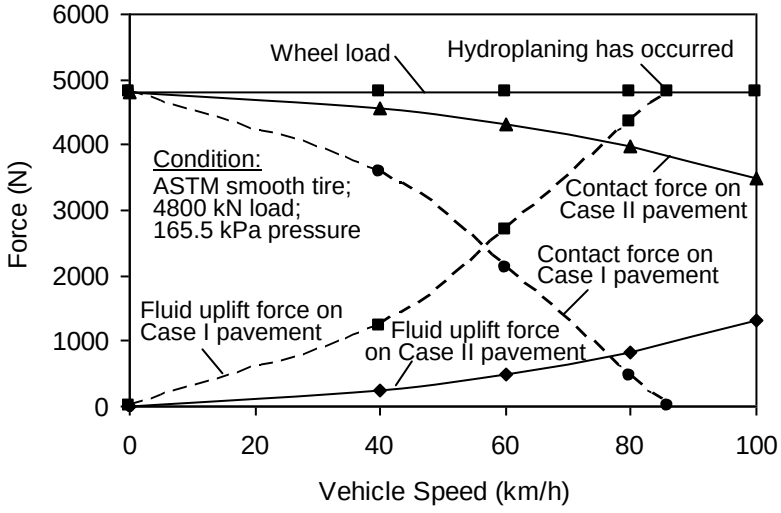

(c)

Figure 4.5: Vertical forces acting on wheel at different speeds: (a) 60 mm/h rainfall intensity, (b) 150 mm/h rainfall intensity, (c) 300 mm/h rainfall intensity

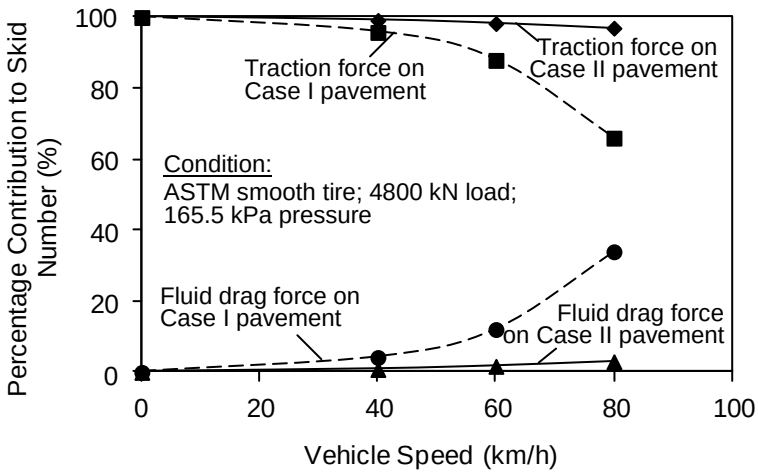

(a)

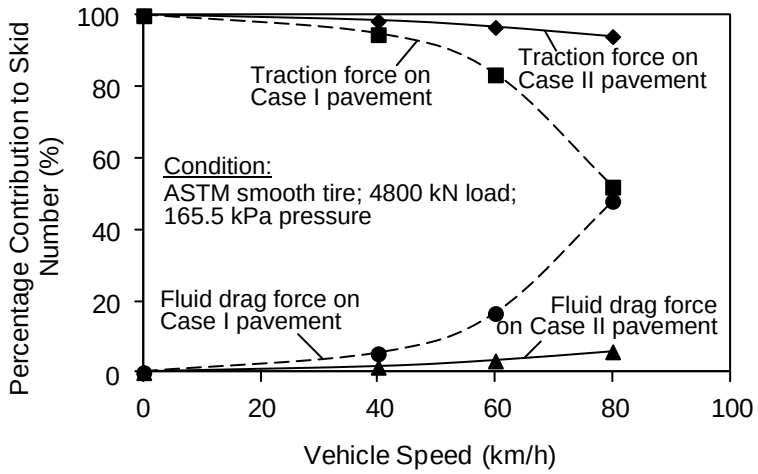

(b)

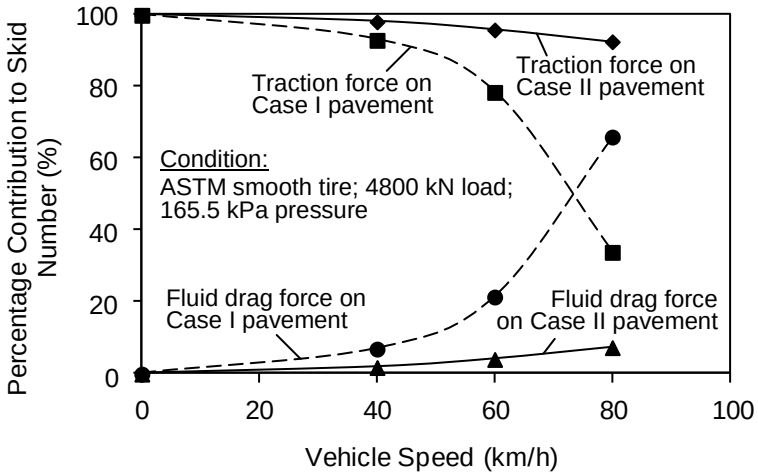

(c)

Figure 4.6: Contribution of traction and drag forces to skid resistance: (a) 60 mm/h rainfall intensity, (b) 150 mm/h rainfall intensity, (c) 300 mm/h rainfall intensity

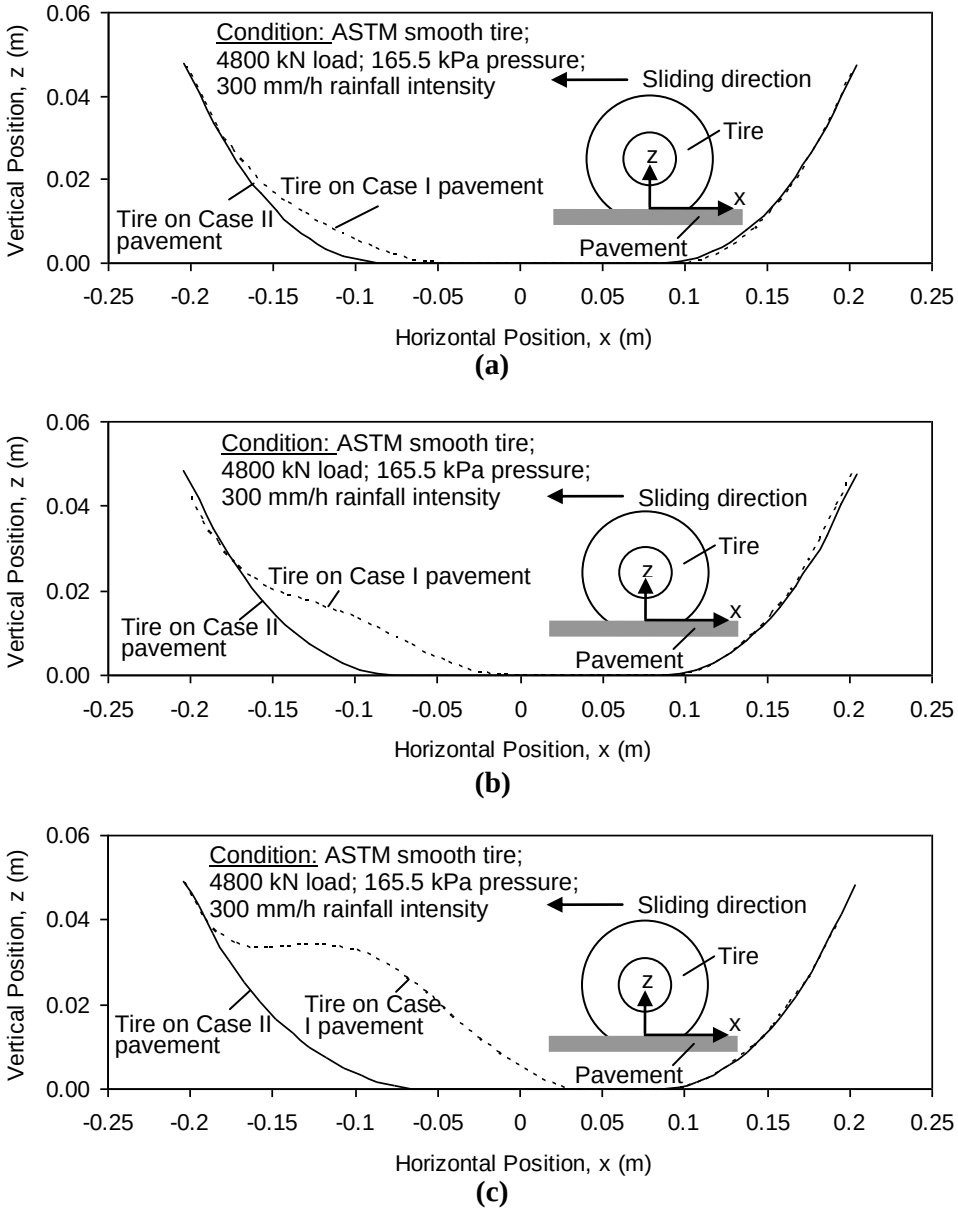

Figure 4.7: Tire deformations at various speeds for 300 mm/h rainfall intensity: (a) 40 km/h vehicle speed, (b) 60 km/h vehicle speed, (c) 80 km/h vehicle speed

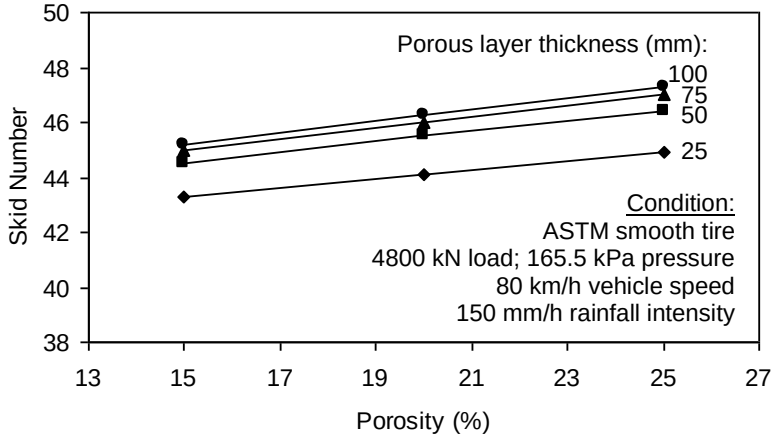

(a)

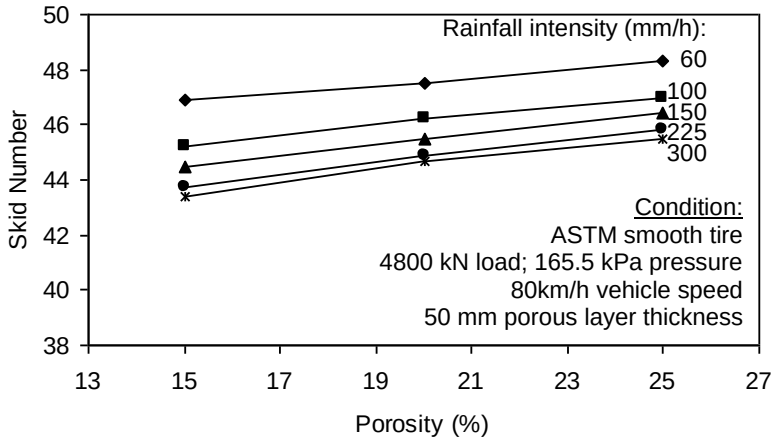

(b)

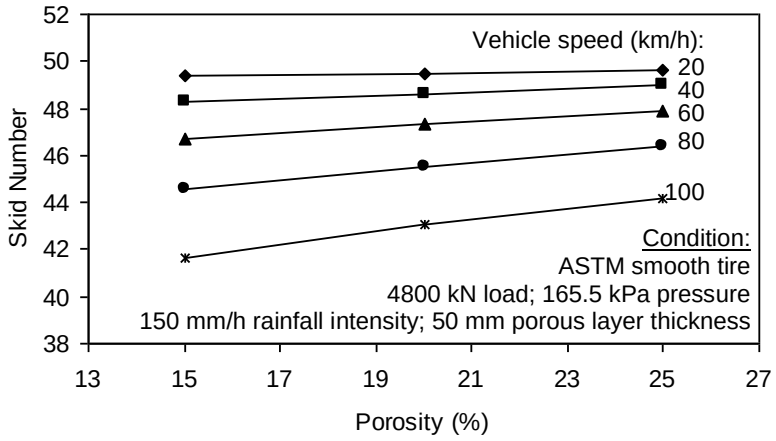

(c)

Figure 4.8: Influence of porosity on skid number: (a) among porous layer thicknesses, (b) among rainfall intensities, (c) among vehicle speeds

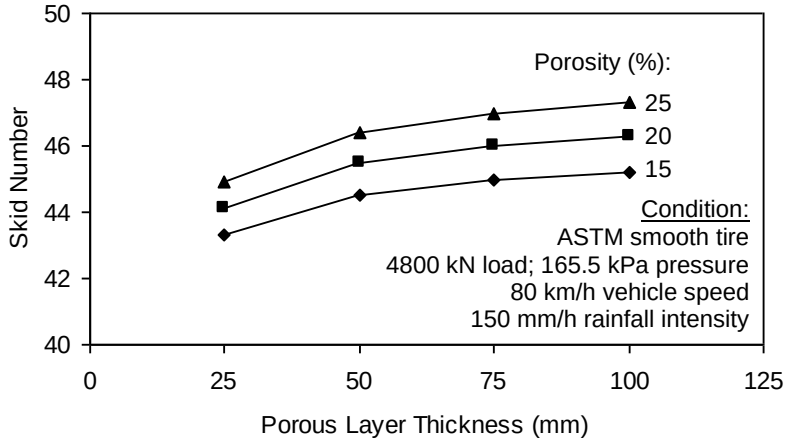

(a)

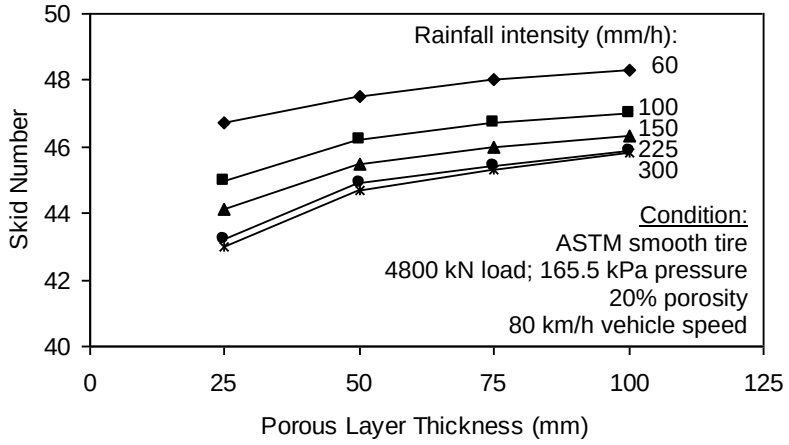

(b)

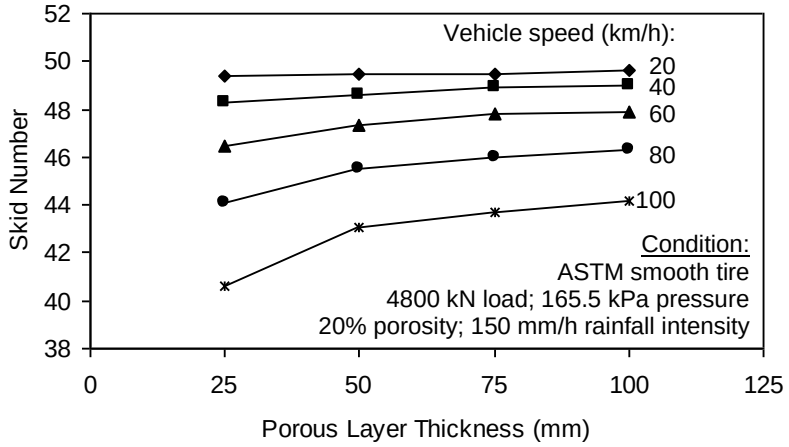

(c)

Figure 4.9: Influence of porous layer thickness on skid number: (a) among porosities, (b) among rainfall intensities, (c) among vehicle speeds

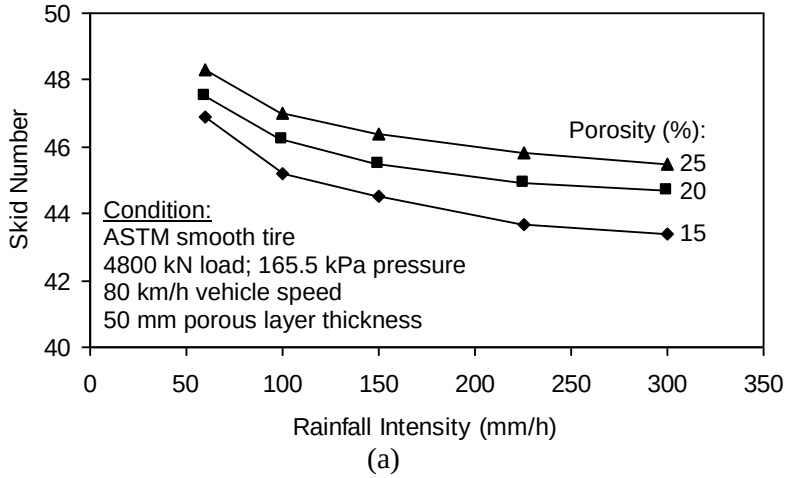

(a)

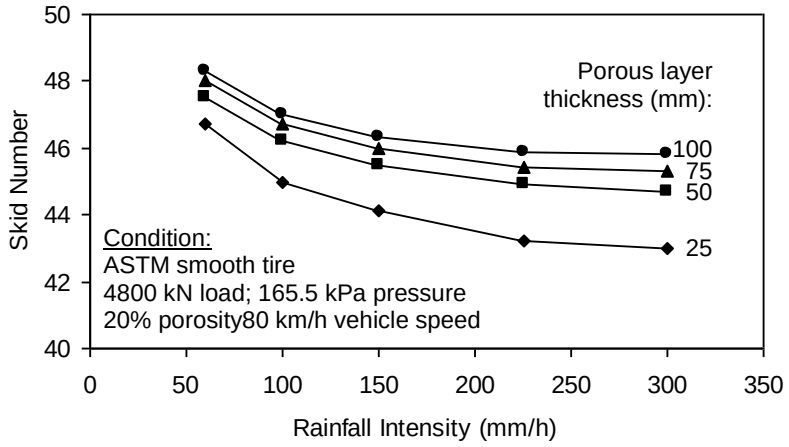

(b)

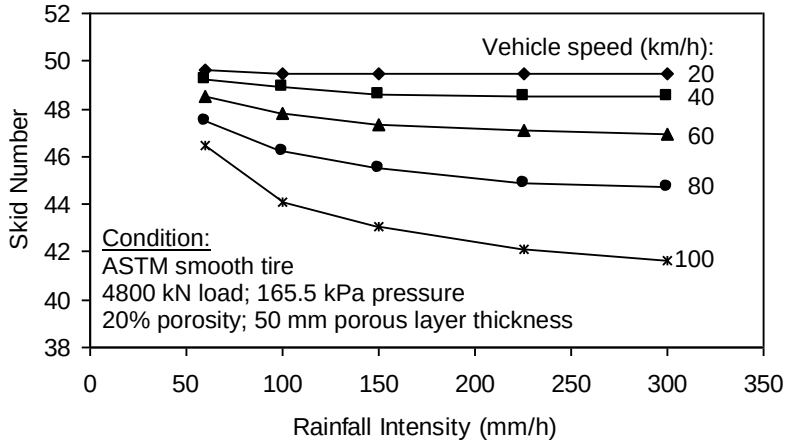

(c)

Figure 4.10: Influence of rainfall intensity on skid number: (a) among porosities, (b) among porous layer thicknesses, (c) among vehicle speeds

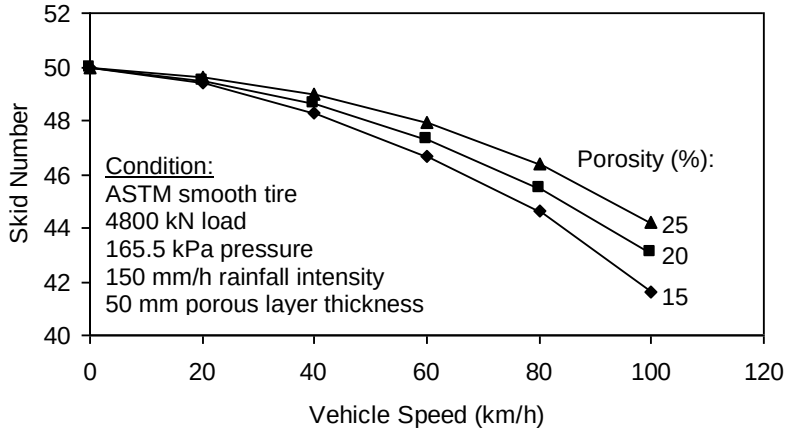

(a)

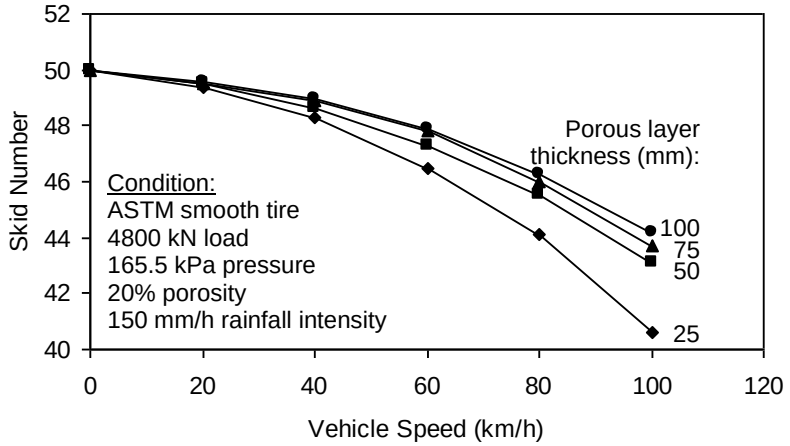

(b)

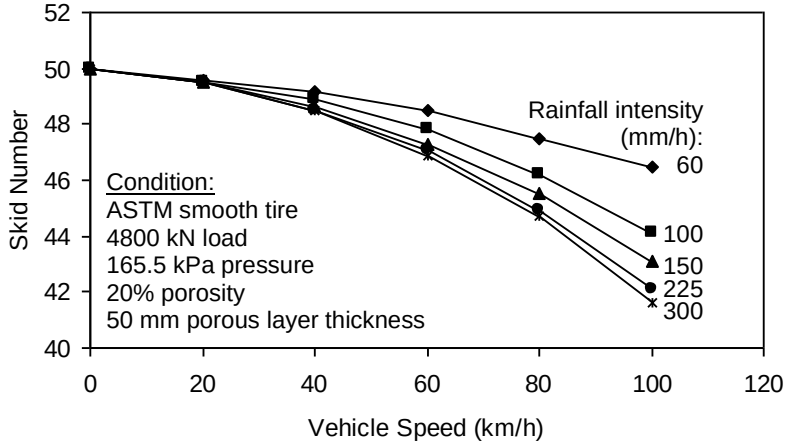

(c)

Figure 4.11: Influence of vehicle speed on skid number: (a) among porosities, (b) among porous layer thicknesses, (c) among rainfall intensities

CHAPTER 5 DEVELOPMENT OF NUMERICAL MODEL FOR TIRE/ROAD NOISE ON POROUS PAVEMENT

Besides skid resistance enhancement, noise reduction is another major benefit brought forth by porous pavements. Most existing studies on acoustical performance of porous pavements to date are experimental in nature (Younger et al., 1994; Bérengier et al ., 1997; Kowalski et al., 2009). Developing a numerical simulation model for tire/road noise on porous pavements is the primary objective of this study. However, the previous approach adopted in skid resistance simulation is inadequate for noise simulation. This is because the acoustical property of a porous surface can not be directed related to its water drainage capacity, although both features are resulted from its high porosity. Porous pavement acoustical property depends on the characteristics of air flow and sound energy dissipation. Therefore, an innovative numerical approach is required to simulate tire/road noise on porous pavements. This chapter presents the development of such a numerical simulation model. The critical issues in the tire/road noise modeling are first addressed. These problems are then solved by finite element method (FEM) and boundary element method (BEM). The appropriate reproduction of porous pavement acoustic absorption is identified as a key issue during model development. In this study, an absorption penal is defined in boundary element method is adopted in this research to numerically represent the acoustical properties of porous surfaces. This pavement model is then integrated with a rolling tire vibration model to evaluate the noise emission around a pneumatic tire that travels on a porous pavement surface. The overall tire/road noise model is then validated against past experimental measurements for both porous and nonporous pavements.

5.1 Issues Considered in Modeling Tire/Road Noise on Porous Pavement

Similar to skid resistance, tire/road noise on porous pavements is a complex phenomenon involving various mechanisms. It is a combination of tire vibration

effect and aerodynamic effect (Sandberg and Ejsmont, 2002; Bernhard and McDaniel, 2005). The former is a result of pavement texture, tire rotation and frictional force, among which the radian excitation induced by pavement texture is the most significant cause of the structure-borne noise. The latter includes air pumping, groove resonance and air resonant radiation, which are more relevant to the air movements between tire tread and pavement surface. The model developed in this study aims to focus on tire wall vibration which is the dominant noise generation mechanism under most traveling conditions (Kim et al., 2007). The other noise generation mechanisms can be covered in the simulation model through a calibration process. Finite element method (FEM) and boundary element method (BEM) are used to formulate the generation and propagation of noise respectively. In the simulation of tire/road noise on porous pavements, problems presented in below subsections should be properly considered.

5.1.1 Pavement Surface Texture

Pavement surface texture induces tire wall vibration and affects the friction at tire-pavement interface. It is important to appropriately represent pavement surface texture in the numerical simulation of tire/road noise. The major challenge lies in the randomness of texture profile and the small scale of texture characteristics. In this work, the spectral analysis in accordance with the technique outlined by ISO 13473-4 standard (ISO, 2008) is adopted to derive the pavement texture spectra from the raw texture profile data measured by high-speed laser profilometers. Specifically, discrete Fourier transform (DFT) method is performed to derive texture spectra. This analysis makes it possible to capture the characteristics of surface asperity distribution (Miller et al., 2012). The DFT is defined by:

$$Z_k = \frac{1}{N}\sum_{i=0}^{N-1} Z_{i,win} e^{-j\left(\frac{2\pi k}{N}\right)i} \tag{5.1}$$

where Z_k is the texture amplitude in the narrow band k, $Z_{i,win}$ is the windowed profile elevation at the discrete point i, and j is the imaginary unit ($j^2 = -1$).

The power spectral density (PSD) can be determined from the DFT results of each narrow band and the total power of a fractional-octave-band is obtained through a summation of all the narrow band power within the window. The pavement texture profile level can then be calculated by:

$$L_{tx,\lambda} = 10 \cdot \log\left(\frac{Z_{p,\lambda}}{a_{ref}^2}\right) = 10 \cdot \log\left(\frac{a_\lambda^2}{a_{ref}^2}\right) \tag{5.2}$$

where $L_{tx,\lambda}$ is the texture profile level (dB) of the fractional-octave-band with a center wavelength λ, $Z_{p,\lambda}$ is the power within the fractional-octave band, α_λ is the root mean square of texture amplitude, and α_{ref} is the reference texture amplitude, 10^{-6} m. In this study, both the 1/3-octave and 1/12-octave bands are used in the representation of texture spectrum.

5.1.2 Rolling Tire Vibration

Most of the tire/road noise generation mechanisms result from tire rotation, especially the tire wall vibration. Tire-pavement interaction is the most important source of rolling tire vibration. Tire deformation and its pre-stress status significantly affect its vibration characteristics and therefore, have to be properly reproduced in the modeling of tire/road noise. Modal analysis is one of the most extensively used methods in tire vibration analysis, and the natural frequencies and mode shapes are fundamental descriptions of tire vibration characteristics. Modal analysis and mode superposition technique are adopted in this study to analyze the rolling tire vibration.

5.1.3 Acoustic-Structure Coupling

Tire/road noise phenomenon involves acoustic radiation and scattering by an elastic structure (i.e. the tire) submerged in an infinite fluid medium (i.e. the air). The interaction between tire walls and surrounding air is an important feature in tire/road

noise modeling. Since the influence of air acoustic pressure on tire wall vibration is negligible and the purpose of the model is for noise prediction, a one-way coupling scheme is adequate for the tire-air interaction. The coupling algorithm transforms the tire vibration velocities or accelerations to the boundary of fluid domain which serve as the radiation source in the acoustic model. This can be realized through the vibro-acoustic transfer vectors (VATV) approach.

5.1.4 Sound Propagation in Free Space

Sound is essentially a sequence of pressure wave propagating in compressible medium, such as air. During propagation, sound waves may be reflected, refracted or attenuated by the medium. The behavior of sound propagation is generally affected by the relationship between density and pressure. The medium viscosity also affects the motion of sound waves and determine the rate at which sound is attenuated. The propagation is also influenced by the motion of the medium itself. Numerical formulations of sound propagation behaviors in the air should be developed to estimate the sound level at a distance from source. Acoustic transfer vector (ATV) concept could be adopted to formulate the relationship between boundary vibration and acoustic pressure field.

5.1.5 Acoustic Absorption of Porous Pavement

Past experimental studies have identified porous pavement as an effective engineering solution to tire/road noise (Bérengier et al., 1997; Praticò and Anfosso-Lédée, 2012). It reduces noise through its acoustic absorption property. Sound energy dissipates when it propagates through the porous pavement layer, primarily due to viscous and thermal effects resulting from the compression and expansion of the air within the pore structure. Sound absorption depends on the complicated pore structure within porous mixtures and the acoustical properties of its materials (i.e. aggregates, binders and additives). It is crucial and essential for the tire/road noise

numerical modeling to appropriately represent the acoustic absorption of porous pavements.

Four of the critical issues (pavement surface texture, rolling tire vibration, acoustic-structure coupling and sound propagation in free space) have already been studied and included into some dense-graded pavement tire/road noise simulation models by the literature (Brinkmeier and Nackenhorst, 2008; Kropp et al., 2012). Similar concepts are adopted in this research study. However, the acoustic properties of porous pavements have not been appropriately considered in existing tire/road noise models (Anfosso-Lédée et al., 2007). This research therefore focuses on integrating the acoustic properties of porous pavements into the numerical tire/road noise prediction model to properly evaluate the noise reduction effects on porous pavements. The modeling of acoustic absorption can be approached by either a phenomenological model or a microstructural model, both of which will be discussed in the next section.

5.2 Numerical Representation of the Acoustic Absorption of Porous Pavement

Porous pavement is characterized by an interconnected pore network within porous surface layer. This interconnected pore network is believed to reduce tire/road noise primarily through two major mechanisms: mitigation in air pumping effect and sound absorption through internal friction (Neithalath et al., 2005). When an incident sound wave impacts a pervious surface, a portion of the acoustic energy is absorbed, while the rest is reflected. Acoustic absorption occurs along the sound propagation within a porous layer and the transmitted sound wave is weakened. The acoustic absorption coefficient of a porous pavement surface layer can be derived from its acoustic impedance. This section discusses the application of various modeling approaches to predict and quantify acoustic absorption of porous pavements using pore structure parameters. Also, the section investigates the numerical representation

of acoustic impedance in BEM simulations. The developed porous pavement model will be used in the development of a tire/road noise numerical simulation model.

5.2.1 Acoustic Characteristics of Porous Pavement

Porous pavement layer is a rigid-frame porous media, whose pore walls do not deform with the air pressure fluctuation within its pore structure. Acoustic wave propagates in rigid-frame porous media by alternating air compression and expansion. In this process, acoustic absorption occurs as a result of energy loss from the viscous effect and thermo-elastic damping (Neithalath et al., 2005). The sound propagation in porous pavement is governed by the effective density and effective bulk modulus of the air within the pore space (Brennan and To, 2001). These quantities are frequency-dependent, complex and non-linear. Acoustic absorption coefficient is a fundamental intuitive parameter commonly used to describe the ability of a particular material in absorbing and transmitting acoustic energy when sound waves collide with it. It is defined as:

$$\alpha = I_a / I_i \tag{5.3}$$

where α is the acoustic absorption coefficient, I_a is the absorbed sound intensity, and I_i is the incident sound intensity. The amount of sound energy absorbed is governed by the acoustic impedance of a porous pavement surface and is frequency-dependent. Acoustic impedance indicates the amount of sound pressure generated by molecule vibrations of an acoustic medium at a given frequency. The characteristic acoustic impedance is an inherent property of a medium, defined by

$$Z_c = \rho_0 c_0 \tag{5.4}$$

where Z_c is the characteristic acoustic impedance, ρ_0 is the density of medium and c_0 is the sound speed in the medium. In a viscous medium, due to the phase difference between pressure and velocity, the specific acoustic impedance will differ from the characteristic acoustic impedance. The specific impedance (Z) is defined as the ratio of sound pressure ($\vec{p}$) to the particle velocity ($\vec{v}$) at the surface of porous material:

$$Z(\omega) = \vec{p}(\omega)/\vec{v}(\omega) \tag{5.5}$$

where ω is the angular frequency. A phase relation generally exists between pressure and particle velocity. Therefore, the specific acoustic impedance is usually expressed as a complex number:

$$Z = R + jM = (r + jm) \cdot Z_c \tag{5.6}$$

where R is the real component of the impedance, representing the resistive part, M is the imaginary component, indicating the reactive part of the impedance, and j is the imaginary unit. The resistive part consists of various loss mechanisms such as thermal motion and viscous effect. Energy is removed from the sound wave and transferred to other objects. The reactive part represents the ability of air to store the kinetic energy of sound wave as potential energy, realized through compression and expansion of air. Energy is not lost, but converted between kinetic and potential forms. The phase of impedance is simply shown as:

$$\varphi = \tan^{-1}(m/r) \tag{5.7}$$

The acoustic absorption coefficient (α) can be theoretically related to the complex acoustic impedance by Equation (5.8).

$$\alpha = \frac{4r}{(r+1)^2 + m^2} \tag{5.8}$$

In practice, the acoustic properties of porous pavements are usually evaluated by the sealed impedance tube approach (ISO, 2010; ASTM, 2012a) in the laboratory on cored samples, or through the extended surface method (ISO, 2002) in the field tests. Both methods measure acoustic absorption through the determination of sound pressure difference between incidental and reflected sound fields. The complex acoustic impedance can be determined from these tests as well, taking into consideration the relationship between acoustic absorption coefficient and acoustic impedance. For a constant acoustic absorption coefficient α, Equation (5.8) degenerates to an equation of circle centering on the real axis at $2/\alpha$-1 with a radius of

$\sqrt{(4/\alpha)\cdot(1/\alpha-1)}$ in the complex plane. When the phase of impedance is obtained from measurement, the real and imaginary components of acoustic impedance can be derived. Details of the theoretical derivation can be found in reference (Möser, 2009).

5.2.2 Modeling the Acoustic Absorption of Porous Pavement

Measurement of pavement acoustic characteristics requires specialized device and high investment, which may not always be available. As a result, various models have been developed to relate the acoustic properties of porous mixture to its composition and volumetric characteristics. Acoustic absorption can be modeled by either phenomenological models (Attenborough and Howorth, 1990; Hamet and Bérengier, 1993; Hubelt, 2003) or microstructural models (Champoux and Stinson, 1992; Neithalath et al., 2005; Kim and Lee, 2010). This section shall introduce the representative phenomenological and microstructural approaches. It was found that the phenomenological model is in close agreement with the microstructural model in the case of porous pavements (Bérengier et al ., 1997). Different models rely on different variables to derive acoustic absorption, therefore, the selection of model depends on what variables are available in the measurement.

5.2.2.1 Phenomenological Model

The phenomenological approach considers the porous mixture and the air within it as a whole dissipative compressible fluid. This method introduces a viscous dissipation resulting from the velocity gradients within the material and a thermal dissipation due to the thermal gradients (Bérengier et al ., 1997). Among the various models, the one developed by Hamet and Bérengier (1993) allows the acoustical characteristics of a porous pavement to be determined using only three parameters (i.e. porosity, tortuosity and airflow resistance). All these parameters can be separately measured by laboratory tests, making this model very attractive to implementation.

In Hamet and Bérengier's model, the dynamic density and bulk modulus are expressed as

$$\rho_g = \rho_{air} q^2 (1 + j\, f_u / f) \tag{5.9}$$

$$K_g = \gamma P_0 \left[1 + (\gamma - 1)/(1 - j\, f / f_\theta)\right]^{-1} \tag{5.10}$$

where ρ_g is the complex dynamic density, K_g is the bulk modulus, ρ_{air} is the density of air, γ is the specific heat ratio (1.4 for ideal gas), q^2 is the media tortuosity, P_0 is the ambient atmospheric pressure and f is the frequency. f_μ and f_θ are functions describing the viscous and thermal dependencies respectively.

$$f_\mu = \phi r_s / (2\pi \rho_{air}\, q^2) \tag{5.11}$$

$$f_\theta = r_s / (2\pi \rho_{air}\, N_{pr}) \tag{5.12}$$

where ϕ is effective porosity, r_s is the air flow resistance of the porous pavement, and N_{pr} is Prandtl number (about 0.71 in the air at 25°C). Using Equations (5.13) and (5.14), the acoustic impedance of porous layer (Z_p) and its complex wave number (k) can be written as Equations (5.15) and (5.16).

$$F_\mu = 1 + j\, f_\mu / f \tag{5.13}$$

$$F_\theta = 1 + j\, f_\theta / f \tag{5.14}$$

$$Z_p = (\rho_{air} c q / \phi) F_\mu^{1/2} \left[\gamma - (\gamma - 1)/F_\theta\right]^{-1/2} \tag{5.15}$$

$$k = k_0 q F_\mu^{1/2} \left[\gamma - (\gamma - 1)/F_\theta\right]^{1/2} \tag{5.16}$$

where c is the homogeneous sound speed in the air, and $k_0 = 2\pi f / c$.

Assuming that the porous surface layer is laid on a perfectly reflecting dense-graded base course, whose impedance could be taken as infinite, surface impedance of the whole porous pavement is derived as:

$$Z = Z_p \coth(-jkl) \tag{5.17}$$

where l is the thickness of the porous surface layer. With this surface impedance, the acoustic absorption coefficient can be calculated from Equation (5.8). This model has

been validated against experimental measurements (Bérengier et al., 1997) and was successfully applied in the analysis of sound propagation over porous pavements (Wai and Kai, 2004).

5.2.2.2 Microstructural Model

The complex pore structure within a porous layer is simplified as individual pores with simple and well-defined geometries in the microstructural models. The entire porous medium field is then assembled by such representative pores. Viscous effects and thermal motions are usually considered separately for each single pore in a microstructural model and the results are corrected by a so-called shape factor to take into account the pore structure complexity, such as the variations in tortuosity and pore size. The acoustic effect at macroscopic scale is then generalized from the corrected single-pore results. Although it is more computationally expensive than a phenomenological model, the microstructural model provides more physical insights of sound propagation mechanisms in the porous medium. This study adopts the model developed by Neithalath et al. (2005), which relates acoustic absorption of porous pavements to three geometric parameters of pore structure (i.e. porosity, characteristic pore size and porous layer thickness).

Recognizing the fact that air is alternatively compressed and expanded when acoustic waves propagate through a porous mixture, Neithalath's model simplifies the pore network as a series of alternating cylinders with varying diameters (see Figure 5.1). Each unit of the pore structure consists of a pore (with diameter D_p and length L_p) and an aperture (with diameter D_a and length L_a). Porosity value (ϕ) is related to the pore structure dimensions and wall thickness (d) through:

$$\phi = \frac{D_a^2 L_a + D_p^2 L_p}{(L_a + L_p)(D_p + d)^2} \tag{5.18}$$

The characteristic pore size (D_p) is defined using the median of all pore sizes larger than 1 mm, which can be obtained from an image analysis on porous mixtures. The

other dimension parameters are related to the pore size and porosity, and can be determined by an iterative process or an optimization algorithm (Losa and Leandri, 2012). The effective porosity is maintained constant in the simplification of a pore structure.

The pore network structure is next modeled using an electro-acoustic analogy consisting of a series of electro resistors and inductors (see Figure 5.1) to simulate the acoustic behavior of porous pavements. The air impedance in a pore (Z_p) is modeled by an inductor, the value of which is a function of the pore diameter (D_p) and can be calculated by:

$$Z_p = -j \cdot \rho_{air} \cdot c \cdot \cot(\omega D_p / c) \tag{5.19}$$

The acoustic impedance of an aperture (Z_a) is modeled by a resister and an inductor, representing the real component (R_a) and the imaginary component (M_a) of acoustic impedance, respectively. The impedance of apertures is thus computed by:

$$Z_a = R_a + j \cdot M_a \tag{5.20}$$

$$R_a = \frac{32\eta L_a}{D_a^2} \cdot \left(\sqrt{1 + \frac{\beta^2}{32}} + \sqrt{\frac{\beta D_a}{4L_a}} \right) \tag{5.21}$$

$$M_a = \omega \rho_{air} L_a \cdot \left(1 + \frac{1}{\sqrt{9 + \beta^2/2}} + \frac{8D_a}{3\pi L_a} \right) \tag{5.22}$$

where η is the air dynamic viscosity, and β is the acoustic Reynolds number deriving from Equation (5.23).

$$\beta = \frac{D_a}{2} \cdot \sqrt{\frac{\omega \rho_{air}}{\eta}} \tag{5.23}$$

For the single-cell situation, the acoustic impedance is given by:

$$Z_1 = Z_a \cdot \frac{D_p^2}{D_a^2} + Z_p \tag{5.24}$$

For a porous layer with thickness *l*, which is composed by *n* cells, the acoustic impedance is determined by applying the electro-acoustic analogy to all the cells and calculated using the following iterative relationship.

$$Z_n = Z_a \cdot \frac{D_p^2}{D_a^2} + \frac{1}{1/Z_p + 1/Z_{n-1}} \tag{5.25}$$

where Z_n is the acoustic impedance of *n*-cell case, and Z_{n-1} is the acoustic impedance of the situation with *n-1* cells.

In the above calculations, air density (ρ_{air}) should be multiplied by a structure factor to take into account that the air in lateral pores appears to be "heavier" than the air in main pores due to the different mechanisms in acoustic energy dissipation. The structure factor (k_s) is defined by Equation (5.26) and is based on the fact that all pores do not contribute equally in sound absorption.

$$k_s = \frac{(L_a D_a^2 + L_p D_p^2) \cdot (L_a D_p^2 + L_p D_a^2)}{(L_a + L_p)^2 D_a^2 D_p^2} \tag{5.26}$$

After the acoustic impedance of porous pavement is determined by Equation (5.25), the absorption coefficient can be derived using Equation (5.8). This model has been validated against experimental measurements (Neithalath et al., 2005) and was applied on the analysis of the acoustic characteristics of porous pavements (Losa and Leandri, 2012).

5.2.3 Validation of the Acoustic Representation of Porous Pavement in BEM

The acoustic representation of porous pavement in the boundary element method (BEM) is next validated through the examination of horn effect reduction on porous pavements. It has been identified that most tire/road noise sources, including tire wall vibration, air pumping, stick-slip and acoustic resonance, exist near the tire-pavement contact patch, where a horn-shape geometry is formed by the tire tread and pavement surface (Sandberg and Ejsmont, 2002). This acoustic horn forces a multi-reflection of sound wave and thus has a significant enlarging effect in its propagation.

The noise amplification resulting from horn effect is found to be 10 to 20 dB (Graf et al., 2002; Kropp et al., 2000). Porous pavement is effective in reducing the horn effect through its absorption of acoustic energy during the multi-reflection process when sound wave propagates in the horn-shape geometry.

5.2.3.1 BEM Model of Horn Effect on Porous Pavement

The boundary element method is used to simulate sound propagation in porous pavement and its resulting reduction in horn effect. BEM is formulated such that integral equations are defined on the domain boundaries and integrations will relate boundary solutions to field point solutions. The benefit of BEM arises from the fact that only the boundaries need to be sub-divided, reducing the problem dimension by one. Furthermore, the infinite domain in acoustic radiation and scattering problem can be more efficiently modeled in this approach.

The linear acoustic theory decomposes an acoustic variable into two terms: a constant one corresponding to a steady state and a fluctuating one representing the perturbations of the constant state. The fluctuations are sufficiently small so that a linear pressure-density relationship stands and all products of acoustic perturbation terms can be neglected. In this case, the wave equation is derived as:

$$\nabla^2 p - \frac{1}{c^2}\frac{\partial^2 p}{\partial t^2} = s \tag{5.27}$$

where p is the acoustic pressure, c is the sound propagation speed in the fluid, t is the time, s is the acoustic source, and ∇^2 is the Laplacian operator. For a harmonic field, the complex pressure amplitude satisfies the Helmholtz equation:

$$\nabla^2 p + k_0^2 p = s \tag{5.28}$$

The particle velocity ($\vec{v}$) is related to the pressure gradient by the Euler equation:

$$grad(p) - jk_0 Z_0 \vec{v} = \vec{0} \tag{5.29}$$

Three types of boundary conditions are used in the study of the horn effect in porous pavements. The tire walls are assumed to be perfectly-reflecting surfaces,

which are acoustically equivalent to zero normal velocity condition $v_n = 0$. Surface impedance gets to infinity and no sound energy is absorbed by such boundaries. This condition is represented by:

$$\frac{\partial p(x_s)}{\partial n} = 0 \tag{5.30}$$

where $p(x_s)$ is the pressure at point x_s on boundary. The boundary condition on porous pavement surface is defined by its surface normal acoustic impedance, which denotes the acoustic absorption properties on boundaries. It can be derived from Equations (5.5) and (5.29):

$$\frac{\partial p(x_s)}{\partial n} - jk_0 \frac{Z_0}{Z(x_s)} p(x_s) = 0 \tag{5.31}$$

Another boundary is defined at the infinity, where the Sommerfeld condition must be satisfied. It specifies that the acoustic pressure approaches zero and no sound energy is reflected.

$$\lim_{x_s \to \infty} |x_s| \cdot \left(\frac{\partial p(x_s)}{\partial x_s} - jk_0 p(x_s) \right) = 0 \tag{5.32}$$

The integral form of Helmholtz equation on boundaries relates the boundary pressure and the normal velocity by a matrix equation:

$$[A]\{p\} = [B]\{v_n\} \tag{5.33}$$

where [*A*] and [*B*] are coefficient matrices. Boundary conditions [Equations (5.30) to (5.32)] are applied to Equation (5.33) to calculate the pressures and particle velocities at the boundaries. The acoustic pressure at any field point is then solved through the integration of boundary solutions:

$$p(x_f) = \{C\}^T \{p\} + \{D\}^T \{v_n\} \tag{5.34}$$

where $\{C\}$ and $\{D\}$ are coefficient vectors derived from integration of Helmholtz equation on boundaries.

$$C_i = \int_{\Omega} N_i(x_s) \frac{\partial G(x_f, x_s)}{\partial n} \cdot d\Omega(x_s) \tag{5.35}$$

$$D_i = -j\rho_{air}\omega \int_{\Omega} N_i(x_s) G(x_f, x_s) \cdot d\Omega(x_s) \tag{5.36}$$

where Ω is the boundary of the calculation domain, $N_i(x_s)$ is the interpolation function for boundary element, and $G(x_f, x_s)$ is the Green function.

Porous pavement is represented by an absorbent panel in the BEM model, on which the acoustic impedance is defined to model its sound absorption properties. In the open space problem of in-field noise measurement, porous pavement is supposed to be infinite horizontally. However, in numerical simulation, the boundary has to have a limited dimension to make sub-division possible. Convergence studies conducted by Anfosso-Lédée (1997) suggested that the finite extension of a boundary can approximate the solutions if the boundary extends over the source and receiver by a distance longer than that between the source/receiver and the boundary and this distance must be longer than one wavelength. This principle is adopted in this study. For the space above pavement surface, the air at 25°C is modeled as the sound propagating medium. The mass density of air is set to be 1.225 kg/m^3 and the sound velocity in it is 340 m/s. Tire walls are modeled by perfectly-reflecting panels according to the geometry of tire used in the test, and a monopole with white noise is adopted as sound source in the simulations. With such a configuration, the acoustic pressure field around the tire-pavement horn is computed from the BEM model.

5.2.3.2 Model Validation Results

The acoustic representation of porous pavement in the BEM model is next validated against published experimental results. The validation work is based on the differences between sound pressure levels on porous and non-porous pavements. Comprehensive measurements conducted by Schwanen et al. (2007) on various types of pavements are used to validate the model.

The experimental set-up is sketched in Figure 5.2. A tire with 195 mm width, 381 mm rim diameter and 310 mm outer radius is placed on the tested surface without vertical loading. Two source positions are selected on the center line of tire tread, 10 and 15 cm from the center of contact patch, respectively. Two receiver positions are defined with the coordinates shown in Figure 5.2. Receiver A is right in front of the tire-pavement contact patch, 428 mm from its center; and Receiver B is perpendicular to the tire center plane, at a distance of 297.5 mm. Both receivers are placed 100 mm above the pavement surface. Two porous pavements and one dense-graded pavement are involved in the model validation work. The acoustic impedance and absorption coefficient of tested pavements were measured by the extended surface method (ISO, 2002) and the results are shown in Figure 5.3.

The effects of porous pavements on sound absorption are represented by the differences in sound pressure levels on porous and dense-graded surfaces. The results computed from the numerical simulations are compared against values measured in the experiments (see Figure 5.4). Model validation is performed for different source positions, receiver locations and porous surfaces to better demonstrate the feasibility of simulation approach. It is seen that the BEM model is capable to predict the main peak frequency of sound absorption on porous pavement, as well as the magnitude of noise reduction at the peak frequency. However, the range of peak frequency detected by receiver B in simulation is wider than that obtained in the measurement. This may result from the setup configuration of experiment. Moreover, it is observed that the errors at high frequencies are larger than those at low frequencies and the estimation of secondary absorption peaks is below satisfaction. Recognizing that the differences between numerical and experimental results shown in Figure 5.4 cover the errors in acoustic impedance and sound pressure level measurements, the accuracy of BEM formulation is considered sufficient for the representation of porous pavement acoustic absorption.

5.3 Development of Tire/Road Noise Simulation Model for Porous Pavement

This section presents the development of an integrated numerical model simulating the tire/road noise phenomenon on porous pavements. An analytical framework capable to predict the rolling tire noise induced by pavement textures is illustrated in Figure 5.5. This framework is developed based on past works on tire-pavement noise simulation using FEM and BEM (Brinkmeier and Nackenhorst, 2008; Kropp et al., 2012). Using this framework, the close-proximity (CPX) noise measurement can be modeled with the pavement surface texture profile serving as a critical input parameter. Four major steps (shaded in Figure 5.5) are performed sequentially in this framework. First, tire deformations and stresses are computed in a dynamic rolling tire analysis. The natural frequencies and mode shapes of tire walls are next computed using a modal analysis, and the tire vibration characteristics are captured through mode superposition with pavement texture excitations. The tire wall vibrations are next inputted into the BEM acoustic model to estimate the sound field around the rolling tire.

5.3.1 Rolling Tire Analysis

Tire deformations at different traveling conditions (i.e. wheel load, inflation pressure and traveling speed) can be very different (Tuononen, 2011). The analyses of rolling tire vibration and tire/road noise generation have to be performed with the correct deformed tire geometry. Moreover, the pre-stress condition of a rolling tire is crucial in the generation of tire natural frequencies and mode shapes. Therefore, it is necessary to produce the appropriate deformed geometry and pre-stress condition of the rolling tire before analyzing its vibration characteristics.

Two major numerical schemes have been developed to analyze rolling tire performance. They are namely steady state rolling analysis and explicit dynamic rolling simulation. The former adopts the arbitrary Lagrangian Eulerian (ALE) description of a rolling tire. The theoretical formulations were presented in detail by

Nackenhorst (2004). Based on this work, a stationary rolling approach was explored by various researchers (Ghoreishy, 2006; Hambleton and Drescher, 2009; Guan et al., 2011). The second method simulates the real-time dynamic behavior of a rolling tire under transient condition using dynamic FEM algorithms. With rapid development in computational capacity, the advantages of transient simulation in the reproduction of actual tire motion have attracted a large amount of research efforts (Hall et al., 2004; Cho et al., 2005; Xia and Yang, 2012).

The explicit dynamic approach is adopted in this study. A relative motion frame of reference is adopted to facilitate the model configuration (Figure 5.6). The wheel is rolling under a specific vertical load without horizontal translation, while the pavement moves horizontally towards the standing wheel at a traveling speed. In the model, only vertical translation is allowed on a cylindrical rigid axle. A pneumatic tire model is assembled onto the axle, with a revolution joint connection defined at the interface between tire rim and the axle, on which the rotational degree of freedom around the axle is released. Frictional contact condition is defined at tire-pavement interface. The pavement is assumed to be rigid and sufficient pavement length is provided in the simulation model to ensure that the tire will experience at least three complete revolutions.

The radial tire is a complex composite structure constructed by a number of rubber components and reinforcements. Its typical cross section is shown in Figure 5.7. An appropriate simplification is necessary to make the numerical computation practicable and efficient. The laminated composite theory (Reddy, 2004) is adopted to convert the multilayer tire component into a single layer, which can then be modeled by shell elements within an FE model. The properties of compound tire materials are assumed to be linear elastic and the values used in the simulation model are derived from actual tire data available in literature (Hall, 2003). In transient analyses, mesh refinement is controlled by the available computational resources and the number of overall time steps (Hall et al., 2004). About 19200 shell elements are used in the tire

rotation model and the mesh is uniformly distributed. As a requirement of the contact analysis, the mesh size of pavement surface should be comparable to that of tire tread.

The analysis is divided into three loading steps. In the first step, a uniformly distributed pressure is applied on the inner surface of tire components to simulate the inflation pressure. Then the vertical wheel load is gradually added onto the axle in the second step, pushing the tire against the pavement surface. Tire rotation is introduced in the third step by applying a translation velocity on pavement and a corresponding angular velocity on tire. The minimum time step is set to be 1×10^{-4} s in the dynamic rolling process to ensure numerical stability. At the beginning of rotation, the model is unstable until the tire has travelled a sufficient length. At least three revolutions should be performed to ensure that the numerical results are reliable. Through the rolling tire analysis, tire wall deformations and stresses are exported as the intermediate solutions to serve as inputs in the following phases.

5.3.2 Tire Modal Analysis

Natural frequencies and mode shapes are essential tire vibration properties considered in the development of tire-pavement noise simulation model. They are related to the geometry and composition of the tire itself. In the tire modal analysis, the frequency response functions of the nodes on tire walls are determined, so that the tire responses to a certain frequency excitation can be derived. Numerical approaches in modal analysis have been explored by various researchers. An analytical method was developed by Soedel and Prasad (1980) to compute the natural frequencies and mode shapes of a tire in contact with pavement from the eigenvalues of non-contacting tire. Kung et al. (1985) obtained the natural frequencies and mode shapes of a radial tire using the doubly curved thin shell elements with smeared-out properties of laminate composite materials. A computational strategy for high frequency response of tires was proposed by Brinkmeier and Nackenhorst (2008), focusing on the more efficient numerical treatment of large scale gyroscopic

eigenvalue problems. The cross section modes and free wave propagation on a stationary tire was analyzed by Sabiniarz and Kropp (2010) using the waveguide finite element approach.

From the mathematical perspective, the essence of modal analysis is to solve the eigen-problem defined in Equation (5.37).

$$[K]\{\phi\} = \lambda[M]\{\phi\} \tag{5.37}$$

where [*K*] is the structure stiffness matrix, [*M*] is the structure mass matrix, $\{\phi\}$ is the eigenvector, and λ is the eigenvalue. For a pre-stressed modal analysis, the stress stiffness matrix [*S*] is included in the [*K*] matrix.

By definition, the eigenvalues are the roots of characteristic polynomial *det*([*K*]- λ[*M*]) = 0, while eigenvectors are the nontrivial solutions of Equation (5.37) corresponding to each λ. Efficient algorithms are available for solving Equation (5.37) in different conditions (Roger et al., 1994; Guo and Lancaster, 2005; Jarlebring et al., 2012). The integrated scheme for large-scale gyroscopic eigenvalue extraction (Brinkmeier and Nackenhorst, 2008) is adopted in this study to generate the natural frequencies and mode shapes for rolling tires.

The equation of vibration for stationary rolling state is:

$$[M]\{\ddot{u}\} + [G]\{\dot{u}\} + [K]\{u\} = 0 \tag{5.38}$$

where [*G*] is gyroscopic matrix and $\{u\}$ is vibration displacement vector. With the time-harmonic assumption $u = e^{i\omega t}\{z\}$, a quadratic eigenvalue problem is derived:

$$\left(-\omega^2[M] + i\omega[G] + [K]\right)\{z\} = 0 \tag{5.39}$$

Based on the problem definition, it is assumed that [*M*] and [*K*] are symmetric, while matrix [*G*] is skew-symmetric. This assumption is generally valid if the friction forces on contact nodes are exclusive from the modal analysis. To take advantage of the ease and efficiency in implementation of linear eigenvalue solver, the quadratic problem is first linearized as:

$$\left(\begin{bmatrix} iG & K \\ K & 0 \end{bmatrix} - \omega \begin{bmatrix} M & 0 \\ 0 & K \end{bmatrix}\right) \begin{Bmatrix} \omega z \\ z \end{Bmatrix} = \begin{Bmatrix} 0 \\ 0 \end{Bmatrix} \tag{5.40}$$

For further mathematical treatment, an identity transformation is introduced (Tisseur and Meerbergen, 2001):

$$\begin{bmatrix} 0 & K^{-1} \\ I & -(iG - \omega M)K^{-1} \end{bmatrix} \left(\begin{bmatrix} iG & K \\ K & 0 \end{bmatrix} - \omega \begin{bmatrix} M & 0 \\ 0 & K \end{bmatrix} \right) \begin{bmatrix} I & \omega I \\ 0 & I \end{bmatrix} = \begin{bmatrix} I & 0 \\ 0 & Q(\omega) \end{bmatrix} \tag{5.41}$$

where $\left[Q(\omega)\right] = -\omega^2 [M] + i\omega [G] + [K]$.

Iterative process is performed to search for the solutions of Equation (5.40). With the above transformation, Equation (5.40) is reformulated as

$$\begin{bmatrix} 0 & K^{-1} \\ I & -(iG - \sigma M)K^{-1} \end{bmatrix}^{-1} \begin{bmatrix} I & 0 \\ 0 & Q(\sigma) \end{bmatrix} \begin{bmatrix} I & \sigma I \\ 0 & I \end{bmatrix}^{-1} \begin{Bmatrix} x_1 \\ x_2 \end{Bmatrix} = \begin{bmatrix} M & 0 \\ 0 & K \end{bmatrix} \begin{Bmatrix} b_1 \\ b_2 \end{Bmatrix} \tag{5.42}$$

$$\Rightarrow \begin{bmatrix} I & -\sigma I \\ 0 & Q(\sigma) \end{bmatrix} \begin{Bmatrix} x_1 \\ x_2 \end{Bmatrix} = \begin{Bmatrix} b_2 \\ Mb_1 - (iG - \sigma M)b_2 \end{Bmatrix} \tag{5.43}$$

where σ is the shift value. The problem is then split into two equations

$$x_1 = b_2 + \sigma x_2 \tag{5.44}$$

$$Q(\sigma)x_2 = Mb_1 - (iG - \sigma M)b_2 \tag{5.45}$$

Providing specific shift value σ, x_2 can be solved from Equation (5.45) with a direct solver, and x_1 is next computed from Equation (5.44).

Modal analysis is performed on the deformed tire geometry obtained from the rolling tire analysis and the pre-stress condition is loaded onto the deformed mesh. The frictional contact condition at tire-pavement interface is replaced by a bounded condition (i.e. degrees of freedom of all the nodes involving in contact are fixed) to eliminate the nonlinearity and asymmetry in numerical formulation. The mode shapes at frequencies up to 3000 Hz are extracted to describe tire wall vibrations in the subsequent mode superposition process. Modes at higher frequencies (larger than 3000 Hz) are neglected as low-order modes were found by Kropp et al. (2012) to be responsible for tire/road noise generation.

5.3.3 Tire Vibration Analysis

When a tire is rolling on a road surface, its dynamic characteristics will create fluctuating forces that excite tire wall vibrations. Analytical and numerical models were extensively used in the studies of tire vibration behavior (Wai and Kai, 2004; Lopez et al., 2007; Rustighi et al., 2008; Waki et al., 2009). Mode superposition method (Bathe, 1996) is widely used in the literature due to its efficiency. This method is used in this study to predict tire vibration resulting from pavement texture excitations. The equation of motion is expressed as:

$$[M]\{\ddot{u}\}+[C]\{\dot{u}\}+[K]\{u\}=\{F\} \tag{5.46}$$

where [*C*] is the damping matrix and $\{F\}$ is the load vector (explained later). A set of modal coordinates y_i is defined so that the displacement vector can be derived from all the mode shapes:

$$\{u\}=\sum_{i=1}^{n}\{\phi_i\}y_i \tag{5.47}$$

where $\{\phi_i\}$ is the shape of mode *i*, and n is the number of modes to be considered. Substituting Equation (5.47) into Equation (5.46) and pre-multiply by a typical mode shape $\{\phi_j\}^T$:

$$\{\phi_j\}^T[M]\sum_{i=1}^{n}\{\phi_i\}\ddot{y}_i+\{\phi_j\}^T[C]\sum_{i=1}^{n}\{\phi_i\}\dot{y}_i+\{\phi_j\}^T[K]\sum_{i=1}^{n}\{\phi_i\}y_i=\{\phi_j\}^T\{F\} \tag{5.48}$$

All the terms where $i\neq j$ vanish due to the orthogonal condition of natural modes. Only the $i=j$ terms remain in Equation (5.48):

$$\{\phi_j\}^T[M]\{\phi_j\}\ddot{y}_j+\{\phi_j\}^T[C]\{\phi_j\}\dot{y}_i+\{\phi_j\}^T[K]\{\phi_j\}y_i=\{\phi_j\}^T\{F\} \tag{5.49}$$

The coefficients of $\ddot{y}_j$, $\dot{y}_j$ and y_j are derived as

$$\{\phi_j\}^T[M]\{\phi_j\}=1 \tag{5.50}$$

$$\{\phi_j\}^T[C]\{\phi_j\}=2\xi_j\omega_j \tag{5.51}$$

$$\{\phi_j\}^T [K]\{\phi_j\} = \omega_j^2 \tag{5.52}$$

where ξ_j is the fraction of critical damping for mode *j*, and $\omega_j = \sqrt{K_j / M_j}$ is the natural circular frequency of mode *j*. Substituting Equation (5.50), (5.51) and (5.52) into Equation (5.49), the equation of motion is obtained:

$$\ddot{y}_j + 2\xi_j \omega_j \dot{y}_i + \omega_j^2 y_i = \{\phi_j\}^T \{F\} \tag{5.53}$$

Equation (5.53) represents *n* uncoupled equations with *n* unknowns y_i (*i* from 1 to *n*). Provided load vector $\{F\}$, the modal coordinates y_i can be efficiently solved and the displacement $\{u\}$ can then be computed from Equation (5.47).

It is noted that the load vector $\{F\}$ in Equation (5.53) is the summation of the loads derived from critical modes and the nodal excitation forces resulting from pavement surface textures. The former is obtained from the tire modal analysis. The latter is computed through a static FE tire model using the measured texture spectrum as a displacement load applied onto the tire contact patch. This evaluation approach is based on the assumption that tire contact patch closely fits the pavement texture. This assumption generally holds when the road surface is not too rough, such that the local displacement caused by a particular vertex is small compared to the tire deformation in the contact patch due to vertical load (Rustighi et al., 2008). The reaction forces on tire tread are computed and the external nodal force spectrum which is applied on all the tire nodes in the tire-pavement contact patch is obtained. Together with the loads computed from the modal analysis, this provides the load vector $\{F\}$ in Equation (5.53), from which tire wall displacements, vibration velocities and accelerations are computed in the frequency domain.

5.3.4 BEM Acoustic Model

The boundary element method is next used to simulate the sound propagation on porous pavement with tire vibration serving as the generation source. Fundamental

BEM theories were introduced in Section 5.2.3.1. The same theory is applied in this BEM acoustic model and the porous pavement acoustic absorption model is integrated in the tire/road noise simulation.

The deformed tire geometry generated from the earlier rolling tire analysis is imported into the BEM model with an acoustic mesh. The vibration velocities on tire surfaces obtained from the tire vibration analysis are then mapped onto the acoustic mesh. The porous pavement surface is modeled as an absorbent panel with a specified frequency-dependant acoustic impedance. The mass density of air is set to be 1.225 kg/m^3 and the sound velocity is 340 m/s. The acoustic pressure in air field around a rolling tire can then be computed together with other acoustic characteristics. The sound pressure level at CPX microphone positions is computed based on the acoustic pressure results obtained from the BEM simulation. It is a logarithmic measure of the effective sound pressure relative to a reference value:

$$L_p = 10 \cdot \log\left(\frac{p}{p_0}\right)^2 \tag{5.54}$$

where L_p is the sound pressure level, p is the root mean square of acoustic pressure at a specific position, and $p_0 = 20\ \mu Pa$ is the standard reference sound pressure.

5.4 Calibration and Validation of Tire/Road Noise Simulation Model

In this section, the tire/road noise simulation model developed in this study is calibrated and validated for both dense-graded and porous pavements using published experimental data in the literature (Schwanen et al., 2007). The sound pressure level spectra and overall noise levels are used in the calibration and validation processes to evaluate the fitness of numerical results comparing to measured data. The CPX noise measurements conducted by Schwanen et al. (2007) are adopted because of the clarity of test conditions and variety of pavement types. It is noted that the measurements are from the same set of field experimental studies used in the validation of acoustic representation of porous pavement in Section 5.2.3.

5.4.1 Calibration of Tire/Road Noise Simulation Model

The proposed model considers tire vibration to be the sole main contributor to tire-pavement noise emission. However, it is recognized that other tire/road noise generation mechanisms exist. Therefore, the developed model has to be calibrated to ensure that it can adequately capture these non-tire vibration mechanisms. Calibration can be achieved through an optimization process which adjusts the modal masses in the tire vibration analysis so that the simulated sound spectrum has an acceptable small error when compared against experimental measurement. The mode shape vector $\{\phi_i\}$ for each mode *i* is unique in shape, but does not have a unique amplitude. It can be scaled when the ratios between vector elements are maintained constant. A scaling constant a_i is defined for mode *i* so that the modal mass m_i is expressed as

$$m_i = \frac{1}{a_i \omega_i} \tag{5.55}$$

where ω_i is the natural frequency of mode i. The scaling constant a_i's are taken as the variables in the optimization process and the objective function is to minimize the difference between simulated and measured noise levels:

$$\min \quad z = \sum \left| L_s - L_m \right| \tag{5.56}$$

where L_s is the simulated sound pressure level in an octave band, and L_m is the value measured in the same band. The summation is taken over 1/3 or 1/12 octave spectrum bands in the frequency range of 315 to 2500 Hz. In practice, thousands of modes contribute to tire vibrations. These modes are divided into groups based on the natural frequencies and an identical scaling constant is assigned to all the modes in the same group. It should be noted that a set of scaling constant a_i is only valid for a particular combination of tire design and pavement surface. The model has to be recalibrated if tire characteristics or pavement properties vary significantly.

5.4.2 Validation of the Model for Dense-Graded Asphalt Pavement

After a proper calibration, the proposed model is next validated against noise measurements on conventional pavement sections with various surface textures. The CPX measurements conducted by Schwanen et al. (2007) are used for this purpose. A Continental slick tire (195/65R15) was tested in the noise measurements on a closed road paved with various types of surface layers. Only dense-graded surfaces with very low acoustic absorption coefficients (i.e. less than 0.1 in most of the interested frequency range) are involved in this section. Information of these examined non-porous surfaces is presented in Table 5.1. CPX method specified in ISO 11819-2 standard (ISO, 2013) was performed to measure the near field noise level. A vehicle with steady speed towed a trailer mounted with test tire, around which microphones were setup at specific close proximity positions. No enclosure was used around the tire since there was no other traffic at the test site. The distance between the test tire and the towing vehicle was more than 5 m to prevent the interference from towing vehicle noise. A-weighted equivalent sound level (both overall level and 1/3-octave bands) is measured along with vehicle speed.

An FE tire model is built based on the geometry and property of test tire and its vibration characteristics are analyzed. Pavement surface texture was measured using laser profilometer on each section and the resulting texture level spectra were available in the project report by Schwanen et al. (2007). Force excitations on tire tread at the contact patch is generated based on the texture spectra. These force excitations induce tire vibrations, which provide the boundary conditions of BEM acoustic model in sound pressure computation.

Wind had a significant influence on the low frequency noise measured in the test, because there is no enclosure used in the experiment. Measured noise data below 300 Hz are considered erroneous and are therefore removed. The upper bound of interested frequency range is set to be 2500 Hz, which is restricted by computational

capacity. Moreover, Cesbron et al. (2009) has shown that high frequency noise generated from air pumping and frictional effect is less dependent on pavement textures, therefore cannot be properly captured by the developed model.

The noise level spectrum measured at 70 km/h traveling speed on an SMA surface with a medium texture depth (S20, MPD = 0.89) is used to calibrate the model. Comparisons between simulated and measured 1/3-octave band spectra are illustrated in Figure 5.8. Comparisons of overall noise levels are shown in Figure 5.9 for all the examined non-porous sections. It is observed that, most simulations provide good estimations of noise spectra and overall noise levels. However, some of the predictions underestimate the overall noise levels. Further observations found that the underestimations happen on surfaces with relatively low MPD values. These errors may result from the absence of air-related mechanisms from the simulation model. Pavements with lower texture depth may generate more air-pumping noise, but this component is not sufficiently captured during model calibration as a high texture level surface was used. Therefore, it is necessary to recalibrate the model for pavement surfaces with low texture depths.

The recalibration work was performed separately for high-texture pavements (MPD above 0.5 mm) and low-texture pavements (MPD below 0.5 mm). Noise measurement on a Stone Mastic Asphalt (SMA) surface (S20, MPD = 0.89) was used to calibrate high-texture model and that on a dense asphalt concrete (DAC) surface (S23, MPD = 0.46) was used for low-texture model. With this effort, two sets of calibrated parameters are made available for pavements with high texture depths and low texture depths respectively. Validation of high-texture and low-texture models were performed on the non-porous pavement sections shown in Table 5.1. The simulated and measured 1/3-octave spectra are illustrated in Figure 5.10, and the simulated overall noise levels and measured results are compared in Figure 5.11 and Table 5.2. It can be seen that with proper calibration, the developed model can predict the overall noise levels as well as the noise spectra on dense-graded pavements. The

errors of overall noise levels are within ±2 dB(A) with the exception of one case and the predicted 1/3-octave spectra can basically describe the measured spectrum shapes.

5.4.3 Validation of the Model for Porous Pavement

The developed tire/road noise model is next validated for porous pavements. The CPX tire/road noise measurements conducted by Schwanen et al. (2007) on porous pavement sections are used for this task. Information of these porous surfaces is presented in Table 5.1 as well. The acoustic absorption coefficients of in-field porous pavements were determined by the extended surface method (ISO, 2002) in the experiment. The magnitude and phase of the complex acoustic impedance were also derived in the measurement, from which the real and imaginary components of acoustic impedance were calculated and then used as input parameters to describe the acoustic properties of porous pavement surfaces in the BEM acoustic model. Other test conditions were maintained the same as those on dense-graded pavements, such as the 195/65R15 slick tire, 3200 N axle load, 1.5 bar tire inflation pressure, and 70 km/h traveling speed.

The overall tire/road noise levels on porous pavements generated from the numerical model are compared against the experimental measurement as shown in Figure 5.12. It can be seen that the simulated results agree well with the experimental measurements. Also seen in Table 5.2, the differences between numerical and experimental overall noise levels are less than 2 dB(A) on all the porous pavement sections. Comparisons between measured and simulated 1/3-octave-band sound level spectra are illustrated in Figure 5.13. It is observed that the predicted spectra basically have similar shapes with the measured ones, with the same increasing and decreasing trend as frequency varies. However, there seems to be a shift between simulated and measured curves, especially for the absorption peaks (i.e. the valley of noise level spectrum). The predicted sound absorption peak commonly appears at a frequency about one 1/3-octave band lower than the measured noise reduction peak. The overall

simulation results may fit the measurements better if the simulated curves were shifted to the higher frequency accordingly.

To account for the frequency shift in simulated noise spectra, an optimization process is adopted to correct the simulation results. Two types of shifting functions are considered in this work, resulting in two objective functions. Type I is to multiply factor α onto the frequency variable of simulated noise spectrum function, while Type II is to apply a power β to the frequency variable. The optimization functions are shown below, corresponding to the two shifting types, respectively.

$$\text{Type I: Min } z = \sum_{f=400}^{2500} \left(S(\alpha f) - M(f) \right)^2 \tag{5.57}$$

$$\text{Type II: Min } z = \sum_{f=400}^{2500} \left(S\left(f^{\beta}\right) - M(f) \right)^2 \tag{5.58}$$

where *S(f)* is the regression function of simulated sound pressure spectrum and *M(f)* is the regression function of measured sound pressure spectrum. These functions could be derived by polynomial curve fitting after applying cubic spline interpolation on the simulated or measured 1/3-octave band noise spectrum. Table 5.3 shows the results of frequency shifting and the fitting quality after shifting. It is seen that both shifting functions can obtain an acceptable agreement between simulated and measured sound level spectra. From the Chi-square and R-square values, it is found that Type I has a slightly higher quality than Type II for most model validation cases. The corrected simulation results with Type I frequency shifting are illustrated in Figure 5.14. Compared to Figure 5.13, it is observed that the agreements between measured and simulated spectra have been significantly improved.

A frequency shift between porous pavement acoustic absorption and noise reduction was observed in past experimental studies (Kuijpers et al., 2007; Peeters and Kuijpers, 2008). It was reported that the highest noise reduction occurs at a frequency approximately 10 - 15% higher respect to the peak in the acoustic absorption curve (Peeters et al., 2010). Based on the model validation results, it was

concluded that the shifting effect of sound absorption is not appropriately addressed in the developed model. This may due to the adoption of the normal incidence acoustic impedance in BEM formulation, which presupposes a local type of reaction on the boundaries, i.e. sound propagation inside the material are neglected. However, this assumption may not be valid in the case of porous pavement because sound propagation within porous surface layer may have a significant influence on the resulted acoustic field. Therefore, porous pavement is an extended reacting surface instead of a local reacting surface. Its boundary condition is much more complex to be introduced in BEM formulation. A two-domain coupling approach was developed to take into account the sound propagation inside the porous medium (Sarradj, 2003). An alternative is to use grazing incidence approximate impedance in the traditional single-domain BEM based on the critical incidence angle (Anfosso-Lédée et al., 2007). Both methods are still under development to date. Due to the software capability limitation, the extended reacting effect cannot be adequately considered in the present model and has to be addressed in future studies.

5.5 Summary

A numerical simulation model of tire/road noise on porous pavements was developed and validated in this chapter. The proposed model recognizes the fact that tire vibration is the most important noise generation mechanism and considers most of the critical issues associated with tire-vibration noise simulation for porous pavements. This includes the representation of pavement surface texture, rolling tire vibration characteristics, acoustic-structure coupling, sound propagation in free space, and most importantly, the acoustic absorption of porous pavements.

Recognizing the critical issues to be addressed in the simulation model, the representation of acoustic absorption properties of porous pavements was identified as a major task in the development of entire tire/road noise model. The acoustic absorption coefficient can be derived from acoustic impedance. The application of

numerical approaches to quantify the acoustic impedance of porous pavement based on its pore structure parameters was discussed. The representative phenomenological model and microstructural model were presented. Although different input parameters are used, the outputs from these two models are in close agreement with each other. Both can be used in the analysis of tire/road noise on porous pavements. The representation of acoustic absorption in BEM formulation was validated against experiments studying horn effect reduction on porous pavements. The modeling of porous pavement acoustic property using BEM was found to be adequate for applications.

The porous pavement acoustic absorption model was next integrated into the tire/road noise simulation model which simulates the near-field noise measurement specified by the ISO 11819-2 standard (ISO, 2013). This model was designed to predict the rolling tire noise induced by pavement textures, focusing on the noise generated by tire vibrations. Four major steps are performed sequentially in the model simulation. First, the dynamic rolling tire analysis computes the deformations and stresses developed on tire walls in its rotation. The tire modal analysis next solves the natural frequencies and mode shapes of a rolling tire. The tire vibration analysis derives the tire vibration characteristics through the mode superposition approach, with the pavement texture spectrum serving as an excitation input. A BEM acoustic model is finally established to estimate the sound field around the tire, using tire wall vibration as the sound generation sources. The acoustic property of porous pavement is represented by the acoustic impedance measured in experiments or derived from mixture volumetric characteristics using either phenomenological or microstructural models.

The entire tire/road noise model was next calibrated and validated against the published experimental data for both conventional and porous pavements. The simulation results were compared against CPX test results measured by Schwanen et al. (2007) on various pavement types using a slick test tire. It was found that a set of

calibrated parameters is only valid for a particular combination of tire designs and pavement types. The model should be recalibrated for significantly different tires or pavement surface properties. It was concluded from model validation cases that with proper calibrations, the simulation results for dense-graded pavements agree well with the experimental measurements on both overall noise level and noise spectrum. The errors in overall noise levels are generally less than 2 dB(A) and the predicted 1/3-octave spectra can basically fit well with the measured spectrum shapes. For porous pavements, the quality of sound level spectra prediction becomes lower with regard to the frequency of noise reduction peak. The predicted noise reduction peaks appear at lower frequencies compared with the measured results. This may due to the local reaction assumption and may be resolved by introducing the extended reacting effect into BEM formulation to incorporate the influence of sound propagation within a porous surface layer on its acoustic absorption characteristics. Nevertheless, the estimations of overall noise levels on porous pavements are still satisfactory and the corrected noise spectra with frequency shifting generally agree with measurements.

The validation work illustrated the ability of the proposed model in predicting the acoustical performance of porous pavements. This model can be used to analyze the critical influencing factors in tire/road noise reduction on porous pavements and may provide useful and valuable information that otherwise is difficult to obtain in experiments.

Table 5.1: Specification and properties of pavement surfaces used in model calibration and validation (Schwanen et al., 2007)

Section No.	Pavement type	Surface layer thickness (mm)	Mean profile depth (mm)	British pendulum number
S01	ISO surface	30	0.39	89.0
S02	thin asphalt layer 2/4	25	0.45	90.5
S03	thin asphalt layer 2/6	25	0.56	91.0
S04	thin asphalt layer 2/6	25	0.75	90.0
S05	thin asphalt layer 4/8	25	0.93	89.5
S19	SMA 0/6	20	0.52	80.5
S20	SMA 0/8	25	0.89	82.0
S21	SMA 0/11	30	1.11	85.5
S22	SMA 0/16	40	1.38	85.5
S23	DAC 0/16	40	0.46	87.5
S40	surface dressing 5/8	N.A.	3.16	N.A.
S41	surface dressing 11/16	N.A.	5.99	N.A.
S24	porous 4/8	25	1.52	90.5
S25	porous 4/8	50	1.58	88.5
S26	porous 4/8 + porous 8/11	25+45	1.42	88.5
S27	porous 4/8 + porous 8/11	25+35	1.51	88.5
S28	porous 4/8 + porous 8/11	35+55	1.44	85.0
S29	porous 8/11	90	2.08	86.0
S30	porous 8/11 + porous 4/8	45+25	2.10	82.5
S31	porous 8/11	45	2.16	85.5

note: N.A. means test value is not available

Table 5.2: Model validation results of overall noise levels on porous and nonporous pavements

Pavement type	Section No.	Measured SPL [dB(A)]	Simulated SPL [dB(A)]	Error [dB(A)]
Dense-graded	S01	86.2	85.5	-0.7
	S02	83.4	82.2	-1.2
	S03	84.0	82.7	-1.3
	S04	84.7	86.2	1.5
	S05	87.9	88.1	0.2
	S19	86.1	85.4	-0.7
	S20	89.8	88.6	-1.2
	S21	91.6	90.7	-0.9
	S22	92.8	92.2	-0.6
	S23	88.4	87.3	-1.1
	S40	97.4	93.4	-4.0
	S41	100.3	100.0	-0.3
Porous	S24	91.1	90.4	-0.7
	S25	88.6	87.5	-1.1
	S26	87.8	87.7	-0.1
	S27	87.7	87.3	-0.4
	S28	87.1	86.0	-1.1
	S29	90.5	89.5	-1.0
	S30	91.1	89.9	-1.2
	S31	94.6	93.3	-1.3

Table 5.3: Results and quality of frequency shifts in simulated sound pressure spectrum correction

	Type I				Type II			
	α	min z	χ^2	R^2	β	min z	χ^2	R^2
S24	0.897	9.11	0.12	0.963365	0.9851	9.70	0.12	0.961022
S25	0.934	31.61	0.41	0.609621	0.9914	33.63	0.44	0.584610
S26	0.967	26.91	0.35	0.541271	0.9969	27.57	0.36	0.530091
S27	0.928	17.96	0.23	0.673844	0.9908	19.58	0.25	0.644579
S28	0.871	3.17	0.04	0.946736	0.9810	3.36	0.05	0.943457
S29	0.880	3.01	0.04	0.975527	0.9825	3.33	0.04	0.972874
S30	0.885	6.24	0.08	0.942494	0.9829	7.75	0.10	0.928563
S31	0.877	15.30	0.19	0.958581	0.9808	13.01	0.16	0.964775

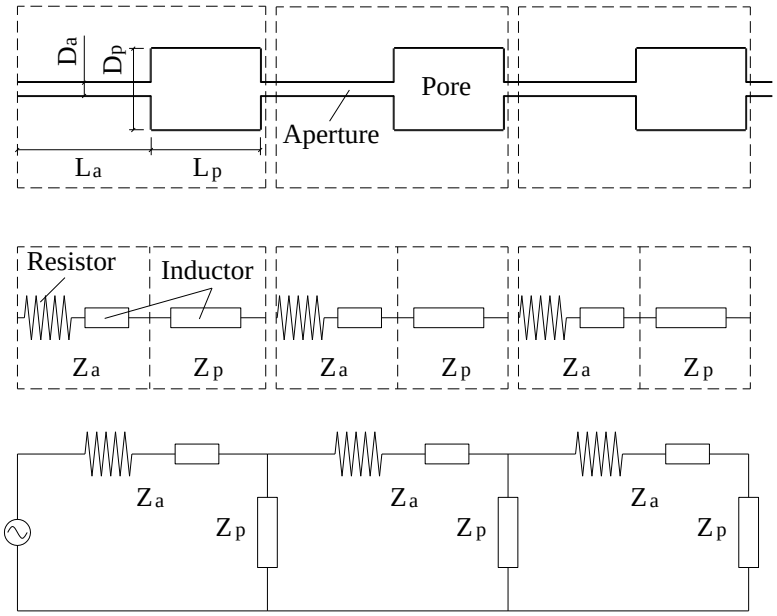

Figure 5.1: Electro-acoustic representation of pore structure (Neithalath et al., 2005)

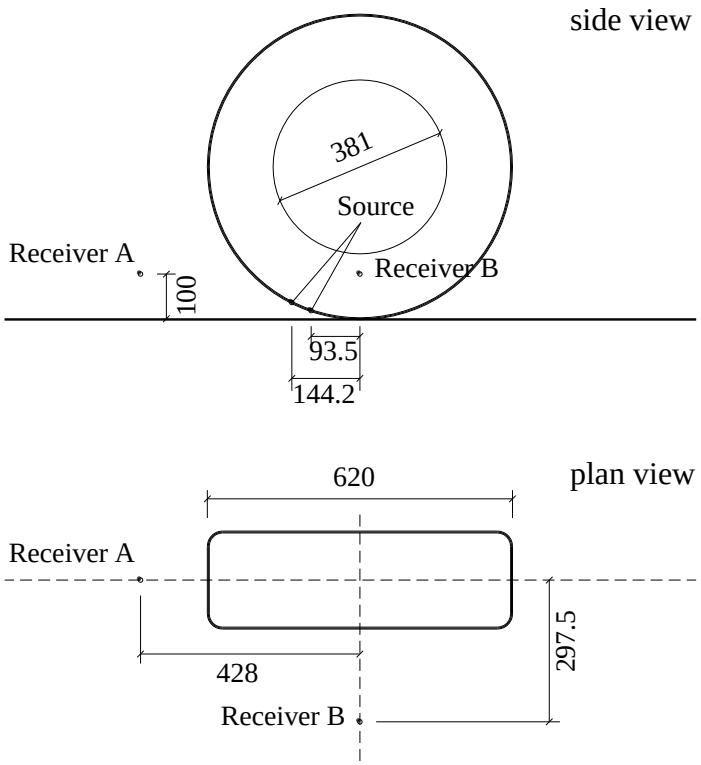

Figure 5.2: Experimental set-up for porous pavement model validation

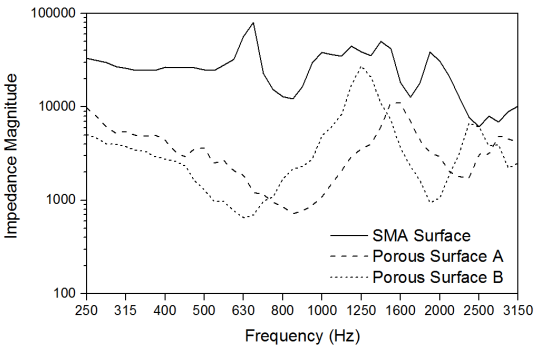

(a) Acoustic Impedance

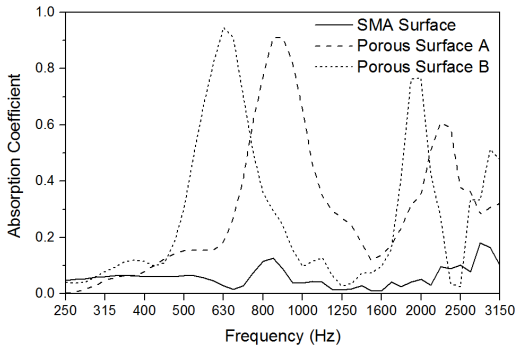

(b) Acoustic Absorption

Figure 5.3: Measured acoustic properties of tested pavements

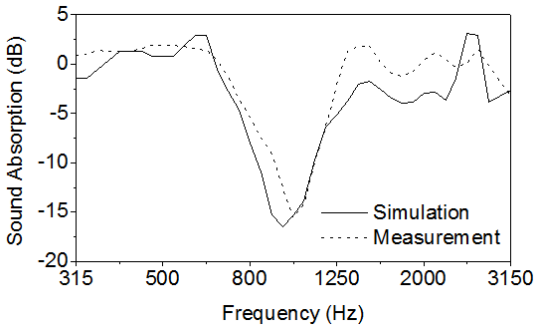

(a) Porous surface A, receiver A, source is 10 cm from the center

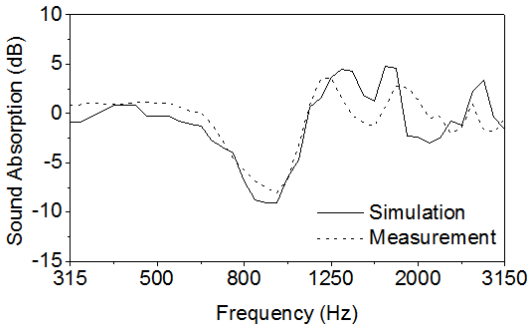

(a) Porous surface A, receiver A, source is 15 cm from the center

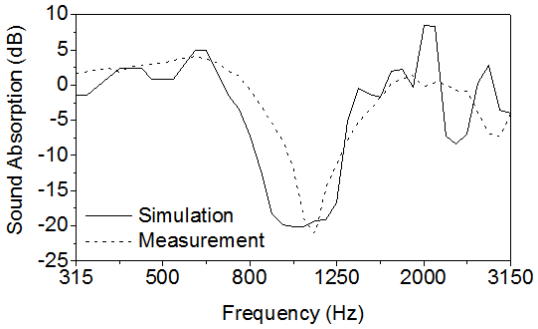

(a) Porous surface A, receiver B, source is 10 cm from the center

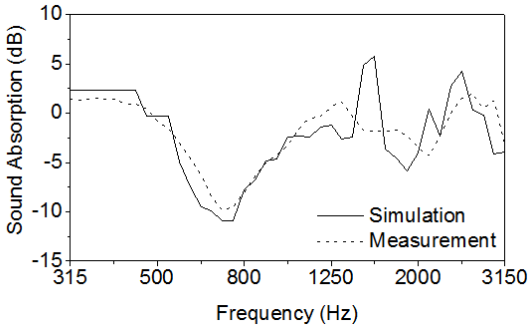

(a) Porous surface B, receiver A, source is 10 cm from the center

Figure 5.4: Model validation results

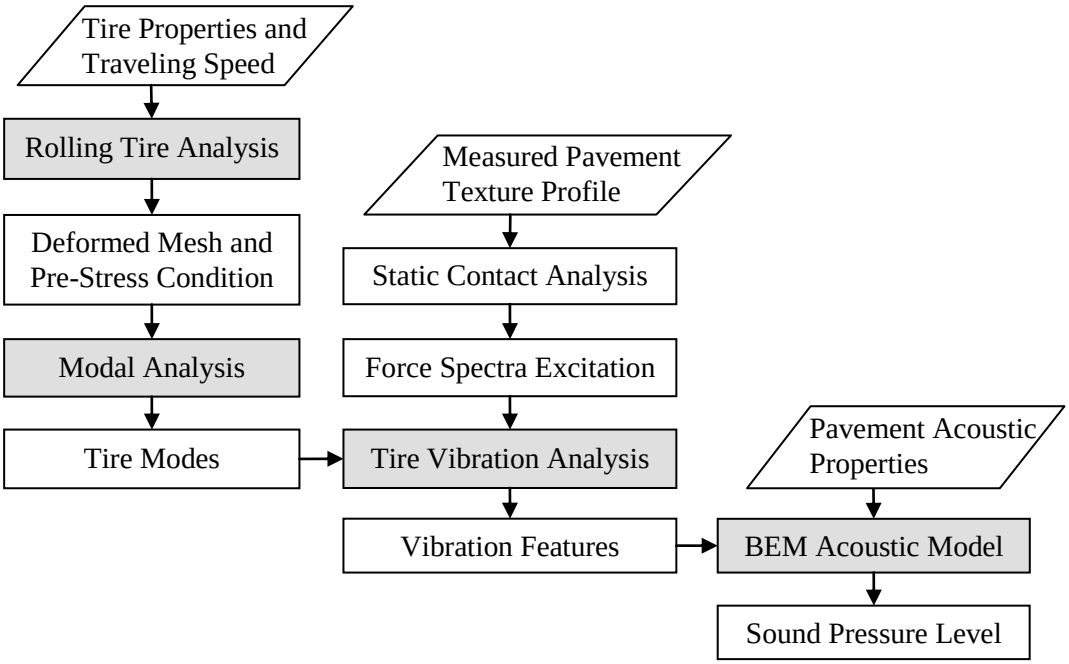

Figure 5.5: Framework of tire-pavement noise prediction model

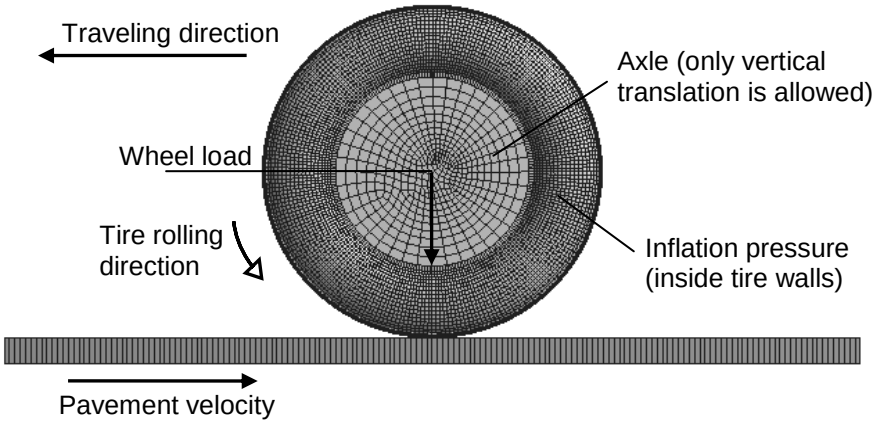

Figure 5.6: Relative motion frame of reference in rolling tire analysis

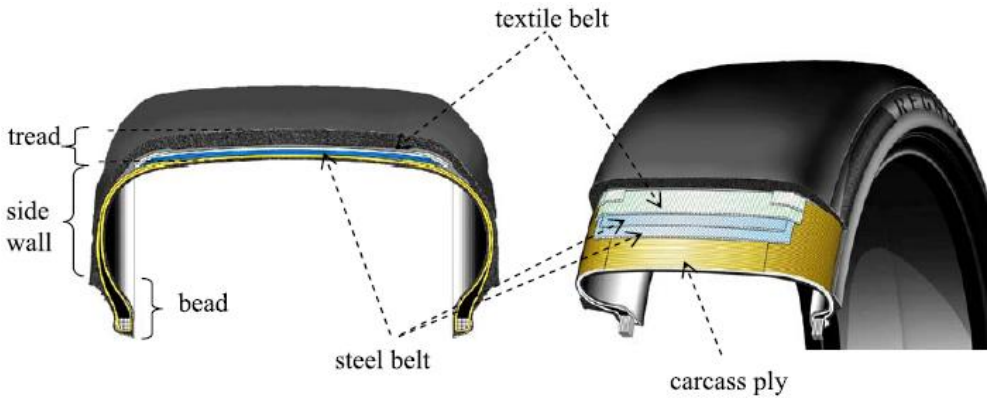

Figure 5.7: Typical cross section of a smooth tire (Waki et al., 2009)

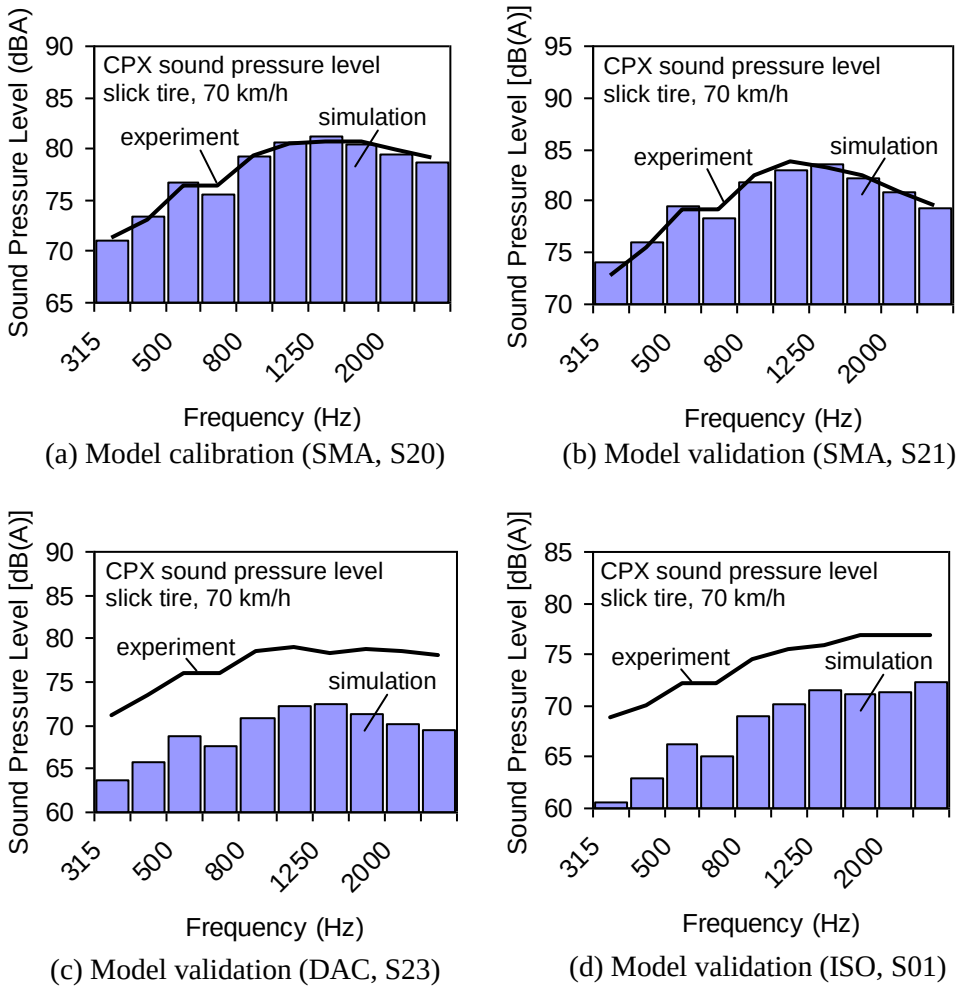

(a) Model calibration (SMA, S20)

(b) Model validation (SMA, S21)

(c) Model validation (DAC, S23)

(d) Model validation (ISO, S01)

Figure 5.8: Illustration of simulated and measured 1/3-octave spectra on dense-graded pavements (refer to Table 5.1 for surface type)

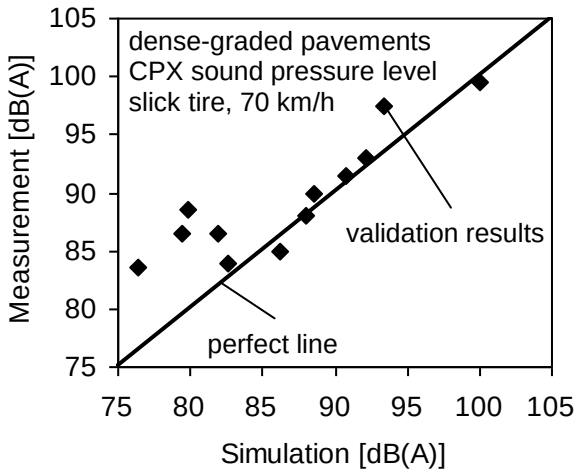

Figure 5.9: Comparison between simulated and measured overall noise levels on dense-graded pavements

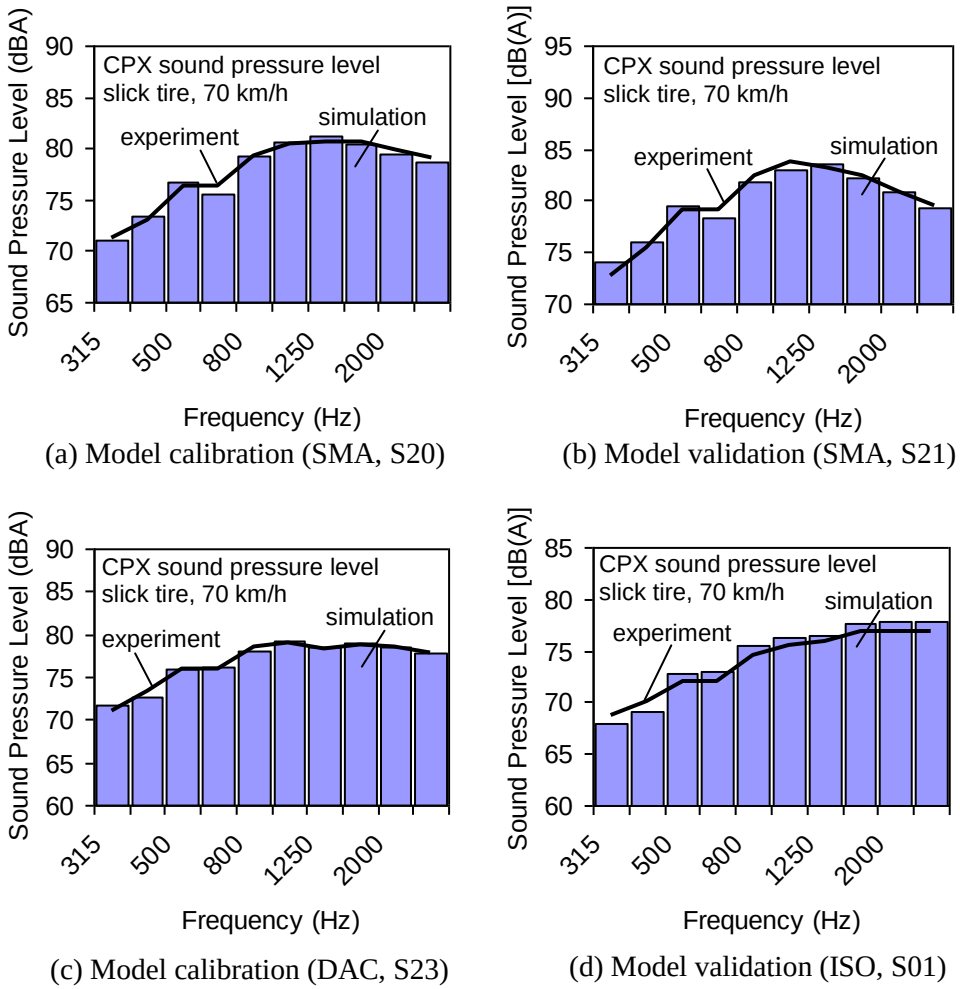

(a) Model calibration (SMA, S20) (b) Model validation (SMA, S21)

(c) Model calibration (DAC, S23) (d) Model validation (ISO, S01)

Figure 5.10: Illustration of simulated and measured 1/3-octave spectra on dense-graded pavements (refer to Table 5.1 for surface type)

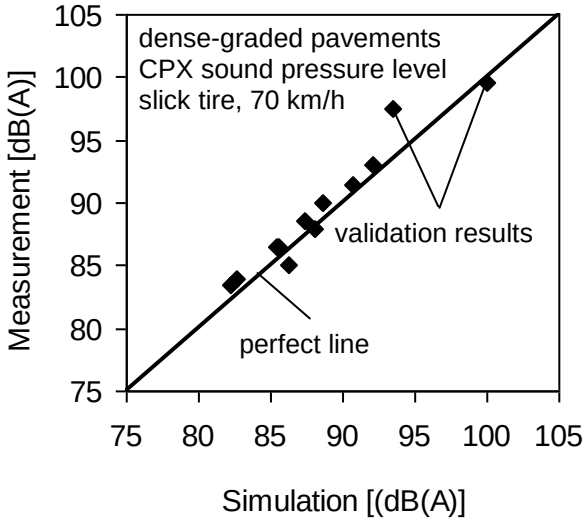

Figure 5.11: Comparison between simulated and measured overall noise levels on dense-graded pavements

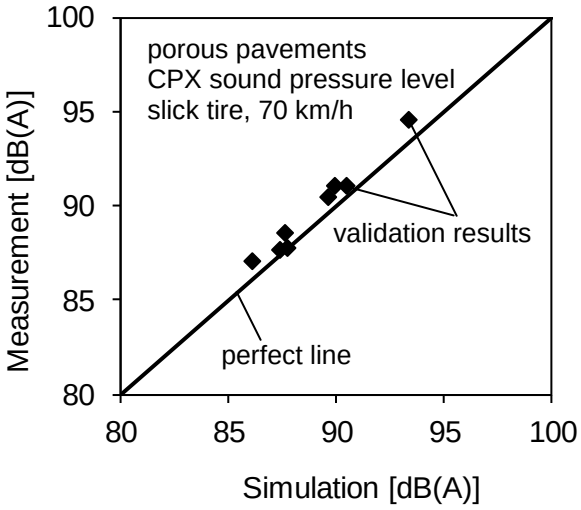

Figure 5.12: Comparison between simulated and measured overall noise levels on porous pavements

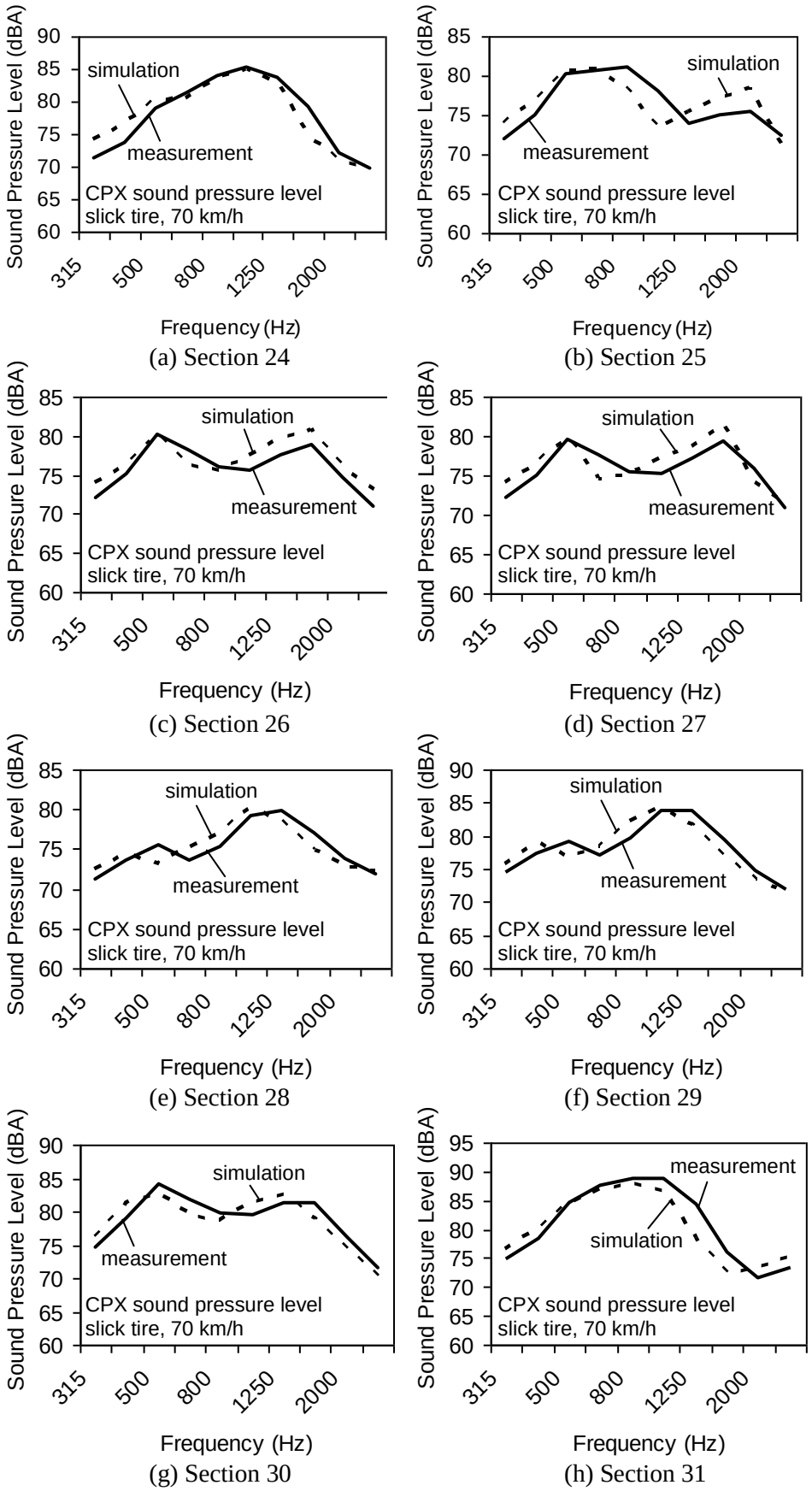

Figure 5.13: Illustration of simulated and measured 1/3-octave-band spectra on porous pavements (refer to Table 5.1 for surface type)

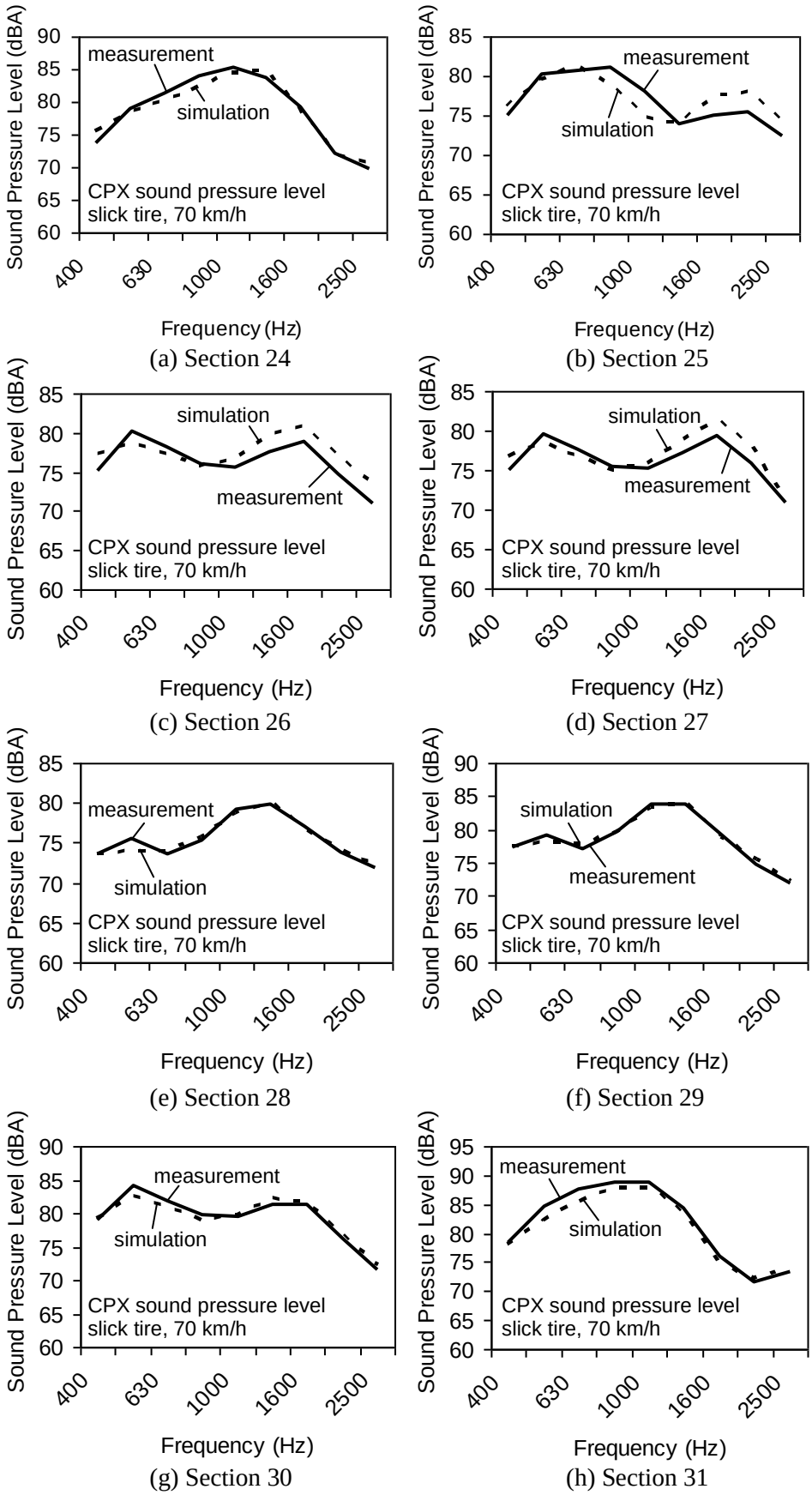

Figure 5.14: Corrected simulated sound pressure spectra on porous pavements (refer to Table 5.1 for surface type)

CHAPTER 6 ANALYSIS OF INFLUENCING FACTORS ON TIRE/ROAD NOISE OF POROUS PAVEMENT

As discussed in Section 2.2.4, various factors in pavement design and vehicle operation can significantly affect the tire/road noise performance of porous pavement. Some critical variables are examined in this chapter for their effects on tire/road noise emission. The porosity and thickness of porous surface layers have been identified as crucial control parameters in porous pavement design. Pavement surface texture is the main excitation of tire vibration noise and travel speed is a critical factor in vehicle operation. The influences of all these factors on the acoustical performance of porous pavement are quantitatively investigated using the analysis framework and numerical simulation model developed in Chapter 5. The overall effect of existence of porous surface layer on tire/road noise is first examined through comparison between porous and nonporous pavements. The effects of above mentioned influencing factors are then studied individually. The analysis presented in this chapter can enhance further understanding in the reduction of tire/road noise on porous pavements and provide preliminary guidelines for porous pavement design considering the acoustical performance.

6.1 Effect of Porous Surface Layer on Tire/Road Noise Performance

Porous pavement technology was initially developed to improve wet-weather skid resistance, but its advantage in traffic noise reduction was soon recognized in the extensive applications. The major functional purpose of porous overlays adopted in Europe today is to control the noise emission level produced by high speed vehicles. This benefit becomes more attractive when considering the high expectation on living environment of the residents near roadways and the high expenses of other noise abatement alternatives such as noise walls. The major mechanism of noise reduction on a porous pavement comes from its acoustic absorption property, which reduces the reflected energy intensity after the sound wave incidents the pavement surface. The

negatively orientated macrotexture may provide a smoother surface for pneumatic tires to travel on, mitigating the texture-induced tire vibrations. Most of the previous studies on the effectiveness of porous surfaces in tire/road noise reduction are experimental in nature (Younger et al., 1994; der Graaff et al., 2005; Kowalski et al., 2009). This makes detailed analysis difficult, primarily due to the requirement of sufficiently long test pavement sections in the complex full scale field test. It is necessary to study this problem from a numerical perspective and apply an appropriate mechanistic analysis framework to predict the acoustical performance of porous and nonporous pavements under identical traveling condition. This section presents an illustrative case study to assess the overall effects of porous surface layer on tire/road noise and interpret how porous pavements reduce traffic noise in regular travel conditions.

6.1.1 Description of the Hypothetical Problem

Past experimental studies have proved that porous pavements produce lower tire/road noise than the conventional dense-graded pavements (Younger et al., 1994; der Graaff et al., 2005; Gibbs et al., 2005; Kowalski et al., 2009; Abbott et al., 2010). This fact is widely accepted and porous pavements are utilized around the world to abate traffic noise pollution. However, there is little improvement in the understanding of tire/road noise reduction mechanism. The expected noise reduction brought forth by a porous surface layer varies largely among studies and the contribution of different noise mitigation mechanisms to overall noise reduction is left investigated. Besides, the relationship between acoustic absorption coefficient and noise reduction remains unclear. The example illustrated in this section attempts to quantify the tire/road noise reduction brought forth by porous surface application while providing insight into major mechanisms.

To investigate noise reduction on porous pavement, the developed numerical model is applied to quantify and compare the acoustical performance of porous and

non-porous pavement surfaces. The following hypothetical problem is defined and analyzed [the values are obtained from in-field experiments performed by Schwanen et al. (2007)]:

A high speed road facility in a residential area is to be rehabilitated using an asphalt overlay. Two alternatives are considered in the design phase where both are adequate in providing excellent skid resistance performance in wet weather:

- Case I: an asphalt surface dressing with aggregate sizes between 5 and 8 mm;
- Case II: a 50 mm thick porous asphalt wearing course with 8 mm nominal maximum aggregate size.

The appearances of these two pavement types are illustrated in Figure 6.1. The surface texture profile of each overlay is measured by a laser profilometer on short trial sections and the mean profile depth (MPD) for Case I and Case II surfaces are determined to be 3.1 mm and 1.5 mm respectively. Surface texture spectra are derived from the measured profiles according to the ISO 13473-4 standard (ISO, 2008) and the results are shown in Figure 6.2. Existing pavement surface is assumed to be acoustically hard, with a zero acoustic absorption for all frequencies. The measured absorption coefficient spectrum of Case II surface is shown in Figure 6.3.

Tire/road noise emission is a critical property considered in the rehabilitation project. The acoustic performance of different alternatives are predicted to assist in the selection of overlay for noise reduction. The developed tire/road noise model is used to simulate CPX noise measurement in accordance to ISO 11819-2 standard (ISO, 2013). A Continental slick tire (195/65R15) is adopted in the simulations with an inflation pressure of 150 kPa and a wheel load of 3200 N. The CPX noise evaluation is based on a vehicle speed of 70 km/h, consistent with model calibration.

6.1.2 Results and Discussions

The surface texture and acoustic absorption of pavement are two critical input parameters in tire/road noise simulation. The differences in these variables on porous

and non-porous surfaces are first discussed. Figure 6.2 presents the texture spectra of the two overlay types (Cases I and II). It was observed that the shapes of the spectra for Case I and II are similar, but the texture level amplitude on Case I is significantly higher than that on Case II in the wavelength range higher than 10 mm. This observation indicates that porous overlay can provide a smoother surface for vehicles to travel on, although it has more open air voids. This is resulted from the negative texture orientation. The Case I pavement surface is assumed to be perfectly reflecting, with zero acoustic absorption coefficient at all frequencies. The acoustic absorption coefficient of porous surface in Case II is shown in Figure 6.3, where two absorption peaks were found at the 800-1000 Hz and 2000-2500 Hz ranges. The primary absorption peak at 800-1000 Hz has a maximum coefficient of about 0.9, while the amplitude for the secondary absorption peak is about 0.6. Acoustic impedance is derived from the absorption coefficient and used as a direct input in the noise simulation model.

The above presented texture spectra and acoustic absorption coefficients are next used as input into the developed and calibrated tire/road noise simulation model. The sound level spectra measured at CPX microphone positions are computed from numerical simulations and the overall noise levels are derived from spectrum outputs. The simulated results are shown in Figure 6.4. The overall noise level on porous asphalt surface is 87.6 dB(A), significantly lower than the 93.8 dB(A) on the surface dressing pavement. From the sound level spectra, it was observed that noise level is lower on porous surface compared to surface dressing overlay in the frequency range from 315 Hz to 2500 Hz. The most significant noise reduction on the porous surface happens at a frequency of about 1250 Hz. This frequency is slightly higher than the frequency of major acoustic absorption peak shown in Figure 6.3. The sound level difference at 1250 Hz is about 12 dB(A) for the two surface types. Another noise reduction peak happens around 2500 Hz, corresponding to the secondary sound

absorption peak of porous surface. Generally, noise reduction is more significant at high frequencies (above 800 Hz) compared to that at low frequencies (below 800 Hz).

The contributions of reduced texture level and increased acoustic absorption capacity are next analyzed separately. First, the effect of surface texture in inducing tire vibration noise is investigated by introducing a Case III surface that has the same surface texture as Case II pavement and a perfectly reflecting acoustic property (zero acoustic absorption). Properties of the three surface types are compared in Table 6.1. The predicted noise spectrum of the "perfectly acoustic hard pavement" (Case III), which has the same texture profile as a porous asphalt layer, is compared with the simulated spectra for Case I and Case II pavements in Figure 6.5. It is observed that the influence of texture difference on tire/road noise emission is insignificant. Some surface texture effects are observed at frequencies below 1000 Hz, while marginal differences occur at higher frequencies. The overall noise level on Case III pavement is 93.3 dB(A), slightly lower than the 93.8 dB(A) on surface dressing pavement. Therefore, it can be concluded that the smoother traveling surface produced by the negative texture orientation of porous pavement is only a secondary component in noise reduction. The mechanisms brought forth by the acoustic absorption capacity of porous surface layer should be the dominant contributors to tire/road noise reduction. This effect could be observed from the differences between the noise spectra of Case II and Case III surfaces (see Figure 6.5).

As indicated by Naithalath et al. (2005), the interconnected pore network may affect tire-generated noise emission primarily through two mechanisms: the decrease in air pumping and the reduction in horn effect. The former occurs by permitting air to escape through the open voids within pavement surface layer. This mechanism is beyond the scope of this study. The later results from the absorption of sound energy during the multi-reflection process when sound waves propagate in the horn-shape geometry formed by tire tread and pavement surface. This effect is examined using a BEM model that predicts the reduction of horn effect on the Case II porous surface.

This model is similar to the BEM model used in tire/road noise simulation, but with a stationary tire and a monopole sound source. The Continental slick tire (195/65R15) is placed on the pavements with and without sound absorbing capacity (e.g. Cases II and III surfaces). The tire surface is assumed to be acoustically hard. A monopole producing white noise is located on the center line of tire tread surface, 10 cm from the center of tire-pavement contact patch. This test configuration is sketched in Figure 6.6, with receivers located at the microphone positions of CPX measurement. The effect of porous surface on sound absorption is captured by the differences in sound pressure levels on porous and non-porous surfaces. Figure 6.7 shows the results computed from the numerical simulations. The maximum reduction of horn effect is found at around 1000 Hz frequency. This agrees well with the frequency of major acoustic absorption peak shown in Figure 6.3. The level of noise reduction at this frequency is more than 15 dB(A). The noise reduction effect fluctuates at high frequencies and a secondary peak is observed at 2000 Hz. These findings indicate that the sound absorbing capacity resulted from the interconnected pores of porous pavement can significantly reduce the horn effect in tire/road noise emission and it should be the dominant contributor to the noise reduction on porous surfaces. It may be possible to optimize the acoustical performance of a porous pavement through adjusting its pore network structure.

6.2 Effect of Influencing Factors on Porous Pavement Tire/Road Noise

The effects of critical influencing factors on tire/road noise performance of porous pavements are analyzed in this section using an illustrative hypothetical case study. The examined variables include porosity, porous layer thickness, texture level and vehicle traveling speed. The analysis considers some interactions between different influencing factors. The hypothetical problem is first defined as a design of porous asphalt overlay. The tire/road noise emissions on the porous surfaces with various design parameters are then predicted by the proposed numerical model. The

simulated results are then analyzed for each individual influencing factor. Several suggestions on porous pavement design are recommended based on the findings in this parametric study.

6.2.1 Description of Hypothetical Problem

A tangent highway section is considered to be rehabilitated by porous asphalt overlay to reduce tire/road noise. The existing dense-graded pavement surface is assumed to be acoustically hard, while the overlaid porous asphalt course should possess a sound absorbing capacity that can eliminate the noise emission for certain frequencies as well as the overall noise level. The porous overlay will have a uniform thickness. Various mixture designs with different porosities, porous layer thicknesses and surface textures are examined. The tire/road noise emissions are evaluated at different vehicle speeds to determine the best design for allowable speeds. The previously developed analysis framework in Chapter 5 is adopted for this purpose.

The porosity levels examined in the parametric study should cover the normal porosity range of porous pavements employed in practice. As presented in Chapter 4, the typical porosity of a new porous surface layer usually ranges from 18% to 22% (Alvarez et al., 2011). Higher porosities up to 25% have also been used to enhance the benefits in skid resistance and tire/road noise (Alvarez et al., 2011). On the other hand, the porosity of porous pavements tends to decrease with time due to clogging. To cater for the deterioration of porosity with time, some agencies have adopted a design terminal value of 15% for porosity (Liu and Cao, 2009). Five porosity levels (i.e. 15%, 17.5%, 20%, 22.5% and 25%) are selected for this study based on the above values.

The levels of porous layer thickness considered in this analysis should cover the normal range of porous surface layer thicknesses used in practice. It is found from extensive review of porous pavement projects that most porous layers used as overlays or wearing courses had thickness varying from 50 mm to 100 mm (Smith,

1992; Moore et al., 2001). Besides, there are also instances where thin porous layers with a thickness of 25 mm were used (Smith, 1992). Porous surface layers in United States are commonly laid in an integer multiple of 1 inch (Moore et al., 2001). Therefore, the porous layer thickness levels examined in this study are selected as 25 mm, 50 mm, 75 mm and 100 mm.

The porous pavement surface texture levels considered in this study should represent the regular texture variations on porous surface in the field. It is difficult to conduct texture profile measurement on porous pavements due to the deep air voids at pavement surface, causing laser sensor to lose focus during high-speed measurement. Therefore, very limited experimental results on porous surface texture could be found in literature. Typical results from the in-situ measurements conducted by Schwanen et al. (2007) are adopted in this study to represent various texture levels on porous surfaces. Figure 6.8 shows four texture spectra obtained from this measurements and are used as excitation input in the noise prediction model. It is observed that large differences exist among porous surface textures, especially at the longer wavelength (i.e. lower frequency). Texture levels at shorter wavelength are less different because pavement microtexture mainly depends on the texture of individual aggregate instead of aggregate gradation. It is noted that type II texture shown in Figure 6.8 is identical with that of Case II in Figure 6.2 because they are measured on the same porous pavement surface.

The vehicle traveling speeds considered in this work should cover the common operating conditions encountered on regular dry roadways. A speed step of 10 km/h is adopted to develop the variation of tire/road noise with traveling speed. Six speed levels are considered in this study, i.e. 50, 60, 70, 80, 90 and 100 km/h.

Neithalath et al. (2005) microstructural model introduced in Section 5.2.2.2 is adopted to derive the acoustical characteristics of each porous overlay surface. Besides porosity and porous layer thickness, other parameters such as the characteristic pore size, pore length, aperture length and aperture diameter are critical

inputs to this model. An analytical approach is performed to establish models for specific porosity values or particular porous layer thicknesses. In an experimental study conducted by Losa and Leandri (2012), a regression relationship between pore length and pore size was proposed for porous asphalt concrete:

$$L_p = 1.92 \cdot D_p + 8.63 \tag{6.1}$$

Pore length (L_p) is related to characteristic pore size (D_p). Considering the porous layer thicknesses studied, the entire length of a pore unit is taken as 25 mm and aperture length are related to pore length by $L_a + L_p = 25$. Aperture diameter is assumed to be a quarter of pore size according to Neithalath (2005). In the analysis, pore wall thickness is fixed at 3.5 mm and the porous layer thickness is fixed at one of the four thickness levels. The characteristic pore size is closely related to porosity and is determined for each porosity level by a trial-and-error approach based on the relationships between pore structure parameters [i.e. pore size (D_p), pore length (L_p), aperture length (L_a) and aperture diameter (D_a)]. The derived input parameters for each pavement design is presented in Table 6.2. There is 1 pore unit in the thickness direction for 25 mm thick porous surface layer, 2 pore units for 50 mm porous layer and so on so forth. With these pore structural parameters, the acoustic impedance and absorption coefficient of each porous overlay surface can be derived from Neithalath microstructure model.

Pavement surface texture is related to porosity and pore size of porous layer. However, the effect of porosity and pore size on surface texture is beyond the scope of this work. Only the four selected typical texture profile levels shown in Figure 6.8 are used in this study to isolate the effect of surface texture on tire/road noise emission. Vehicle speed also affects the texture level spectrum experienced by a tire traveling on the same road surface. Texture excitation spectra at different speeds can be derived from the relationship among speed, wavelength and frequency.

$$f = v/\lambda \tag{6.2}$$

where f is frequency (Hz), v is vehicle speed (m/s) and λ is wavelength (m). Basically, a texture spectrum will shift towards the higher frequency at a higher vehicle speed. Different vehicle speeds are used as inputs to the rolling tire analysis (see Figure 5.5) to compute the pre-stress condition, and deformed tire geometry under different traveling conditions. Tire vibration at each speed is then generated from tire vibration analysis with corresponding pavement texture excitation spectrum. The frequency-dependent acoustic impedance of porous overlay is next used in the BEM acoustic model to predict its acoustical performance. The sound pressure spectra and the overall noise levels are obtained from numerical simulations and compared among alternative porous overlays.

6.2.2 Influence of Porosity

Past experimental studies have shown that porous surfaces with different porosities and pore structures may present quite different acoustical characteristics (Schwanen et al., 2007). However, the quantitative effect is still unclear. Section 6.1 had shown that the significant noise reduction on porous pavement surfaces is mainly a result of the pavement acoustic absorption ability. Therefore, porous pavement design should also consider the influence of porosity on its acoustic property if traffic noise reduction is one of the primary purposes of porous surface application. This section analyzes the porosity effect based on numerical results of tire/road noise simulation model. The efforts focus on the estimation of surface acoustic absorption of different porous surface layers and the prediction of rolling-tire noise levels on each surface.

The acoustic absorption coefficients of alternative porous mixture designs with various porosities are derived from Neithalath et al. (2005) model. The results for the 50 and 100 mm porous layer thickness are illustrated in Figure 6.9. It can be observed that porosity does not have a significant influence on the peak absorption frequency, although the absorption peak shifts slightly towards the lower frequency

side with an increase in porosity value. However, porosity does affect the magnitude of primary absorption peak. In the examined porosity range (15% - 25%), the maximum acoustic absorption coefficient decreases with an increase in porosity. The relative reduction at primary absorption peak is about 25% when the porosity increases from 15% to 25%. This is mainly a result of declination in the real component of acoustic impedance, which represents the resistive part of energy lost. The decrease of acoustic absorption with porosity increase may seem counterintuitive at the first glance, but it is reasonable and inevitable when considering the mechanisms of Neithalath's model. The increase of porosity comes from two parts in the microstructure model, the increase of pore size and the decrease of aperture length. The impedance of air inside the pores is modeled as a resistor, which is inversely related to the pore size. The frictional losses of sound energy occur mainly in the apertures, thus the reduced aperture length also leads to a reduced absorption. These results are consistent with the observations by Neithalath et al. (2005). Comparing with the acoustic coefficients of 50 mm thick porous layers, it was found that the primary absorption peaks occur at lower frequencies and a secondary absorption peak appears at around 2200 Hz on 100 mm porous layers.

Figure 6.10 demonstrates the noise spectra generated by a rolling slick tire on the various porous surfaces shown in Figure 6.9, subjected to the identical Type II texture level as shown in Figure 6.8. The acoustical performance of a perfectly acoustic hard surface with the same texture level (i.e. Case III surface as shown in Table 6.1) is also generated numerically and plotted as a basis for comparison. It is seen that, with the same thickness, porous surfaces produce similar tire rolling noise spectra, although different porosity values exist in the porous mixtures. Taking the 50 mm case [Figure 6.10 (a)] as an example, all the five sound pressure level spectra have similar shapes with the maximum noise reductions occurring at around 1600 Hz. The maximum noise reductions may result from the peak sound absorbing capacity of porous pavements, which happens at about 1400 Hz [see Figure 6.9 (a)]. Considering

the frequency-shift correction factor, the noise reduction peak agrees with the sound absorption peak. The differences in the magnitudes of sound pressure spectra on various surfaces are quite marginal at frequencies below 800 Hz, but are more significant at higher frequencies, especially at the peak noise reduction frequency. In the examined porosity range, sound pressure level at about 1600 Hz increases with the increase of porosity value. The difference is about 3 dB(A) when porosity increases from 15% to 25%. The situation on 100 mm thick porous surface layers is similar to that on 50 mm ones, except that the primary noise reduction peaks happen at a lower frequency around 800 Hz. It is also observed that the spectrum shapes are significantly different between 50 mm and 100 mm thick porous courses. The influence of porous layer thickness on tire/road noise reduction will be discussed in detail in the next sub-section.

Figure 6.11 compares the simulated overall noise levels emitted from a tire rolling on various porous pavement surfaces. Noise level of the perfectly acoustic hard surface is also shown in the figure as a shaded bar for comparison. It can be seen that for the same porous layer thickness, the overall noise level increases with the increase in pavement surface porosity. For pavements with 50 mm thick porous layers, the overall noise level is 87.50 dB(A) at 15% porosity, and 88.74 dB(A) at a porosity value of 25%. For pavements with 100 mm thick porous layers, the overall noise level at 15% and 25% porosity is 85.02 dB(A) and 86.14 dB(A) respectively. The differences in overall noise levels due to porosity variations for both thickness levels are more than 1 dB(A). A research study in New Zealand (Dravitzki, 2006) has indicated that a 1 dB(A) change in overall noise level could be noticeable and annoying to public, especially when the existing noise level is high, refuting the previous understanding that a noise change of 3 dB(A) is just noticeable to most people. Taking this into consideration, it can be concluded that although the difference in overall noise level brought forth by altering the porosity value of porous surface layer may not be significant, it may still be beneficial to public.

To summarize, with the same pavement texture and porous layer thickness, tire/road noise on porous surfaces increases with an increase in porous layer porosity in 15% to 25% porosity range and the increasing trend is generally linear. Porosity variation does not alter the noise spectrum shape much at 1/3 octave bands. A porous mixture design with a lower porosity should be adopted from the perspective of tire/road noise reduction, provided the premise of sufficiently superior frictional performance and clogging resistance durability.

6.2.3 Influence of Porous Layer Thickness

In addition to porosity, the thickness of porous surface layer is also a critical factor in porous pavement design that can affect the acoustical characteristics of a porous pavement system. At least two effects are brought forth through variations in porous layer thickness. Firstly, a thicker porous course may be capable to dissipate more acoustic energy in the sound propagation process, since the sound wave has travel a longer distance within the porous medium. Secondly, the difference in porous layer thickness may alter the spectrum shape of acoustic absorption coefficient, making the absorption peak appear at a different frequency or changes the number of peaks in the 300 to 2500 Hz frequency range (Wai and Kai, 2004; Losa and Leandri, 2012). Therefore, it is possible to adjust porous layer thickness during the design phase to optimize traffic noise reduction. For this purpose, the influence of porous layer thickness on tire/road noise performance of porous pavements is analyzed using the developed numerical simulation model. Similar to the previous sections, research efforts are also focused on estimating the surface acoustic impedance of various porous surfaces and predicting the rolling-tire noise levels on each surfaces using the derived acoustic properties.

Figure 6.12 illustrates the absorption coefficients of porous pavements with various surface layer thicknesses, at three porosity levels. It is seen from the figure that porous layer thickness significantly affects peak absorption frequency. This may

be due to the interferences and phase differences between the sound wave traveling directly from source to receiver, wave reflected by pavement surface and wave penetrating into porous layer and reflected by the dense-grade base (Abbott et al., 2010). The primary absorption peak moves towards lower frequency due to the increase in porous layer thickness. The peak absorption occurs at about 2200 Hz on a 25 mm thick porous pavement surface and appears at about 700 Hz on a 100 mm thick porous layer. Along with the primary absorption peak shifting to lower frequency, a secondary peak may appear in the interested frequency range from the higher frequency side. Such a secondary peak can be observed on 100 mm porous layer at about 2200 Hz. Furthermore, porous layer thickness also affects the magnitude of absorption coefficient. In the examined range of porous layer thickness, the maximum acoustic absorption coefficient increases with the increase of porous layer thickness. The relative increase in primary absorption peak is about 20% when porous layer thickness increases from 25 mm to 100 mm. This is expected because more acoustic energy will dissipate when the sound wave travels a longer distance in the porous pavement layer.

Figure 6.13 illustrates the simulated noise spectra on porous pavements with various surface layer thicknesses and porosity values, subjected to the identical Type II texture level as shown in Figure 6.8. The acoustical performance of a perfectly acoustic hard surface (i.e. Case III in Table 6.1) is also shown in the figure. It can be seen that porous pavements may generate very different tire rolling noise spectra if porous layers with different thicknesses are used in pavement construction or rehabilitation, despite the same porosity level. Taking the case of 20% porosity [see Figure 6.13 (b)] as an example, the sound spectrum shapes differ from each other with the maximum noise reduction occurring at different frequencies. The primary noise reduction peak moves towards the lower frequency with the increase of porous layer thickness, appearing at 2500 Hz, 1600 Hz, 1000 Hz and 800 Hz, respectively, for porous layer with a 25 mm, 50 mm, 75 mm and 100 mm thickness. As previously

observed, the maximum noise reduction may result from the peak sound absorbing capacity of a porous pavement. From Figure 6.12 (b), the peak absorption frequency is observed to be around 2200 Hz, 1400 Hz, 900 Hz and 700 Hz for porous surfaces with 25, 50, 75 and 100 mm thicknesses respectively. Taking the frequency-shift correction factor into consideration, the frequencies of noise reduction peaks agree with the frequencies of sound absorption peaks. Sound pressure level differences on various porous surfaces are insignificant at frequencies below 630 Hz, but are large at higher frequencies [up to 10 dB(A) for some particular frequencies]. Similar observations can be made on porous surfaces with 15% and 25% porosities, with slight differences in sound level magnitudes.

Figure 6.14 compares the overall noise levels emitted from a slick tire rolling on different porous pavement surfaces. Noise level on the perfectly acoustic hard surface is also shown in the figure. The overall noise levels are derived from the simulated spectra in Figure 6.13. It is seen that, for the same porosity level, the overall noise level decreases with an increase in porous layer thickness. The noise reduction performance of porous pavement is superior with thicker porous layer. For pavements with a 15% porosity, the overall noise level is 89.08 dB(A) when the porous layer thickness is 25 mm, and 85.02 dB(A) when the thickness is 100 mm. The overall noise levels at 25 and 100 mm porous course thickness are 89.77 and 85.58 dB(A) for 20% porosity and 90.45 and 86.14 dB(A) for 25% porosity, respectively. The difference in overall noise levels due to porous layer thickness variations is more than 4 dB(A) in the examined thickness range. This is much more significant than the influence of porosity on tire/road noise. The dependency of noise reduction on porous layer thickness is nonlinear. The noise level difference between 50 mm and 75 mm is about 0.8 dB(A), while it is around 1.5 dB(A) when porous layer thickness increase from 25 to 50 mm or from 75 to 100 mm. This indicates that 50 mm thick porous layer may be the most cost effective for tire/road noise reduction.

100 mm porous layer could be used to enhance the noise reduction only when the additional material cost is reasonable.

The above observations indicate that tire/road noise on porous surfaces decreases with an increase in porous layer thickness with a nonlinear trend when porosity and texture are maintained identical. Porous layer thickness significantly affects the noise spectrum shape, making the noise reduction peak move towards a lower frequency as the porous layer thickness increases. Porous pavement design with a thicker porous surface layer could be adopted in the perspective of tire/road noise reduction if material cost is acceptable.

6.2.4 Influence of Pavement Surface Texture

Pavement surface texture is directly involved in the tire-pavement interaction, affecting not only friction but also tire/road noise. Surface texture essentially results from composition and property of pavement materials, especially the size, gradation and angularity of aggregates. It varies with pavement age and traffic loading, due to weather impact and tire abrasion. The porous surface texture characteristics have two opposing influences on tire/road noise generation. The negative texture orientation formed by large aggregates provides a flat traveling surface, which can mitigate the tire-pavement impact occurring at contact patch. On the contrary, due to the adoption of larger aggregates and open air voids on pavement surface, porous pavement may exhibit a more aggressive texture profile, which increases texture level and enhances excitation on tire vibration. Although it is expected that surface texture is related to the porosity and pore size of pavement material, it is also observed that pavements with the same porosity value may possess different surface texture levels and result in different noise levels (Schwanen et al., 2007). Besides, the texture level of an identical pavement varies in its service life, causing differences in tire/road noise emission as well. Therefore, it is necessary to investigate the influence of pavement

surface texture on rolling tire noise, independently from porosity, porous layer thickness and other material properties.

Figure 6.15 shows the noise spectra produced by a rolling slick tire on porous pavements with various surface texture levels and identical acoustical characteristics, derived for the case of 20% porosity and 50 mm thickness. It is found that, with the same porosity value and porous layer thickness, porous pavements may generate very different tire/road noise levels if different surface textures are exhibited by porous layers. The spectrum shapes differ marginally from each other, with all the maximum noise reductions happening at the same frequency (around 1600 Hz in the illustrated case). This may be a result of the similar texture spectrum shapes as shown in Figure 6.8 and the identical acoustic absorption coefficient for all surfaces. The magnitude of sound pressure levels vary significantly on different surfaces. The differences at some particular frequencies can be as high as 15 dB(A). They tend to be larger at low frequencies and smaller at very high frequencies.

Figure 6.16 compares the overall noise levels generated by a rolling slick tire on different porous pavement surfaces. The overall noise levels are derived from the sound level spectra shown in figure 6.15. It is seen that, for pavements with the same porosity and porous layer thickness, the overall noise level increases with the surface texture level. For the illustrated case (20% porosity and 50 mm porous layer thickness), the overall noise level is 91.03 dB(A) on Type I porous surface and 77.27 dB(A) on Type IV surface. The difference is 13.76 dB(A). This difference is very significant in the sense of traffic noise reduction. However, considering the need for recalibration of the proposed tire/road noise prediction model for pavements with largely different texture levels (as discussed in Section 5.4.2), the result presented may overestimate the effect of pavement surface texture on tire/road noise. Besides the texture level spectrum, the mean profile depth (MPD) of each porous pavement was also measured in the experiment. Figure 6.16 (b) shows the variation of overall noise level with MPD value. It is obvious that tire/road noise level increases with an

increase in porous surface MPD in a nonlinear manner. The overall noise level increases faster at lower MPD values.

The above observations indicate that tire/road noise on porous surfaces increases with the increase in surface texture level and mean profile depth. Pavement surface texture does not alter the noise spectrum shape much, but it determines the magnitude of noise level. Porous surface with a lower macrotexture level should be used on the purpose of tire/road noise reduction if it does not adversely affect skid resistance.

6.2.5 Influence of Vehicle Speed

Sections 6.2.2 to 6.2.4 had discussed the influence of porous pavement properties on tire/road noise emission. Besides pavement surface, vehicle also plays an important role in the generation of tire/road noise. Vehicle traveling speed may be the most crucial vehicle-related influencing factor and is investigated in this section. Vehicle speed affects noise generated through both tire vibration mechanisms and aerodynamic mechanisms. Two effects can be directly captured by the developed simulation model: changes in tire modes resulted from rotational speed variation and alterations in texture spectrum due to translational speed variation. The deformed geometry of a rolling tire also changes with vehicle speed. It has been observed in the experimental studies that tire/road noise increases when a vehicle travels at a higher speed on conventional pavements. This is expected because tire vibrates more violently at higher rotation speed and impacts with pavement surface more heavily. Besides, air pumping effect is more intense at higher speed as well. A log-linear relationship between vehicle travel speed and overall tire/road noise level had been developed on various dense-graded pavements (Sandberg and Ejsmont, 2002) (as illustrated in Section 2.2.4.1). Although the increasing trend should be maintained on porous pavement, the log-linear relationship may not be adequate with the same parameters. This section attempts to analyze this problem numerically, examining the

influence of vehicle speed on tire/road noise emitted on porous pavements. Noise levels at different vehicle speeds on various porous surfaces are estimated through numerical simulations. Results are analyzed to develop the relationship between speed and noise level on porous pavements.

The noise spectra generated by a rolling slick tire at various vehicle speeds on a porous pavement surface with a 50 mm layer thickness and 20% porosity are shown in Figure 6.17(a). It is observed that the spectrum shapes of tire/road noise at different traveling speeds are similar on the same porous pavement, but their magnitudes are quite different. All the six spectra have troughs around 1600 Hz, indicating the maximum noise reduction on the particular pavement surface resulted from its peak absorbing capacity. The spectrum of lower vehicle speed is below that of higher speed. The differences between sound pressure levels are larger at higher frequencies. The noise level difference at 350 Hz is 4.7 dB(A) when vehicle speed increases from 50 km/h to 100 km/h, while it is 13.2 dB(A) at 2500 Hz for the same speed increment. It was also observed that the increasing rate of noise spectrum magnitude is larger at lower vehicle speeds and gets smaller with an increase in speed.

Figure 6.17(b) illustrates the overall noise levels emitted from a rolling tire traveling at different speeds on an identical porous pavement surface (20% porosity and 50 mm thickness). The overall noise levels are derived from the simulated sound level spectra shown in Figure 6.17(a). It is observed from the figure that on the same porous pavement, the overall noise level increases as the vehicle speed increases. For the porous surface layer with a 50 mm thickness and 20% porosity, the overall noise level is 83.15 dB(A) at 50 km/h traveling speed and 91.66 dB(A) at 100 km/h, resulting in an increment of 8.51 dB(A). Such a difference is very significant in the perspective of traffic noise control, therefore, reducing traveling speed is an effective measure to reduce traffic noise in highly residential areas. Comparing the noise levels between each pair of adjacent speeds, it was found that the difference is significantly larger at lower speeds. This is consistent with the observation from sound level

spectra in Figure 6.17(a). The overall noise level grows 3.14 dB(A) when vehicle speed increases from 50 km/h to 60 km/h, but only 0.79 dB(A) from 90 km/h to 100 km/h.

Figure 6.18 shows the increase in overall noise levels with vehicle speed for different porous pavements with identical porous layer thickness (50 mm) but various porosity values. It is observed that overall noise level increases with vehicle speed in a similar nonlinear manner for all the tested surfaces. When vehicle speed increases from 50 km/h to 100 km/h, the overall noise level increases by 8.02 dB(A) on a porous surface with 15% porosity and 9.03 dB(A) on a surface with 25% porosity. The rate of increase is larger at lower speeds and gets smaller at higher speeds. The difference between 15% and 25% porosity is 0.74 dB(A) at 50 km/h vehicle speed and 1.75 dB(A) at 100 km/h. Influence of porosity on overall noise level is basically uniform. This is consistent with the linear increasing trend observed from Figure 6.11.

Figure 6.19 shows the variation in overall noise levels with vehicle speed on porous pavements with identical porosity value (20%) and different porous layer thicknesses. The overall noise level increases with vehicle speed in a nonlinear manner for all the tested porous surfaces. When vehicle speed increases from 50 km/h to 100 km/h, overall noise level grows 7.85 dB(A) for 25 mm porous layer thickness and 9.05 dB(A) for 100 mm case. The increasing rate of overall noise level with increasing vehicle speed is larger at lower speed. On the other hand, difference in overall noise level between different porous layer thicknesses is larger at lower speeds. The difference between 25 mm and 100 mm porous layer thicknesses is 4.74 dB(A) at 50 km/h and 3.54 dB(A) at 100 km/h. It was also observed that the influence of porous layer thickness on overall noise level is unequal. The difference between 50 mm and 75 mm thicknesses is less than that between 25 mm and 50 mm, as well as that between 75 mm and 100 mm.

The curves in Figures 6.18 and 6.19 suggest a potential log-linear relationship between tire/road noise level and vehicle speed on porous pavements. The traditional

noise-speed model as shown in Equation (2.26) seems to be valid on porous surfaces. Linear regression method is used to determine the log-linear relationship in describing the noise increase with vehicle speed on porous pavements. The regression results are shown in Table 6.3. It is seen that all the R-square values are larger than 0.95, indicating good agreements between empirical model and numerical model.

Concluded from the above observations, tire/road noise on a particular porous pavement increases with vehicle speed in a log-linear manner. The variations in vehicle speed do not significantly affect noise spectrum shape, but they have an effect on sound level magnitude. The influence of vehicle speed on tire/road noise is slightly larger on the pavement with a higher porosity and a thinner porous layer. The effect of porosity on noise reduction is more significant at higher speeds, while the influence of porous layer thickness is larger at lower speeds. In porous pavement design, speed variation on road should be taken into consideration to optimize the acoustic performance of a pavement surface.

6.3 Summary

This chapter investigated the effects of several critical influencing factors of tire/road noise on porous pavements using the developed numerical simulation model. The parametric study is defined based on hypothetical cases with surface texture levels measured on field porous pavements (Schwanen et al., 2007) and acoustical properties derived from microstructural model (Neithalath et al., 2005).

The simulation model was first adopted to study the overall effect of porous pavement layer on tire/road noise emission. This application attempted to quantify and interpret the reduction of tire/road noise achieved by employing porous surfaces, comparing with conventional dense-graded surfaces. Sound pressure level spectra and overall noise levels on the two surface types were compared. The illustrative case study proved that porous pavement is effective in reducing tire/road noise level, especially at higher frequency. The difference in the overall noise level is 6.2 dB(A)

between the examined surfaces, and the sound pressure level is the lowest on porous surface. It was also observed that the most significant noise reductions on porous pavements happen at the frequencies slightly higher than the peak of acoustic absorption coefficient. The dominant contributor to noise reduction on porous pavements was identified as the sound absorbing capacity resulted from the interconnected air voids within porous surface layers, while the smoother traveling plane resulted from negative texture orientation is a secondary component in tire/road noise abatement.

The developed numerical framework was next used to analyze the influences of crucial pavement characteristics and vehicle operating conditions on tire/road noise emission. The numerical model enables systematic study on the effects of individual factors (e.g. porous layer porosity, porous layer thickness, pavement surface texture and vehicle speed) through a hypothetical case study. Several findings were obtained from the simulations and analyses conducted in this study:

- Tire/road noise on porous pavements increases with an increase in surface layer porosity in a linear manner for the porosity range of 15% to 25%, provided identical pavement texture and porous layer thickness. The noise spectrum shapes remain similar on pavements with identical porous layer thickness but different porosity values. The influence of porosity is more obvious near the noise reduction peak. The noise reductions resulted from a specific porosity variation are similar for different porous layer thicknesses.

- Tire/road noise on porous pavements decreases with an increase in porous layer thickness in a nonlinear manner, provided identical texture and porosity. Differences in noise levels are less significant between pavements with 50 mm and 75 mm porous layers. Variations in porous layer thickness alter the shape of noise spectrum. Noise reduction peak moves towards lower frequencies with the increase in porous layer thickness. The benefits of increasing porous layer thickness are slightly more substantial for porous pavements with higher porosities.

- Tire/road noise emission on porous pavements increases with an increase in pavement surface texture level and mean profile depth when porosity and thickness are identical. The increasing trend with MPD is nonlinear. The variations in pavement surface texture marginally affect the noise spectrum shape, but significantly alter the noise level magnitude. The influence of surface texture is more obvious at lower frequencies.

- Tire/road noise on a particular porous pavement increases with vehicle speed in a log-linear manner. Speed variation hardly affects the noise spectrum shape, but it does influence the sound level magnitude. The effect of vehicle speed on tire/road noise is slightly larger on pavements with higher porosities and thinner porous layers.

Based on these findings, some recommendations could be made for porous pavement design from the standpoint of tire/road noise reduction. A lower porosity value in the normal porosity range (i.e. 15% to 25%) should be adopted in the porous surface layer to better utilize its advantages in sound absorption, provided that there is sufficient skid resistance performance and clogging resistance durability. It not only mitigates tire/road noise more effectively, but also reduces the adverse effect of increasing vehicle speed on tire/road noise emission. Thicker porous layer should also be adopted in pavement design for the same reasons if cost effectiveness is acceptable. It is crucial to maintain the negative texture orientation on porous pavement surfaces and reduce the profile level of macrotexture to further decrease tire/road noise level. Moreover, speed variations on the road should also be taken into consideration to optimize the acoustical performance of a porous pavement surface.

Table 6.1: Properties of examined pavements

Pavement	Surface type	Texture spectrum	Acoustic absorption
Case I	Asphalt surface dressing	Case I in Figure 6.2	0
Case II	Porous asphalt	Case II in Figure 6.2	Figure 6.3
Case III	Perfectly acoustic hard surface	Case I in Figure 6.2	0

Table 6.2: Pore structure parameters for mixtures with different porosity values

Porosity	Pore diameter (mm)	Aperture diameter (mm)	Pore length (mm)	Aperture length (mm)
15.0%	3.350	0.838	15.062	9.938
17.5%	3.742	0.936	15.815	9.185
20.0%	4.130	1.033	16.560	8.440
22.5%	4.505	1.126	17.280	7.720
25.0%	4.880	1.220	18.000	7.000

Table 6.3: Logarithmic linear models for speed-dependency of overall noise level on various porous pavements

Porosity	Thickness (mm)	A	B	R^2
15.0%	50	38.449	26.438	0.976
17.5%	50	37.013	27.375	0.970
20.0%	50	35.718	28.247	0.978
22.5%	50	34.425	29.111	0.981
25.0%	50	32.919	30.104	0.981
20.0%	25	41.758	25.859	0.967
20.0%	75	33.963	28.733	0.977
20.0%	100	30.079	29.906	0.978

(a) Case I: surface dressing (b) Case II: porous asphalt

Figure 6.1: Appearance of rehabilitation surface types

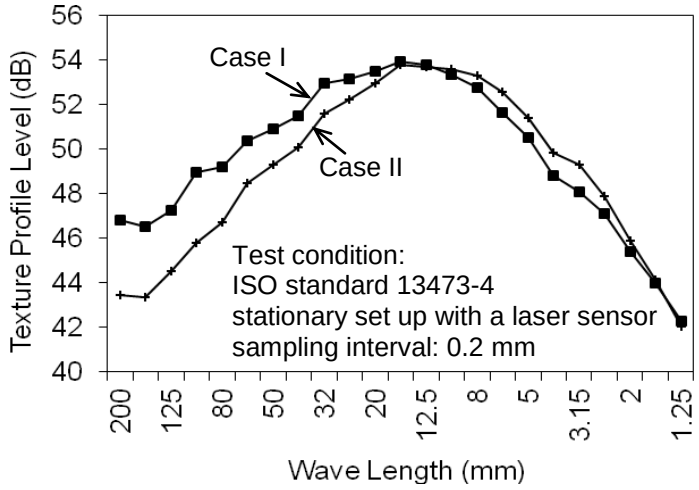

Figure 6.2: Texture spectra of rehabilitation surface types

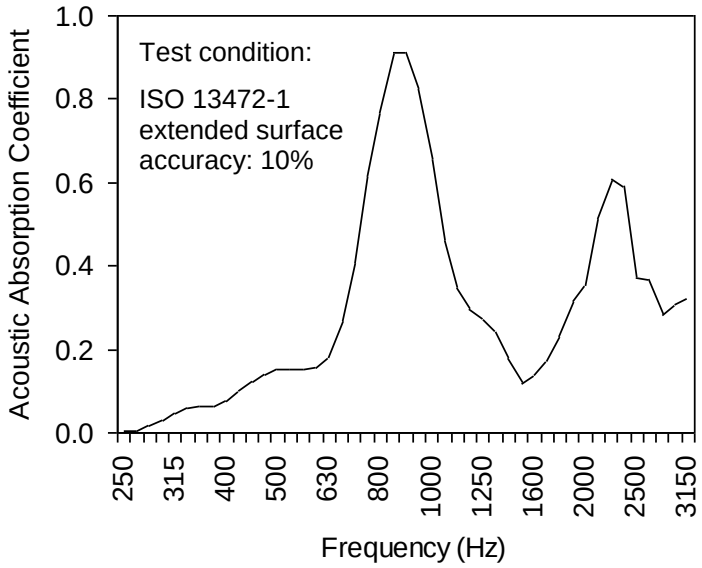

Figure 6.3: Acoustic absorption coefficient of Case II surface (porous asphalt)

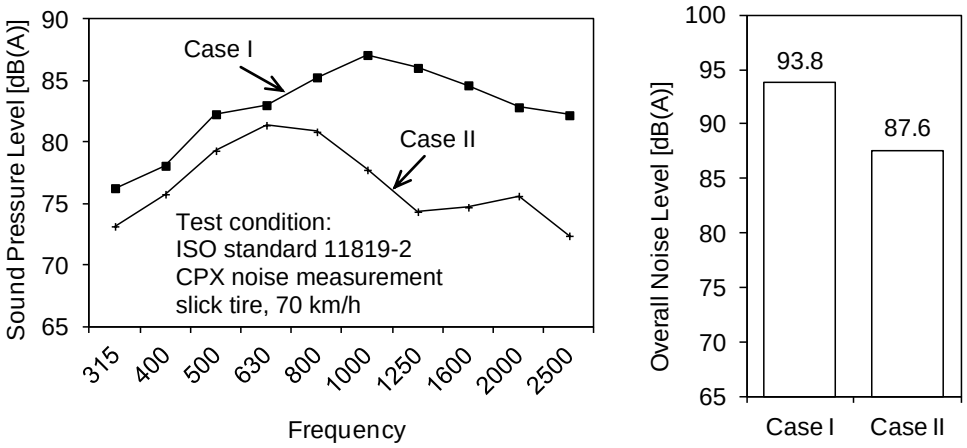

Figure 6.4: Predicted tire/road noise on Case I and Case II pavements

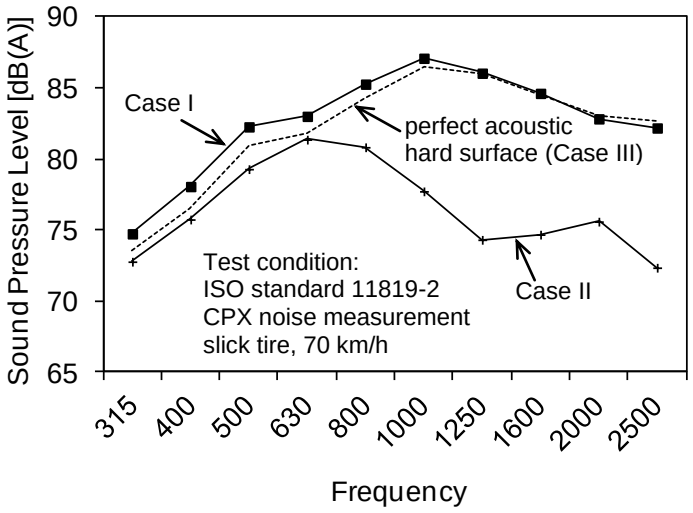

Figure 6.5: Comparison between noise spectra of various pavements

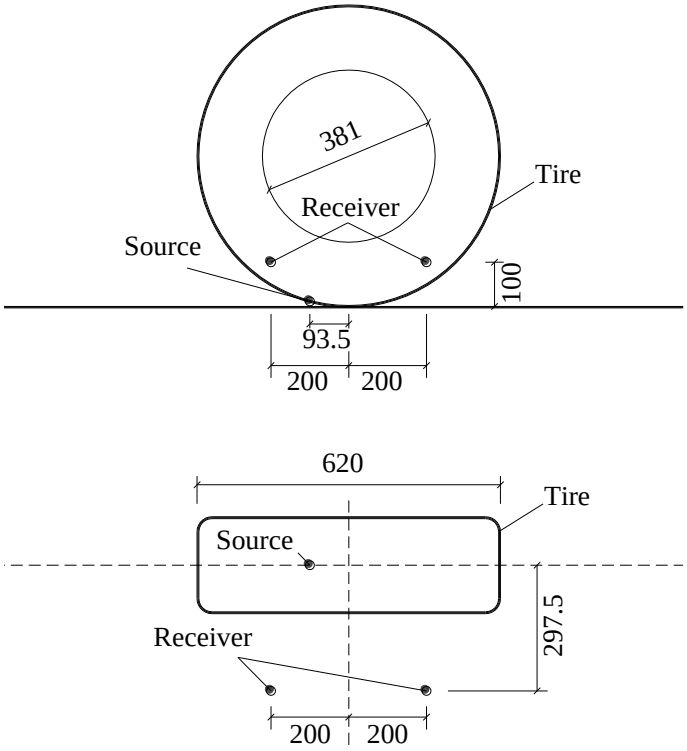

Figure 6.6: Horn effect measurement configuration

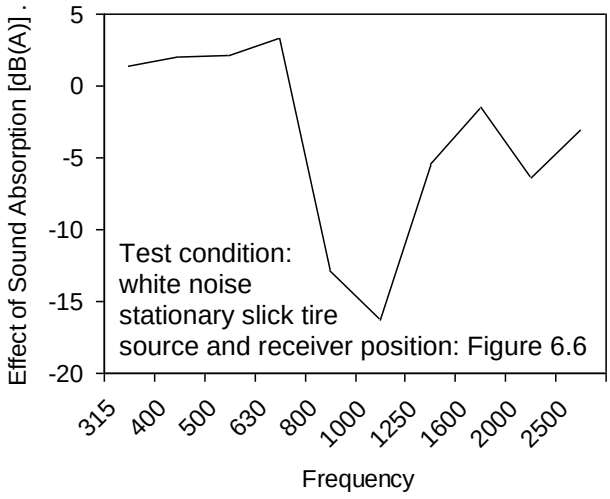

Figure 6.7: Horn effect reduction on Case II porous pavement

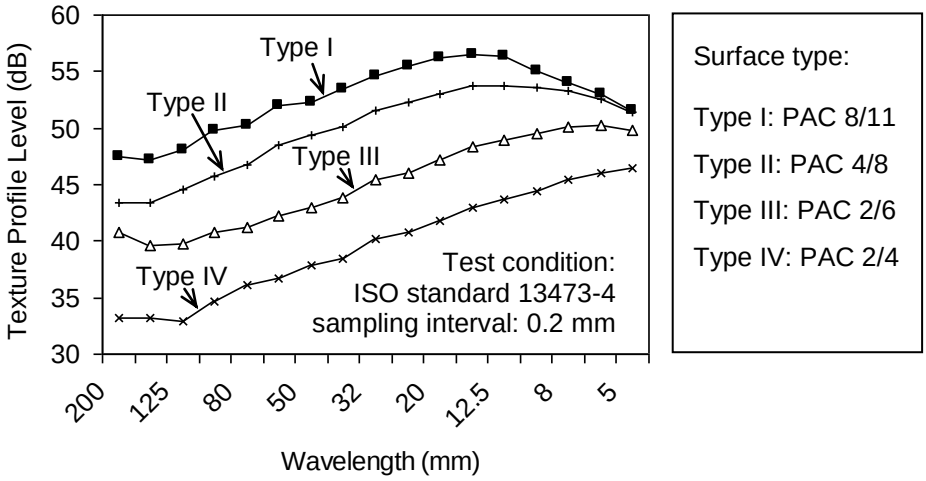

Figure 6.8: Illustration of typical surface texture profile levels on porous pavements (Schwanen et al., 2007)

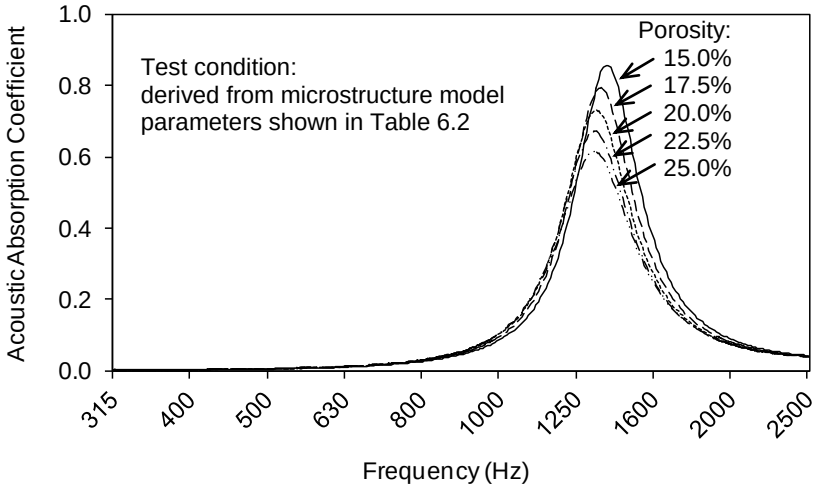

(a) 50 mm porous layer thickness

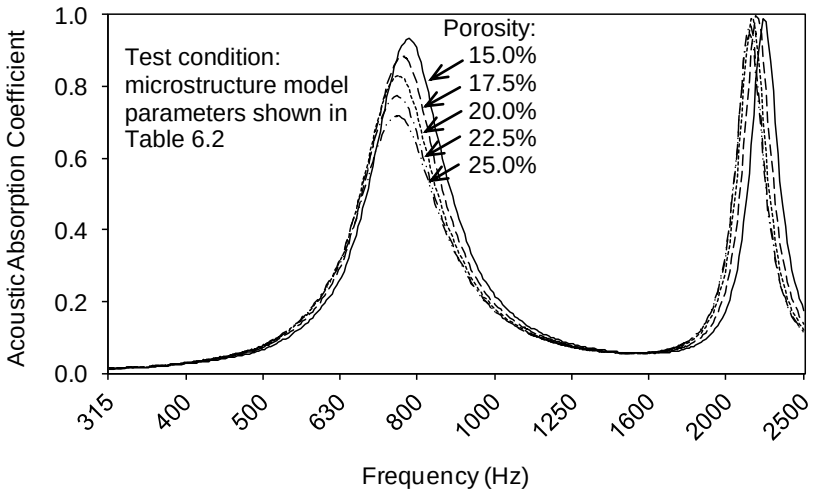

(b) 100 mm porous layer thickness

Figure 6.9: Acoustic absorption coefficient of different porous mixtures derived from microstructural model

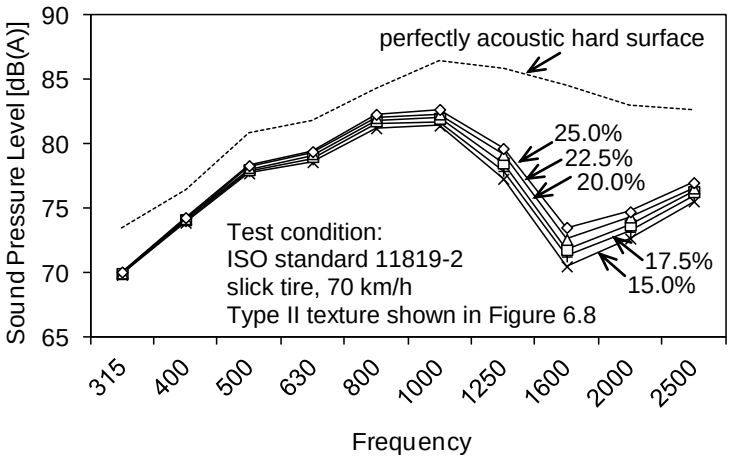

(a) 50 mm porous layer thickness

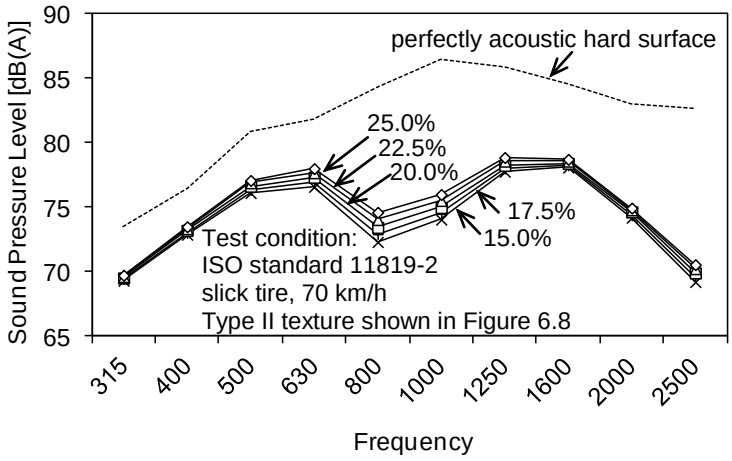

(b) 100 mm porous layer thickness

Figure 6.10: Tire/road noise spectra for porous surfaces with different porosity values

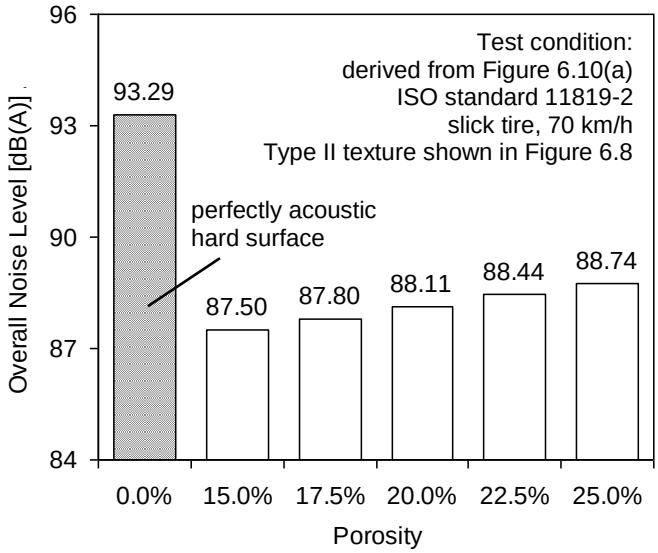

(a) 50 mm porous layer thickness

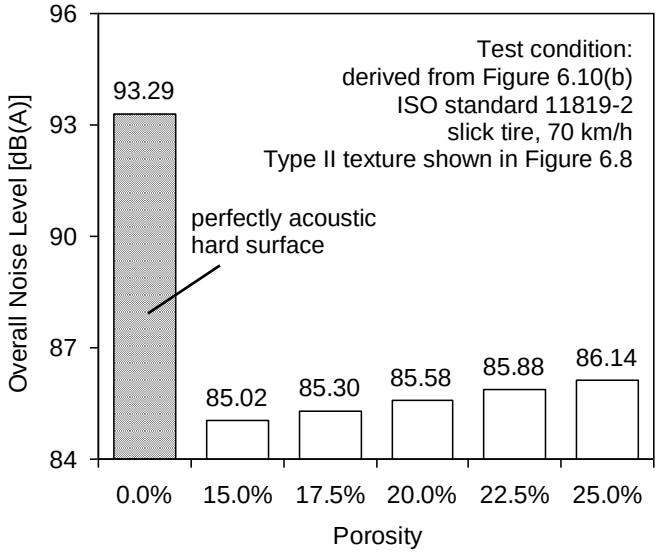

(b) 100 mm porous layer thickness

Figure 6.11: Overall tire/road noise levels for porous surfaces with different porosity values

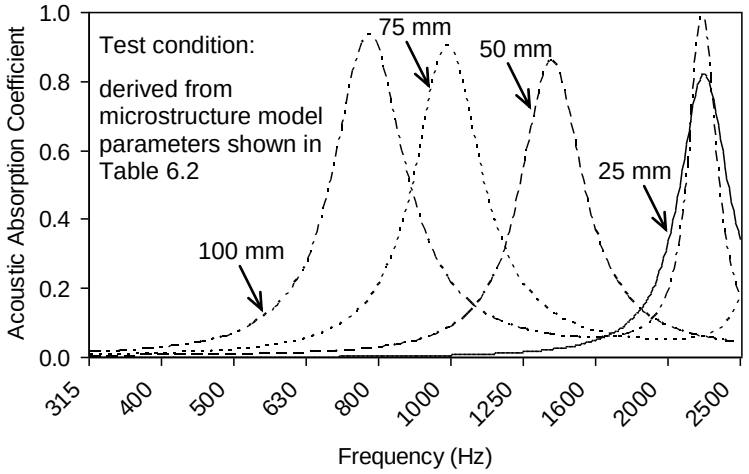

(a) 15% porosity

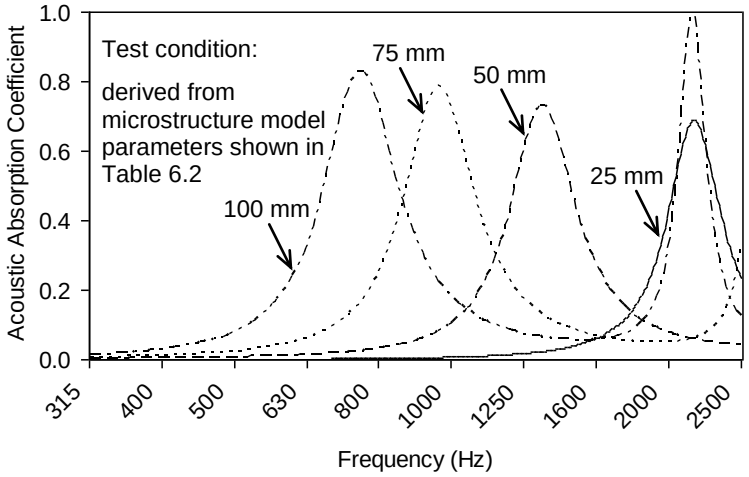

(b) 20% porosity

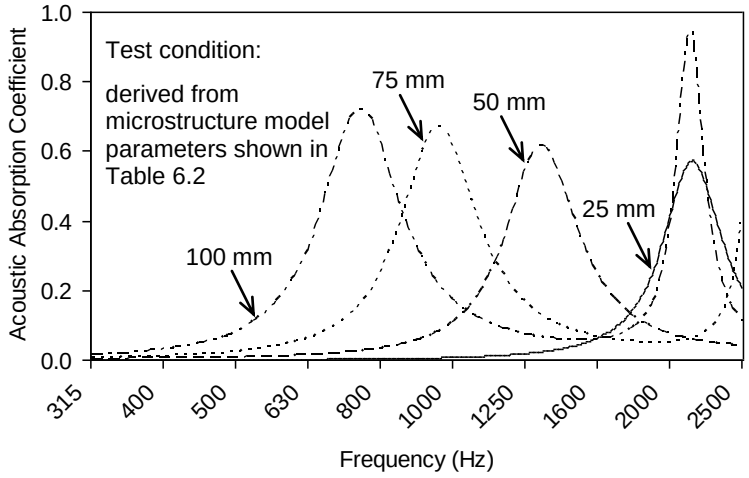

(c) 25% porosity

Figure 6.12: Acoustic absorption coefficient of different porous surfaces derived from microstructural model

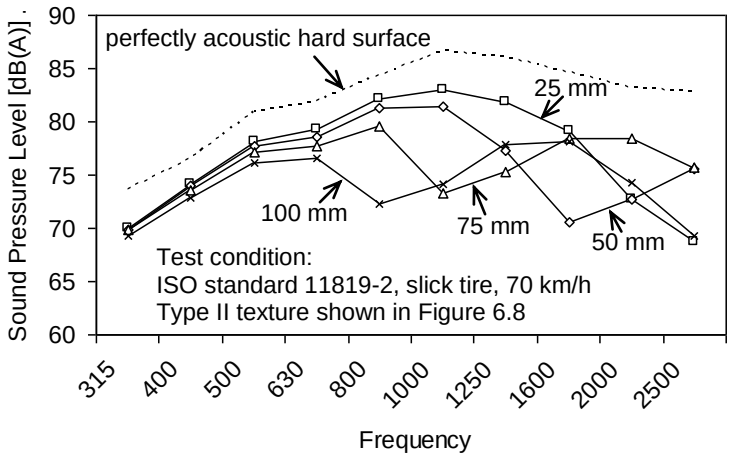

(a) 15% porosity

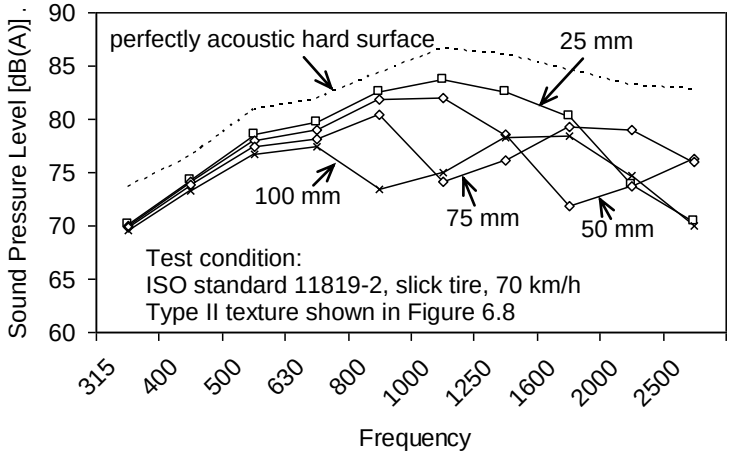

(b) 20% porosity

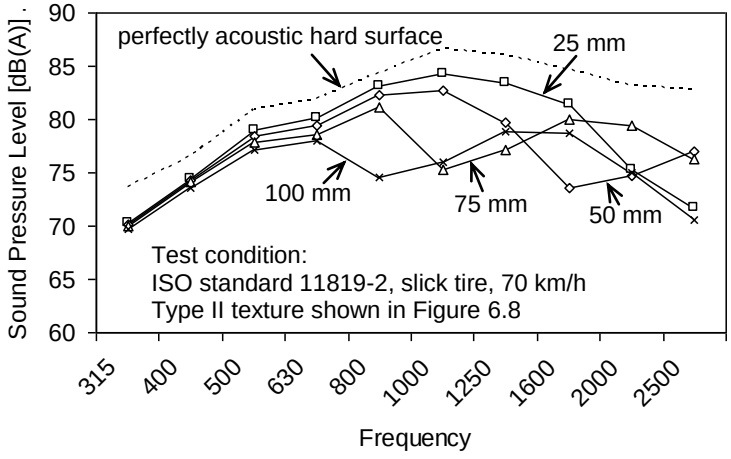

(c) 25% porosity

Figure 6.13: Tire/road noise spectra for porous pavements with different porous layer thicknesses

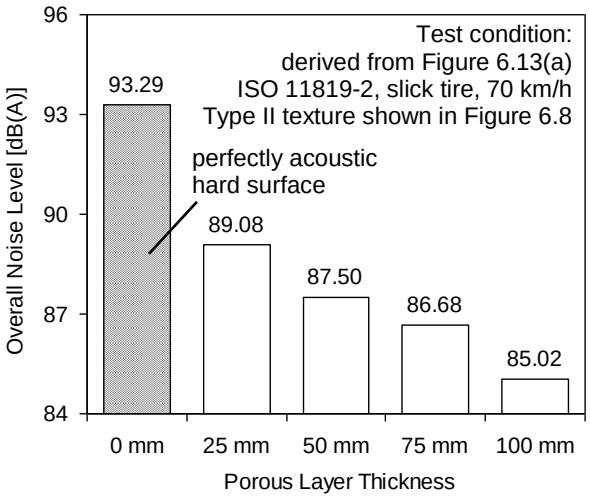

(a) 15% porosity

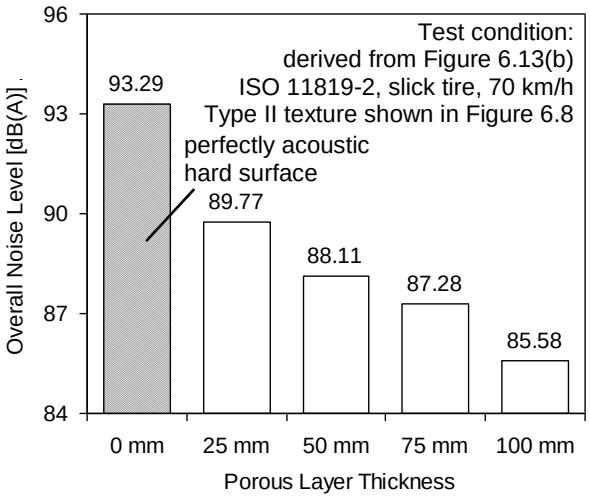

(b) 20% porosity

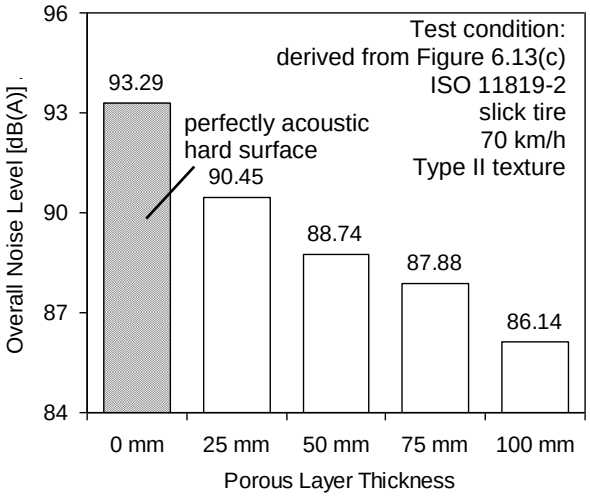

(c) 25% porosity

Figure 6.14: Overall tire/road noise levels for porous pavements with different porous layer thicknesses

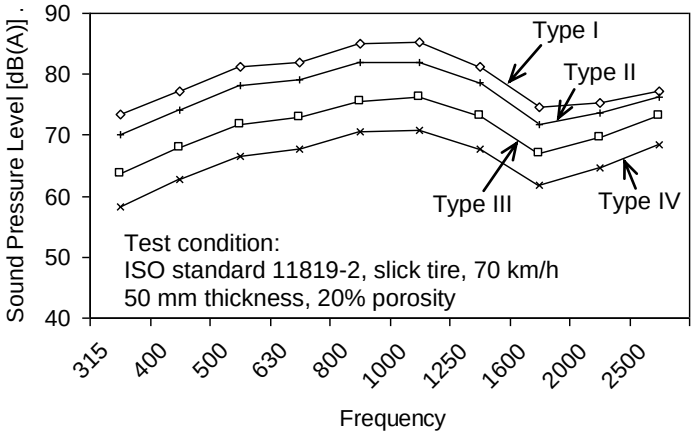

Figure 6.15: Tire/road noise spectra for porous pavements with different surface textures

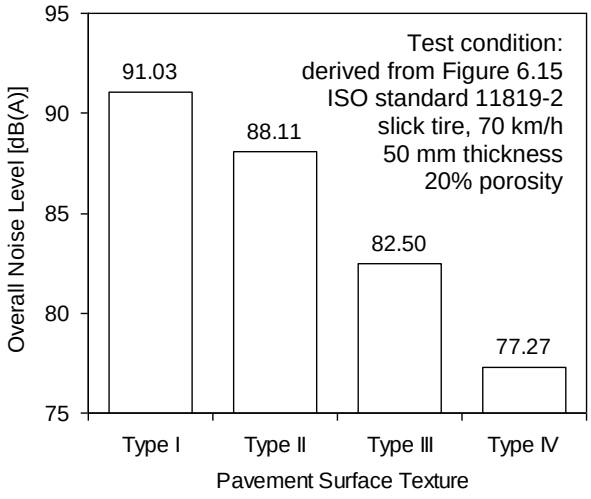

(a) overall noise level vs. texture type

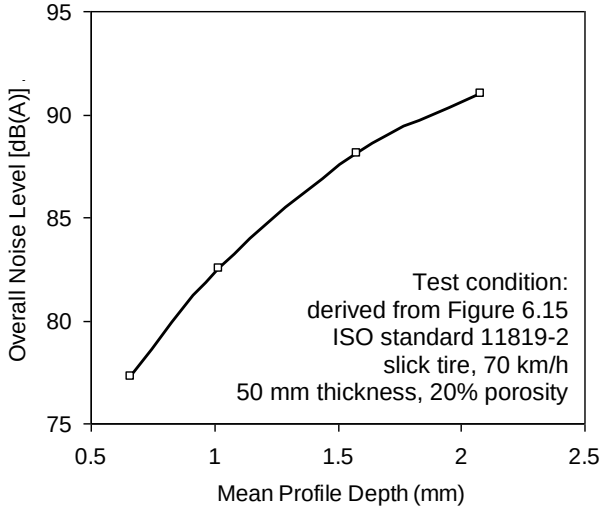

(b) overall noise level vs. mean texture depth

Figure 6.16: Overall tire/road noise levels for porous pavements with different surface textures

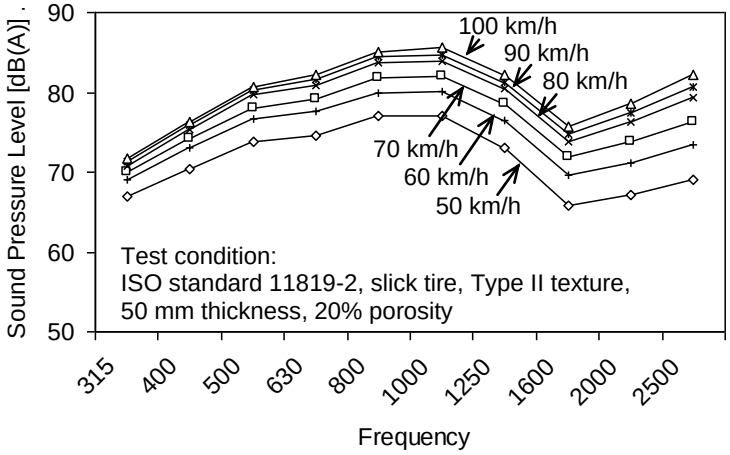

(a) sound pressure level spectrum

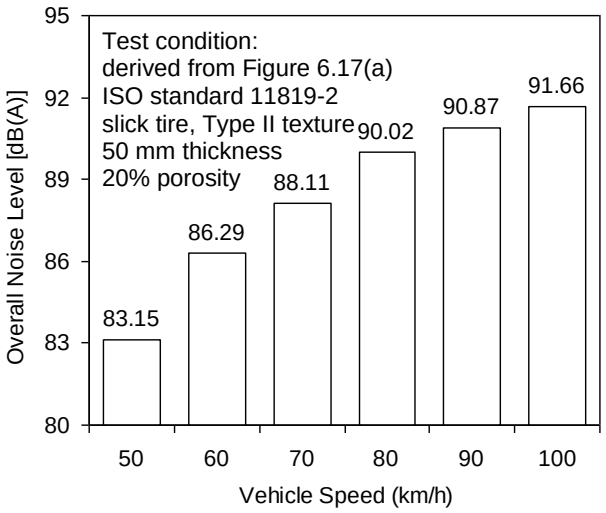

(b) overall noise level

Figure 6.17: Variation of tire/road noise with vehicle speed on a porous pavement with 50 mm porous layer thicknesses and 20% porosity

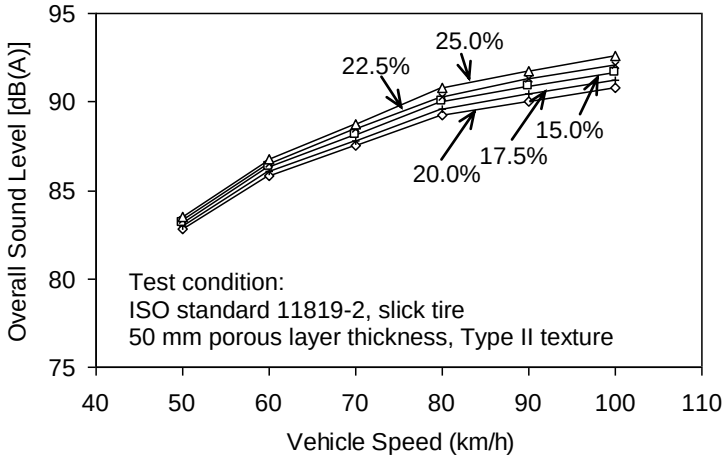

Figure 6.18: Variation of overall noise level with vehicle speed on porous pavements with different porosity values

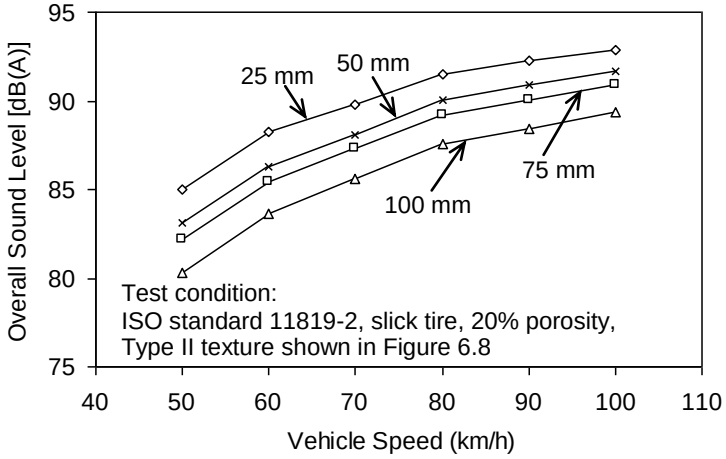

Figure 6.19: Variation of overall noise level with vehicle speed on porous pavements with different porous layer thicknesses

CHAPTER 7 INTEGRATING SKID RESISTANCE AND TIRE/ROAD NOISE PERFORMANCES INTO POROUS MIXTURE DESIGN

Although porous surface layers serve mainly the functional purposes in most applications, current porous pavement design specifications did not consider frictional and acoustical performance. Porosity is taken as the control parameter in most of the existing design methods (Mallick et al., 2000; BSI, 2005; Putman and Kline, 2012; ASTM, 2013a), while permeability is an optional criterion in some of them (Khalid and Pérez, 1996; Putman and Kline, 2012). It is presumed in the porous mixture design that functional performances should be adequate if the volumetric and composition requirements are satisfied. However, this assumption may not be true, based on findings reported by various agencies around the world (Gibbs et al., 2005; Abbott et al., 2010). This presents a challenge to porous pavement design, especially in the case where improving skid resistance or reducing tire/road noise is the major purpose of porous surface application. Therefore, it is necessary to analytically predict the frictional and acoustical performance in the design stage of porous pavement project. This chapter attempts to explore the integration of numerical evaluations of skid resistance and tire/road noise into the current porous mixture design procedures.

7.1 Overview of the Existing Porous Mixture Design Methods

Despite the fact that porous pavement technologies have evolved for more than half a century, there is still no unified design methodology accepted by different countries. Even within the same country, different agencies may use different design specifications as well. United States and Europe are the leaders in porous pavement technologies to date, although many other countries, such as Japan and Australia also developed their own standards. Representative design methods are briefly introduced in this section to understand the status of current practice and provide basis for further

progresses. The considerations in functional performance are found to be inadequate in the currently available methods.

7.1.1 United States Design Method

Porous pavement is known as open-graded friction courses (OGFC) in United States, although the porosity level of a traditional OGFC is slightly lower than that of a regular porous asphalt surface. With the adoption of modified asphalt in mix design, the new generation OGFC now possesses a similar porosity level as the porous surfaces out of United States. The first formalized design procedure in United States was developed by the Federal Highway Administration (FHWA) in 1974. There are currently more than 20 different approaches used across the United States (Putman and Kline, 2012), among which, the method developed by the National Center for Asphalt Technology (NCAT) in 2000 (Mallick et al., 2000) is the most influential and was standardized by ASTM in 2004 (ASTM, 2013a). Four major steps are considered in the porous mixture design: 1) selection of appropriate materials; 2) development of aggregate gradation; 3) determination of optimum asphalt content; and 4) evaluation of mix performance.

In mixture design, the materials that need to be selected include aggregates, asphalt binders and stabilizing additives. The requirements on aggregate quality for porous mixtures are similar to those for stone matrix asphalt (SMA) mixture. Polishing resistance and durability have been identified as the most important properties (Cooley et al., 2009). The angularity, abrasion resistance, particle shape and cleanliness are also considered. The selection of asphalt binder should be based on environment, weather and traffic at the site, as well as the expected performance of the porous surface. A wide range of asphalt binders could be used and graded in accordance with either Superpave performance grading system, viscosity grading procedure or penetration grading system. Modified asphalt cements can significantly improve porous mixture performance, so are highly recommended. The functions of

stabilizing additives used in porous mixture include reducing draindown potential, increasing mixture strength and improving durability. Cellulose fibers, mineral fibers, polymers or rubber particles may be used as additive. Fiber stabilizers are typically added into the mixture at a content of 0.2% to 0.5% of the total mixture mass. Table 7.1 summarizes the material selection criteria specified by ASTM standard (ASTM, 2013a).

The next step in porous mixture design is to develop an aggregate gradation that guarantees the desirable air void content in the total mixture and the existence of stone-on-stone contact in coarse aggregate skeleton. The porous mixture gradations may potentially be characterized by the nominal maximum aggregate size (NMAS) as defined in Superpave. Highway agencies in the United States have developed various recommended master gradations for different NMAS (most commonly 9.5, 12.5, 19 and 25 mm). Examples are shown in Table 7.2. In the design process, engineers first determine the adopted NMAS and a specified master gradation is then selected. Three trial gradations within the recommended grading range should be selected and mixed with a trial asphalt content (typically between 6.0% and 6.5%). Additive should be included if it is going to be used in the actual mixture. Specimens are then prepared using the Superpave gyratory compactor with a compaction effort of 50 gyrations. The condition of stone-on-stone contact is defined achieved when the percent voids among the coarse aggregates of compacted mixture (VCA_{mix}) is less than that of coarse aggregates obtained by the dry-rodded test (VCA_{DRC}), with coarse aggregates defined as the fraction larger than the No.4 sieve. The air void content of compacted porous mixture can be determined based on its bulk specific gravity and the theoretical maximum density measured on loose sample. Of the three trial gradations, the one with the highest air void content (minimum acceptable is generally 18%) and a VCA_{mix} equal to or less than VCA_{DRC} is considered optimum and should be adopted as the desired gradation.

Although there is no specific approach that can identify an absolute optimum asphalt binder content, methods resulting in a range of allowable binder contents have been widely developed. The procedures used in the United States can be divided into three categories: methods using compacted specimens; methods using oil absorption test; and methods based on visual observation. Compacted specimen approach is the most popular and scientific methodology which is adopted by most highway agencies. In this method, the optimum asphalt content is determined based on test results of air voids, asphalt draindown and durability. Specimens compacted with 50 gyrations are produced using the selected gradation and at least three asphalt contents in increments of 0.5%. The air voids calculated from bulk specific gravity and theoretical maximum density should be at least 18%, and higher air void contents are desirable. The asphalt draindown is tested at a temperature 15 °C higher than the anticipated production temperature and the maximum permissible draindown is 0.3% by total mixture mass. Cantabro abrasion test may be used to examine the durability of designed mixtures. The average abrasion loss on unaged specimens should not exceed 20%. For aged porous mixture, the average loss should be below 30% and the loss for any individual specimen should not exceed 50%. Laboratory permeability test is optional in this step, with a magnitude greater than 100 m/day being recommended. The optimum asphalt content could be determined based on the above requirements. If none of the designs satisfies all the criteria, the mixture needs to be further adjusted.

The last step of porous mixture design involves performance evaluation. The predominant type of performance testing to date is moisture sensitivity test using the modified indirect tensile test with five freeze/thaw cycles. The desired retained tensile strength ratio (TSR) should be at least 80%. The moisture susceptibility may also be evaluated through the boil test or a loaded-wheel tester (Cooley et al., 2009). If the mixture fails to meet the requirement of moisture susceptibility, anti-strip additives

such as hydrated lime may be used. The stiffness of porous mixture, rutting resistance and short-term raveling resistance may also be examined in the design.

7.1.2 European Design Method

Similar approaches to the above-presented U.S. design method are also used in Europe, with some diversities among countries. A major difference, comparing to the U.S. method, lies in the fact that specimens in Europe are commonly fabricated using the Marshall compactor with 50 blows on each side. The penetration grading system is more widely used in Europe instead of the PG-grade. The desired air void contents of European designs are commonly higher than that of U.S. design, such as 20% in the Netherland and Spain, 21% in Belgium, 22% in Switzerland, and 26% in Denmark (Alvarez et al. 2006). Besides, the mixture properties considered in the design, as well as the test methods and evaluation criteria are also different among European countries.

Danish road standards use asphalt draindown and volumetric composition to determine the maximum asphalt content, and consider the resistance to water damage, aging and disintegration in the selection of minimum binder content. Hamburg wheel tracking test is also employed to assess rutting resistance performance. Permeability test is not requested, but some practices and recommendations have been made by the Danish Road Institute (Alvarez et al. 2006). Porous mixture design in Belgium requires optimizing the aggregate gradation using the software PradoWin (Programs for Road Asphalt Design Optimization) (BRRC, 2009). The target air void content is obtained in this software considering the characteristics of each material. Volumetric property measurement and Cantabro test are conducted to determine the optimum binder content. The loss of mass in Cantabro test should be lower than 20%. Spain also determines the minimum asphalt content based on the Cantabro test, and the maximum binder content is selected based on air voids and draindown test. Typical binder contents are around 4.5%. The commonly adopted binder is a 60/70 or 80/100

pen asphalt with polymer modification. Besides, indirect tension test, wheel tracking test and laboratory permeability measurement are also used in Spanish porous mixture design (Khalid and Pérez, 1996).

Another type of porous mixture design methods used in Europe is the recipe approach. British standard BS 4987-1 (BSI, 2005) defines the material compositions of two kinds of porous asphalt mixtures: PA 6/20 for highways and PA 2/10 for other applications. For the 6/20 mm gradation, the asphalt grade 100/150 or 160/200 pen is recommended at a content of 3.7% or 4.5% (modified) by the mass of total mixture. The same asphalt grade is used for the 2/10 mm gradation at an optimum content of 5.2%. The modifiers listed in the standard include fibers, natural rubber and styrene butadiene rubber. It is recommended to include 2% by mass of total aggregates of hydrated lime in the mixture to minimize stripping and increase stiffness. Although hydraulic conductivity is measured in the field after placement, the permeability is not involved in the mixture design process. Recipe approach is also employed in the Netherlands, supplemented by some property tests. Two types of porous mixture have been specified, named PA 0/11 and PA 0/16, respectively. Asphalt binder is applied at a content of about 4.5% by weight of aggregates, whereas hydrated lime is also involved in the mixture. Mixture performances may be evaluated by indirect tensile strength, rotating surface abrasion, Cantabro and semi-circular bending tests as well, especially for research purposes (van der Zwan et al., 1990).

From the extensive review of existing porous mixture design methods in the U.S. and Europe, it was found that skid resistance and tire/road noise performances are not taken into consideration in porous mixture design. Attentions had been put on the moisture sensitivity and durability of porous mixture. Functional properties are commonly considered adequate if the aggregate gradation, asphalt binder content, layer thickness and compaction specifications are satisfied in the field. Permeability measurement is the only test adopted to assess the functional performance of a porous

mixture, but it is optional and conducted on the finished pavement in most design methods that involved this test. This is definitely insufficient for the prediction of frictional and acoustical performances of porous pavement. It is therefore necessary to develop an analytical framework based on numerical simulation models to more scientifically and mechanistically evaluate the functional performance. From this sense, the models developed in this research work are candidates to be integrated into the porous mixture design procedures.

7.2 Development of Analysis Framework

Recognizing the necessity of incorporating skid resistance and tire/road noise performances into the porous mixture design procedures, an analytical framework is developed in this section based on the existing design approaches and the developed numerical simulation models. It is worth noting that, at this stage of study, only the overall concept and partial specific technologies of the whole analysis framework are available. Although mechanistic models are used in performance prediction, valuation of functional benefits and determination of design criteria are still heavily subjective. Nevertheless, the approach proposed in this study could serve as an effective supplement to the current engineering practices.

7.2.1 Identification of Key Variables

It is essential to assume that the porous mixture obtained from existing design methods are adequate in structural capacity, durability and moisture sensitivity. Some critical parameters measured on such designed mixtures could be used as inputs into numerical models to forecast functional performance of finished porous pavements. To identify the critical variables inputted in the skid resistance and tire/road noise simulations is the first task in framework development. Several requirements apply to the selection of key variables. First of all, the combination of these variables should be capable to determine the drainage capacity and acoustic absorption of a porous

surface. Second, they should be controllable or measurable in laboratory. Third, key variables should be uncorrelated with each other. Furthermore, skid resistance and tire/road noise should be sensitive to the key variables.

Porosity is one of the critical variables because it is closely related to the water- and air-permeability of a porous mixture. Although no clear correlation between porosity and permeability has been found in the past experimental studies (Chuai, 1998; Liu and Cao, 2009; Kuang et al., 2011), it has been a consensus among pavement engineers that a larger porosity will result in a higher permeability. Porosity level determines how much space is occupied by connected air voids within a porous layer which could be used to discharge water and absorb sound energy. It is a basic indicator of water drainage and acoustic absorption capacity of porous pavements. Porosity can be easily measured by various volumetric approaches on laboratory-compacted specimens. It commonly varies from 15% to 25% in practice.

Porosity cannot uniquely decide the permeability of a porous surface because other volumetric parameters, such as tortuosity, connectivity, pore shape and pore size, also have significant influences. These variables are heavily correlated with each other and it is very difficult to quantify them in mixture design. However, all of these parameters are related to aggregate size, which can be strictly controlled in mixture design. It is noticed that a particular gradation is usually followed in existing design methods, but the majority of aggregates used in a porous mixture fall in a specific sieve size. In the present simulation models, only a characteristic aggregate size is needed to determine the characteristic pore size. The nominal maximum aggregate size (NMAS) could be adopted as the characteristic aggregate size in the numerical simulations. It is commonly within the sieve size range from 9.5 mm to 19 mm.

Besides the porosity and aggregate size of porous mixture, the porous layer thickness is another parameter in the determination of drainage capacity and acoustic absorption. It was demonstrated in previous chapters that an increasing porous layer

thickness can improve the drainage capacity and enhance the wet skid resistance of a porous pavement. On the other hand, the thickness of porous surface layer also affects the peak frequency of its acoustic absorption coefficient and alters the tire/road noise reduction effect significantly. Porous layer thickness is specified in pavement design, commonly within the range of 25 mm to 100 mm.

The above-discussed variables (porosity, aggregate size and porous layer thickness) are also the common parameters in both skid resistance and tire/road noise models. Friction coefficient is a key parameter in skid resistance model and texture level is the one in tire/road noise model. Although friction coefficient is related to texture level, it is impractical to capture their influences on skid resistance and tire/road noise using an identical indicator because they contribute to different mechanisms in the two phenomena. The friction coefficient depends more on pavement microtexture, while the macrotexture plays a more fundamental role in exciting tire vibration noise. Both parameters can be measured in laboratory.

7.2.2 Quantification of Safety and Comfort Benefits

In order to quantitatively evaluate the functional benefits brought forth by the application of porous surface layers, appropriate indices have to be developed to represent the advantages of porous pavements in skid resistance enhancement and tire/road noise reduction. It is difficult to employ an clear-cut benefit estimate technique, not only because studies to establish the relationships between pavement friction and travel safety is still undergoing, but also due to the difficulty in assigning a monetary value on the comfort and health effects of traffic noise (Ahammed and Tighe, 2010). The perception of noise annoyance depends not only on physical attributes, but also to a certain extent on subjective parameters and socio-culture environment (Martín et al., 2006). Therefore, a compromise has to be reached based on empirical relationships raised from past research studies and subjective estimations on the demands of each individual project.

7.2.2.1 Estimation of Safety Benefit

The benefits of skid resistance improvement may be estimated according to the potential reduction in the count and severity of wet-weather crashes. Although the relationship between surface friction and crash risk is difficult to quantify, past studies have provided some useful insights on the decreasing trend of crashes with the increase of wet-pavement friction. The road research group of the Organisation for Economic Cooperation and Development (OECD, 1984) revealed a linear crash-friction relationship with a decreasing rate of about 0.045 acc/MVM per unit increase of skid number at 40 mph (see Figure 7.1). Nonlinear relationships have also been suggested from other research studies (McLean and Foley, 1998; Wallman and Aström, 2001) (see Figure 7.2). Because many other factors contribute to crashes as well (such as road geometry, vehicle speed and traffic condition), it should not be expected to accurately predict accident frequency from skid resistance alone (Henry, 2000). In a statistical analysis of the effect of wet-pavement friction on highway safety, Ivan et al. (2012) developed crash-friction models for various roadway and operation characteristics (curve classification, grade, intersection, driveway, shoulder width, rural/urban area, and speed limit). The negative binominal regression was adopted to estimate model coefficients. Table 7.3 illustrates some typical results of exponents of consolidated SN_{40} coefficients, which indicate the multiplicative factor of crash count variation for a unit increase in SN_{40} measurement. The above research findings may be used to estimate the safety benefits obtained from skid resistance improvement, but one should be very careful to apply such empirical relationships because no consensus have been reached among the pavement engineering practitioners.

Economic appraisal is considered as a formal practice in the roadway safety management process developed by the Federal Highway Administration (FHWA, 2013). For each potential porous mixture, the installation and maintenance costs over

its service life are first computed. The annual crashes on the existing pavement is then estimated based on historical observed crash frequency. AASHTO (2010) proposed several methods for predicting roadway safety, such as the long-term average value, safety performance functions and empirical Bayes method. The estimated annual crashes on the existing surface is multiplied by the crash modification factor (CMF) obtained from past researches, based on the skid resistance improvement, to predict the annual crashes on the finished porous pavement. Crash reduction is derived from the values with and without porous layer. The estimated annual crash reduction is next converted to a monetary benefit by multiplying appropriate average crash costs. Many agencies developed their own crash costs. Table 7.4 illustrates an example, by severity level, based on an FHWA report (Council et al., 2005). The monetary benefit in a given year is converted to present value by multiplying the present value factor. With these, the estimated annual benefit can be summed and divided by the present value of treatment cost to estimate the benefit-cost ratio. The above steps should be repeated for each candidate mixture design and the extreme cases. The extreme cases are used to define the bounds of a feasible solution range and the benefit-cost ratio for each design corresponds to a value within this range.

7.2.2.2 Estimation of Noise Reduction Benefit

The valuation of tire/road noise reduction is not as straightforward as that of skid resistance improvement. The benefit of noise abatement is a more complicated problem involving people's health and comfort, environmental concern, real estate price near the roadway, as well as impact on working productivity. It is quite difficult to include all these aspects into a single analysis and it is impracticable to represent some effects in monetary values. Therefore, there is no economical model that enables the computation of overall benefit/cost for the whole society associated with noise exposure. The existing research studies on noise reduction benefit are focused

on a particular aspect and quantify the benefit using either cost of abatement, cost of illness, contingent valuation or hedonic price method (Becker and Lavee, 2003).

Cost of abatement was used as the minimal estimate of noise damage in some early studies. The benefit from a noise-reducing measure must be at least equal to the price paid for this action. This approach is a very rough estimation in the case where no better alternatives are available. It actually ignores the true value of the benefit, which is probably higher than the cost involved. For a multi-purpose measure, the benefits may be much more than just noise abatement. Cost of illness is another approach to estimate noise damage. It makes use of health expenditures to measure the economic cost associated with hearing loss caused by environmental noise. It is also quite difficult to obtain reliable results by this method because there is no specific evidence providing a correlation between hearing loss and traffic noise contribution. Contingent valuation method (CVM) is a very popular technique in transportation policy analyses, which is also widely used in the valuation of noise abatement. This method is developed based on a "willing to pay (WTP)" concept, which estimates the amount of money a representative sample of the public would like to pay to achieve a given amount of noise reduction. This is a closer estimation of the subjective value on noise abatement of each individual, but problems lie in the residents' general lack of familiarity in the "given amount of noise reduction". The WTP value varies dramatically from person to person and it is difficult to cover a sufficient sample of population with extensive socioeconomic backgrounds. Another popular technique in estimating the true value of noise reduction is the hedonic price method (HPM). The real estate price is commonly used as a proxy of the WTP for a quieter apartment in this approach, taking the assumption that the attribute vector determines the price and noise is one such attribute. The separate effect of noise reduction on the real estate price is then evaluated as the monetary benefit. HPM is more objective compared to CVM because the real estate price comes from the

market instead of individuals. The limitations of this approach lies in the assumptions of a perfect equilibrium in the housing market and the full awareness of information among participants.

Although no existing method is able to accurately valuate the overall noise abatement benefit, many useful findings have been achieved in past research works. Becker and Lavee (2003) used HPM to evaluate the benefits brought forth by a new noise standard in Israel with a linear noise depreciation sensitivity index, and found a 1.2% increase of average urban property value per 1 dB noise reduction. The increasing rate in rural areas was found to be 2.2%. Martín et al. (2006) examined the relationships between traffic noise exposure and annoyance in Spain and found a linear correlation between annoyance and the measured noise level (see Figure 7.3). The CVM was also adopted in the same study and found that 50% of the population was willing to pay 7.22 € on average per person per year to reduce noise contamination. Arsenio et al. (2006) used the stated choice model to valuate the road traffic noise. Some typical results of household monthly valuations for one unit change in noise level are illustrated in Table 7.5. The Department for Environment, Food and Rural Affairs of UK published a guideline on economic analysis of noise pollution (DEFRA, 2013). The marginal value of noise impact was estimated in this guideline to convert changes in noise exposure to monetary values, which could then be incorporated into a cost benefit analysis. Table 7.6 provides the values specified in this guide.

The noise measurements in the above studies are basically the far-field sound pressure level detected in the residential along the roadways. It is difficult to calculate this far-field noise level from the CPX near-field noise level obtained from numerical simulation model because of the variations in traffic volume, traffic composition and distance between vehicle tire and sound receivers. However, the essential concept of these studies are still applicable, considering the fact that far-field noise is a

combination of all the near-field sources after propagation. Based on the extensive review of past researches on the valuation of noise abatement benefit (Becker and Lavee, 2003; Arsenio et al., 2006; Martín et al., 2006; DEFRA, 2013), it is concluded that linear and geometric relationships are commonly found between noise variation and its worth. Regression curves were developed and the noise level associated with each feasible mixture design can be related to a benefit value on this curve.

7.2.3 Design Procedures

Recognizing the critical variables in porous pavement design and the benefit estimating techniques in pavement performance evaluation, an analysis framework is introduced to integrate wet-pavement skid resistance and tire/road noise into the design process of porous mixture.

7.2.3.1 Overall Workflow

Figure 7.4 shows the workflow of proposed framework. Existing porous mixture design approaches have specific methods (such as Los Angeles test, penetration test and Marshall test) to select materials, aggregate gradation and asphalt content to produce a durable structure with a desired porosity. Using specimens designed by such an approach, the crucial characteristics of compacted porous mixture can be measured from various laboratory experiments, among which the mixture porosity, aggregate size and porous layer thickness are selected as critical parameters in porous mixture design. These variables determine the drainage capacity and acoustic absorption of a porous pavement.

The workflow next develops in two tracks, one on skid resistance and the other on tire/road noise. The numerical simulation models developed in this study were adopted to predict the performance of each alternative mixture. A simplified pore network model was built using the critical variables to reproduce the drainage capacity of a given thickness of porous layer. The standard lock-wheel skidding test

(ASTM, 2011a) is then simulated on the simplified porous layer using a finite element model to predict the skid number at the standard condition. The predicted skid number (SN_p) is compared to the required value (SN_r) derived from design criterion on skid resistance performance. If SN_p is larger than SN_r, a skid resistance performance index (SPI) can be designated and the mixture design passes friction requirement. If not, one should adjust the aggregate gradation and/or asphalt content and redo the mixture design.

A simplified pore network structure was developed to reproduce the acoustic absorption property of the same porous surface layer. The sound pressure level in a standard CPX noise measurement (ISO, 2013) is predicted using the developed tire/road noise simulation model. The predicted sound pressure level (SPL_p) is compared to the allowable value (SPL_r) derived from the design criterion on tire/road noise. If SPL_p is lower than SPL_r, the mixture design passes the acoustic requirement and an acoustical performance index (API) could be assigned to it. When both criteria are satisfied, the particular mixture design is considered adequate in functional performance. In order to compare among multiple qualified mixtures, a functional performance index (FPI) is derived from a linear superposition of SPI and API. The weighting factors, α and β, are project-specific and heavily dependent on the experts' subjective judgments.

7.2.3.2 Design Criteria on Skid Number and Sound Pressure Level

It is important to understand that there is no identical design criterion which is universally applicable to all porous pavement projects. The terminal skid number and noise level (values at the end of pavement service life or the time of rehabilitation) should be determined according to project location, road classification, design speed, traffic composition, terrain topography and meteorological condition. The design criteria on functional performance (initial values at the beginning of pavement service

life) can then be derived from the terminal requirements, taking account of various long-term effects.

Minimum Skid Number Requirement

Although the lock-wheel skid number is considered as an important indicator of wet-weather traveling safety on high-speed road facilities, transportation agencies in the U.S. have never developed standards for minimum skid resistance requirement (Ahammed and Tighe, 2010). This is not unexpected because it is difficult to set a unique minimum skid number for the huge and complex road network. However, some tentative guidelines and recommendations have been made for desired skid number by various organizations and researchers. Jayawickrama et al. (1996) surveyed 48 states on the practices of skid resistance control and suggested that the minimum skid number measured by ASTM E274 skid trailer should be 30 for low volume roadways and 35 to 38 for high volume roadways. The Transportation Association of Canada (TAC, 1997) applied a grading system to identify the low-friction sections and initiate possible countermeasures. Improvement or maintenance is recommended if SN is less than 31 and there is an accident problem; maintain the surveillance and take corrective action if SN is between 31 and 40; and no action is required if SN is larger than 40. Britain makes a more comprehensive requirement for the desired minimum friction levels based on roadway category, geometric condition, pavement gradient and approaches. The investigatory level of the SCRIM friction coefficient ranges from 0.35 at 50 km/h for a motorway to 0.60 at 20 km/h for a sharp bend (Gargett, 1990).

The specified minimum friction level can be used as terminal skid resistance requirement. If the measurement follows ASTM E274 standard, the result obtained is named terminal SN. It is well understood that skid number declines with pavement age, mainly due to the polishing and abrasive effects of accumulative traffic loading. This long-term depreciation may become more severe on a porous pavement surface

because the clogging of pore network will significantly reduce its drainage capacity. Kowalski et al. (2009) observed the frictional performance of a porous friction course (PFC) section in a four year's period. The skid number variation was found around 9 SN units during this period. Rezaei et al. (2011) developed an empirical model to predict the skid number variation with traffic load on asphalt pavements. It was found that the skid number dropped faster at the early life and became stable after a certain amount of traffic loading. The overall skid number lost for PFC surface was about 20 SN units in its whole life. Besides of pavement aging, seasonal effects influence the long-term variation of skid number as well. Temperature and precipitation are the main reasons to the seasonal fluctuation. It was known that skid number decreases with increased temperature and its value is higher when measured after rain (Moyer, 1959; Saito and Henry, 1983). Given an appropriate estimation of the long-term effects caused by pavement aging and seasonal influence, the skid resistance criterion for a newly-paved porous surface can be derived from the terminal SN requirement.

Maximum Noise Level Requirement

There is no specification or guideline on acceptable maximum noise level available to date from pavement engineering perspective, but the guidance on traffic noise at highway neighborhoods has been developed by environmental agencies (Ahammed and Tighe, 2010). In a Federal Highway Administration technical advisory (Gee, 2005), tire/road noise are recommended to be taken into consideration when selecting pavement surface types for highways and bridges. Despite the lack of official guidelines, several research studies have explored the desirable pavement acoustical performance. Kuemmel et al. (2000) indicated that an appropriate surface should exhibit a maximum noise level of 83 dB(A) in a pass-by measurement at 97 km/h. Rasmussen et al. (2008) suggested a target sound intensity level for PCC pavement surfaces between 100 and 105 dB(A) in the on-board sound intensity measurement at 97 km/h. It is noticed that the acoustical performance of different

types of pavement significantly differ from each other and the recommendations are not applicable for all locations. Therefore, the acoustic requirement of a pavement should be developed individually according to public perception and noise abatement criteria. The distance to nearby neighborhood should also be considered to connect public perception with close proximity noise level.

The acceptable maximum noise level can be used as the terminal acoustical requirement. If measured with the CPX method, the result is denoted as terminal SPL. To determine the acceptable level for a newly constructed or rehabilitated porous pavement, the deterioration of its acoustical performance with time should be taken into account. This mainly results from the clogging of pore network, which reduces the sound absorption capacity of porous surface layer and increases the air pumping effect. The Danish Road Institute measured tire/road noise on porous pavements for 7 years (Raaberg et al., 2011). The noise level variation in this period was 5 to 6 dB(A). The temperature effect on tire/road noise should also be considered in the derivation of design criterion. Bueno et al. (2011) reported that increasing pavement temperature lead to a reduction in the CPX noise level assessed at a rate of 0.06 dB(A)/°C at a 50 km/h vehicle speed. Mechanisms associated with both vibration and friction may be affected by temperature variation. Traffic composition is another factor taken into account, recognizing the fact that heavier vehicles are commonly noisier than lighter ones. With proper estimations on long-term effect, temperature influence and traffic composition, the acceptable maximum CPX noise level for a new porous surface can be derived from the terminal SPL.

7.2.3.3 Determination of SPI, API and FPI

The determinations of skid resistance performance index (SPI), acoustical performance index (API) and functional performance index (FPI) are subjective in nature. It heavily relies on the practitioners' experiences and knowledge. All the three indices are defined on a scale from 0 to 10, with 0 indicating the lower bound of the

acceptable pavement performance range and 10 indicating its upper bound. If cost is not a constraint in porous mixture design, the indices can be directly defined on the absolute values of skid number and noise level. However, this is not the case in most porous pavement applications. The cost-benefit analysis is commonly adopted when cost constraint is taken into consideration. In this study, SPI and API are determined using the benefit valuation techniques previously presented in Section 7.2.2, and the FPI is derived by a linear superposition of SPI and API.

The benefit-cost ratio of a porous mixture with regards to its skid resistance performance can be estimated using the procedures illustrated in Section 7.2.2.1. The boundary values of SPI (i.e. 0 and 10) are defined by the lowest and highest ratios calculated from the extreme cases selected from extensive combinations of feasible values of design variables (i.e. porosity, aggregate size and porous layer thickness). Recognizing that the extreme cases may not occur at the boundary of feasible range of design variables, advanced techniques are needed to detect the highest and lowest benefit-cost ratios from a limited number of numerical simulations. Artificial neural network (ANN) is a promising alternative for this purpose and will be adopted in this study. When the extreme cases are determined, each of the possible mixture designs should have a benefit-cost ratio within the feasible range formed by the highest and lowest ratios, which in turn corresponds to an integer SPI value between 0 and 10. The subjective part of SPI derivation comes into the picture at this point. That is how to define the relationship between benefit-cost ratio and SPI index. It depends on the strength of cost constrain, the preference of individual project and the dispersion of candidate benefit-cost ratios. The determination of correspondence between benefit-cost ratio and SPI value relies on engineers' experience and agencies' policy.

To avoid double counting the cost in mixture comparison, the determination of API is directly based on the simulated tire/road noise level instead of performing a benefit-cost analysis. The boundaries of API are defined by the lowest and highest

noise levels obtained from the extreme cases. Due to the monotonous relationships between tire/road noise level and the value of design parameters, the extreme cases must occur on the boundaries of feasible design range. Each design parameter has a lowest feasible value and a highest feasible value, therefore, there are altogether 8 (2 × 2 × 2) cases available as candidates of extreme cases. After deciding the extreme cases, each alternative mixture design should present a tire\road noise level within the feasible range formed by the highest and lowest levels, corresponding to an integer API value between 0 and 10. Section 7.2.2.2 showed that either a linear or geometric relationship can be assumed between noise abatement and its benefit. The simulated noise levels of two extreme cases are used to determine the parameters in the assumed relationship. The API value for each candidate mixture design is read from the resulted curve according to the simulated noise level.

FPI denotes a combined functional performance index covering both safety and noise considerations. It is a linear superposition of SPI and API with weighting factors α and β, respectively (see Figure 7.4). Factors α and β represent the relative importance of frictional and acoustical performances in the assessment of overall functional performance, and their summation should be a unit. The values of α and β are project-specific and determined based on experts' judgments, at this stage of study, according to the purposes of a particular porous surface application. The FPI value is calculated for each candidate mixture design (i.e. mixtures satisfying both criteria in skid resistance and tire/road noise). After comparison, the mixture with the highest FPI value should be selected as the final design.

7.2.3.4 Improving Design Efficiency through Artificial Neural Network

The analysis framework presented in the above section provide the possibility to incorporate skid resistance and tire/road noise performances of a finished pavement into porous mixture design. The core components of this framework is the numerical simulation models presented in this study (circled by a dash box in Figure 7.4), which

are used to predict the lock-wheel skid number and CPX noise level from the mixture design parameters. However, such numerical simulations may turn out to be a tedious work when there is a large number of candidate mixtures available. Furthermore, it is difficult to extensively examine all the possible combinations of design parameters in the determination of extreme cases when the benefits of porous surfaces are valuated and the performance indices are mapped. Therefore, it is necessary to facilitate the integration of functional performance in the porous mixture design through advanced mathematical techniques based on a limited number of simulation results in advance. Artificial neural network (ANN) is a well-developed technique being used in highly nonlinear fitting without the need of recognizing regression function. It is adopted in this study to develop a fast estimation of the functional performance prediction from a number of numerical simulation results. A two-layer feed-forward neural network is used because of its simplicity in topology and ease in application.

The feed-forward neural network is characterized by its single-directional information flow: from the input nodes, through the hidden nodes and to the output nodes, with no directed cycles in the connections. The architecture of the two-layer feed-forward network adopted in this study is shown in Figure 7.5, where a nonlinear hidden layer and a linear output layer work together to make predictions from the input data. The essence of this neural network is to perform space conversion on all the input vectors through a set of nonlinear activation functions in the hidden layer. After conversion, linear weights are applied onto the nodes of hidden layer and the final outputs of the network are presented as a linear combination of the activation functions of inputs and neuron parameters:

$$\varphi(\vec{x}) = \sum_{i=1}^{N} w_i f(\vec{x}) \tag{7.1}$$

where N is the number of neurons in the hidden layer, $\vec{x}$ is the input vector, $f(\ )$ is the activation function applied on the hidden nodes and w_i is the weight of neuron i in the

linear output layer. The universal approximation theorem (Cybenko, 1989) states that a feed-forward neural network with a single hidden layer containing a finite number of neurons is able to arbitrarily closely approximate any continuous functions on the compact subsets of $\mathbf{R}^n$. This holds only for restricted classes of activation functions. In this application, the network applies a sigmoid function as the activation function:

$$f(\vec{x}) = \frac{1}{1+e^{-a_i(\vec{x}-\vec{c}_i)}} \tag{7.2}$$

The model parameters a_i, $\vec{c}_i$ and w_i are calibrated through minimizing the differences between network outputs and observed data, which is named "training" in the ANN techniques. Multi-layer networks are commonly trained using the back-propagation (BP) strategy, where the output values are compared with the "correct answers" to calculate the value of a predefined error-function. The error is then fed back to the network. Using this information, the training algorithm adjusts the weights of each connection, backwardly from the output layer to the hidden layer, in order to reduce the value of error function. After repeating the training process for sufficient cycles, the network usually converges to a state with a small error. The network used in this study is trained by the Levenberg-Marquardt algorithm, also known as the damped least squares method. This method interpolates between the Gauss-Newton algorithm and gradient descent method. It is recommended as a faster BP algorithm, although it does require more computer memory. After proper training, the network can be used to perform function interpolation, approximation or classification.

A BP neural network is established in this study to efficiently extract highly accurate performance predictions for porous mixtures with arbitrary feasible design parameter values based on a number of numerical simulation results. The input vector has three elements, representing porosity, aggregate size and porous layer thickness, respectively. The outputs contain fluid uplift force, fluid drag force and tire/road noise reduction. The training data are prepared based on the normal practicable range

of each design parameter. Porous mixtures with five porosity levels (15.0, 17.5, 20.0, 22.5 and 25%), four nominal aggregate size levels (9.5, 12.5, 16.0 and 19 mm) and four porous layer thickness levels (25, 50, 75 and 100 mm) are selected to train the neural network. The target fluid uplift force and drag force developed in a standard lock-wheel skidding test are generated using the skid resistance simulation model for each mixture, and target noise reduction is derived from the tire/road noise simulation model with a typical mild texture excitation. The skid number is not taken as a direct output of the neutral network because it can be easily derived from the fluid forces providing the coefficient of friction. The overall noise level is not suitable to serve as a neural network output because it subjects to the pavement surface texture, which may make the network too complicated when being included into the ANN model inputs. The finalized overall tire/road noise level is computed in such a manner that the noise reduction value generated from the neural network is deducted from the simulated overall noise level on a pseudo pavement with the same surface texture as the designed porous mixture, but no acoustic absorbing capacity.

The neural network is first trained using 70% out of the 80 ($5 \times 4 \times 4$) sets of data and then validated against another 15% randomly-sampled mixture designs and tested by the remaining 15%. Over-fitting is a major problem that may occur during ANN training, where the error on training set is very small, but that on new data set is large. If the number of parameters in the network is much smaller than the number of data in training set, over-fitting is unlikely to occur. However, the size of training set in the current study is relatively small. Therefore, to limit the power of network, the number of nodes in hidden layer should be just enough to provide an adequate fit. The technique of early stopping is also adopted to improve the generalization of the network. Figure 7.6 shows the performance of the developed network. Figure 7.7 to 7.9 illustrate some derived results from this network. This network can be next used in the porous mixture design to replace the elements circled by the dash box in Figure

7.4. It significantly improves the efficiency of performance evaluations. The sample size of training data used in this study is restricted by computational capacity and time constraints in the numerical simulations of skid resistance and tire/road noise. The network quality can be further improved when more training cases are available.

7.3 Application of the Proposed Analysis Framework

The above developed analysis framework is next further elaborated through a hypothetical case study. The assumptions and problem definition are first presented. The mixture design procedures introduced in the previous section are then performed to incorporate functional performance into the porous mixture selection process. The resulting mixture design is considered to be the optimum solution.

7.3.1 Description of the Hypothetical Problem

An in-service highway section is suffering from two problems: high accident-tendency caused by insufficient wet skid resistance and over-irritating traffic noise emitted from high-speed vehicles. A porous surface layer is to be installed in the rehabilitation of this highway section in order to solve both problems. The following information is made available at the time of mixture design.

- The design rainfall intensity is 100 mm/h. Considering road geometry and drainage capacity, the critical water film thickness for safety evaluation is computed to be 1.2 mm.
- The temperature variation in a year is from 5 °C (in winter) to 35 °C (in summer) at the project location.
- The design speed for road geometry is 90 km/h. This is also applicable in the frictional and acoustical performance design.
- The design service life is 10 years, within which regular maintenance will be performed to prevent porous surface failure from clogging.

- According to the local pavement agency's recommendation, the terminal skid number acting on a worn tire at the design speed should be at least 31.
- According to the environmental agency's requirement, the average noise level in the nearby residential should be lower than 65 dB(A). This can be converted to a 97 dB(A) CPX noise level at the design speed, taking into account the traffic composition on roadway and the distance from roadway to residence.
- The linear crash-friction relationship proposed by the Organization for Economic Cooperation and Development (OECD, 1984) is adopted in this case study, with a decreasing rate of 0.045 acc/mvm per unit increase in skid number. Geometric relationship is assumed between noise level variation and its quantified worth. The relative importance of frictional and acoustical performances is set to be 0.6 : 0.4.
- Six mixture designs with variations in nominal max aggregate size and porosity value (see Table 7.7) are produced in the laboratory. All these mixtures satisfy the requirements in structural strength, drainage capacity, moisture susceptibility and durability. Two levels of porous layer thickness is under consideration, namely 40 mm and 60 mm.
- Only the material cost is taken into consideration. The other costs are assumed identical for all the candidate mixtures. The cost of material does not only differ with thickness, but also increases with porosity due to high-viscosity asphalt or additives used. The relative cost ratio for each mixture is shown in Table 7.7.

7.3.2 Framework Application

The developed analysis framework is next performed step by step on the illustrative hypothetical case study. The derivation follows the workflow shown in Figure 7.4, and the artificial neural network technology is applied to facilitate the performance prediction.

Step 1: Design Criterion Determination

The most unfavorable skid number occurs on a smooth tire traveling on the flooded pavement (with a 1.2 mm water film) at the design speed (i.e. 90 km/h). This value on an old pavement after 10 years of service is required to be 31. The numerical simulation could be directly conducted at this most-unfavorable condition, but for the generalization of the approach, simulations are performed according to the standard condition specified in ASTM E274 (ASTM, 2011a) at 80 km/h. Therefore, speed and water thickness corrections should be made on the terminal SN. This can be achieved through a parametric analysis as in Chapter 4. Although the corrections may not be identical for every mixtures, to unify the standard, the worst case values are used here. The speed correction in the specific condition is -1.0 SN units from 90 to 80 km/h, and that for water film thickness is 1.8 from 1.2 to 0.5 mm. The deterioration of skid number with pavement age is assumed to be 15 SN units within its first 10 years' life according to Rezaei et al.'s model (2011), and the seasonal fluctuation of skid number in the project area is taken as 4.2 SN units. Combining the terminal SN value with the long-term effects, the design criterion on skid number is determined as

$$SN_r = 31 - 1.0 + 1.8 + 15 + 4.2 = 51 \tag{7.3}$$

The acceptable maximum tire/road noise should be corrected by the vehicle speed as well. This can be achieved through a parametric analysis similar with that in Chapter 6. Again, the worst case is adopted in this study. The speed correction for the given condition is found to be -1.0 dB(A) from 90 to 80 km/h. The increase of CFX noise level with pavement age is assumed to be 8 dB(A) in the first 10 years' service life, and the seasonal effect on tire/road noise due to temperature variation is derived to be -0.9 dB(A) based on Bueno et al.'s work (2011) . Combining the terminal CFX sound pressure level with the long-term effects, the design criterion on tire/road noise is determined as

$$SPL_r = 97 - 1.0 - 8 - 0.9 = 87.1 \text{ dB(A)} \tag{7.4}$$

Step 2: Functional Performance Prediction

An artificial neural network was developed based on numerical simulation results to enhance the efficiency of performance predictions. The network training data cover the whole variation ranges of design parameters used in this case study. It is considered adequately accurate to generate fluid forces and noise reductions from this network. Tables 7.8 and 7.9 show the predictions of functional performance, with the wet-pavement friction coefficients measured in the laboratory on compacted specimens of each mixture design. The "generated noise" in Table 7.9 is obtained from the tire/road noise simulation performed on an ideal surface with the texture of examined porous specimen but without any acoustic absorption ability. It is observed that the predicted skid number for Mixtures A-40 and F-40 is lower than the design criterion (SN = 51) and the predicted noise level for Mixtures B-40, D-40 and F-40 is higher than the 87.1 dB(A) noise criterion. Therefore, these four mixtures do not satisfy the functional requirements and should be removed from the candidates. The extreme cases within the practicable ranges are also extracted from the ANN technique. The upper and lower bounds of tire/road noise can be directly obtained from the network outputs, while those for safety benefit should account for material cost difference, which is a best estimation from the information available.

Step 3: Functional Performance Valuation

The approach of safety benefit quantification was presented in Section 7.2.2.1. The lowest skid number obtained from the neural network is adopted as the baseline of safety valuation. The differences between predicted skid number and the baseline are used to calculate the potential accident reduction for each mixture design, taking the decreasing rate of 0.045 acc/mvm per unit increase in skid number. The variation of skid number with pavement age is assumed the same for all the mixtures, therefore, the SN differences maintain identical with time. The reduction in monetary loss is proportional to the reduction in accident count. The coefficient is taken as L, which could be derived based on the proportions of accidents with various severities. The

present value of monetary benefit is derived with the present value factor at a given interest rate *r*. It is then divided by the material cost to estimate the benefit-cost ratio:

$$B/C = \frac{AR \cdot L \cdot \left[\frac{(1+r)^{10}-1}{r(1+r)^{10}}\right]}{Cost} = \frac{AR}{Cost} \cdot Z \tag{7.5}$$

where *AR* is the accident reduction per million of vehicle-mile. Z is a constant for various mixtures, provided constant *L* and r. Therefore, the benefit-cost ratio could be presented by accident reduction rate and the relative cost. The same procedures are also performed on the extreme cases of mixtures with regards to safety benefits. The calculation results are shown in Table 7.10.

The quantification of acoustic benefit was introduced in Section 7.2.2.2. Since there is no reliable approach available to date in the valuation of overall benefit of tire/road noise reduction, simple relationships observed in previous studies may be adopted in practice. Geometric growth is assumed in this study to describe the relationship between tire/road noise reduction and its value. The parameters in this relationship can be defined by the extreme noise levels.

Step 4: Performance Index Calculation

Skid resistance performance index (SPI) is defined on a linear scale of 0 to 10, with the extreme cases serving as upper and lower bounds. Acoustical performance index (API) is defined on a geometric scale with the same range. The values of these two indices are listed in Table 7.11. The indices for each candidate mixture design are then easily read from the table based on its safety benefit-cost ratio or tire/road noise level. The functional performance index (FPI) is then derived by linear superposition of SPI and API, letting the weighting factor α and β take the values of 0.6 and 0.4, respectively. The performance indices of each mixture are shown in Table 7.12.

Step 5: Optimal Design Selection

Comparing FPI among candidate mixture designs, it is obvious that Mixture E-40 possesses the highest FPI value. Therefore, in this particular project, Mixture E-

40 (produced from 12.5 mm aggregates with a 24.4% porosity and 40 mm porous layer thickness) should be selected as the final design considering the optimization of functional performance.

7.4 Summary

This chapter developed an analytical framework to integrate the evaluations of functional performance into porous mixture design process, based on the simulated skid number and noise level from the numerical models. This analysis approach is a powerful supplement to the current porous mixture design procedures, where functional performance is not properly taken into consideration. Although the proposed analysis framework, to some extent, contains subjective judgments and uncertainties, it provides an effective and convenient technical strategy to select porous mixture according to its functional performance. This approach should be helpful in the practical applications of porous pavements.

The existing porous mixture design approaches were firstly reviewed in this chapter. Emphasis was focused on the methods used in the U.S. and Europe, because they are the current leaders in porous pavement technique. It was concluded that, in the existing design procedures, emphasis is mainly made on durability and moisture sensitivity of porous mixture. The functional performance is normally considered adequate if the porosity criterion is satisfied. Permeability measurement on finished pavement surface is optional in some specifications, where it serves as the only test evaluating porous mixture functions. Existing mixture design methods are considered to be inadequate because the major purposes of porous surface applications are to enhance skid resistance and/or to reduce traffic noise. This up-to-date review revealed the necessity of developing an analysis framework based on some mechanistic simulation models to predict the functional performance in the design phase of a porous pavement.

An analytical framework was next developed to incorporate frictional and acoustical performance evaluations into the design procedures of porous mixture. The basic idea of the framework is to numerically predict skid number and noise level on a porous pavement using the critical parameters measured on alternative mixtures. The predicted values are then compared with the design criteria and converted to some normalized performance indices. Porosity, aggregate size and porous layer thickness are selected as the critical mixture properties to be used in the skid resistance and tire/road noise simulations, because they are easily measurable or controllable in the laboratory, and can determine the drainage capacity and acoustic absorption of a porous surface layer. The design criterion for skid resistance is determined from the minimum desired skid number of a specific old pavement and the long-term effects caused by pavement aging and seasonal variation. The acoustic criterion is derived in a similar way, combining the acceptable maximum noise level with the long-term effects and temperature influences. The terminal skid number and noise level should take into consideration of the project location, road classification, design speed, traffic composition, terrain topography and meteorological condition. Approaches have been developed in some past studies to valuate the benefit of skid resistance enhancement and tire/road noise reduction. These methods were introduced and adopted in this study to quantitatively evaluate the advantages brought forth by the adoption of porous surfaces. A cost-benefit analysis is necessary in this step when cost constrain is considered. Based on the benefit quantification, performance indices for skid resistance and tire/road noise are defined on a scale of 0 to 10, from which a functional performance index is derived by a linear superposition. To further improve the efficiency of this analysis framework, the artificial neural network technique was adopted to generate a fast estimation of the functional performance from a number of numerical simulation results. A two-layer feed-forward neural network was trained, validated and applied in this study to replace the most tedious part of the framework.

The analysis framework was next applied in an illustrative case study. The mixture selection procedures considering skid resistance and tire/road noise performances were demonstrated. This case study exhibited the feasibility of developed framework in selecting an optimum porous mixture design with favorable frictional and acoustical performances. However, the analysis framework can be further improved. The determination of SPI, API and FPI is still reliant on experts' experiences. Future research efforts can be made to provide a more objective interpretation of these indices.

Table 7.1: Criteria on material properties for porous mixture design (ASTM, 2013a)

Material	Property	Test method	Requirement
Course aggregates	Abrasion resistance	Los Angeles abrasion test	< 30%
	Angularity	Fractured face test	Two crushed faces > 90% One crushed faces > 95%
	Particle shape	Flat and elongated test	< 10% (ratio of 5:1)
Fine aggregates	Cleanliness	Sand equivalent test	> 45%
	Angularity	Uncompacted voids content	> 40%
Asphalt binder	Grade	PG-grade	One or two grades stiffer than normally used at the project location
	Modified asphalt		Polymer modified or rubber modified asphalt
Additives	Dosage rate	Draindown test	< 0.3 %

Table 7.2: Examples of recommended master gradation for OGFC

Sieve size	Percent passing			
	Oregon 25 mm	ASTM 12.5 mm	Texas 12.5 mm	California 9.5 mm
25 mm	99 - 100	100	100	100
19 mm	85 - 96	100	100	100
12.5 mm	55 - 70	85 - 100	95 - 100	100
9.5 mm	40 - 56	35 - 60	50-80	90 - 100
4.75 mm	10 - 23	10 - 25	0-8	29 - 36
2.36 mm	5 - 16	5 - 10	0-4	7 - 18
0.075 mm	1 - 5	2 - 4	0-4	0

Table 7.3: Illustrative crash modification factors for a unit increase in SN_{40} (Ivan et al., 2012)

Curve type	Driveway	Wet crashes
No curve	Yes	0.9846
	No	1.0208
Mild	Yes	0.9292
	No	0.9624
Severe	Yes	0.9499
	No	0.9838
Isolated	Yes	0.9292
	No	0.9658
Non-isolated	Yes	0.9965
	No	1.0358

Table 7.4: Example of the comprehensive crash costs (in 2011 dollars)

Crash severity	Estimated cost ($)
Fatal	4,008,900
Disabling injury	216,000
Evident injury	79,000
Possible injury	44,900
Property damage only	7,400

Table 7.5: Household monthly valuations for a unit change in noise level (Arsenio et al., 2006)

Noise level variation	Change rating	Value per unit change in noise level (€)
30 - 31	2.62	5.58
35 - 36	2.91	6.20
40 - 41	3.19	6.79
45 - 46	3.48	7.41
50 - 51	3.77	8.03

Table 7.6: Values of changes in noise exposure (DEFRA, 2013)

L_{Aeq}, 18hr (dB)		£ per household per dB change (per year, 2010 prices)		
Low	High	Amenity	Health	Total
55	56	34.80	0.00	34.80
56	57	37.40	0.48	37.88
57	58	40.00	2.70	42.70
58	59	42.70	4.16	46.86
59	60	45.30	5.67	50.97
60	61	48.00	7.22	55.22
61	62	50.60	8.82	59.42
62	63	53.20	10.47	63.67
63	64	55.90	12.17	68.07
64	65	58.50	13.92	72.42
65	66	61.10	15.71	76.81
66	67	63.80	17.56	81.36
67	68	66.40	19.45	85.85
68	69	69.00	21.39	90.39
69	70	71.70	23.37	95.07
70	71	74.30	25.41	99.71
71	72	76.90	27.49	104.39
72	73	79.60	29.62	109.22
73	74	82.20	31.81	114.01
74	75	84.90	34.03	118.93
75	76	87.50	36.31	123.81
76	77	90.10	38.64	128.74
77	78	92.80	41.01	133.81
78	79	95.40	43.43	138.83
79	80	98.00	45.90	143.90
80	81	98.00	48.42	146.42

Table 7.7: Parameters of candidate mixture designs

Mixture code	Porosity (%)	Aggregate size (mm)	Thickness (mm)	Relative cost
A-40	18.2	12.5	40	1.00
A-60	18.2	12.5	60	1.38
B-40	18.6	16.0	40	1.05
B-60	18.6	16.0	60	1.41
C-40	20.8	12.5	40	1.10
C-60	20.8	12.5	60	1.47
D-40	21.3	16.0	40	1.12
D-60	21.3	16.0	60	1.51
E-40	24.4	12.5	40	1.15
E-60	24.4	12.5	60	1.56
F-40	23.7	16.0	40	1.18
F-60	23.7	16.0	60	1.61

Table 7.8: Skid resistance performance of candidate mixture designs

Mixture code	Fluid uplift force (N)	Fluid drag force (N)	Wet friction coefficient	Skid number
A-40	454.6	81.8	0.54	50.6
A-60	364.6	65.6	0.54	51.3
B-40	392.3	70.8	0.55	52.0
B-60	317.8	58.0	0.55	52.6
C-40	380.8	69.2	0.54	51.2
C-60	303.5	55.7	0.54	51.7
D-40	343.7	62.4	0.56	53.3
D-60	273.2	50.0	0.56	53.9
E-40	315.9	57.3	0.55	52.6
E-60	244.2	45.6	0.55	53.2
F-40	310.7	56.0	0.53	50.7
F-60	240.2	44.7	0.53	51.3
Upper bound	224.8	39.0	0.59	57.0
Lower bound	1073.7	194.1	0.53	45.2

Table 7.9: Tire/road noise performance of candidate mixture designs

Mixture code	Noise reduction [dB(A)]	Generated noise [dB(A)]	CPX noise level [dB(A)]
A-40	5.45	92.08	86.63
A-60	6.89	92.08	85.19
B-40	4.69	92.15	87.46
B-60	6.12	92.15	86.03
C-40	5.27	91.42	86.15
C-60	6.55	91.42	84.87
D-40	4.40	92.37	87.97
D-60	5.54	92.37	86.83
E-40	4.79	90.66	85.87
E-60	5.89	90.66	84.77
F-40	4.14	91.98	87.84
F-60	4.99	91.98	86.99
Upper bound	2.18	92.40	90.22
Lower bound	9.54	91.30	81.76

Table 7.10: Safety benefit valuation of candidate mixture designs

Mixture code	Skid number	Δ SN	Accident reduction (acc/mvm)	Relative cost	Benefit-cost ratio
A-40	50.6	5.4	0.24	1.00	0.243
A-60	51.3	6.1	0.27	1.38	0.198
B-40	52.0	6.8	0.31	1.05	0.291
B-60	52.6	7.4	0.33	1.41	0.235
C-40	51.2	6.0	0.27	1.10	0.244
C-60	51.7	6.5	0.29	1.47	0.200
D-40	53.3	8.1	0.36	1.12	0.325
D-60	53.9	8.7	0.39	1.51	0.258
E-40	52.6	7.4	0.33	1.15	0.289
E-60	53.2	8.0	0.36	1.56	0.229
F-40	50.7	5.5	0.25	1.18	0.211
F-60	51.3	6.1	0.27	1.61	0.170
Upper bound	57.0	11.8	0.53	1.33	0.400
Lower bound	45.2	0.0	0.00	0.94	0.000

Table 7.11: Scale definition of SPI and API

Scales	0	1	2	3	4	5	6	7	8	9	10
B/C	0.00	0.00 | 0.04	0.04 | 0.08	0.08 | 0.12	0.12 | 0.16	0.16 | 0.20	0.20 | 0.24	0.24 | 0.28	0.28 | 0.32	0.32 | 0.36	0.36 | 0.40
SPL_p	> 90.22	89.88 | 90.22	89.51 | 89.88	89.10 | 89.51	88.63 | 89.10	88.08 | 88.63	87.44 | 88.08	86.65 | 87.44	85.64 | 86.65	84.21 | 85.64	81.76 | 84.21

Table 7.12: Performance index calculation

Mixture code	B/C	SPL_p	SPI	API	FPI
A-40	0.243	86.63	7	8	7.4
A-60	0.198	85.19	5	9	6.6
B-40	0.291	87.46	8	6	7.2
B-60	0.235	86.03	6	8	6.8
C-40	0.244	86.15	7	8	7.4
C-60	0.200	84.87	6	9	7.2
D-40	0.325	87.97	9	6	7.8
D-60	0.258	86.83	7	7	7.0
E-40	0.289	85.87	8	8	8.0
E-60	0.229	84.77	6	9	7.2
F-40	0.211	87.84	6	6	6.0
F-60	0.170	86.99	5	7	5.8

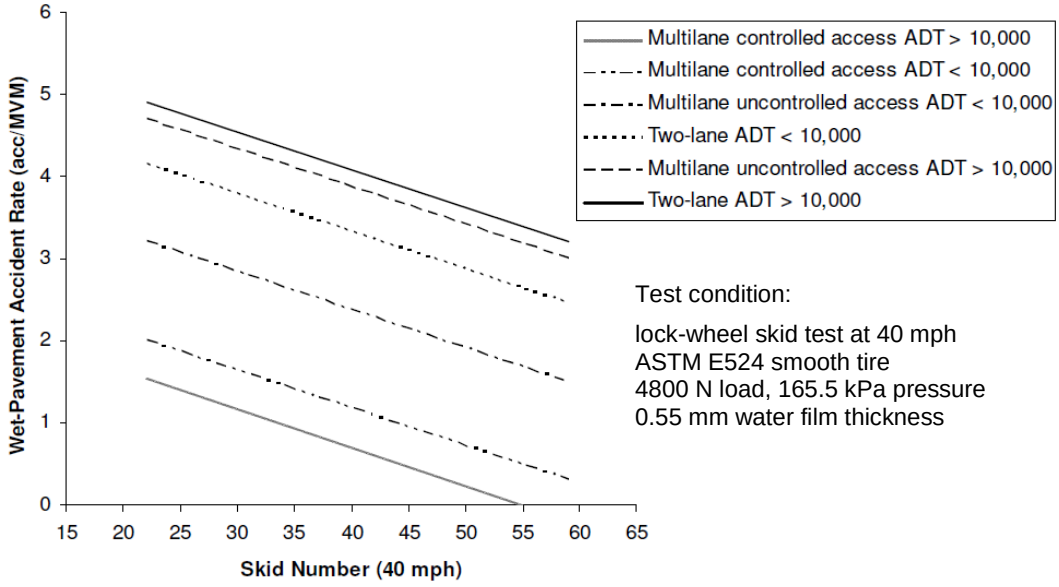

Figure 7.1: Illustrated linear relationship between wet-pavement crashes and skid number (OECD, 1984)

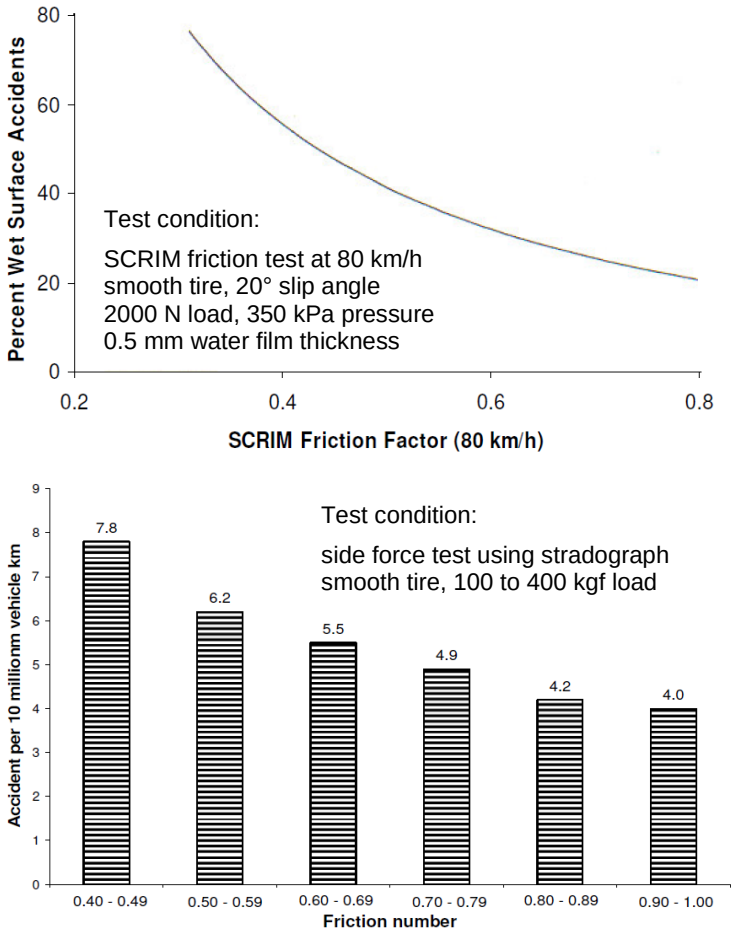

Figure 7.2: Illustrated nonlinear relationship between crashes and friction (McLean and Foley, 1998; Wallman and Aström, 2001)

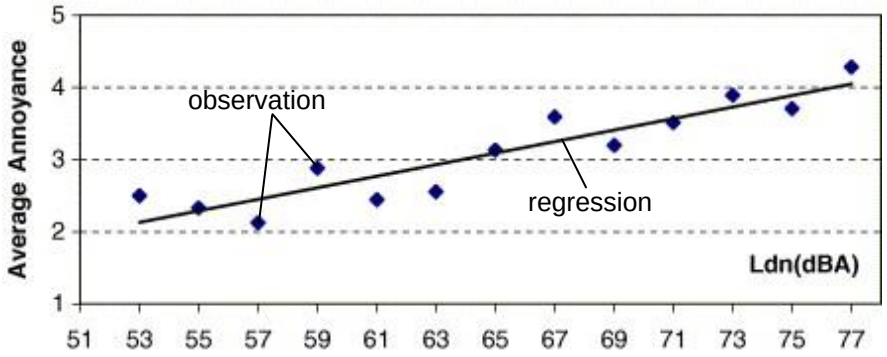

Figure 7.3: Average annoyance produced by traffic noise (Martín et al., 2006)

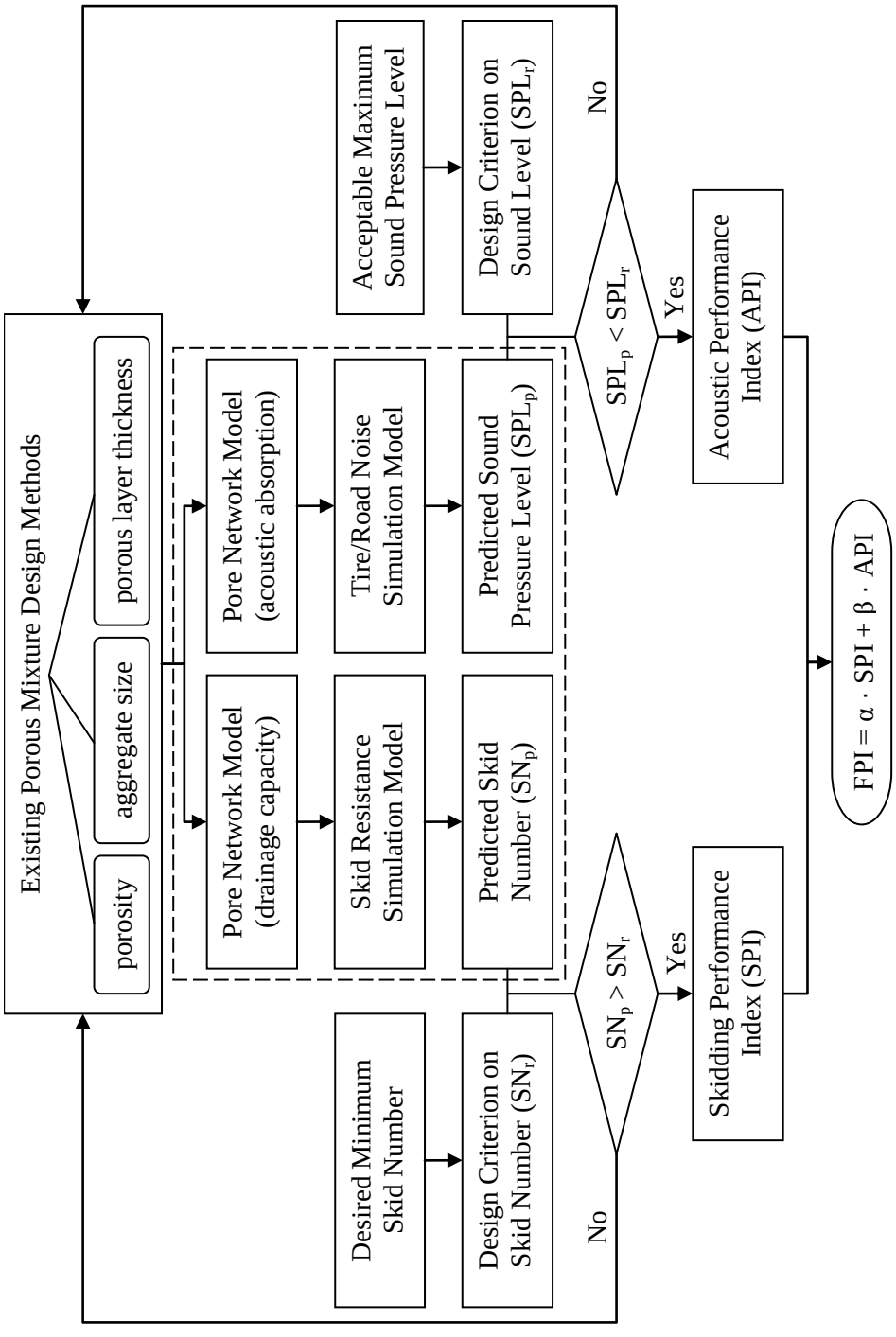

Figure 7.4: Analysis framework to integrate frictional and acoustical performances into porous mixture design

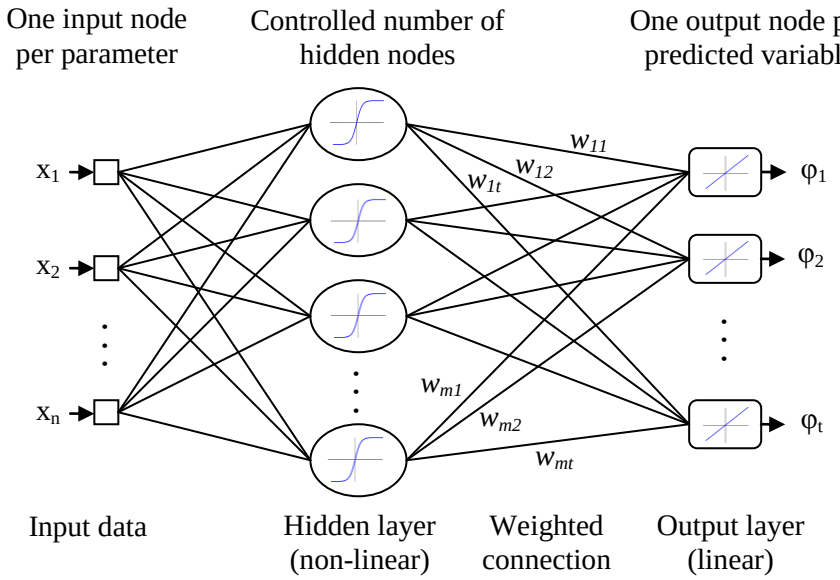

Figure 7.5: Topology of a two-layer feed-forward neutral network

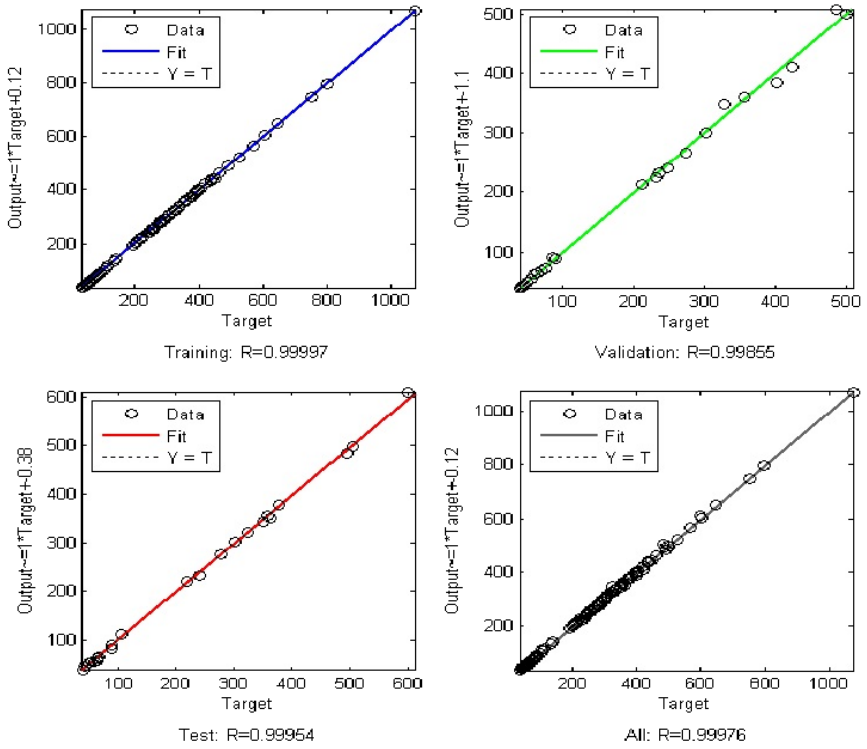

(a) Fluid force

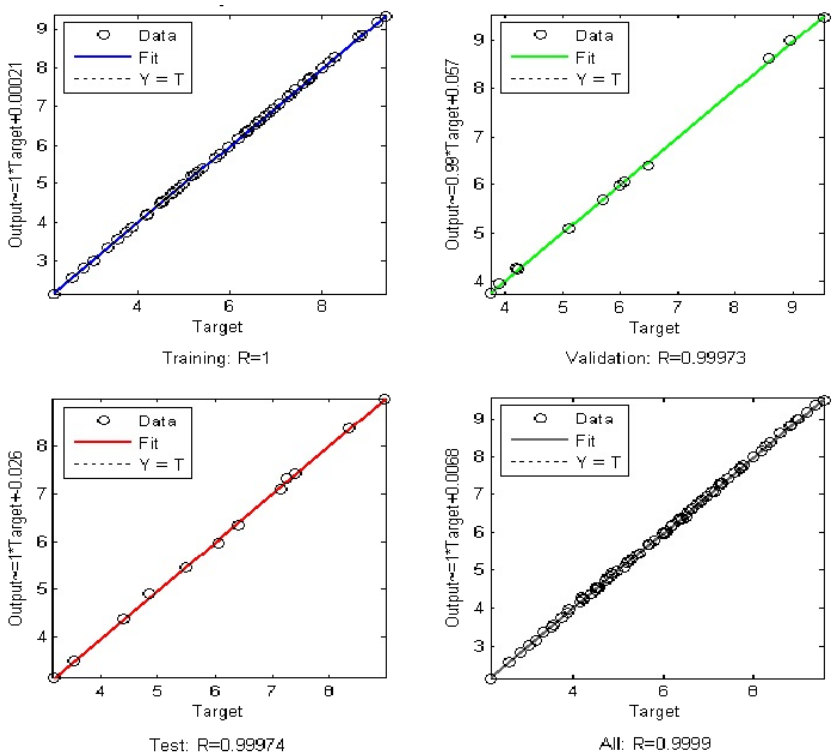

(b) Noise reduction

Figure 7.6: Regression plots of ANN training, validation and test

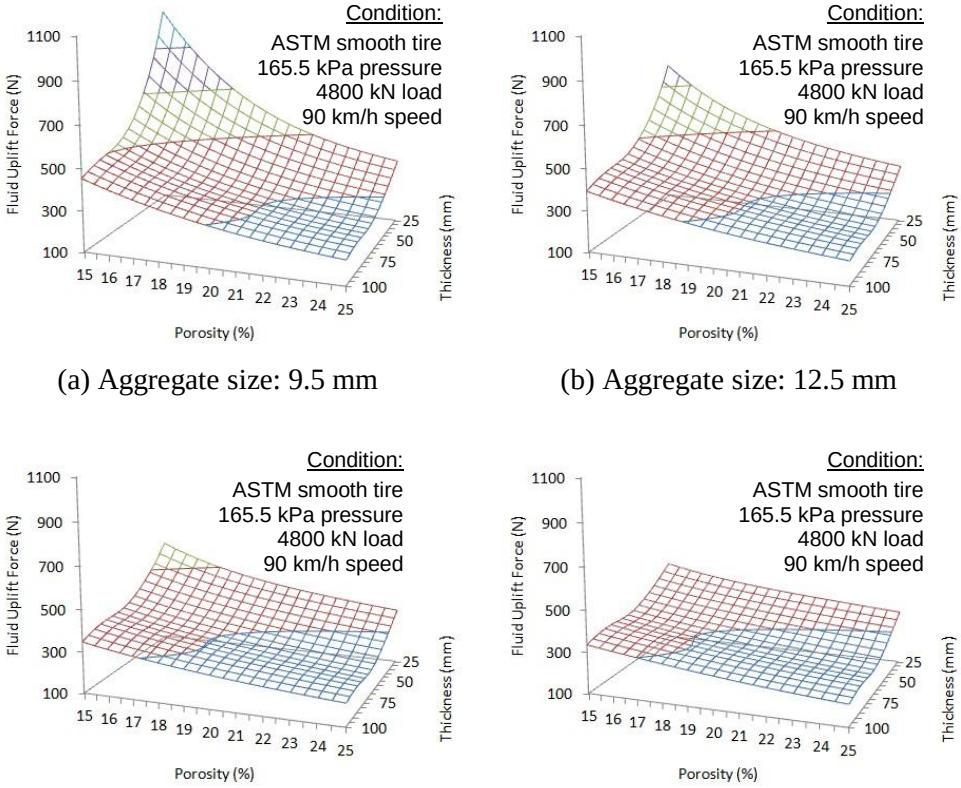

(a) Aggregate size: 9.5 mm

(b) Aggregate size: 12.5 mm

(c) Aggregate size: 16 mm

(d) Aggregate size: 19 mm

Figure 7.7: Fluid uplift force for various aggregate sizes derived from the artificial neural network

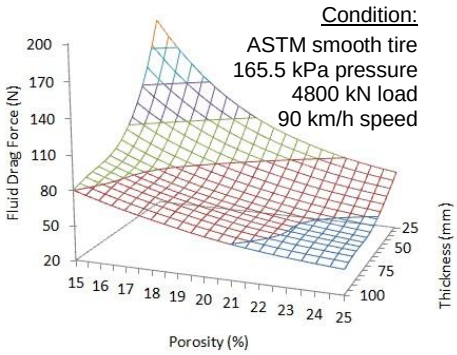

(a) Aggregate size: 9.5 mm

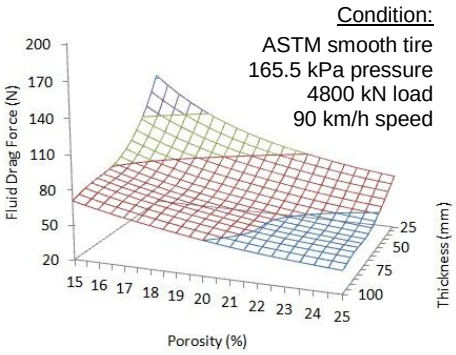

(b) Aggregate size: 12.5 mm

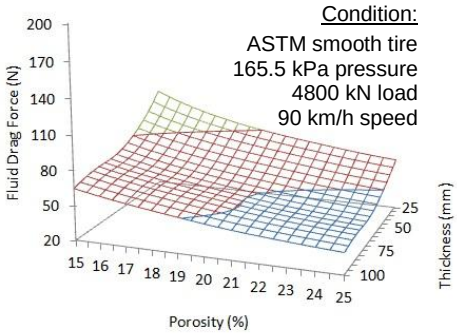

(c) Aggregate size: 16 mm

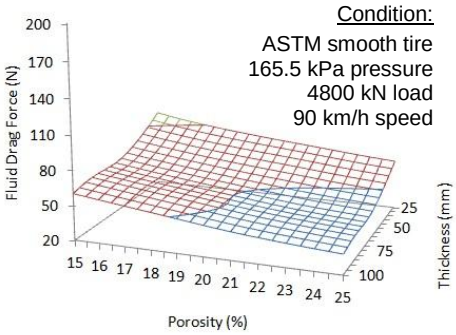

(d) Aggregate size: 19 mm

Figure 7.8: Fluid drag force for various aggregate sizes derived from the artificial neural network

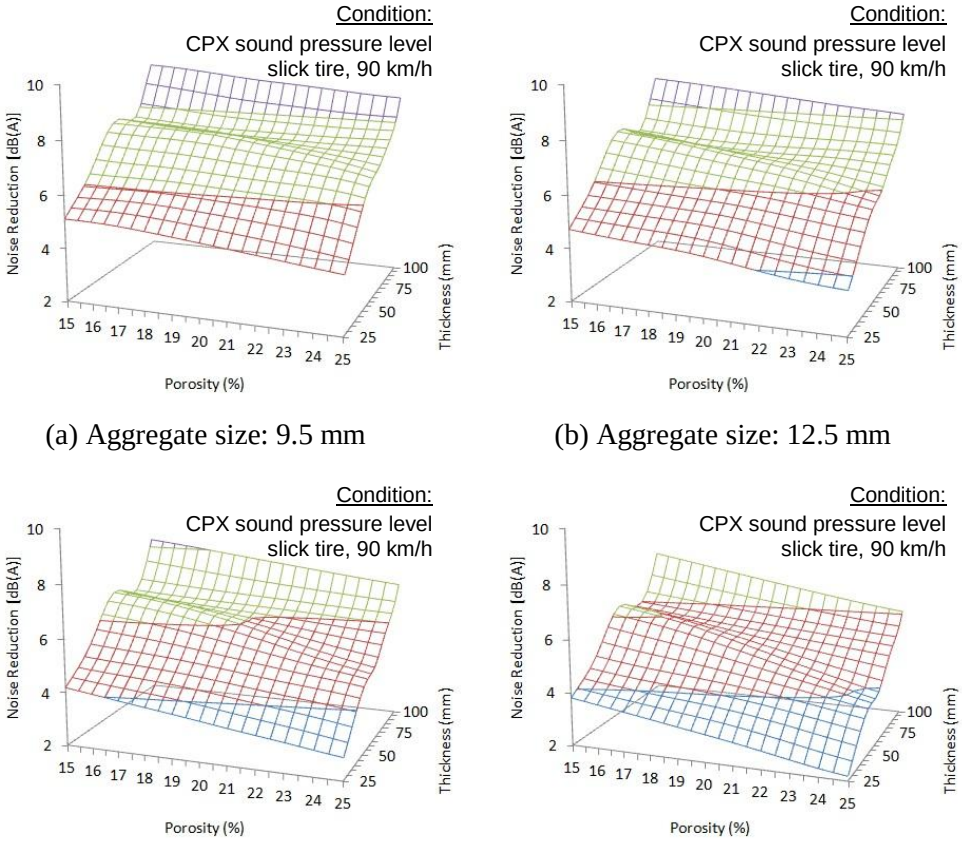

(a) Aggregate size: 9.5 mm

(b) Aggregate size: 12.5 mm

(c) Aggregate size: 16 mm

(d) Aggregate size: 19 mm

Figure 7.9: Noise reduction for various aggregate sizes derived from the artificial neural network

CHAPTER 8 CONCLUSIONS AND RECOMMENDATIONS

This chapter shall present the conclusions of this study drawn from the works described in the previous chapters and the recommendations for future research based on the limitations of present study. After examining the main research objectives, the critical aspects in the development of the skid resistance model and tire/road noise model on porous pavements are summarized. Analyses of influencing factors are presented for porous pavement frictional and acoustical performances, respectively and the major findings are presented and discussed. The development of integrated mixture design approach considering functional performance of porous pavements are also summarized. Several limitations with regards to the current model formulations and applications are identified and some research recommendations are then provided accordingly with suggestions on the potential research avenues.

8.1 Conclusions of Research

Wet pavement skid resistance and tire/road noise are two crucial functional performances of modern pavements. Porous pavement is found to be superior in both aspects. Understanding of the mechanisms and influencing factors in skid resistance enhancement and tire/road noise reduction is essential in the applications of porous pavement technique to benefit from its functional advantages. This research attempts to approach this problem in a numerical perspective. The primary purposes of this study are to develop numerical simulation models for skid resistance and tire/road noise evaluations on porous pavements using the finite element method (FEM) and the boundary element method (BEM), and apply the proposed models to analyze the mechanisms and critical influencing factors. Based on the results and findings, these two functional performances shall be integrated into the design procedures of porous mixture.

8.1.1 Numerical Modeling of Skid Resistance on Porous Pavement

The first part of this research work involved the development of a numerical simulation model on the wet skid resistance performance of porous pavements. This model involves most of the critical issues associated with a numerical skid resistance modeling, including the fluid-structure interaction, turbulent flow, frictional contact formulation, multiphase free-surface flow and, most importantly, drainage capacity of porous pavements.

The reproduction of porous pavement drainage capacity has been achieved through an iterative process based on the simulation of outflow tests. A geometrically simple pore network of a 3D grid structure is proposed to simplify the complex pore space and make the simulation numerically feasible. The simplified pore network model is calibrated to make sure that it presents a similar drainage capacity as the in-field porous pavements. The calibration is conducted on the dimensions of pores and the spacing between successive pores, taking the measured porosity, permeability as well as clogging potential into consideration.

The simplified porous pavement model is integrated with a numerical skid resistance model which simulates the lock-wheel trailer test as specified by ASTM E274 standard (ASTM, 2011a). The formulation of skid resistance model involves the theories in both solid mechanics and fluid dynamics. The tire sub-model and the fluid sub-model are coupled in the computation through a fluid-structure interaction (FSI) algorithm. The solid contact between tire tread and pavement surface is modelled by a nonlinear frictional contact algorithm and the turbulent flow is modelled by the k-ε turbulence model. The multiphase flow technique is adopted to include both water and air into the simulation and define the water film thickness by the free surface of water. The structure model (i.e. tire, pavement and contact algorithm) is calibrated against measured tire foot prints, and the fluid model (i.e. water and air) is defined according to the standard properties at test conditions.

The whole porous pavement skid resistance model has been validated against field experiments conducted by Younger et al. (1994). The simulation results show satisfactory agreements with the measurements, with an absolute error within ±2 SN units. This demonstrates the feasibility and capability of the developed FEM model in reproducing lock-wheel skid number on porous pavements. This model can be used to predict the skid resistance performance of a particular porous pavement, provided its drainage capacity (represented by porosity and outflow time) and wet coefficient of friction at low speeds (represented by SN_0). The developed model can also be used to quantify those variables that are difficult to measure in experiments. The behaviours of tire and water observed from the numerical simulations should be useful in interpreting the mechanisms of skid resistance enhancement on porous pavements.

8.1.2 Factors Affecting Skid Resistance on Porous Pavement

The developed model was next applied to investigate the mechanisms of skid resistance on porous pavements and analyze the critical influencing factors. The effect of porous surfaces on skid resistance was first studied through a detailed comparison between tire skidding behaviours on porous and non-porous pavements. It was found that the fluid uplift force developing on a porous pavement is significantly reduced comparing with that on a non-porous pavement and the tire deformation is less severe as well. A better contact status can be maintained between the tire tread and porous pavement surface even at high speeds. The traction force dominates skid resistance on porous pavements in the practical speed range, while fluid drag force is a secondary component. These could be essential to interpret the development of the superior skid resistance performance on porous pavements.

The influences of some crucial pavement parameters and vehicle operating conditions on porous pavement skid resistance were next analyzed using the proposed simulation model. The surface porosity, porous layer thickness, rainfall intensity and vehicle speed were investigated as the major influencing factors. The availability of

mechanistic model enables one to study, in detail, the effects of individual factors as well as their interactions. The following findings can be made from the analysis:

- The skid resistance of porous pavements in wet weather increases when either the porosity or the thickness of porous surface layer increases, but decreases when either the rainfall intensity or vehicle speed increases.
- The skid resistance increases with porosity approximately linearly in the porosity range of 15% to 25%. The beneficial effect of porosity is more prominent in the situations with thicker porous surface layer, higher rainfall intensity and higher vehicle speed.
- The increasing rate of skid resistance with porous layer thickness is more pronounced for a thinner porous layer, and tends to level as the porous surface layer becomes thicker than 75 mm. The benefits from increasing porous layer thickness are more substantial for pavements with higher porosity, and operating conditions under higher rainfall intensity and higher vehicle speed.
- The reduction rate of skid resistance with the increase of rainfall intensity is higher at low rainfall intensity levels. The adverse effects of rainfall intensity on the frictional performance of porous surface are more significant for pavements with lower porosity and thinner porous layer thickness, and at higher travel speeds.
- Skid resistance reduction becomes more and more significant as vehicle speed increases. The adverse effects of speed are more critical in the cases of lower porosity, thinner porous layer and higher rainfall intensity.

Based on these findings, some recommendations could be made for porous pavement design from the standpoint of wet-weather driving safety. Higher porosity is preferred to better utilize its advantage in skid resistance improvement as long as it does not adversely affect the structural and other functional performances of a porous pavement. It also reduces the negative effects of rainfall intensity and vehicle speed, so that a more consistent driving behavior can be maintained on rainy days. The

findings also suggested that, from the skid resistance point of view, a minimum of 50 mm thickness of porous surface layer should be used. Porous surfaces thicker than 75 mm may not be cost-effective because they provide marginal further skid resistance improvement.

8.1.3 Numerical Modeling of Tire/Road Noise on Porous Pavement

The next part of this research work focused on developing a numerical model to simulate the tire/road noise phenomena on porous pavements. The proposed FEM-BEM model recognized tire vibration as a dominant noise generation mechanism and included most of the critical problems associated with the simulation of tire-vibration noise for porous pavements, such as the representation of pavement surface texture, characterization of tire vibration, acoustic-structure coupling, sound propagation in free space, and most importantly, acoustic absorption of porous surface layers.

The numerical description of the acoustic absorption characteristics of porous pavements has been identified as the most crucial component to be addressed in the development of the entire tire/road noise model. It was understood that the acoustic absorption coefficient can be theoretically derived from the acoustic impedance, but the laboratory impedance measurements are not always available. Therefore, some previously developed computational approaches should be adopted to quantify the acoustic impedance of porous surfaces based on their pore geometry parameters. The representative phenomenological and microstructural models with different input parameters were discussed, which were found in close agreement with each other. Theoretically, either of them can be used in the analysis of tire/road noise on porous pavements, and the microstructural model developed by Neithalath et al. (2005) were adopted in this research. The numerical representation of porous pavement acoustic absorption in the BEM formulation was next examined using the experimental results of horn effect reduction on porous pavements. Such modeling of porous surfaces was found adequate for engineering applications.

The porous pavement acoustic absorption model was next integrated into the tire/road noise simulation model to simulate the CPX noise measurement specified by the ISO 11819-2 standard (ISO, 2013). This model is able to estimate the rolling tire vibration noise induced by pavement textures on porous pavements. Four major steps are conducted in a sequential manner. First, a dynamic rolling tire analysis computes the deformations and stresses developing on tire walls when a specific tire rotates in a given traveling condition. A tire modal analysis next solves the natural frequencies and mode shapes of the rolling tire. A tire vibration analysis then derives the vibration velocities and accelerations on tire walls through mode superposition excited with the pavement surface texture. The vibration characteristics are used as sound sources in an acoustic BEM model to generate sound field around the rolling tire. The acoustic properties of porous pavements in the BEM model are represented by the acoustic impedance measured in experiments or derived from computational models.

The developed tire/road noise simulation model was calibrated and validated against experimental measurements conducted by Schwanen et al. (2007) for both dense-graded and porous pavements. It is important to notice that a set of calibration parameters is only valid for a restricted range of tire and pavement types. The model needs to be recalibrated if the tire or pavement surface properties vary significantly. The numerical predictions agree well with the experimental results on non-porous surfaces for both overall noise level and noise spectrum. The errors in overall noise levels were less than 2 dB(A) and the simulated 1/3-octave spectra basically fitted with the measured shapes. However, for porous surfaces, the quality of spectrum prediction is lower with regards to the peak noise reduction frequency. The simulated noise reduction peaks appeared at frequencies lower than that of measured spectra. This may be resulted from the local reaction assumption and may be resolved by including extended reacting effects into porous pavement simulation. Nevertheless, the estimations of overall noise level on porous pavements were still satisfactory and the noise spectra corrected by a frequency shifting approach agree better with the

measurements. The model validation demonstrated the feasibility of proposed model in evaluating the acoustical performance of porous pavements. This model provides the possibility of efficient examinations on various scenarios without the needs for extensive experiments. It can also be used to understand the mechanisms of tire/road noise reduction on porous pavements and analyze its influencing factors.

8.1.4 Factors Affecting Tire/Road Noise on Porous Pavement

The developed numerical model was next adopted to study the overall effect of porous pavements on the reduction of tire/road noise and investigate the effects of factors affecting tire/road noise. The function of porous surface in tire/road noise abatement was first studied through a detailed comparison between sound pressure level spectra and overall noise levels on porous and nonporous pavements. The illustrative case study demonstrated that porous pavement can effectively reduce tire/road noise. The sound pressure level emitted from a rolling tire is lower on a porous surface than that on a dense-graded pavement in the whole interested frequency range from 350 Hz to 2500 Hz, resulting in a significantly decreased overall noise level. It is found that the maximum noise reductions on a porous surface happen at a frequency slightly higher than its acoustic absorption peak. Between the two potential sources of tire/road noise reduction on porous surfaces, the acoustic absorption resulted from interconnected air voids was identified as the dominant contributor, while the negatively oriented macrotexture serves as a secondary contributor.

The developed numerical simulation model was next applied in analyzing the influences of critical pavement properties and vehicle operating condition on tire/road noise emission. Surface porosity, porous layer thickness, pavement surface texture and vehicle speed were investigated as the major factors affecting tire/road noise. The availability of mechanistic model enables a systematic study on the effects of individual factors. The following findings have been drawn from the analysis:

- Tire/road noise increases in a linear manner with the increase of surface layer porosity in the normal porosity range of 15% to 25%. Noise spectrum shapes are similar on pavements with identical porous layer thickness but different porosities. The magnitudes of noise level slightly differ among various surfaces, and it is more obvious near the noise reduction peak. The benefits of porosity variation on overall noise level present an insignificant amount in the overall tire/road noise emission.

- Tire/road noise on porous pavements decreases as porous layer thickness increases and the declining trend is nonlinear. Noise variation is less significant when porous layer thickness changes between 50 and 75 mm, comparing with that in lower or higher thickness ranges. Variations in porous layer thickness alter the noise spectrum shape significantly, by moving the reduction peak towards lower frequency with the thickness increase. It was also found that the benefits of increasing porous layer thickness are slightly more substantial on pavements with higher porosities.

- Tire/road noise emission on porous pavements increases as pavement texture level or mean profile depth increases. The variations in pavement surface texture marginally affect the noise spectrum shape, but significantly affect the noise level magnitude. The texture effect is more obvious at lower frequencies and the noise incremental resulted from a specific amount of texture increase is larger at a lower mean texture depth.

- Tire/road noise level on porous pavements increases with vehicle speed in a logarithmic-linear manner. Speed variation hardly affects noise spectrum shape, but it affects sound level magnitude significantly. The effect of vehicle travel speed on tire/road noise is slightly larger on porous pavements with higher porosities and thinner porous layers. The effect of porosity level on noise reduction is more significant at higher speeds, while that of porous layer thickness is larger at lower speeds.

Some recommendations could be made for porous pavement design from the standpoint of acoustical traveling comfort. A lower porosity in the normal range (i.e. 15% to 25%) should be adopted to better utilize its advantages in sound absorption, provided sufficient skid resistance and clogging resistance. It can reduce the negative effect of vehicle speed increase as well. The numerical analysis also suggested thicker porous layer to be used in pavement design, with the cost effectiveness in restriction. The negative texture on porous surfaces should be maintained and the macrotexture level should be restrained to make a flatter traveling plane.

8.1.5 Integrating the Frictional and Acoustical Performances into the Porous Mixture Design

The last part of this research work focused on the development of an analysis framework to consider the skid resistance and tire/road noise performances in porous mixture design, based on skid numbers and noise levels predicted from the developed numerical simulation models. From the review of some current porous mixture design methods, it was concluded that the existing specifications only pay attentions to the durability and moisture sensitivity of porous mixtures. The functional performance is assumed acceptable if the requirements in material composition and porosity level are fulfilled, although permeability measurement on pavement surfaces after placement is optional in some countries. This is inadequate for the efficient applications of porous pavement techniques, especially when their major objectives are to improve traveling safety and comfort. Therefore, it is important to develop an analytical framework to consider the functional performance in porous mixture design based on mechanistic simulation models.

The primary workflow of the proposed approach is to predict the skid number and noise level on a finished porous pavement using the developed numerical models with the control variables of an alternative mixture design as input parameters. The results are then compared with design criteria and scalar performance indices are

designated to mixtures satisfying both the frictional and acoustical requirements. The optimum design is finally selected according to the functional performance index. Considering their applicability and significance, the porosity value, aggregate size and porous layer thickness were selected as the control variables in porous mixture design to be input into the skid resistance and tire/road noise simulation models. The design criteria were determined based on the minimum desired skid number or the maximum acceptable CPX noise level of a specific old pavement and the long-term effects caused by pavement aging, seasonal variation and temperature influences. The specific terminal skid number and noise level should consider the project location, road classification, design speed, traffic composition, terrain topography, as well as meteorological condition. Approaches developed in past studies were adopted to quantify the safety and comfort benefits brought forth by porous surfaces. A cost-benefit analysis should be involved if the cost constrain plays a role in the design. The performance indices for skid resistance and tire/road noise were defined on an integer scale of 0 to 10, from which the overall functional performance index can be derived using linear superposition. A two-layer feed-forward artificial neural network was established from the numerical simulation results to improve the efficiency of functional performance estimation.

Application of the proposed framework was demonstrated through a case study. Mixture design procedures considering frictional and acoustical performances were performed based on the problem definition. This framework provides an effective and efficient approach in selecting porous mixture taking the functional performance into consideration. It should serve as a useful tool to improve the current practice of porous mixture design and help to spread the effective applications of porous pavement technologies.

8.2 Recommendations for Further Research

As an early exploration in numerically investigating the skid resistance and tire/road noise performances of porous pavements, the works presented in this thesis are far from perfection. Several limitations could be identified in the formulations and applications of the proposed numerical simulation models. Based on the current work, the following areas are recommended for future research.

8.2.1 Improvement to Porous Pavement Skid Resistance Model

The current model only considered the lock-wheel skidding situation of the smooth tire, since this is the most adverse scenario in wet-pavement skid resistance. However, the realistic wheel braking behaviors are much more complicated and most of the tires used in practice have tread patterns. Tire slip conditions (i.e. slip ratio and slip angle) should be properly included into the numerical simulation model to better represent the braking and corning scenarios. The stationary rolling approach with the arbitrary Lagrangian Eulerian (ALE) formulation (Nackenhorst, 2004) is a promising methodology in the slip tire modeling, which could overcome the disadvantages of time- and resource-consuming dynamic simulations. Tires with tread patterns or grooves should also be included in the future model to more accurately describe the realistic tire-pavement-fluid interaction.

As a result of the restrictions in computational capacity and limitations in reported measurements, a simplified grid pore network geometry is adopted in this study to represent the porous surface layer and reproduce the drainage capacity of a porous pavement. Although this approach is feasible to provide results with adequate accuracy, it is quite complicated and tedious to perform the iterative calibration based on the measured outflow time. Advanced formulations of porous medium should be developed to describe the water flow behavior in skid resistance on porous pavements. The difficulties may lie in the formulation of the boundary condition at porous layer surface, where water can flow into, flow out of and flow parallel to the porous layer.

8.2.2 Improvement to Porous Pavement Tire/Road Noise Model

The four-step tire/road noise model developed in this research work is mainly based on the tire vibration mechanism, since this is the most crucial noise generation mechanism for a smooth tire rolling on a rough surface. Air-related noise generation mechanisms are not involved in model formulation, but covered by model calibration. Although air turbulence noise is negligible at highway speeds, air pumping noise near the tire-pavement contact patch should be included in the simulation model because it is a significant component in the overall tire/road noise and porous pavements can effectively reduce the air pumping effect. However, boundary element method (BEM) may be powerless in capturing the air pumping noise. Computational fluid dynamics (CFD) is a potential method to simulate the air pumping phenomenon, provided an appropriate description of the relative motions among tire, pavement and air.

The acoustic absorption capacity of a porous pavement is represented by the measured or derived normal acoustic impedance spectrum in the developed model, due to the restrictions in both measurement data and BEM formulation. The use of normal acoustic impedance presumes a local reaction condition, which may not be valid in the case of porous pavements. Extended reaction should be considered in the modeling of porous pavement acoustic properties. The input parameter should be able to describe the surface acoustic impedance at any incidence angle. Grazing incidence approximate impedance (Anfosso-Lédée et al., 2007) may be a promising approach, provided that detailed measurements on porous mixture properties are made available. The two-domain BEM technique and acoustic FEM are also possible solutions to this problem, with different requirements in their applications.

8.2.3 To Improve the Porous Pavement Design Procedures

The analysis framework developed in this study incorporate the consideration of functional performance into porous mixture selection based on the comparison of functional performance indices (FPI) among alternative mixture designs. Although

mechanistic models are used in the predictions of skid number and noise level, the valuation of safety and comfort benefits and the projection of performance indices are largely subjective. This causes the proposed framework to rely heavily on the experts' experiences and judgments. More scientific methodologies should be developed in the quantification of benefits brought forth by a porous pavement installation. This has to be based on a large amount of practices in various porous pavement projects. The appropriate valuation of comfort and health effects may present great difficulties in this task, because one has to include the subjective perceptions and socio-culture influence into the appraisal of traffic noise. Future research efforts should also be put on the development of a more objective interpretation of the performance indices. This includes not only the projection rules from benefit value to index level, but also the approach to determine the weighting factors in combining multiple performance indices into a final PFI. Moreover, the current analysis framework covers only skid resistance and tire/road noise. More functional performances, such as the roughness, rutting resistance and rolling resistance, could be integrated into the framework when they can be mechanically evaluated from mixture parameters. Considering the fact that most tires traveling on roads have certain tread patterns and depths, it is also necessary to develop the relationships between smooth tire performance and ribbed tire performance based on future experimental and numerical analysis.

8.2.4 Application of Developed Models in Porous Pavement Maintenance

Besides assisting porous pavement design, the developed numerical models can also be applied in porous pavement maintenance to better retain the superior skid resistance and acoustical performances. One of the major tasks in porous pavement maintenance is to remove dusts and debris from air voids, because the clogging effect could dramatically decrease the functional performances. The proposed models can be used to predict the variations in skid resistance and tire/road noise with clogging level under different travelling conditions. Analysis on the simulation results can help

pavement engineers to determine the critical clogging level for routine maintenance. Combined with a clogging analysis, the time and method for air void cleaning can be decided with a sounder basis.

REFERENCES

1. AASHTO (2010). Highway Safety Manual. American Association of State Highway and Transportation Officials, Washington D.C.
2. AASHTO (2011a). A Policy on Geometric Design of Highways and Streets, American Association of State Highway and Transportation Officials, Washington D.C.
3. AASHTO (2011b). Standard Method of Test for Measurement of Tire/Pavement Noise Using the On-Board Sound Intensity (OBSI) Method. American Association of State Highway and Transportation Officials, Washington D.C.
4. Abbott, P. G., Morgan, P. A., and McKell, B. (2010). A Review of Current Research on Road Surface Noise Reduction Techniques. Transport Research Laboratory, Wokingham, UK.
5. Abbott, P. G., and Phillips, S. M. (1996). Vehicle Noise Levels Derived from the Statistical Pass-By Method and Road Surface Texture. NOISE-CON 1996, Seattle, Washington.
6. Abustan, I., Hamzah, M. O. and Rashid, M. A. (2012). A 3-Dimensional Numerical Study of a Flow Within a Permeable Pavement. International Journal of Sustainable Development, 4(2), 37-44.
7. Acharya, R. C., van der Zee, S. E. A. T. M., and Leijnse, A. (2004). Porosity-Permeability Properties Generated with a New 2-Parameter 3D Hydraulic Pore-Network Model for Consolidated and Unconsolidated Porous Media. Advances in Water Resources, 27, 707-723.
8. Agrawal, S. K., and Henry, J. J. (1977). Technique for Evaluating Hydroplaning Potential of Pavement. Transportation Research Record, 633, 1-7.

9. Ahammed, M. A., and Tighe, S. L. (2010). Pavement Surface Friction and Noise: Integration into the Pavement Management System. Canadian Journal of Civil Engineering, 37, 1331-1340.

10. Al-Masaeid, H. R. (1997). Impact of Pavement Condition on Rural Road Accidents. Canadian Journal of Civil Engineering, 24(4), 523-531.

11. Al-Qadi, I. L., Elseifi, M. A., and Yoo, P. J. (2004). Pavement Damage Due to Different Tires and Vehicle Configurations. Virginia Tech Transportation Institute, Blacksburg, Virginia.

12. Albert, B. J., and Walker, J. C. (1968). Tire to Wet Road Friction at High Speeds. Rubber Chemistry and Technology, 41(4), 753-779.

13. Alvarez, A. E., Martin, A. E., and Estakhri, C. K. (2011). Optimizing the Design of Permeable Friction Course Mixture. Transportation Research Record, 2209, 26-33.

14. Alvarez, A. E., Martin, A. E., Estakhri, C. K., Button, J. W., Glover, C. J., and Jung, S. H. (2006). Synthesis of Current Practice on the Design, Construction, and Maintenance of Porous Friction Courses. FHWA Report 06/0-5262-1, Texas Transportation Institute, Austin, Texas.

15. Amontons, G. (1699). De La Resistance Caus'ee Dans Les Machines. Memoires de l'Academie Royale, A, 257-282.

16. Anderson, D. A., Huebner, R. S., Reed, J. R., Warner, J. C., and Henry, J. J. (1998). Improved Surface Drainage of Pavement. Transportation Research Board, National Research Council, Washington D.C.

17. Anfosso-Lédée, F. (1997). Application de la Méthode des Equations Intégrales à la Modélisation du Bruit aux Abords des Routesb: Interaction Chaussée/Ecran Antibruit. Proc., Études et recherches des Laboratoires des Ponts et Chaussées . Série environnement et génie urbain Laboratoire central des ponts et chaussées.

18. Anfosso-Lédée, F., Dangla, P., and Bérengier, M. (2007). Sound Propagation Above a Porous Road Surface with Extended Reaction by Boundary Element Method. The Journal of the Acoustical Society of America, 122(2), 731-736.

19. Anfosso-Lédéé, F., and Do, M. T. (2002). Geometric Descriptors of Road Surface Texture in Relation to Tire/Road Noise. Transportation Research Record, 1806, 160-167.

20. Anonymous (1971). Truck Tire Noise. Rubber Manufacturers Association, Washington D.C.

21. Anonymous (1980). Foreign Research in Tire Noise. Office of Noise Abatement and Control, U.S. Environmental Protection Agency, Washington D.C.

22. ANSYS (2009a). ANSYS Workbench User's Guide. ANSYS, Inc.

23. ANSYS (2009b). ANSYS Structural Analysis Guide. ANSYS, Inc.

24. ANSYS (2009c). ANSYS CFX-Solver Modeling Guide. ANSYS, Inc.

25. ANSYS (2009d). ANSYS Reference for the Mechanical APDL and Mechanical Applications. ANSYS, Inc.

26. ANSYS (2009e). ANSYS CFX-Solver Theory Guide. ANSYS, Inc.

27. ANSYS (2009f). ANSYS CFX-Pre User's Guide. ANSYS, Inc.

28. Anupam, K. (2011). Numerical Simulation of Vehicle Hydroplaning and Skid Resistance on Grooved Pavement. Ph.D thesis, National University of Singapore, Singapore.

29. Arsenio, A., Bristow, A. L., and Wardman, M. R. (2006). Stated Choice Valuation of Traffic Related Noise. Transportation Research Part D: Transport and Environment, 11(1), 15-31.

30. ASTM (2004). Standard Test Methods for Measurement of Skid Resistance on Paved Surfaces Using a Passenger Vehicle Diagonal Braking Technique. ASTM E503, ASTM International, West Conshohochen, Pennsylvania.

31. ASTM (2006). Standard Test Method for Measuring Pavement Macrotexture Depth Using a Volumetric Technique. ASTM E965, ASTM International, West Conshohochen, Pennsylvania.

32. ASTM (2008a). Standard Specification for Standard Rib Tire for Pavement Skid-Resistance Tests. ASTM E501, ASTM International, West Conshohochen, Pennsylvania.

33. ASTM (2008b). Standard Specification for Standard Smooth Tire for Pavement Skid-Resistance Tests. ASTM E524, ASTM International, West Conshohochen, Pennsylvania.

34. ASTM (2008c). Standard Specification for P225/60R16 97S Radial Standard Reference Test Tire. ASTM F2493, ASTM International, West Conshohochen, Pennsylvania.

35. ASTM (2009a). Standard Practice for Calculating Pavement Macrotexture Mean Profile Depth. ASTM E1845, ASTM International, West Conshohochen, Pennsylvania.

36. ASTM (2009b). Standard Test Method for Side Force Friction on Paved Surfaces Using the Mu-Meter. ASTM E670, ASTM International, West Conshohochen, Pennsylvania.

37. ASTM (2009c). Standard Test Method for Measuring Pavement Macrotexture Properties Using the Circular Track Meter. ASTM E2157, ASTM International, West Conshohochen, Pennsylvania.

38. ASTM (2009d). Standard Test Method for Measuring Paved Surface Frictional Properties Using the Dynamic Friction Tester. ASTM E1911, ASTM International, West Conshohochen, Pennsylvania.

39. ASTM (2009e). New Practice for Measurement of Tire/Pavement Noise Using the On-Board Sound Intensity (OBSI) Method, ASTM WK26025, ASTM International, West Conshohochen, Pennsylvania.

40. ASTM (2011a). Standard Test Method for Skid Resistance of Paved Surfaces Using a Full-Scale Tire. ASTM E274, ASTM International, West Conshohochen, Pennsylvania.

41. ASTM (2011b). Standard Test Method for Friction Coefficient Measurements Between Tire and Pavement Using a Variable Slip Technique. ASTM E1859, ASTM International, West Conshohochen, Pennsylvania.

42. ASTM (2012a). Standard Test Method for Impedance and Absorption of Acoustical Materials Using a Tube, Two Microphones and a Digital Frequency Analysis System. ASTM E1050, ASTM International, West Conshohochen, Pennsylvania.

43. ASTM (2012b). Terminology Relating to Vehicle-Pavement Systems. ASTM E867, ASTM International, West Conshohochen, Pennsylvania.

44. ASTM (2013a). Standard Practice for Open-Graded Friction Course (OGFC) Mix Design. ASTM D7064, ASTM International, West Conshohochen, Pennsylvania.

45. ASTM (2013b). Standard Test Method for Measuring Surface Frictional Properties Using the British Pendulum Tester. ASTM E303, ASTM International, West Conshohochen, Pennsylvania.

46. ASTM (2013c). Standard Test Method for Stopping Distance on Paved Surfaces Using a Passenger Vehicle Equipped with Full-Scale Tires. ASTM E445, ASTM International, West Conshohochen, Pennsylvania.

47. Attenborough, K., and Howorth, C. (1990). Models for the Acoustic Characteristics of Porous Road Surfaces. International Tire/Road Noise Conference, Goteborg, Sweden, 177-191.

48. Ayadi, A., Picoux, B., Lefeuve-Mesgouez, G., Mesgouez, A., and Petit, C. (2012). An Improved Dynamic Model for the Study of a Flexible Pavement. Advances in Engineering Software, 44(1), 44-53.

49. Bakker, A. A. M., van Blokland, G. J., Bobbink, E., van Grunsven, G. F. C., van Hinthem, P. E., van Leeuwen, J. J. A., van Mulken, G. N. M., Reinink, F., Reubsaet, J., and van Vliet, W. J. (2012). CPX Trailer Comparison Round Robin Test Data Analysis. CROW, Ede, the Netherlands.

50. Balmer, G. G., and Gallaway, B. M. (1983). Pavement Design and Controls for Minimizing Automotive Hydroplaning and Increasing Traction. Frictional Interaction of Tire and Pavement, W. E. Meyer, and J. D. Walters, ed., Ameriacn Society for Testing and Materials, West Conshohochen, Philadelphia, 167-190.

51. Barry, J. H., and Henry, J. J. (1981). Short-Term, Weather-Related Skid Resistance Variations. Transportation Research Record, 836, 76-81.

52. Bathe, K. J. (1996). Finite Element Procedures, Prentice-Hall, Englewood Cliffs, New Jersey.

53. Bathe, K. J., and Wilson, E. L. (1973). NONSAP-A General Finite Element Program for Nonlinear Dynamic Analysis of Complex Structures. The 2nd International Conference of Structural Mechanics in Reactor Technology, Berlin, Germany.

54. Beckenbauer, T. (2001). Akustische Eigenschaften von Fahrbahnoberflaechen. Strasse+Autobahn, 54(10), 553-561.

55. Becker, N., and Lavee, D. (2003). The Benefits and Costs of Noise Reduction. Journal of Environmental Planning and Management, 46(1), 97-111.

56. Bendtsen, H. (1998). Porous Asphalt and Noise Reduction over a Long Period. EURO-NOISE, Munich, Germany.

57. Benedetto, A. (2002). A Decision Support System for the Safety of Airport Runways: the Case of Heavy Rainstorms. Transportation Research Part A, 36(8), 665-682.

58. Benedetto, A. and Umiliaco, A. (2014). Evaluation of Hydraulic Permeability of Open-Graded Asphalt Mixes Using a Full Numerical Simulation. Journal of Materials in Civil Engineering, 26(4), 599-606.

59. Bennert, T. A., Fee, F., Sheehy, E., Jumikis, A., and Sauber, R. W. (2005). Comparison of Thin-Lift Hot-Mix Asphalt Surface Course Mixes in New Jersey. Transportation Research Record, 1929, 59-68.

60. Berckmans, D., Kindt, P., Sas, P., and Desmet, W. (2010). Evaluation of Substitution Monopole Models for Tire Noise Sound Synthesis. Mechanical Systems and Signal Processing, 24(1), 240-255.

61. Bérengier, M. C., Stinson, M. R., Daigle, G. A., and Hamet, J. F. (1997). Porous Road Pavements: Acoustical Characterization and Propagation Effects. The Journal of the Acoustical Society of America, 101(1).

62. Berge, T. (1996). Noise Control of In-Use Vehicles - New Norwegian Legislation. INTER-NOISE 96, Liverpool, UK.

63. Bergmann, M. (1980). Noise Generation by Tire Vibrations. INTER-NOISE 80, Miami, Florida.

64. Bernhard, R. J., and McDaniel, R. S. (2005). Basics of Noise Generation for Pavement Engineers. Transportation Research Record, 1941, 161-166.

65. Bhushan, B. (2002). Introduction to Tribology, John Wiley and Sons, New York.

66. Bolton, J. S., Song, H. J., Kim, Y. K., and Yeon, J. K. (1998). The Wave Number Decomposition Approach to the Analysis of Tire Vibration. NOISE-CON 1998, Ypsilanti, Michigan.

67. Boullosa, R. R., and Lopez, A. P. (1987). Traffic Noise Spectra in Dry and Wet Street Conditions. Noise Control Engineering Journal, 29(2).

68. Bowden, F. P., and Tabor, D. (1964). The Friction and Lubrication of Solids, Clarendon Press, Oxford, UK.

69. Brackbill, J. U., Kothe, D. B., and Zemach, C. (1992). A Continuum Model for Modeling Surface Tension. Journal of Computational Physics, 100, 335-354.

70. Brennan, M. J., and To, W. M. (2001). Acoustic Properties of Rigid-Frame Porous Materials - An Engineering Perspective. Applied Acoustics, 62(7), 793-811.

71. Brewer, R. A. (1971). Epoxy-Asphalt Open-Graded Pavement as a Skid-Resistant Treatment on the San Francisco-Oakland Bay Bridge. Highway Research Board Special Report 116, 42-47.

72. Brick, H. (2009). Application of the Boundary Element Method to Combustion Noise and Half-Space Problems. Ph.D. thesis, Chalmers University of Technology, Gothenburg, Sweden.

73. Brinkmeier, M., and Nackenhorst, U. (2008). An Approach for Large-Scale Gyroscopic Eigenvalue Problems with Application to High-Frequency Response of Rolling Tires. Computational Mechanics, 41(4), 503-515.

74. Brinkmeier, M., Nackenhorst, U., Petersen, S., and von Estorff, O. (2008). A Finite Element Approach for the Simulation of Tire Rolling Noise. Journal of Sound and Vibration, 309(1), 20-39.

75. Brown, R. (1996). Physical Testing of Rubber, Chapman & Hall, London, UK.

76. Browne, A. L. (1975). Mathematical Analysis for Pneumatic Tire Hydroplaning. Surface Texture Verses Skidding: Measurements, Frictional Aspects, and Safety Features of Tire-Pavement Interaction, J. G. Rose, ed., American Society for Testing and Materials, West Conshohochen, Philadelphia, 75-94.

77. Brownie, R. B. (1977). Porous Friction Surface Runway at USNAS Dallas, Texas. Naval Construction Battalion Center.

78. BRRC (2009). Asphalt Mix Design. Belgian Road Research Center, Brussels, Belgium.

79. Bschorr, O. (1985). Reduction of Tire Noise. INTER-NOISE 85, Munich, Germany.

80. BSI (2000a). Methods for Measuring the Skid Resistance of Pavement Surfaces: Test Method for Measurement of Surface Skid Resistance Using the GripTester Braked Wheel Fixed Slip Device. BS 7941-2, British Standards Institution, London, UK.

81. BSI (2000b). Sampling and Examination of Bituminous Mixtures for Roads and Other Paved Areas: Methods of Test for the Determination of Texture Depth. BS 598-105, British Standards Institution, London, UK.

82. BSI (2005). Coated Macadam (Asphalt Concrete) for Roads and Other Paved Areas - Part 1: Specification for Constituent Materials and for Mixtures. BS 4987-1, British Standard Institution, London, UK.

83. BSI (2006). Bituminous Mixtures: Material Specifications: Porous Asphalt. BS EN 13108-7, British Standards Institute, London, UK.

84. BSI (2009). Tests for Mechanical and Physical Properties of Aggregates: Determination of the Polished Stone Value. BS EN 1097-8, British Standards Institution, London, UK.

85. Bueno, M., Luong, J., Viñuela, U., Terán, F., and Paje, S. E. (2011). Pavement Temperature Influence on Close Proximity Tire/Road Noise. Applied Acoustics, 72(11), 829-835.

86. Burchett, J. L., and Rizenbergs, R. L. (1980). Seasonal Variations in the Skid Resistance of Pavements in Kentucky. Transportation Research Record, 788, 6-14.

87. Cameron, A. (1976). Basic Lubrication Theory, Wiley, New York.

88. Camomilla, G., Malgarini, M., and Gervasio, S. (1990). Sound Absorption and Winter Performance of Porous Asphalt Pavement. Transportation Research Record, 1265, 1-8.

89. Cao, C. (2010). Skid Resistance and Hydroplaning Analysis of Rib Truck Tire. Master thesis, National University of Singapore, Singapore.

90. Carslaw, H. S., and Jaeger, J. C. (1959). Conduction of Heat in Solids, Oxford University Press, London, UK.

91. Cenek, P. D., Davies, R. B., Loader, M., and McLarin, M. W. (2004). Crash Risk Relationships for Improved Safety Management of Roads. The New Zealand Transport Agency, Wellington, New Zealand.

92. Cesbron, J., Anfosso-Lédéé, F., Duhamel, D., Yin, H. P., and Houédec, D. L. (2009). Experimental Study of Tire/Road Contact Forces in Rolling Conditions for Noise Prediction. Journal of Sound and Vibration, 320(1), 125-144.

93. Champoux, Y., and Stinson, M. R. (1992). On Acoustical Models for Sound Propagation in Rigid Frame Porous Materials and the Influence of Shape Factors. The Journal of the Acoustical Society of America, 92(2).

94. Charbeneau, R. J., and Barrett, M. E. (2008). Drainage Hydraulics of Permeable Friction Courses. Water Resources Research, 44.

95. Charbeneau, R. J., Klenzendorf, J. B., and Barrett, M. E. (2011). Methodology for Determining Laboratory and in Situ Hydraulic Conductivity of Asphalt Permeable Friction Course. Journal of Hydraulic Engineering, 137(1), 15-22.

96. Cho, J. R., Kim, K. W., Jeon, D. H., and Yoo, W. S. (2005). Transient Dynamic Response Analysis of 3-D Patterned Tire Rolling over Cleat. European Journal of Mechanics - A/Solids, 24(3), 519-531.

97. Choubane, B., Holzshuher, D. R., and Gokhale, S. (2003). Precision of Locked Wheel Testers for Measurement of Roadway Surface Friction Characteristics. State Materials Office, Florida.

98. Chuai, C. T. (1998). Measurement of Drainage Properties of Porous Asphalt Mixtures. Ph.D thesis., National University of Singapore, Singapore.

99. Clapp, T. G., and Eberhardt, A. C. (1984). Spectral Correlation Techniques Applied to Evaluate Noise and Safety Tradeoffs in Tire/Pavement Interaction. Journal of Vibration, Acoustics, Stress and Reliability in Design, 106(2), 258-262.

100. Clapp, T. G., Eberhardt, A. C., and Kelley, C. T. (1987). Tire/Pavement Contact Force Modeling - Investigation of the Tire/Pavement Interaction Mechanism: Phase III - Final Report. U.S. Department of Transportation, Washington D.C.

101. Clapp, T. G., Eberhardt, A. C., and Kelley, C. T. (1988). Development and Validation of a Method for Approximating Road Surface Texture-Induced Contact Pressure in Tire-Pavement Interaction. Tire Science and Technology, 6(1), 2-17.

102. Clemmer, H. F. (1958). Supplemental Tests of Pavement Skidding Resistance with a 3-Wheel Trailer. Highway Research Board Bulletin, 186, 48-53.

103. Cooley, L. A., Brumfield, J. W., Mallick, R. B., Mogawer, W. S., Partl, M., Poulikakos, L., and Hicks, G. (2009). Construction and Maintenance Practices for Permeable Friction Courses. Transportation Research Board, Washington D.C.

104. Coulomb, C. A. (1785). Theorie des Machines Simpes, En Ayant Egard au Frottement de Leurs Parties, et la Roideur des Ordages. Mem Math Phys Paris, x, 161-342.

105. Council, F., Zaloshnja, E., Miller, T., and Persaud, B. (2005). Crash Cost Estimates by Maximum Police-Reported Injury Severity Within Selected Crash Geometries. Federal Highway Administration, U.S. Department of Transportation, Washington D.C.

106. Cybenko, G. (1989). Approximations by Superpositions of Sigmoidal Functions. Mathematics of Control, Signals, and Systems, 2(4), 303-314.

107. Dahir, S. H., Henry, J. J., and Meyer, W. E. (1979). Seasonal Skid Resistance Variations. Federal Highway Administation, Harrisburg, Pennsylvania.

108. Dare, T., and Bernhard, R. (2009). Predicting Tire-Pavement Noise on Longitudinally Ground Pavements Using a Nonlinear Model. INTER-NOISE 09, Wttawa, Canada.

109. Dare, T. P. (2012). Generation Mechanisms of Tire-Pavement Noise. Ph.D. thesis, Purdue University, West Lafayette, Indiana.

110. Davis, R. M. (2001). Comparison of Surface Characteristics of Hot-Mix Asphalt Pavement Surfaces at the Virginia Smart Road. Master thesis, Virginia Polytechnic Institute and State University, Blacksburg, Virginia.

111. De Toffol, S., Laghari, A. N., and Rauch, W. (2009). Are Extreme Rainfall Intensities More Frequent? Analysis of Trends in Rainfall Patterns Relevant to Urban Drainage Systems. Water Science and Technology: A Journal of the International Association on Water Pollution Research, 59(9), 1769-1776.

112. DEFRA (2013). Noise Pollution: Economic Analysis. Department for Environment, Food and Rural Affairs, London, UK.

113. Delanne, Y., and Gothie, M. (2005). Influence of Road Wetness on the Skid Resistance Performance of Tires. Bulletin des Laboratoires des Ponts et Chaussees, 255, 23-34.

114. Dell'Acqua, G., De Luca, M., Russo, F., and Lamberti, R. (2012). Analysis of Rain-Related Crash Risk on Freeway Pavements in Porous and Dense Asphalt. Transportation Research Board 91st Annual Meeting, Washington D.C.

115. den Boer, L. C., and Schroten, A. (2007). Taffic Noise Reduction in Europe: Health Effects, Social Costs and Technical and Policy Options to Reduce Road and Rail Traffic Noise. Delft, the Netherlands.

116. der Graaff, D. F., Peeters, A. A. A., and Peeters, H. M. (2005). Tyre/Road Noise Measurements of Truck Tyres. Ministry of Transport, Public Works and Water Management, the Netherlands.

117. Desaguliers, J. T. (1734). A Course of Experimental Philosophy. London, UK.

118. Descornet, G. (2000). Vehicle Noise Emission on Wet Road Surfaces. INTER-NOISE 00, Nice, France.

119. Descornet, G., and Sandberg, U. (1980). Road Surface Influence on Tire Noise. INTER-NOISE 80, Miami, Florida.

120. Deuss, H. (1994). The Skid Resistance of Porous Asphalt Wearing Courses in the Netherlands. European Asphalt Magazine, 28-29.

121. Dijks, A. (1976). Influence of Tread Depth on Wet Skid Resistance of Tires. Transportation Research Record, 621, 136-147.

122. Donavan, P. R. (2008). Comparative Measurements of Tire/Pavement Noise in Europe and the United States - NITE I. INTER-NOISE 08, Shanghai, China.

123. Donavan, P. R., and Lodico, D. M. (2009). Measuring Tire-Pavement Noise at the Source. Transportation Research Board of the National Academies, Washington D.C.

124. Donavan, P. R., and Lodico, D. M. (2009). Tire/Pavement Noise of Test Track Surfaces Designed to Replicate California Highways. INTER-NOISE 09, Ottawa, Canada.

125. Donavan, P. R., and Oswald, L. J. (1980). The Identification and Quantafication of Truck Tire Noise Sources Under on-Road Operating Conditions. INTER-NOISE 80, Miami, Florida.

126. Dravitzki, V. (2006). Keeping a Cap on Noise. Land Transport New Zealand, Wellington, New Zealand.

127. Dubois, G., Cesbron, J., Yin, H. P., Anfosso-Ledee, F., and Duhamel, D. (2013). Statistical Estimation of Low Frequency Tyre/Road Noise from Numerical Contact Forces. Applied Acoustics, 74(9), 1085-1093.

128. Dugan, E. L., and Burroughs, C. B. (2003). Measurement of Automobile Tire Tread Vibration and Radiated Noise. NOISE-CON 2003, Cleveland, Ohio.

129. Eberhardt, A. C. (1984). Development of a Transient Response Model for Tire/Pavement Interaction. INTER-NOISE 84, Honolulu, Hawaii.

130. Ejsmont, J. A. (1982). Comparison of Road and Laboratory Measurements and Influence of Some Tire Parameters on Generation of Sound. Swedish Road and Transport Research Institute, Borlänge, Sweden.

131. Ejsmont, J. A. (1990). Side Force Influence on Tire/Road Noise. International Tire/Road Noise Conference 1990, Gothenburg, Sweden.

132. Ejsmont, J. A. (1992). Halas Opon Samochodowych - Wybrane Zagadnienia. Zeszyty Naukowe Politechniki Gdanskiej Nr 498, Mechanika L XVIII.

133. Ejsmont, J. A. (2000). Tire/Road Noise Simulation for Optimization of the Tread Pattern. INTER-NOISE 00, Nice, France.

134. Ejsmont, J. A., and Mioduszewski (1994). Influence of Ambient Temperature on Tire/Road Noise when Measuring with the Drum Method. Mechanical Faculty, Technical University of Gdansk, Gdansk, Poland.

135. Ejsmont, J. A., and Sandberg, U. (1988). Cornering Influence on Tire/Road Noise. INTER-NOISE 88, Avignon, France.

136. Ejsmont, J. A., and Taryma, S. (1982). Halas Opon Samochodow Osobowych Poruszajacych Sie po Suchych Nawierzchniach Asfaltowych I Betonowych. Technical University of Gdansk, Gdansk, Poland.

137. EU (1996). Future Noise Policy - European Commission Green Paper. European Commission, Brussels, Belgium.

138. Ferguson, B. K. (2005). Porous Pavements, CRC Press, Boca Raton, Florida.

139. FHWA (1990). Open Graded Friction Courses. Federal Highway Administration, Washington D.C.

140. FHWA (1998). FHWA Material Notebook. Fedral Highway Administration, Washington D.C.

141. FHWA (2013). Crash Modification Factors in Practice - Quantifying Safety in the Roadway Safety Management Process. Federal Highway Administration, U.S. Department of Transportation, Washington D.C.

142. Flintsch, G. W., De Leon, E., McGhee, K. K., and Al-Qadi, I. L. (2003). Pavement Surface Macrotexture Measurement and Applications. Transportation Research Record, 1860, 168-177.

143. Fong, S. (1998). Tyre Noise Predictions from Computed Road Surface Texture Induced Contact Pressure. INTER-NOISE 98, Christchurch, New Zealand.

144. Forster, S. W. (1989). Pavement Microtexture and its Relation to Skid Resistance. Transportation Research Record, 1215, 151-164.

145. Franklin, R. E., Harland, D. G., and Nelson, P. M. (1979). Road Surfaces and Traffic Noise. Transport and Road Research Laboratory, Crowthorne, UK.

146. Fuentes, L., Gunaratne, M., and Hess, D. (2010). Evaluation of the Effect of Pavement Roughness on Skid Resistance. Journal of Transportation Engineering, 136(7), 640-653.

147. Fujikawa, T., Koike, H., Oshino, Y., and Tachibana, H. (2005). Definition of Road Roughness Parameters for Tire Vibration Noise Control. Applied Acoustics, 66(5), 501-512.

148. Fujikawa, T., Koike, H., Oshino, Y., and Tachibana, H. (2006). Road Texture for Abating Truck Tire Noise Generation. INTER-NOISE 06, Honolulu, Hawaii.

149. Fujiwara, T., Meiarashi, S., Namikawa, Y., and Hasebe, M. (2005). Reduction of Equivalent Continuous A-Weighted Sound Pressure Levels by Porous Elastic Road Surfaces. Applied Acoustics, 66, 766-778.

150. Fwa, T. F., and Ong, G. P. (2008). Wet-Pavement Hydroplaning Risk and Skid Resistance: Analysis. Journal of Transportation Engineering, 134(5), 182-190.

151. Fwa, T. F., Tan, S. A., and Guwe, Y. K. (1999). Laboratory Evaluation of Clogging Potential of Porous Asphalt Mixtures. Transportation Research Record, 1681, 43-49.

152. Gallaway, B. M., Ivey, D. L., Hayes, G., Ledbetter, W. B., Olson, R. M., Woods, D. L., and Schiller, J. R. F. (1979). Pavement and Geometric Design Criteria for Minimizing Hydroplaning. Federal Highway Administration, Washington D.C.

153. Gandhi, P. M., Colucci, B., and Gandhi, S. P. (1991). Polishing of Aggregates and Wet-Weather Accident Rates for Flexible Pavements. Transportation Research Record, 1300, 71-79.

154. Gargett, T. (1990). The Introduction of a Skidding-Resistance Policy in Great Britain. Surface Characteristics of Roadways: International Research and Technologies, W. E. Meyer, and J. Reichert, eds., American Society for Testing and Materials, Philadelphia, Pennsylvania, 30-38.

155. Gauterin, F., and Ropers, C. (2005). Modal Tyre Models for Road Noise Improvement. Vehicle System Dynamics: International Journal of Vehicle Mechanics and Mobility, 43(Supplement 1), 297-304.

156. Gee, K. W. (2005). Surface Texture for Asphalt and Concrete Pavements. Federal Highway Administration, Washington D.C.

157. Gelosa, E., and Cervi, E. (1999). Predictive Model of Noise due to Tire Structural Vibration. 1st International Colloquium on Vehicle Tyre Road Interaction, Rome, Italy.

158. Gengenback, W. (1968). Experimental Investigation of Tires on Wet Tracks. Automobiltechnische Zeitschrift, 70, 310-316.

159. Ghoreishy, M. H. R. (2006). Finite Element Analysis of Steady Rolling Tyre with Slip Angle: Effect of Belt Angle. Plastics, Rubber and Composites, 35(2), 83-90.

160. Gibbs, D., Iwasaki, R., Bernhard, R., Bledsoe, J., Carlson, D., Corbisier, C., Fults, K., Hearne, T., McMullen, J. K., Newcomb, D., Roberts, C. P., Rochat, J., Scofield, L., and Swanlund, M. (2005). Quiet Pavement Systems in Europe. Federal Highway Administration, Washington D.C.

161. Giles, C. G. (1963). Some Recent Developments in Work on Skidding Problems at the Road Research Laboratory. Highway Research Record, 46, 43-59.

162. Giles, C. G., and Lander, F. T. W. (1956). The Skid-Resisting Properties of Wet Surfaces at High Speeds: Exploratory Measurements with a small Breaking Force Trailer. Journal of the Royal Aeronautical Society, 60, 83-94.

163. Giles, C. G., and Sabey, B. E. (1959). A Note on the Problem of Seasonal Variation in Skidding Resistance. The First International Skid Prevention Conference, Virginia.

164. Giles, C. G., and Sabey, B. E. (1959). Recent Investigations on the Rubber Hysteresis in Skidding Resistance Measurements. The First International Skid Prevention Conference, Virginia.

165. Gillespie, T. D. (1992). Fundamentals of Vehicle Dynamics. Society of Automotive Engineers (SAE), Warrendale, Pennsylvania.

166. Gough, V. E. (1958). Friction of Rubber. The Engineer, 701-704.

167. Gough, V. E. (1959). Discussion of Paper by D. Tabor. Revue Generale Du Caoutchouc, 36(10), 1409.

168. Graf, R. A. G., Kuo, C. Y., Dowling, A. P., and Graham, W. R. (2002). On the Horn Effect of a Tyre/Road Interface, Part I: Experiment and Computation. Journal of Sound and Vibration, 256(3), 417-431.

169. Greenwood, J. A., and Tabor, D. (1958). The Friction of Hard Slider and Lubricated Ruber: The Importance of Deformation Losses. Proceedings of the Physical Society, 71(6), 989-1001.

170. Gross, W. A., Matsck, L. A., Castelli, V., Eshel, A., Vohr, J. H., and Wildmann, M. (1980). Fluid Film Lubrication, Wiley, New York.

171. Guan, Y., Zhao, G., and Cheng, G. (2011). 3-Dimensional Non-Linear FEM Modeling and Analysis of Steady-Rolling of Radial Tires. Journal of Reinforced Plastics and Composites, 30(3), 229-240.

172. Guisset, P., and Augusztinovicz, F. (1999). TINO Noise Emission: Analysis and Prediction Models. First International Colloquium on Vehicle Tyre Road Interaction, Rome, Italy.

173. Guo, C. H., and Lancaster, P. (2005). Algorithms for Hyperbolic Quadratic Eigenvalue Problems. Mathematics of Computation, 74(252), 1777-1791.

174. Haas, R., Hudson, W. R., and Zaniewski, J. P. (1994). Modern Pavement Management, Krieger Pub. Co, Malabar, Florida.

175. Haisler, W. E. (1977). AGGIE I. A Finite Element Program for Non-Linear Structural Analysis., Texas A&M University, College Station, Texas.

176. Hall, J. W., Smith, K. L., Titus-Glover, L., Wambold, J. C., Yager, T. J., and Rado, Z. (2009). Guide for Pavement Friction. Transportation Research Board of the National Academies, Washington D.C.

177. Hall, W. (2003). Finite Element Modelling and Simulation for a Smart Tyre. Ph.D. thesis, University of Warwick, Coventry, UK.

178. Hall, W., Mottram, J. T., and Jones, R. P. (2004). Finite Element Simulation of a Rolling Automobile Tyre to Understand its Transient Macroscopic Behaviour. Proceedings of the Institution of Mechanical Engineers, Part D: Journal of Automobile Engineering, 218(12), 1393-1408.

179. Hambleton, J. P., and Drescher, A. (2009). On Modeling a Rolling Wheel in the Presence of Plastic Deformation as a Three- or Two-Dimensional Process. International Journal of Mechanical Sciences, 51(11), 846-855.

180. Hamet, J. F., and Bérengier, M. C. (1993). Acoustical Characteristics of Porous Pavements: A New Phenomenological Model. INTER-NOISE 93, Leuven, Belgium, 641-646.

181. Hamet, J. F., and Klein, P. (2000). Road Texture and Tire Noise. INTER-NOISE 00, Nice, France.

182. Hamrock, B. J. (1994). Fundamentals of Fluid Film Lubrication, McGraw-Hill, New York.

183. Hegmon, R. R. (1969). The Contribution of Deformation Losses to Rubber Friction. Rubber Chemistry and Technology, 42(4), 1122-1135.

184. Henry, J. J. (1986) Tire Wet-Pavement Traction Measurement: A State-of-the-Art Review. Conference of Tire Pavement Interface, Columbu, Ohio.

185. Henry, J. J. (2000). Evaluation of Pavement Friction Characteristics: A Synthesis of Highway Practice. Transportation Research Board, National Research Council, Washington D.C.

186. Henry, J. J., and Meyer, W. E. (1983). The Simulation of Tire Tractions on Wet Pavements. 18th International Automobile Technical Congress, Hamburg, Germany, 121-128.

187. Hershfield, D. M. (1984). Extreme Rainfall Intensities. Archives for Meteorology, Geophysics, and Bioclimatology Series B, 35(1-2), 67-80.

188. Highway Research Board (1972). Skid Resistance. Highway Research Board, Washington D.C.

189. Hirt, C. W. and Nichols, B. D. (1981). Volume of Fluid (VOF) Method for the Dynamics of Free Boundaries. Journal of Computational Physics, 39(1), 201-225.

190. Holmes, K. E. (1970). Braking Force/Braking Slip Measurements Over a Range of Conditions Between 0 and 100 Percent Slip. Road Research Laboratory, Crowthorne, Berkshire.

191. Hori, H., and Furusato, N. (2001). Development of Porous Asphalt Pavement Using Rubber Particles. Journal of Pavement Engineering, 6, 11-18.

192. Horne, W. B. (1969). Results from Studies of Highway Grooving and Texturing at NASA Wallops Station. NASA Langley Research Center, Hampton, Virginia.

193. Horne, W. B., and Dreher, R. C. (1963). Phenomena of Pneumatic Tire Hydroplaning. National Aeronautics and Space Administration.

194. Hossain, M., Scofield, L. A., and Meier, W. R. J. (1992). Porous Pavement for Control of Highway Runoff in Arizona: Performance to Date. Transportation Research Record, 1354, 45-54.

195. Hubelt, J. (2003). Modeling of Porous Asphalt as Extended Reacting Absorber Using the Transmission-Line-Matrix-Method (TLM). EURO-NOISE 03, Naples, Italy.

196. Huddleston, I. J., Zhou, H., and Hicks, R. G. (1991) Performance Evaluation of Open-Graded Asphalt Concrete Mixtures Used in Oregon. Asphalt Paving Technology 1991, Seattle, Washington.

197. Huddleston, I. J., Zhou, H., and Hicks, R. G. (1993). Evaluation of Open-Graded Asphalt Concrete Mixture Used in Oregon. Transportation Research Record, 1427, 5-12.

198. Isenring, T., Koester, H., and Scazziga, I. (1990). Experiences with Porous Asphalt in Switzerland. Transportation Research Record, 1265, 41-53.

199. Ishida, S. M. M., Fujiwara, T., Hasebe, M., and Nakatsuji, T. (1996). Noise Reduction Characteristics of Porous Elastic Road Surfaces. Applied Acoustics, 47(3), 239-250.

200. ISO (1997a). Acoustics - Measurement of the Influence of Road Surfaces on Traffic Noise - Part 1: Statistical Pass-By Method. ISO 11819-1, International Organization for Standardization, Geneva, Switzerland.

201. ISO (1997b). Characterization of Pavement Texture by Use of Surface Profiles - Part 1: Determination of Mean Profile Depth. ISO 13473-1, International Organization for Standardization, Geneva, Switzerland.

202. ISO (2002). Acoustics - Measurement of Sound Absorption Properties of Road Surfaces in Situ - Part 1: Extended Surface Method. ISO 13472-1, International Organization for Standardization, Geneva, Switzerland.

203. ISO (2003). Tyres - Coast-By Methods for Measurement of Tyre-to-Road Sound Emission. ISO 13325, International Organization for Standardization, Geneva, Switzerland.

204. ISO (2008). Characterization of Pavement Texture by Use of Surface Profile - Part 4: Spectral Analysis of Surface Profiles. ISO/TS 13473-4, International Orgnization for Standardization, Geneva, Switzerland.

205. ISO (2010). Acoustics - Measurement of Sound Absorption Properties of Road Surfaces in Situ - Part 2: Spot Method for Reflective Surfaces. ISO 13472-2, International Organization for Standardization, Geneva, Switzerland.

206. ISO (2013). Acoustics - Method for Measuring the Influence of Road Surfaces on Traffic Noise - Part 2: Close-Proximity Method (Draft). ISO/DIS 11819-2, International Organization for Standardization, Geneva, Switzerland.

207. Ivan, J. N., Ravishanker, N., Jackson, E., Aronov, B., and Guo, S. (2012). A Statistical Analysis of the Effect of Wet-Pavement Friction on Highway Traffic Safety. Journal of Transportation Safety & Security, 4(2), 116-136.

208. Ivannikov, A., Haberkorn, U., and Langenberg, H. (1998). Einflussgrössen auf Reifen/Fahrbahn-Geräusche eines LKW bei Unterschiedlichen Fahrbedingungen. Forschungsvereinigung Automobiltechnik e.v., Germany.

209. Iwai, S., Miura, Y., Koike, H., and Levy, G. (1994). Inflence of Porous Asphalt Pavement Characteristics on the Horn Amplification of Tire/Road Contact Noise. INTER-NOISE 94, Yokohama, Japan.

210. Izevbekhai, B. I. (2012). Tire-Pavement Interaction Noise of Concrete Pavements. Ph.D. thesis, University of Minnesota, Minneapolis, Minnesota.

211. Jackson, N. M., Choubane, B., Holzschuher, C., and Gokhale, S. (2005). Measuring Pavement Friction Characteristics at Variable Speeds for Added Safety. Journal of ASTM International, 2(10).

212. Jarlebring, E., Michiels, W., and Meerbergen, K. (2012). A Linear Eigenvalue Algorithm for the Nonlinear Eigenvalue Problem. Numerische Mathematik, 122(1), 169-195.

213. Jayawichrama, P. W., Prasanna, R., and Senadheera, S. P. (1996). Survey of State Practices to Control Skid Resistance on Hot-Mix Asphalt Concrete Pavements. Transportation Research Record, 1536, 52-58.

214. Jayawickrama, P. W., and Graham, G. L. (1995). Use of Skid Performance History as Basis for Aggregate Qualification for Seal Coats and Hot-Mix Asphalt Concrete Surface Courses. Transportation Research Record, 1501, 31-38.

215. Jayawickrama, P. W., and Thomas, B. (1998). Correction of Field Skid Measurements for Seasonal Variations in Texas. Transportation Research Record, 1639, 147-154.

216. Jeong, J. Y., and Jeong, H. Y. (2013). Hydroplaning Simulation of a Tire in Thin Water Using FEM and an Estimation Method and its Application to Skid Number Estimation. International Journal of Automotive Technology, 14(2), 325-331.

217. Johnson, A. R., Tanner, J. A., and Mason, A. J. (1999). Quasi-Static Viscoelastic Finite Element Model of an Aircraft Tire. National Aeronautics and Space Administration, Langley Research Center, Hampton, Virginia.

218. Kandhal, P. S., and Mallick, R. B. (1998). Open Graded Asphalt Friction Course: State of the Practice. National Center for Asphalt Technology, Auburn, Alabama.

219. Kelly, J. D. (1968). Factors Affecting Passenger Tire Traction on the Wet Road. Society of Automotive Engineers, SAE Technical Paper 680138.

220. Khalid, H., and Pérez, F. (1996). Performance Assessment of Spanish and British Porous Asphalts, E & FN Spon, London, UK.

221. Kilmer, R. D. (1976). Test Procedures for Future Tire Noise Regulations. SAE Highway Tire Noise Symposium, San Francisco Society of Automotive Engineers, Warrendale, Pennsylvania.

222. Kim, B. S. (2003). Sound Radiation due to Tire Tread Vibration. JSME International Journal. Ser. C, Mechanical Systems, Machine Elements and Manufacturing, 46(2), 675-682.

223. Kim, B. S., Kim, G. J., and Lee, T. K. (2007). The Identification of Sound Generating Mechanisms of Tyres. Applied Acoustics, 68(1), 114-133.

224. Kim, H. K., and Lee, H. K. (2010). Acoustic Absorption Modeling of Porous Concrete Considering the Gradation and Shape of Aggregates and Void Ratio. Journal of Sound and Vibration, 329(7), 866-879.

225. Kim, S., Jeong, W., Park, Y., and Lee, S. (2006). Prediction Method for Tire Air-Pumping Noise Using a Hybrid Technique. Journal of the Acoustical Society of America, 119(6), 3799-3812.

226. Kim, Y. J., and Bolton, J. S. (2004). Effects of Rotation on the Dynamics of a Circular Cylindrical Shell with Application to Tire Vibration. Journal of Sound and Vibration, 275(3), 605-621.

227. Kinsler, L. E., Frey, A. R., Coppens, A. B., and Sanders, J. V. (2000). Fundamentals of Acoustics, John Wiler & Sons, Inc, New York.

228. Klein, P., and Hamet, J. F. (2007). Tyre/Road Prediction with the HyRoNE Model. INTER-NOISE 07, Istanbul, Turkey.

229. Koiki, H., Fujikawa, T., Oshino, Y., and Tachibana, H. (1999). Generation Mechanism of Tire/Road Noise Part 2: Pipe Resonance in Tread Groove of Tire. INTER-NOISE 99, Fort Lauderdale, Florida.

230. Kokkalis, A. G., and Panagouli, O. K. (1998). Fractal Evaluation of Pavement Skid Resistance Variations. I: Surface Wetting. Chaos, Solitons and Fractals, 9(11), 1875-1890.

231. Köllman, A. (1993). Ermittlung des Standes der Technik Hinsichtlich der Geräuschemission von PKW-Reifen. FIGE GmbH, Herzogenrath, Germany.

232. Kowalski, K., McDaniel, R. S., Shah, A., and Olek, J. (2009). Long-Term Monitoring of Noise and Frictional Properties of Three Pavements: Dense-Graded Asphalt, Stone Matrix Asphalt, and Porous Friction Course. Transportation Research Record, 2127, 12-19.

233. Kozhevnikov, I. F. (2012). Vibrations of a Rolling Tyre. Journal of Sound and Vibration, 331(7), 1669-1685.

234. Kroger, M., Lindner, M., and Popp, K. (2004). Inflence of Friction on Noise and Vibrations of Tyres. INTER-NOISE 04, Prague, Czech Republic.

235. Kropp, W. (1989a). Structure-Borne Sound on a Smooth Tyre. Applied Acoustics, 26(3), 181-192.

236. Kropp, W. (1989b). A Simple Model of Wave Excitation and Propagation on a Rolling Tire. Workshop on Rolling Noise Generation, Technical University of Berlin, Berlin, Germany.

237. Kropp, W. (1992). Ein Modell zur Beschreibung des Rollgeräusches eines Unprofilierten Gürtel reifens auf Rauher Straßenoberfläche . VDI Verl ., Düsseldorf.

238. Kropp, W., Bécot, F. X., and Barrelet, S. (2000). On the Sound Radiation from Tires. Acta Acoustica, 86(5), 769-779.

239. Kropp, W., Sabiniarz, P., Brick, H., and Beckenbauer, T. (2012). On the Sound Radiation of a Rolling Tyre. Journal of Sound and Vibration, 331(8), 1789-1805.

240. Kuang, X., and Fu, Y. (2013). Coupled Infiltration and Filtration Behaviours of Concrete Porous Pavement for Stormwater Management. Hydrological Processes, 27(4), 532-540.

241. Kuang, X., Sansalone, J., Ying, G., and Ranieri, V. (2011). Pore-Structure Model of Hydraulic Conductivity for Permeable Pavement. Journal of Hydrology, 399, 148-157.

242. Kuemmel, D. A., Sonntag, R. C., Jaeckel, J. R., Crovetti, J. A., Becker, Y. Z., and Satanovsky, A. (2000). Using a Road Surface Analyzer to Explain Noise Characteristics of Portland Cement Concrete Pavement Surface Texture. Transportation Research Record, 1716, 144-153.

243. Kuijpers, A., and van Blokland, G. (2001). Tyre/Road Noise Models in the Last Two Decades: A Critical Evaluation. INTER-NOISE 01, the Hague, the Netherlands.

244. Kuijpers, A. H. W. M. (2001). Further Analysis of the Sperenberg Data – Towards a Better Understanding of the Processes Influencing Tyre/Road Noise. M+P raadgevende ingenieurs b.v., 's-Hertogenbosch, the Netherlands.

245. Kuijpers, A. H. W. M., Peeters, H. M., Kropp, W., and Beckenbauer, T. (2007). Acoustic Optimization Tool - Modeling Refinements in the SPERoN Framework. M+P Consulting Engineers, Vught, the Netherlands.

246. Kulakowski, B. T., Harwood, D., Hiltunen, D., Mason, J., Meyer, W. E., Simoniau, S., and Wambold, J. C. (1990). Skid Resistance Manual. Federal Highway Administration, Washington D.C.

247. Kulakowski, B. T., and Meyer, W. E. (1989). Skid Resistance of Adjacent Tangent and Nontangent Sections of Roads. Transportation Research Record, 1215, 132-136.

248. Kummer, H. W. (1966). Unified Theory of Rubber and Tire Friction. Philadelphia.

249. Kummer, H. W., and Meyer, W. E. (1967). Tentative Skid-Resistance Requirements for Main Rural Highways. Highway Research Board, Washington D.C.

250. Kung, L. E., Soedel, W., Yang, T. Y., and Charek, L. T. (1985). Natural Frequencies and Mode Shapes of an Automotive Tire with Interpretation and

Classification Using 3-D Computer Graphics. Journal of Sound and Vibration, 102(3), 329-346.

251. Lamm, R., Mailaender, T., and Psarianos, B. (1999). Highway Design and Traffic Engineering Handbook, McGraw-Hill, New York.

252. Lander, F. T. W., and Williams, T. (1968). The Skidding Resistance of Wet Runway Surfaces with Reference to Surface Texture and Tire Conditions. Road Research Laboratory, Crowthorne, UK.

253. Landsberger, B. J., DeMoss, J., and McNerney, M. (2001). Effects of Air and Road Surface Temperature on Tire Pavement Noise on an ISO 10844 Surface. Society of Automotive Engineers, Warrendale, Pennsylvania.

254. Langousis, A., and Veneziano, D. (2009). Extreme Rainfall Intensities and Long-Term Rainfall Risk from Tropical Cyclones. European Geosciences Union General Assembly, European Geosciences Union, Vienna, Austria.

255. Larsson, K. (2000). A Rolling Contact Model Using Green's Functions. INTER-NOISE 00, Nice, France.

256. Larsson, K., Barrelet, S., and Kropp, W. (1999). Modelling of Tangential contact Forces. The 2nd Convention of the European Acoustics Association – Forum Acousticus, Berlin, Germany.

257. Lee, Y. P. K. (2005). Analyzing Laboratory Skid Resistance Test Using Finite Element Modeling. Ph.D thesis, National University of Singapore, Singapore.

258. Legret, M., Colandini, V., and Le Marc, C. (1996). Effects of a Porous Pavement with Reservoir Structure on the Quality of Runoff Water and Soil. Science of the Total Environment, 189-190, 335-340.

259. Leland, T. J. W., and Taylor, G. R. (1965). An Investigation of the Influence of Aircraft Tire Tread Wear on Wet Runway Braking. National Aeronautics and Space Administration, Springfield, Virginia.

260. Leland, T. J. W., Yager, T. J., and Joyner, U. T. (1968). Effects of Pavement Texture on Wet Runway Braking Performance. National Aeronautics and Space Administration, Washington D.C.

261. Leonardo, d. V., and MacCurdy, E. (1948). The Notebooks of Leonardo da Vinci, Jonathan Cape, London, UK.

262. Liu, K. W., Alvarez, A. E., Martin, A. E., Dossey, T., Smit, A., and Estakhri, C. K. (2010). Synthesis of Current Research on Permeable Friction Courses: Performance, Design, Construction, and Maintenance. Texas Department of Transportation and Fedral Highway Administration, Austin, Texas.

263. Liu, Q., and Cao, D. (2009). Research on Material Composition and Performance of Porous Asphalt Pavement. Journal of Materials in Civil Engineering, 21(4), 135-140.

264. Liu, Y. (2004). Evaluation of British Pendulum Tester for Laboratory Pavement Skid Resistance Measurements. Master thesis, National University of Singapore, Singapore.

265. Liu, Y., Fwa, T. F., and Choo, Y. S. (2003). Finite-Element Modeling of Skid Resistance Test. Journal of Transportation Engineering, 129(3), 316-321.

266. Lopez, I., Blom, R. E. A., Roozen, N. B., and Nijmeijer, H. (2007). Modelling Vibrations on Deformed Rolling Tyres - A Modal Approach. Journal of Sound and Vibration, 307(3-5), 481-494.

267. Losa, M., and Leandri, P. (2012). A Comprehensive Model to Predict Acoustic Absorption Factor of Porous Mixes. Materials and Structures, 45(6), 923-940.

268. Losa, M., Leandri, P., and Bacci, R. (2010). Empirical Rolling Noise Prediction Models Based on Pavement Surface Characteristics. Road Materials and Pavement Design, 11(Supplement 1), 487-506.

269. Lowne, R. W. (1970). The Effect of Road Surface Texture on Tire Wear. Wear, 15(1), 57-70.

270. Lui, W. K., and Li, K. M. (2004). A Theoretical Study for the Propagation of Rolling Noise Over a Porous Road Pavement. Journal of the Acoustical Society of America, 116(1), 313-322.

271. Mak, K. L., Lee, S. H., Ho, K. Y., and Hung, W. T. (2011). Developing Instantaneous Tyre/Road Noise Profiles: A Note. Transportation Research Part D: Transport and Environment, 16(3), 257-259.

272. Mallick, R. B., and El-Korchi, T. (2013). Pavement Engineering: Principles and Practice, Taylor & Francis, Boca Raton, Florida.

273. Mallick, R. B., Kandlal, P. S., Cooley, L. A., and Watson, D. E. (2000). Design, Construction and Performance of New Generation Open-Graded Friction Course. Journal of the Association of Asphalt Paving Technologists, 69, 391-423.

274. Marick, L. (1959). Frictors in Tires that Influence Skid Resistance, Part II: The Effect of Tread Design. The First International Skid Prevention Conference, Virginia Council of Highway Investigation and Research, Virginia, 155-162.

275. Martin, G. E. (1939). Report on Committee on Anti-Skid Properties of Road Surfaces. 19th Highway Research Board Annual Meeting, Washington D.C., 126-128.

276. Martín, M. A., Tarrero, A., González, J., and Machimbarrena, M. (2006). Exposure-Effect Relationships Between Road Traffic Noise Annoyance and Noise Cost Valuations in Valladolid, Spain. Applied Acoustics, 67, 945-958.

277. Masad, E., Al-Rousan, T., Button, J., Little, D., and Tutumluer, E. (2005). Test Methods for Characterizing Aggregate Shape, Texture and Angularity. National Research Council, Washington D.C.

278. Maycock, G. (1967). Experiments on Tire Tread Patterns. Road Research Laboratory, Crowthorne, UK.

279. Mayora, P. J. M., and Piña, J. R. (2009). An Assessment of the Skid Resistance Effect on Traffic Safety Under Wet-Pavement Conditions. Accident Analysis and Prevention, 41(4), 881-886.

280. McDaniel, R. S., Thornton, W. D., and Dominguez, J. G. (2004). Field Evaluation of Porous Asphalt Pavement. North Central Superpave Center, Purdue University, West Lafayette, Indiana.

281. McGhee, K. K., and Clark, T. M. (2010). Functionally Optimized Wearing Course: Installation Report. Transportation Research Record, 2180, 150-155.

282. McGhee, K. K., Clark, T. M., and Hemp, C. C. (2009). A Functionally Optimized Hot-Mix Asphalt Wearing Course: Part I: Preliminary Results. Virginia Transportation Research Council, Charlottesville, Virginia.

283. McGovern, C., Rusch, P., and Noyce, D. A. (2011). State Practices to Reduce Wet Weather Skidding Crashes. Federal Highway Administration, U.S. Department of Transportation, Washington D.C.

284. McLean, J., and Foley, G. (1998). Road Surface Characteristics and Condition – Effects on Road Users. ARRB Transport Research Ltd, Vermont South, Australia.

285. Meng, L. (2002). Truck Tire/Pavement Interaction Analysis by the Finite Element Method. Ph.D thesis, Michigan State University, East Lansing, Michigan.

286. Mercer, J. S. (1958). Locked Wheel Skid Performance of Various Tires on Clean, Dry Road Surfaces. Highway Research Board Bulletin, 186, 8-25.

287. Meyer, W. E. (1991). Pavement Texture Significance and Measurement. Standardization News, 19(2), 28-31.

288. Michael, H. L., and Grunau, D. L. (1956). Development of Skid Testing in Indiana. Highway Research Board Bulletin, 139, 60-78.

289. Miller, T., Swiertz, D., Tashman, L., Tabatabaee, N., and Bahia, H. U. (2012). Characterization of Asphalt Pavement Surface Texture. Transportation Research Record, 2295, 19-26.

290. Miró, R., Pèrez-Jimènez, F., Martìnez, A. H., Reyes-Ortiz, O., Paje, S. E., and Bueno, M. (2009). Effect of Crumb Rubber Bituminous Mixes on Functional Characteristics of Road Pavements. Transportation Research Record, 2126, 83-90.

291. Molisani, L. R., Burdisso, R. A., and Tsihlas, D. (2003). A Coupled Tire Structure/Acoustic Cavity Model. International Journal of Solids and Structures, 40(19), 5125-5138.

292. Moore, D. F. (1966). Prediction of Skid-Resistance Gradient and Drainage Characteristics for Pavement. Highway Research Record, 131, 181-203.

293. Moore, D. F. (1969). A History of Research on Surface Texture. Wear, 13(6), 381-412.

294. Moore, D. F. (1972). The Friction and Lubrication of Elastomers, Pergamon Press, Oxford, UK.

295. Moore, D. F. (1975). Principles and Applications of Tribology, Pergamon Press, Oxford, UK.

296. Moore, D. F., and Geyer, W. (1972). A Review of Adhesion Theories for Elastomers. Wear, 22(2), 113-141.

297. Moore, D. F., and Geyer, W. (1974). A Review of Hysteresis Theories for Elastomers. Wear, 30(1), 1-34.

298. Moore, L. M., Hicks, R. G., and Rogge, D. F. (2001). Design, Construction, and Maintenance Guidelines for Porous Asphalt Pavements. Transportation Research Record, 1778, 91-99.

299. Möser, M. (2009). Engineering Acoustics: An Introduction to Noise Control, Springer Berlin Heidelberg, Berlin,Germany.

300. Moyer, R. A. (1933). Skidding Characteristics of Road Surfaces. Thirteenth Highway Research Board Annual Meeting, Washington D.C.

301. Moyer, R. A. (1935). Further Skidding Tests with Particular Reference to Curves. Fourteenth Highway Research Board Annual Meeting, Washington D.C., 123-130.

302. Moyer, R. A. (1959). A Review of the Variables Affecting Pavement Slipperiness. The First International Skid Prevention Conference, Virginia, 411-433.

303. Moyer, R. A. (1963). California Skid Tests with Butyl Rubber Tires and Report of Visit to Road Research Laboratories in Europe Engaged in Skid Prevention Research. Highway Research Record, 28, 32-62.

304. Mullen, W. G. (1972). Skid Resistance and Wear Properties of Aggregates for Paving Mixtures. North Carolina State University, Raleigh, North Carolina.

305. Muthukrishnan (1990). Effects of Material Properties on Tire Noise. Society of Automotive Engineers, Warrendale, Pennsylvania.

306. Nackenhorst, U. (2004). The ALE-Formulation of Bodies in Rolling Contact. Computer Methods in Applied Mechanics and Engineering, 193(39), 4299-4322.

307. Nakahara, D., Nota, E., and Endo, K. (2004). Utilization of Pavement Quality Pervious Concrete and its Performance. 9th Symposium on Concrete Pavement, Istanbul, Turkey.

308. NCHRP (1978). Open-Graded Friction Courses for Highways. Synthesis of Highway Practice, Transportation Research Board, National Research Council, Washington D.C.

309. Neithalath, N., Marolf, A., Weiss, J., and Olek, J. (2005). Modeling the Influence of Pore Structure on the Acoustic Absorption of Enhanced Porosity Concrete. Journal of Advanced Concrete Technology, 3(1), 29-40.

310. Nelson, P. M. (1986). Rubber Tyre Noise Generation. Wear, 113(1), 171-174.

311. Nelson, P. M., and Phillips, S. M. (1997). Quieter Road Surfaces. TRL Annual Review 1997, Transport Research Laboratory, Crowthorne, UK, 25-37.

312. Newton, P. W., Baum, S., Bhatia, K., Brown, S. K., Cameron, S., Foran, B., Grant, T., Mak, S. L., Memmott, P., Mitchell, V. G., Neate, K., Smith, N. C., Stimson, R., Pears, A., Tucker, S., and Yencken, E. D. (2001). Australia State of the Environment Report 2001: Human Settlements Theme Report. The Commonwealth Scientific and Industrial Research Organisation, Canberra, Australia.

313. Nicholls, J. C. (1998). Asphalt Surfacing, CRC Press, London, UK.

314. Nichols, F. P., Dillard, J. H., and Alwood, R. L. (1956). Skid Resistant Pavement in Virginia. Highway Research Board Bulletin, 139, 35-58.

315. Nilsson, N. Å. (1979). Possible Method of Reducing External Tyre Noise. The International Tire Noise Conference 1979, Stockholm, Sweden.

316. Nilsson, N. Å. (1980). External Tire/Road Noise from Trailing Contact Edge - the Excitation Process. IFM Akustikbyrån AB, Stockholm, Sweden.

317. Nilsson, N. Å. (1982). Principles in the Control of External Tire/Road Noise. INTER-NOISE 82, San Francisco, California.

318. Nilsson, N. Å., Bennerhult, O., and Soederqvist, S. (1980). External Tire/Road Noise: Its Generation and Reduction. INTER-NOISE 80, Miami, Florida.

319. Nilsson, N. Å., Söderqvist, S., and Bennerhult, O. (1979). Air-Resonant Radiation - An Experimental Study: Measurement Methods. IFM Akustikbyrån AB, Stockholm, Sweden.

320. O'Boy, D. J., and Dowling, A. P. (2009). Tyre/Road Interaction noise - Numerical Noise Prediction of a Patterned Tyre on a Rough Road Surface. Journal of Sound and Vibration, 323(1), 270-291.

321. OECD (1984). Road Surface Characteristics - Their Interaction and Their Optimisation. Organisation for Economic Cooperation and Development, Road Research Group, Paris, France.

322. Offenberg, M. A., Wade, D. J. and Weiss, Jr. C. A. (2010). Report on Pervious Concrete. American Concrete Institute, Farmington Hill, Michigan.

323. Ong, G. P., and Fwa, T. F. (2006). Transverse Pavement Grooving Against Hydroplaning I: Simulation Model. Journal of Transportation Engineering, 132(6), 441-448.

324. Ong, G. P., and Fwa, T. F. (2007a). Wet-Pavement Hydroplaning Risk and Skid Resistance: Modeling. Journal of Transportation Engineering, 133(10), 590-598.

325. Ong, G. P., and Fwa, T. F. (2007b). Prediction of Wet-Pavement Skid Resistance and Hydroplaning Potential. Transportation Research Record, 2005, 160-171.

326. Ong, G. P., and Fwa, T. F. (2008). Wet-Pavement Hydroplaning Risk and Skid Resistance: Analysis. Journal of Transportation Engineering, 134(5), 182-190.

327. Ong, G. P., and Fwa, T. F. (2010). Modeling Skid Resistance of Commercial Trucks on Highways. Journal of Transportation Engineering, 136(6), 510-517.

328. Oshino, Y., Mikami, T., and Tachibana, H. (2001). Study of Road Surface Indices for the Assessment of Tire/Road Noise. INTER-NOISE 01, the Hague, the Netherlands.

329. Oswald, L. J., and Arambages, A. (1983). The Noise Mechanisms of Cross Groove Tire Tread Pattern Elements. NOISE-CON 83, New York.

330. Page, B. G. (1977). New and Innovative Methods and Materials for Pavement Skid Resistance. Federal Highway Administration, Sacramento, California.

331. Page, G. C. (1993). Open Graded Friction Courses - Florida's Experience. Transportation Research Record, 1427, 1-4.

332. Pagotto, C., Legret, M., and Le Cloirec, P. (2000). Comparison of the Hydraulic Behaviour and the Quality of Highway Runoff Water According to the Type of Pavement. Water Research, 34(18), 4446-4454.

333. Paje, S. E., Bueno, M., Terán, F., and Vi nuela, U. (2007). Monitoring Road Surfaces by Close Proximity Noise of the Tire/Road Interaction. Journal of the Acoustical Society of America, 122(5), 2636-2641.

334. Pasindu, H. R. (2011). Incorporating Risk Considerations in Airport Runway Pavement Maintenance Management. Ph.D thesis, National University of Singapore, Singapore.

335. Peeters, B., Ammerlaan, I., Kuijpers, A., and van Blokland, G. (2010). Reduction of the Horn Effect for Car and Truck Tyres by Sound Absorbing Road Surfaces. INTER-NOISE 2010, Lisbon, Portugal.

336. Peeters, B. and Kuijpers, A. (2008). The Effect of Porous Road Surfaces on Radiation and Propagation of Tyre Noise. EURO-NOISE 08, Paris, France.

337. Peeters, B., and van Blokland, G. (2007). The Noise Emission Model for European Road Traffic. M+P consulting engineers, Vught, The Netherlands.

338. Pelletier, J. D., Cline, M., and DeLong, S. B. (2007). Desert Pavement Dynamics: Numerical Modeling and Field-Based Calibration. Earth Surface Processes and Landforms, 32(13), 1913-1927.

339. Pelletier, R. F. (1976). Demonstration Project No. 10, Improved Skid Resistant Pavements. Federal Highway Administration, Arlington, Virginia.

340. Pelloli, P. (1976). Road Surface Characteristics and Hydroplaning. Transportation Research Record, 624, 27-32.

341. Persson, B. N. J. (1998). On the Theory of Rubber Friction. Surface Science, 401(3), 445-454.

342. Phillips, S., and Abbott, P. (2001). Factors Affecting Statistical Pass-By Measurements. INTER-NOISE 01, the Hague, the Netherlands.

343. Phillips, S. M., Morgan, P. A., and Watts, G. R. (1999). Development of Methods for Understanding Tyre/Road Noise Generation and Propagation. INTER-NOISE 99, Fort Lauderdale, Florida.

344. PIARC (1991). Surface Characteristics. XIX World Road Congress, Permanent International Association of Road Congresses, Marrakech, Morocco.

345. PIARC (1995). International PIARC Experiment to Compare and Harmonize Texture and Skid Resistance Measurements. Permanent International Association of Road Congresses, World Road Association, Paris, France.

346. PIARC (2005). International PIARC Experiment to Compare and Harmonize Texture and Skid Resistance Measurements. Permanent International Association of Road Congresses, World Road Association, Paris, France.

347. Pinkus, O., and Sterlicht, B. (1961). Theory of Hydrodynamic Lubrication, McGraw-Hill, New York.

348. Plotkin, K. J., Montroll, M. L., and Fuller, W. R. (1980). The Generation of Tire Noise by Air Pumping and Carcass Vibration. INTER-NOISE 80, Miami, Florida.

349. Praticò, F. G., and Anfosso-Lédée, F. (2012). Trends and Issues in Mitigating Traffic Noise Through Quiet Pavements. Procedia-Social and Behavioral Sciences, 53, 203-212.

350. Putman, B. J., and Kline, L. C. (2012). Comparison of Mix Design Methods for Porous Asphalt Mixtures. Journal of Materials in Civil Engineering, 24(11), 1359-1367.

351. Raaberg, J., Schmidt, B., and Bendtsen, H. (2011). Technical Performance and Long-Term Noise Reduction of Porous Asphalt Pavements. Danish Road Institute, Copenhagen, Denmark.

352. Ranieri, V., Antonacci, M. C., Ying, G., and Sansalone, J. J. (2010). Application of Kozeny-Kovàcs Model to Predict the Hydraulic Conductivity of Permeable Pavements. Transportation Research Record, 2195, 168-176.

353. Ranieri, V., Ying, G., and Sansalone, J. J. (2012). Drainage Modeling of Roadway Systems with Porous Friction Courses. Journal of Transportation Engineering, 138(4), 395-405.

354. Rasmussen, R. O., Bernhard, R. J., Sandberg, U., and Mun, E. P. (2007). The Little Book of Quieter Pavement. FHWA Report IF-08-004, Federal Highway Administration, Washington, D.C.

355. Rasmussen, R. O., Mun, E., Karamihas, S., and Chang, G. (2006). Relating Pavement Texture to Tire-Pavement Noise. INTER-NOISE 06, Honolulu, Hawaii.

356. Rasmussen, R. O., Sohaney, R., and Wiegand, P. (2011). Measuring and Reporting Tire-Pavement Noise Using On-Board Sound Intensity (OBSI). National Concrete Pavement Technology Center, Iowa State University, Ames, Iowa.

357. Rasmussen, R. O., Whirledge, R., Turner, D., Light, R., Ferragut, T., and Wiegand, P. (2008). Identifying Quieter Concrete Pavements Using On-Board Sound Intensity. Transportation Research Board 87nd Annual Meeting, Washington D.C.

358. Reddy, J. N. (2004). Mechanics of Laminated Composite Plates and Shells: Theory and Analysis, CRC Press, Boca Raton, Florida.

359. Reynolds, O. (1886). On the Theory of Lubrication and its Application to Mr Beauchamp Tower's Experiments Including an Experimental Determination of the Viscosity of Olive Oil. Philosophical Transactions of the Royal Society of London, 177, 157-234.

360. Rezaei, A., Masad, E., and Chowdhury, A. (2011). Development of a Model for Asphalt Pavement Skid Resistance Based on Aggregate Characteristics and Gradation. Journal of Transportation Engineering, 137(12), 863-873.

361. Richard, J., Ruhala, R. J., and Burroughs, C. B. (1998). Separation of Leading Edge, Trailing Edge, and Sidewall Noise Sources from Rolling Tires. NOISE-CON 1998, Ypsilanti, Michigan.

362. Roe, P. G., Parry, A. R., and Viner, H. E. (1998). High and Low Speed Skidding Resistance: The Influence of Texture Depth. Transport Research Laboratory, Crowthorne, UK.

363. Roger, G. G., John, G. L., and Horst, D. S. (1994). A Shifted Block Lanczos Algorithm for Solving Sparse Symmetric Generalized Eigenproblems. SIAM Journal on Matrix Analysis and Applications, 15(1), 228-272.

364. Ronneberger, D. (1985). Directivity of Tire/Road Noise Radiation. INTER-NOISE 85, Munich, Germany.

365. Rose, J. G., and Gallaway, B. M. (1977). Water Depth Influence on Pavement Friction. Journal of Transportation Engineering, 103(4), 491-506.

366. Ruhala, R. J., and Burroughs, C. B. (1998). Separation of Leading Edge, Trailing Edge, and Sidewall Noise Sources from Rolling Tires. NOISE-CON 1998, Ypsilanti, Michigan.

367. Ruhala, R. J., and Burroughs, C. B. (2008). Localization of Tire/Pavement Noise Source Regions. Noise Control Engineering Journal, 56(5), 318-331.

368. Rustighi, E., Elliott, S. J., Finnveden, S., Gulyás, K., Mócsai, T., and Danti, M. (2008). Linear Stochastic Evaluation of Tyre Vibration Due to Tyre/Road Excitation. Journal of Sound and Vibration, 310(4–5), 1112-1127.

369. Ryell, J., Corkill, J. T., and Musgrove, G. R. (1979). Skid Resistance of Bituminous-Pavement Test Sections: Toronto By-Pass Project. Transportation Research Record, 712, 51-61.

370. Ryszard, W. (2001). Measurement of Tyre/Road Noise in Longitudinal Slip Conditions. INTER-NOISE 01, the Hague, the Netherlands.

371. Sabey, B. E. (1966). Road Surface Texture and the Change in Skidding Resistance with Speed, Road Research Laboratory, London, UK.

372. Sabiniarz, P., and Kropp, W. (2010). A Waveguide Finite Element Aided Analysis of the Wave Field on a Stationary Tyre, Not in Contact with the Ground. Journal of Sound and Vibration, 329(15), 3041-3064.

373. Saemann, E. U., and Schmidt, H. (2002). Schallmessungen bei der Entwicklung von Reifen mit Geringem Vorbeifahrtpegel. Zeitschrift für Lärmbekämpfung, 49(2), 59-62.

374. Saito, K., and Henry, J. J. (1983). Mechanistic Model for Predicting Seasonal Variations in Skid Resistance. Transportation Research Record, 946, 29-38.

375. Saito, K., Horiguchi, T., Kasahara, A., Abe, H., and Henry, J. J. (1996). Development of Portable Tester for Measuring Skid Resistance and its Speed Dependency on Pavement Surfaces. Transportation Research Record, 1536, 45-51.

376. Sandberg, U. (1982). Will Tire/Road Noise Limit Vehicle Noise Reductions? INTER-NOISE 82, Washington D.C.

377. Sandberg, U. (1984). Six Decades of Vehicle Noise Abatement - But What Happened to the Tire? Spring Conference Acoustics, Institute of Acoustics, UK.

378. Sandberg, U. (1987). Noise and the Road - Is There a Conflict Between Requirements for Safety and Noise? Ingénieurs de l'Automobile, 76-84.

379. Sandberg, U. (1997). A New Porous Pavement with Extended Acoustical Lifetime and Useful Even on Low-Speed Roads. INTER-NOISE 97, Budapest, Hungary.

380. Sandberg, U. (2001). The Effect of Regulations on Road Vehicle Noise - Final Report by the I-INCE Working Party on Noise Emissions of Road Vehicles. Noise News International, 9(3), 147-206.

381. Sandberg, U., and Descornet, G. (1980). Road Surface Influence on Tire/Road Noise - Part I. INTER-NOISE 80, Miami, Florida.

382. Sandberg, U., and Ejsmont, J. A. (1984). Three Basic Methods for Measurement of Tire/Road Noise. INTER-NOISE 84, Honolulu, Hawaii.

383. Sandberg, U., and Ejsmont, J. A. (1992). Selection of Tires with Regard to Noise Emission. Swedish National Road and Transport Research Institute (VTI), Linköping, Sweden.

384. Sandberg, U., and Ejsmont, J. A. (2002). Tyre/Road Noise Reference Book, INFORMEX, Kisa, Sweden.

385. Sandberg, U., and Ejsmont, J. A. (2007). Inflence of Tyre Rubber Hardness of Tyre/Road Noise Emission. INTER-NOISE 07, Istanbul, Turkey.

386. Sarradj, E. (2003). Multi-Domain Boundary Element Method for Sound Fields in and Around Porous Pavement, Acustica/Acta Acustica, 89, 21-27.

387. Savkoor, A. R. (1965). On the Friction of Rubber. Wear, 8(3), 222-237.

388. Scavuzzo, R. W., Charek, L. T., Sandy, P. M., and Shteinhauz, G. D. (1994). Influence of Wheel Resonance on Tire Acoustic Cavity Noise. SAE Technical Paper, Series No. 940533.

389. Schaaf, K., and Ronneberger, D. (1982). Noise Radiation from Rolling Tires – Sound Amplification by the Horn-Effect. INTER-NOISE 82, San Francisco, California.

390. Schlichting, H. (1960). Boundary Layer Theory, McGraw-Hill, New York.

391. Schulze, K. H., and Beckman, L. (1965). Skid Resistance. American Society for Testing and Materials, West Conshohochen, Pennsylvania, 42-49.

392. Schwanen, W., van Leeuwen, H. M., Peeters, A. A. A., van Blokland, G. J., Reinink, H. F., and Kropp, W. (2007). Acoustic Optimization Tool RE3: Measurement Data Kloosterzande Test Track. Delft, the Netherlands.

393. Scofield, L. (2009). Development of the Next Generation Low Maintenance Concrete Surface. National Conference on Preservation, Repair and Rehabilitation of Concrete Pavements, St. Louis, Missouri.

394. Sextro, W. (2007). Dynamical Contact Problems with Friction: Models, Methods, Experiments and Applications, Springer, Berlin, Germany.

395. Shen, W., Shan, L., Zhang, T., Ma, H., Cai, Z., and Shi, H. (2013). Investigation on Polymer–Rubber Aggregate Modified Porous Concrete. Construction and Building Materials, 38, 667-674.

396. Smith, H. A. (1992). Performance Characteristics of Open-Graded Friction Courses. Transportation Research Board, National Research Council, Washington D.C.

397. Soedel, W., and Prasad, M. G. (1980). Calculation of Natural Frequencies and Modes of Tires in Road Contact by Utilizing Eigenvalues of the Axisymmetric Non-Contacting Tire. Journal of Sound and Vibration, 70(4), 573-584.

398. Srirangam, S. K. (2009). Study of Hydroplaning Characteristics of Rib Tires By Analytical Simulation. Master thesis, National University of Singapore, Singapore.

399. Stachowiak, G. W., and Batchelor, A. W. (2005). Engineering Tribology, Elsevier Butterworth-Heinemann, Amsterdam.

400. Staughton, G. C., and Williams, T. (1970). Tyre Performance in Wet Surface Conditions. Transport and Road Research Laboratory, Crowthorne, UK.

401. Steere, L. B. (1976). Skid Number-Speed Gradient Testing in Colorado. Colorado State Department of Highways, Denver, Colorado.

402. Stempihar, J. J., Pourshams-Manzouri, T., Kaloush, K. E., and Rodezno, M. C. (2012). Porous Asphalt Pavement Temperature Effects for Urban Heat Island Analysis. Transportation Research Record, 2293, 123-130.

403. Steven, H. (1989). Investigations on a Measuring Method for the Tire-Road-Noise of Passenger Cars. A Workshop on Rolling Noise Generation, Berlin, Germany.

404. Steven, H. (1991). Summary of the Results of the UBA Research Project Development of a Measuring Procedure for Car Tire-Road Noise. FIGE GmbH, Herzogenrath, Germany.

405. Steven, H., Küppers, D., van Blokland, G. J., van Houten, M. H., and van Loon, R. (2000). International Validation Test for the Close Proximity Method (CPX). M+P Raadgevende ingenieurs bv, 's-Hertogenbosch, the Netherlands.

406. Steven, H., and Pauls, H. (1990). Entwicklung eines Messverfahrens für das Reifen-Fahrbahn-Geräusch. FIGE, Herzogenrath, Germany.

407. Stinson, K. W., and Roberts, C. P. (1933). Coefficient of Friction Between Tires and Road Surfaces. 13th Highway Research Board Annual Meeting, Washington D.C., 169-188.

408. Storeheier, S. Å., and Sandberg, U. (1990). Vehicle Related Parameters Affecting Tire/Road Noise. INTROC 90, Gothenburg, Sweden.

409. Stutzenberger, J. W., and Havens, J. H. (1958). A Study of the Polishing Characteristics of Limestone and Sandstone Aggregates to Pavement Slipperiness. Highway Research Board Bulletin, 186, 58-81.

410. Tabor, D. (1959). The Importance of Hysteresis Loss in the Friction of Lubricated Rubber. The First International Skid Prevention Conference, Virginia.

411. TAC (1997). Pavement Design and Management Guide. Transportation Association of Canada, Ottawa, Ontario.

412. Tan, S. A., Fwa, T. F., and Chuai, C. T. (1999). A New Apparatus for Measuring the Drainage Properties of Porous Asphalt Mixes. Journal of Testing and Evaluation, 27(1), 57-62.

413. Tanner, J. A. (1996). Computational Methods for Frictional Contact with Applications to the Space Shuttle Orbiter Nose-Gear Tire. National Aeronautics and Space Administration, Langley Research Center, Hampton, Virginia.

414. The Highways Agency (1997). Design Manual for Roads and Bridges: Geotechnics and Drainage: Drainage the Stationery Office, Norwich, UK.

415. The Highways Agency (2004). Design Manual for Roads and Bridges: Pavement Design and Maintenance: Surfacing and Surfacing Material. The Stationery Office, Norwich, UK.

416. Tisseur, F., and Meerbergen, K. (2001). The Quadratic Eigenvalue Problem. SIAM Review, 43(2), 235-286.

417. Trant, J. J. P. (1959). NACA Research on Friction Measurements. The First International Skid Prevention Conference, Virginia Council of Highway Investigation and Research, Virginia, 297-308.

418. Tuononen, A. J. (2011). Laser Triangulation to Measure the Carcass Deflections of a Rolling Tire. Measurement Science and Technology, 22.

419. Ullrich, S., and de Veer, H. (1978). Geräuschmessungen von Pkw-Reifen am Innentrommelprüfstand der Bundesanstalt fur Strassenwesen. Bundesanstalt fur Strassenwesen, Bergisch-Gladbach, Germany.

420. Umiliaco, A. and Benedetto, A. (2012). Unsteady Flow Simulation of Water Drainage in Open-Graded Asphalt Mixtures. Procedia - Social and Behavioral Sciences, 53, 346-355.

421. Underwood, M. C. P. (1981). Lorry Tire Noise. Transport and Road Research Laboratory, Crowthorne, UK.

422. van der Zwan, J. T. (2011). Developing Porous Asphalt for Freeway in the Netherlands: Reducing Noise, Improving Safety, Increasing Service Life. TR News, 272, 22-29.

423. van der Zwan, J. T., Goeman, T., Gruis, H. J. A. J., Swart, J. H., and Oldenburger, R. H. (1990). Porous Asphalt Wearing Courses in the Netherlands: State of the Art Review. Transportation Research Record, 1265, 95-110.

424. van Heystraeten, G., and Moraux, C. (1990). Ten Years' Experience of Porous Asphalt in Belgium. Transportation Research Record, 1265, 34-40.

425. Varterasian, J. H. (1969). Quieting Noise Mathematically - Its Application to Snow Tires. Society of Automotive Engineers, Warrendale, Pennsylvania.

426. Veith, A. G. (1983). Tires-Roads-Rainfall-Vehicles: The Traction Connection. Frictional Interaction of Tire and Pavement, W. E. Meyer, and J. D. Walter, eds., American Society for Testing and Materials, West Conshohochen, Philadelphia, 3-40.

427. Veith, A. G. (1986). The Most Complex Tire-Pavement Interaction: Tire Wear. The Tire Pavement Interface, M. G. Pottinger, and M. G. Yager, ed., American Society for Testing and Materials, West Conshohochen, Pennsylvania, 125-158.

428. von Meier, A. (1992). Thin Porous Surface Layers - Design Principles and Results Obtained. The Mitigation of Traffic Noise in Urban Areas, Nantes, France.

429. von Meier, A., van Blokland, G. J., and Heerkens, J. C. P. (1990). Noise Optimized Road Surfaces and Further Improvements by Tyre Choice. INTROC 90, Gothenburg, Sweden.

430. Wai, K. L., and Kai, M. L. (2004). A Theoretical Study for the Propagation of Rolling Noise Over a Porous Road Pavement. The Journal of the Acoustical Society of America, 116(1), 313-322.

431. Waki, Y., Mace, B. R., and Brennan, M. J. (2009). Free and Forced Vibrations of a Tyre Using a Wave/Finite Element Approach. Journal of Sound and Vibration, 323(3-5), 737-756.

432. Wallman, C. G., and Aström, H. (2001). Friction Measurement Methods and the Correlation Between Road Friction and Traffic Safety - Literature Review. Swedish National Road and Transport Research Institute, Linköping, Sweden.

433. Wambold, J. C., Henry, J. J., and Hegmon, R. R. (1986). Skid Resistance of Wet-Pavement Accidents Sites. The Tire Pavement Interface, M. G. Pottinger, and M. G. Yager, eds., American Society of Testing and Materials, West Conshohochen, Pennsylvania, 47-60.

434. Watanabe, T., Tomita, N., Kishinami, S., Yamaguchi, H., Konishi, S., and Kawana, A. (1987). Noise Generation Mechanism of Cross-Bar Tires and Its Countermeasures. JSAE Review, 8(2), 56-62.

435. White, A. M. (1958). Test for Coefficients of Friction by the Skidding Car Method on Wet and Dry Surfaces. Highway Research Board Bulletin, 186, 26-34.

436. Williams, M. L., Landel, R. F., and Ferry, J. D. (1955). Temperature Dependence on Relaxation Mechanisms in Amorphous Polymers. Journal of American Chemical Society, 77, 3701-3707.

437. Williams, T., and Meades, J. K. (1975). Effects of Tread Pattern Depth and Tire Grooving on Lorry Tire Skidding Resistance. Transport and Road Research Laboratory, Crowthorne, UK.

438. Wolshon, B. (2004). Geometric Design of Streets and Highway. Handbook of Transportation Engineering, M. Kutz, ed., McGraw-Hill, New York, 13.11-13.21.

439. Woodside, A. R., and Woodward, W. D. H. (2002). Wet Skid Resistance. Highways, C. A. O'Flaherty, ed., Butterworth Heinemann, 479-499.

440. Wozniak, R. (2002). Hala Opon w Warunkach Wystepowania Znacznych sil Stycznych w Strefie Styku Opony z Jezdnia. Ph.D thesis, Technical Univeersity of Gdansk, Gdansk, Poland.

441. Wozniak, R., and Taryma, R. (2004). Investigations in Tyre/Road Noise in Longitudinal Slip Conditions. INTER-NOISE 04, Prague, Czech Republic.

442. Wu, C.-L., and Nagi, M. (1995). Optimizing Surface Texture of Concrete Pavement, Portland Cement Association, Skokie, Ill.

443. Wullens, F., Kropp, W., and Jean, P. (2004). Quasi-3D Versus 3D Contact Modelling for Tyre/Road Interaction. INTER-NOISE 04, Prague, Czech Republic.

444. Xia, K., and Yang, Y. (2012). Three-Dimensional Finite Element Modeling of Tire/Ground Interaction. International Journal for Numerical and Analytical Methods in Geomechanics, 36(4), 498-516.

445. Xing, M., Chen, S., Wang, B., and Wei, S. (2010). Research on Influence of Aggregate Gradation on the Performance of Porous Asphalt Pavement. Integrated Transportation Systems - Green, Intelligent, Reliable, 3738-3746.

446. Xu, G., Yin, C., and Yang, J. (2010). Early Age Field Performance Assessment of Porous Asphalt Pavement on Yan-Tong Expressway in China. Transportation Research Board 89th Annual Meeting, Washington D.C.

447. Xu, P., and Yu, B. (2008). Developing a New Form of Permeability and Kozeny-Carman Constant for Homogeneous Porous Media by Means of Fractal Geometry. Advances in Water Resources, 31, 74-81.

448. Yandell, W. O. (1971). A New Theory of Hysteric Sliding Friction. Wear, 17(4), 229-244.

449. Yang, B., Huang, Q., and Zhao, Y. (2009). Impact Analysis of Low-Noise Asphalt Pavement to Improve the Urban Environment. International Conference on Management and Service Science, Wuhan/Beijing, China.

450. Yang, J. (2013). Tire-Pavement Noise Simulation and Analysis. Ph.D thesis, National University of Singapore, Singapore.

451. Yoshiki, M., Tatsuo, N., and Katsuro, K. (2005). Evaluation of Porous Concrete Pavements in Japan. Eighth International Conference on Concrete Pavement: Innovations for Concrete Pavement: Technology Transfer for the Next Generation, Colorado Springs, Colorado, 462-473.

452. Younger, K., Hicks, R. G., and Gower, J. (1994). Evaluation of Porous Pavements Used in Oregon, Final Report. Oregon Department of Transportation, Salem, Oregon.

453. Yu, B., and Lu, Q. (2013). Bayesian Model for Tyre/Asphalt Pavement Noise. Proceedings of the Institution of Civil Engineers, 166(4), 241-252.

454. Yum, K., Hong, K., and Bolton, J. S. (2006). Experimental Relationship Between Tire Structural Wave Propagation and Sound Radiation. INTER-NOISE 06, Honolulu, Hawaii.

455. Zoeppritz, H. P. (1977). An Overview of European Measuring Methods and Techniques. Transportation Research Record, 621, 75-82.